UNIVERSITY OF TURIN

DOCTORAL SCHOOL IN NATURAL SCIENCES

Ph.D. PROGRAM IN
PAHARMACEUTICAL AND BIOMOLECULAR SCIENCES

CYCLE XXXIV

DETERMINATION OF DRUGS PERMEABILITY ON MUCUS MODELS BY HPLC-MS

BY

COSMIN STEFAN BUTNARASU

DOCTORAL THESIS

SUPERVISOR: PROF. SONIA VISENTIN

Ph.D. PROGRAMME COORDINATOR: PROF. ROBERTA CAVALLI
2020/2021

SCIENTIFIC DISCIPLINE: CHIM/08 - PHARMACEUTICAL
CHEMISTRY

DOCTORAL SCHOOL IN NATURAL SCIENCES

Ph.D. PROGRAM IN
PAHARMACEUTICAL AND BIOMOLECULAR SCIENCES
XXXIV cycle

UNIVERSITY OF TURIN
2020/2021

DOCTORAL THESIS

DETERMINATION OF DRUGS PERMEABILITY ON MUCUS MODELS BY
HPLC-MS

Candidate	Dr. Cosmin Stefan Butnarasu
Supervisor	Prof. Sonja Visentin
Jury Members	Prof. Giuseppe Ermondi (internal member) University of Turin Department of Molecular Biotechnology and Health Sciences
	Prof. Giuseppe Ciccarella (reviewer) University of Salento Department of Biological and Environmental Sciences and Technologies
	Prof. Thomas Crouzier (reviewer) KTH - Royal Institute of Technology, Stockholm School of Engineering Sciences in Chemistry, Biotechnology and Health – Division of Glycoscience
Head of the Doctoral School	Prof. Alberto Rizzuti
Ph.D. Program Coordinator	Prof. Roberta Cavalli

ABSTRACT

A constitutive layer of mucus covers all the non-keratinized epithelia in the body ensuring lubrication and protection against external threats. Its selective permeability is governed by mucins which are complex and heavily glycosylated proteins that form a tridimensional network around which mucus organize. Mucus can represent a strong barrier to tackle even for oral or pulmonary administered drugs, especially in mucus-related disorders where mucus is overproduced. Moreover, implications of mucins have been reported also in the oncogenesis and metastasis of adenocarcinomas. Yet, despite the critical role played on drug absorption, still little is known about the molecular characteristics leading to selective mucin and mucus binding.

Here, different approaches have been adopted to highlight the mechanisms ruling the binding of drugs with mucin and mucus. Furthermore, since mucin is recognized as a cancer biomarker, the detection of mucin mediated by fluorescent probes was investigated as well.

At first, mucin was used as a model of mucus to study the interaction with different drugs employed in cystic fibrosis (CF) therapy. Yet, mucin-based solutions fail to mimic the tridimensional structure of mucus, therefore an *in vitro* CF mucus model that reproduces both the composition and the rheological properties of pathological mucus was engineered following a modular approach. The mucus model was coupled to the state-of-the-art permeability platform (PAMPA) recreating a mucosal surface with a substantial high throughput capacity. Then, the mucus permeability platform was used to study how mucus impacts the passive diffusion of 45 drugs, showing that the CF mucus model was not a mere physical barrier but it behaves like an interactive filter. Besides, since the overproduction of mucus during respiratory diseases impedes pulmonary delivery of therapeutics, a novel class of intrinsically mucoadhesive and glycosylated mucin-based nanoparticles that have been called *mucosomes*, was developed. The outstanding drug loading capacity, the proven *in vitro* and *in vivo* safety, as well as the intrinsic glycosylation and mucoadhesivity, makes mucosomes a promising drug carrier for respiratory diseases. Eventually, fluorescent probes called squaraines were used to investigate the possibility to detect mucin following a fluorescence turn-on mechanism. The availability of a fluorometric test capable of detecting mucin at serum level would be of great help in identifying at an early-stage people at risk of adenocarcinomas.

LIST OF PUBLICATIONS AND MANUSCRIPTS

This thesis is structured into 4 main chapters. Within each chapter, the reader is given a comprehensive introduction of the topic to provide him/her the background knowledge to appreciate the scientific evidence produced in the thesis. Overall, the thesis is a summary of the publications or manuscripts listed below. At the end of each chapter, the reader will find a short overview of the results reported in the Author's paper(s) related to that specific chapter. For experimental details, the reader is invited to consult the Appendix part where the published papers/manuscripts, dealing with mucin/mucus (Manuscript I-V), are fully attached.

MANUSCRIPT I

Mucin binding to therapeutic molecules: the case of antimicrobial agents in cystic fibrosis
<u>Butnarasu C.</u>, Barbero N., Pacheco D., Petrini P., Visentin S.
International Journal of Pharmaceutics, 2019, 10, 136-144, DOI 10.1016/j.ijpharm.2019.04.032

MANUSCRIPT II

Disassembling the complexity of mucus barriers to develop a fast screening tool for early drug discovery
Pacheco D., <u>Butnarasu C.</u>, Briatico Vangosa F., Pastorino L., Visai L., Visentin S., Petrini P.
Journal of Materials Chemistry B, 2019, 7, 4940-4952, DOI 10.1039/C9TB00957D

MANUSCRIPT III

Cystic fibrosis mucus model to design more efficient drug therapies
<u>Butnarasu C.</u>, Caron G., Pacheco D., Petrini P., Visentin S.
Molecular Pharmaceutics, 2022, 19, 2, 520-531,
DOI 10.1021/acs.molpharmaceut.1c00644

MANUSCRIPT IV

Mucosomes: intrinsically mucoadhesive glycosylated mucin nanoparticles as multi drug delivery platform
Butnarasu C., Petrini P., Bracotti F., Visai L., Guagliano G., Fiorio Pla A., Sansone E., Petrillo S., Visentin S.
(Under review in Advanced Healthcare Materials)

MANUSCRIPT V

Squaraine dyes as fluorescent turn-on sensors for the detection of porcine gastric mucin: a spectroscopic and kinetic study
Butnarasu C., Barbero N., Barolo C., Visentin S.
Journal of Photochemistry and Photobiology B: Biology, 2020, 205, 111838, DOI 10.1016/j.jphotobiol.2020.111838

MANUSCRIPT VI

A PI3Kγ mimetic peptide triggers CFTR gating, bronchodilation, and reduced inflammation in obstructive airway diseases
Ghigo A., Murabito A., Sala V., Pisano A., Bertolini S., Gianotti A., Caci E., Montresor A., Premchandar A., Pirozzi F., Ren K., Della Sala A., Merigotti M., Richter W., de Poel E., Matthey M., Caldrer S., Cardone R., Civiletti F., Costamagna A., Quinney N., Butnarasu C., Visentin S., Ruggiero M., Baroni S., Geninatti Crich S., Ramel D., Laffargue M., Tocchetti C., Levi R., Conti M., Yun-Lu X., Melotti P., Sorio C., De Rose V., Facchinetti F., Fanelli V., Wenzel D., Fleischmann B., Mall M.., Beekman J., Laudanna C., Gentzsch M., Lukacs Gergely., Pedemonte N., Hirsch E.
*(*Accepted on *Science Translational Medicine*)

MANUSCRIPT VII

Squaraine dyes: interaction with bovine serum albumin to investigate supramolecular adducts with aggregation-induced emission (AIE) properties
Barbero N., Butnarasu C., Visentin S., Barolo C.
Chemistry – An Asian Journal, 2019, 14(6), 896-903, DOI 10.1002/asia.201900055

MANUSCRIPT VIII

Interaction of squaraine dyes with proteins: looking for more efficient fluorescent turn-on probes
Butnarasu C., Barbero N., Barolo C., Visentin S.

ACKNOWLEDGEMENTS

TABLE OF CONTENTS

LIST OF FIGURES

specific proteins can restore their fluorescence. (C) Increase of fluorescence induced by different concentrations of mucin. (D) Absorption spectrum of SQ in the presence of mucin. Mucin might act as a desolvating agent favoring the solubilization of SQ aggregates......... 39

LIST OF TABLES

ACRONYMS

A

adsorption, distribution, metabolism, excretion (ADME), 21
airway surface liquid (ASL), 13

C

chimeric antigen receptor T-Cell (CAR-T), 36
chronic obstructive pulmonary disease (COPD), XIV, 12, 14, 26, 53
coronavirus disease 2019 (COVID-19), 31, 57

cyclic adenosine monophosphate (cAMP), 12, 26, 27
cysteine-knot (CysK), 4, 5
cysteine-rich domains (CysD), 2, 3, 4, 5
cystic fibrosis (CF), V, XIV, XV, 2, 5, 6, 10, 12, 13, 14, 17, 18, 19, 23, 24, 25, 26, 27, 28, 32, 41, 42, 43, 52
cystic fibrosis transmembrane conductance regulator (CFTR), IX, XIV, 2, 5, 12, 13, 14, 27, 52
cytoplasmic tail (CT), 3

1 MUCINS

Mucins are a family of high molecular weight, rod-like and heavily glycosylated proteins. They are not exclusive of vertebrates, and can be found in almost all eukaryotes.[1] In humans, mucins are produced and secreted by goblet cells and submucosal glands mucus or are tethered to cell membranes.[2] Mucins are characterized by a rich chemical diversity, since they combine a long protein backbone linked to carbohydrates. Most of the amino acids within the peptide core are covalently O-linked to sugars called glycans, which make up to 80-90% of the molecular mass of the protein.[3] The main properties attributed to mucins include barrier properties, dynamicity, hydration, lubrication, and bioactivity.[4] Among them, one of the most important characteristic is their ability to form gels which makes mucins key components in most gel-like secretions enabling boundary lubrication with very low friction coefficients. Because of their ability to retain huge volumes of water, mucins are the major macromolecular components of mucus. These large proteins assemble into enormous polymers that build a tridimensional scaffold around which mucus is organized.

1.1. MUCIN SUBTYPES

To date, mucins include 21 mucin-type glycoproteins, all of them belonging to the *MUC* gene family. According to their localization, mucins have been classified in transmembrane and secreted mucins (Table 1). The differences between the two groups are also given by the different composition of their domains, the different biosynthetic pathways, and the different posttranscriptional modifications.

Transmembrane mucins (membrane-tethered mucins) are anchored to the apical side of epithelial cells by a transmembrane domain, and are involved in the formation of the glycocalyx. This class consists of several mucins that differ in length, domains composition, and mainly on the cytoplasmic signaling.[5] They can be further classified in three groups: the SEA (sea urchin-enterokinase-agrin) mucins, the NIDO-AMOP-VWD (*nidogen*-like, *A*dhesion-associated domain in *M*UC4 and *O*ther *P*roteins, and *v*on *W*iellebrand *D* domain) mucins, and a group without specific protein domains other than mucin domain.[6] The intracellular domain is

a distinctive feature of transmembrane mucins and it is involved in signaling pathways thanks to the presence of (supposed) phosphorylation sites. On the contrary, the extracellular domains (mucin domain) often consist of long internal repeat domains that are highly glycosylated (PTS), a common trait also present in secreted mucins.

The secreted mucins are the key components of mucus because endows mucus with its characteristic viscoelastic properties.[7] These mucins can be further classified into insoluble gel-forming mucins and soluble mucins. All the gel-forming mucins share a similar structural assembly. In particular, the presence of cysteine-rich domains (CysD) at both the N- and C-terminus, allow mucins to form oligomers, and consequently to construct a tridimensional network.[8]

1.2. THE STRUCTURE OF MUCINS

Mucins are structurally diverse but share similar structural features (Figure 1-1). All of them have a variable number of tandem repeats rich in hydroxy-amino acids serine and threonine along with proline, called PTS domains.[9] The PTS domains are characterized by dense O-linked oligosaccharide chains called glycans, thanks to, mucins gain resistance to proteolysis. Among the most common O-linked glycans there are mannose, xylose, N-acetylglucosamine, fucose and sialic acid.[10,11] The linked carbohydrate chains are negatively charged because of the presence of sialic acid and sulfated sugars (especially galactose, N-acetyl-galactosamine, and N-acetyl-glucosamine).

The overall negative charge contributes to the stiffness of the mucin, which is important for their viscoelastic properties.

A short sequence of hydrophobic amino acids residues assembles into the transmembrane domain, characteristic of membrane-bound mucins. This domain continues intracellularly forming the C-terminal cytoplasmic tail which plays active functions in intracellular signaling.

MUC3, MUC12, and MUC17, contains on their intracellular domain PDZ-binding motifs, which are key components in the trafficking and in the formation and function of signal transduction complexes.[12] For instance, through PDZ-binding motifs, these mucins communicate with the cystic fibrosis (CF) transmembrane conductance regulator (CFTR) chloride channel.

Other common protein domains within transmembrane mucins are the sea urchin-enterokinase-agrin (SEA) domain, the *nidogen*-like (NIDO), and the *A*dhesion-associated domain in *M*UC4 and *O*ther *P*roteins (AMOP), however, in addition of knowing that they are extracellular domains, their roles are not yet completely deciphered. It is known that

Table 1: List of human mucins. Adapted from Hansson G. (*Annu. Rev. Biochem.* 2020) [6].

Mucins	Domain structure	Number of amino acids	Typical localization
TM mucins			
SEA			
MUC1	PTS-SEA-TM-CT	1,255	General
MUC3	PTS-SEA-TM-CT	> 2,541	Intestine
MUC12	PTS-SEA-TM-CT	5,478	Intestine
MUC13	PTS-SEA-TM-CT	512	Intestine
MUC16	(PTS-SEA)$_{33}$-TM-CT	22,152	General
MUC17	PTS-SEA-TM-CT	4,493	Intestine
NIDO-AMOP-VWD			
MUC4	PTS-NIDO-AMOP-VWD-TM-CT	5,284	General
Others			
MUC15	PTS-TM-CT	334	General
MUC21	PTS-TM-CT	566	Esophagus
MUC22	PTS-TM-CT	1,733	Esophagus
Secreted mucins			
Gel forming			
MUC2	VWD1-VWD2-VWD3-PTS(CysD)-VWD4-CT	5,130	Intestine
MUC5AC	VWD1-VWD2-VWD3-PTS(CysD)-VWD4-CT	5,654	Lung, stomach
MUC5B	VWD1-VWD2-VWD3-PTS(CysD)-VWD4-CT	5,703	Lung, saliva
MUC6	VWD1-VWD2-VWD3-PTS-CT	5,534	Stomach
Monomeric			
MUC7	PTS	377	Saliva
MUC20	PTS	709	Kidney/urinary tract

Abbreviations: AMOP, adhesion associated domain; CT, cytoplasmic tail; NIDO, nidogen domain; PTS, Pro-Thr-Ser; domain; SEA, sea urchin-eneterokinase-agrin; TM, transmembrane; VWD, von Wiellebrand D domain.

SEA domains are highly conserved and they undergo post-translational cleavage. It has been proposed that this domain may act as

a breaking point that can dissociate before the plasma membrane is breached when mechanical forces are applied to cell surfaces.[13,14]

At the N- and C-terminus (cysteine-knot, CysK), as well as interspaced between the PTS domains, gel forming mucins have cysteine-rich domains (CysD), which are implicated in forming disulfide bonds and mucin multimers.

Gel-forming mucins share a common protein domain (VWD) with von Willebrand factor (VWF), a protein essential for blood clotting. Recently, it has been proposed that mucins and von Willebrand factor have a common mechanism to form linear polymers based on disulfide-rich bridges.[15] Similar to PTS domains, VWD undergoes extensive posttranslational modification resulting in the addition of O- and N-linked glycans.[16]
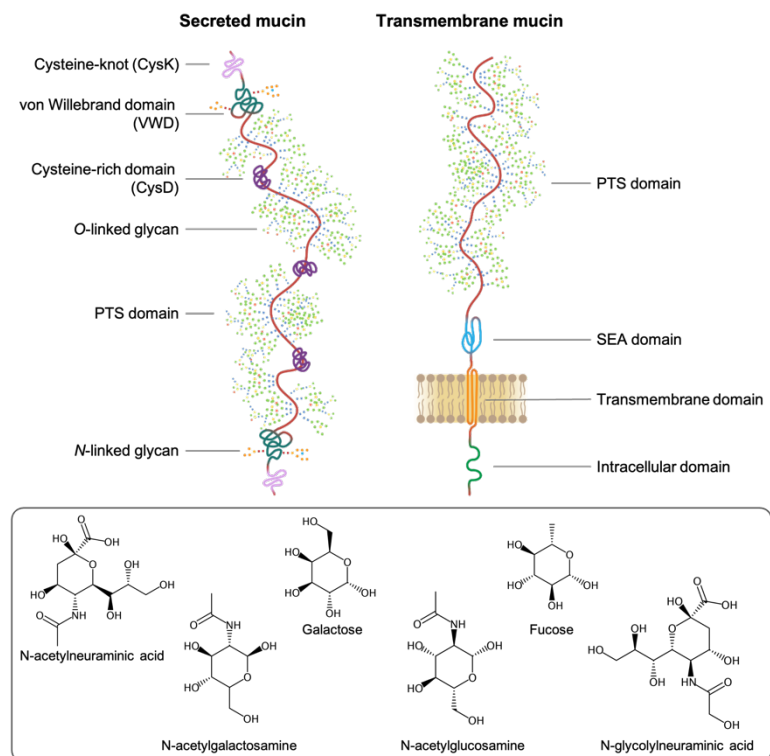
Figure 1-1. Schematic representation of secreted and transmembrane mucins with their most representative domains. On the bottom, the most common carbohydrates constituting the glycan chains.

1.3. INTERACTION OF DRUGS WITH MUCIN

Mucins are one of the most complex glycoproteins present in nature. Because of the simultaneously presence of hydrophilic, hydrophobic, and negatively charged domains, mucins have a huge binding capacity. In fact, lipophilic drugs may interact with the naked portions of mucins (*i.e.*, CysK, VWD, CysD), while hydrophilic molecules may engage mucins either through H-bonding or, if positively charged, by electrostatic interactions on the negatively charged glycans.[17,18] The big picture sees mucins' tridimensional framework preventing the penetration of noxious particles and small molecules by a complex size and interactional filtering activity. In mucus-related disorders (see Chapter 2.2 below) such as cystic fibrosis (CF), the barrier activity of mucins is strengthened as a result of overexpression of mucins, mucus dehydration, and acidification. Therefore, it is clear that the binding of drugs to mucins can alter their pharmacokinetics and bioavailability.

Mucin binding to therapeutic molecules: the case of antimicrobial agents used in cystic fibrosis – overview

«*The work presented in this section was published in the journal* International Journal of Pharmaceutics *and it is attached as full article in Appendix A*»

Given the high binding capacity exerted by mucins, in this thesis, focus was set on studying the binding between molecules of interest in CF and porcine gastric mucin (PGM). Drugs with strong binding to mucin could be less effective because not available on their biological target. The proof of concept of using mucin to mimic mucus is widely reported in the literature.[19–21]

The interaction was investigated by absorbance and steady-state fluorescence spectroscopies (for experimental details, the reader is invited to consult Appendix A). Such approach was previously applied in our group by Pontremoli *et al.*, to study the binding of theophylline, cephalexin and prednisolone to mucin.[22] Since CF patients are subjected to recurrent infections of the airways, here eight compounds (7-aminocephalosporanic acid, ceftazidime, aztreonam, ampicillin, CFTR$_{inh}$-172, tobramycin, levofloxacin, rifampicin) have been selected among the antibiotics used in the CF therapy, with the only exception of CFTR$_{inh}$-172 which, instead, is an inhibitor of the cystic fibrosis transmembrane conductance regulator (CFTR) protein. The tryptophan fluorescence is extremally sensitive to the local environment, therefore it can be exploited to investigate the interaction of small molecules with

proteins (Figure 1-2, A). Experimentally, the binding was observed by measuring the quenching of fluorescence of mucin upon addition of increasing concentrations of the drug (Figure 1-2, B). It was found that only ceftazidime, aztreonam, CFTR$_{inh}$-172 and levofloxacin interact with the protein as the fluorescence of mucin linearly decreased in the presence of the drug. The measured equilibrium association and dissociation constants (K_a and K_d) indicates moderate affinity toward mucin (Figure 1-2, D). From the clinical point of view, the mild affinity could explain why, after all, these drugs are routinely used in the CF therapeutic regimes. By changing the temperature of the system, it was determined that the quenching mechanism is mostly collisional, meaning that the interaction occurs when mucin is in the excited-state (Figure 1-2, C). In addition, variation of systems' temperature can give information about thermodynamic parameters (*i.e.*, $\Delta H°$, $\Delta S°$ and $\Delta G°$) that can be used to describe the nature of the binding. Accordingly, in spite of expectations, it was found that the driving force of the binding are mainly governed by hydrophobic interactions. Interestingly, no binding is observed with the aminoglycoside tobramycin, which is known to interact with mucin.[21] Since tobramycin has five positive charges at pH 7.4, it can strongly bind the negatively charged glycans of mucin by electrostatic interactions.

Overall, the fluorometric monitoring could clarify some aspects of the binding, however, limitations intrinsic to the spectroscopic approach could underestimate the number of possible interactions that can be established with such a complex protein as mucin (*e.g.*, tobramycin results). Moreover, the same mucin might be a too simplistic model of mucus, as it fails to mimic the tridimensional architecture of mucus.
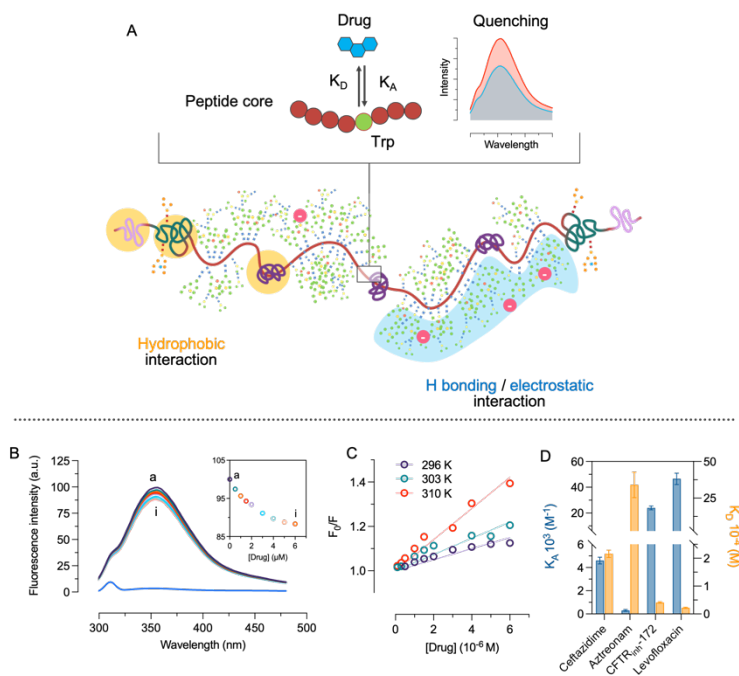
Figure 1-2. Mucin is a glycoprotein with a huge binding capacity. (A) Due to the multiversity of functional groups, mucins can interact with molecules of both hydrophilic or hydrophobic nature, as well as with positively charged drugs. The intrinsic fluorescence of mucin can be exploited by monitoring the fluorescence of tryptophan (Trp), which is extremally sensitive to environmental changes (*e.g.*, polarity). Quenching of proteins can be used to determine the extent of binding to the protein. (B) Steady state fluorescence spectra of mucin in the presence of ceftazidime. The inset on (B) depicts the quenching of fluorescence of mucin upon increasing the concentration of ceftazidime. (C) Changing the temperature of the system allow to discriminate between static and dynamic quenching, namely if the interaction takes place in the ground or excited state of the protein. Stern-Volmer plots illustrates the variation of collisional quenching with the variation of the temperature. The higher the temperature, the stronger the quenching. (D) Equilibrium association (K_a) and dissociation (K_d) constants measured by steady-state fluorescence spectroscopy at 37 °C.

2 MUCUS

Nature endowed us with two mechanisms to protect ourselves against environmental threats such as toxins, pollutants and pathogens: the first consisting in shielding the living cells of the body with a coating of death cells (*e.g.,* skin), while the second being the coating of the cells with a dynamic hydrogel called mucus. Usually, mucus is thought as something disgusting, actually it is a valuable tool of our body.

Within the human body, all the wet epithelia are lined by mucus. It harbors and nourish our intestinal flora, and at the same time, protects the underlying cells against noxious agents, pollutants and invading pathogens.[3,23–25] Yet, the mechanism behind mucus' protective effect is still not completely clear. Some of the unanswered questions surrounding mucins and mucus are starting to be revealed, thanks also to the outstanding research made within the Glycoscience landscape, but much more has yet to be learned.

The skeleton around which mucus organize is build up by mucins. Once secreted, mucins undergo massive swelling process, entrapping large volumes of water, and assemble into polymeric glycoconjugates forming a tridimensional network. Mucus is constantly secreted at low rate, however, external stimuli, such as presence of bacterial toxins, irritating substances and inflammatory mediators, or mechanical stimuli, can induce mucus overproduction.[26–28] The daily secretion of mucus is about 10 *l,* but large part of it (9.8 *l*) is reabsorbed and recycled.[29] The secretion is dependent of the anatomical site, mostly being at the gastrointestinal (GI) and respiratory tract, but mucus is released also at ocular, vaginal, and pancreatic districts. The thickness of mucus extensively varies both within and between the different organs. For instance, at gastrointestinal level the layer of mucus become thicker from the upper to the lower GI tract, spanning from 100 to 800 μm, respectively.[30] Similarly, in the airways, the layer of mucus is thinner, varying from 10-30 μm at tracheal level, to 2-5 μm in the smaller bronchi.[30]

Mucus has a heterogeneous composition. Even if mucins are the most important constituents, many other proteins are harbored within mucus. These proteins can be classified in four different groups including defensive proteins (*e.g.*, elastase, α- and β-defensines, lysozymes and lactoferrins), growth factors, structural proteins and generic

glycoproteins.[31] But also, fragments of nucleic acids and lipids, such as cholesterol and phospholipids, can be present, especially in pathological conditions,[32,33] where their concentration changes the rheology of mucus. The hydration and tonicity of mucus are finely regulated by its electrolyte content (Na^+, Cl^-, Mg^{2+}, Ca^{2+}, K^+, CO_3^{2-}), which despite being less than 1% of the total mass, play a crucial role on the viscoelastic properties of the hydrogel.[34]

2.1.   BARRIER PROPERTIES OF MUCUS

One of the most outstanding capacity of mucus is its ability to be a dynamic semipermeable network allowing the exchange of gasses, nutrients and hormones, whilst impeding the penetration of environmental threats. The barrier properties of mucus are mainly orchestrated by the crosslinked network of mucins, which establish a spider web-like sticky filter, controlling the diffusion of small and macromolecules (Figure 2-1).

As a first filtering mechanism, particles are excluded on the basis of their size, namely the diffusion is reduced if the particle is larger than the mesh spacing between mucin fibers. The average pore size of the mucin mesh varies significantly with the location, composition and disease state.[35] It has been estimated that the average pore size of cervicovaginal mucus (CVM) is roughly 340 ± 70 nm[36], while that of intestinal mucus being around 200 nm[37]. Respiratory mucus was found to be permeable to 200 nm polyethylene glycol (PEG) coated particles, whereas diffusion of 500 nm particles was hampered.[38] In disease conditions such as CF, the mucin mesh shrinks forming smaller average pore sizes around 140 $\pm$ 50 nm.[39,40]

In contrast, particles smaller than the average mesh size theoretically diffuse through the pores as long as they are inert to the interactional filter exposed by mucus. Because of its heterogeneous composition, mucus provides a broad range of possible interactions that can be established with molecules of hydrophilic as well as hydrophobic nature. Here, mucins play the key role in binding exogenous compounds. The abundance of negative charges and hydrophilic portions given by the glycans, and the hydrophobic residues on the naked domains, allows mucin to engage molecules by electrostatic, H-bonding and hydrophobic interactions. Thus, mucin can selectively control the diffusion of those molecules small enough to penetrate the mucin mesh. For example, it has been proved that identically sized particles of 10 nm, but with different surface properties, have different diffusion profiles through mucus.[41] The barrier effect driven by electrostatic interactions is more evident on polycationic compounds. It has been proved that the aminoglycoside

tobramycin which has 5 positive charges at pH 7.4, strongly binds the negatively charged glycans of mucin.[21] Lipophilic particles will tend to bind non-specifically to the naked portions of mucins and their permeability will be limited also by their low solubility in an aqueous environment as mucus is (*i.e.*, 95% water).[21] Indeed, as reported in Appendix A, the driving force for the binding of several drugs to PGM was found to be mainly governed by hydrophobic interactions. Yet, mucins are just one of the components contributing to the interaction filtering of mucus. All the other components of mucus such as lipids, fragments of DNA, and proteins, can similarly contribute on retention of particles into the mucus matrix.
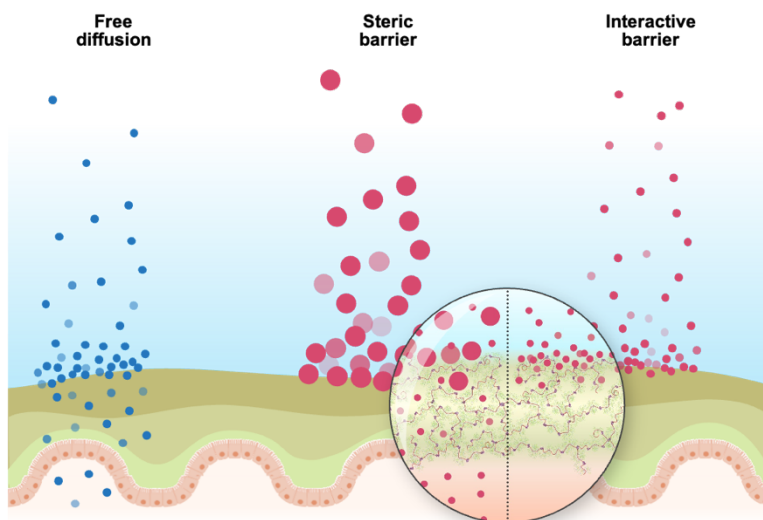
Figure 2-1. The steric and interactive barriers of mucus. Drugs larger than the mesh spacing between mucin fibers are stacked within mucus because too big to cross the mucus mesh. Similarly, drugs smaller than the mesh, but able to interact with mucus components are equally retained by mucus. On the contrary, particles that are small enough and relatively inert to any of the mucus components can freely diffuse through the mucus layer and eventually absorbed.

2.2.   MUCINS AND MUCUS RELATED DISORDERDS

Malfunctions of mucins/mucus is an important factor in human diseases, both in the causation (etiology) of the illness or in the exacerbation of dysfunctions originated from different mechanisms.[42] A

key role is played by mucins in the so called *mucus-related disorders* like cystic fibrosis (CF) and chronic obstructive pulmonary disease (COPD). Nevertheless, implication of mucins have been found also in different malignancies such as adenocarcinomas of various tissues (see Chapter **Error! Reference source not found.**).

2.2.1. *Respiratory diseases*

If on one hand, weakening of mucus barriers makes us more vulnerable to environmental threats, paradoxically an overproduction of mucus or dysfunctional clearance are hallmarks of the pathogenesis of all the mucus-related disorders. Among them, COPD and CF are the most representative cases with similar pathophysiological events. These effects involve mucus persistence to epithelial surfaces, airway obstruction, chronic bacterial infection with recurrent pulmonary exacerbations, inflammation with persistent leukocyte accumulation. The infection and inflammation processes are strictly intertwined. The permanent presence of bacteria participates in the inflammatory process contributing to a vicious cycle where mucus alteration, infection, and inflammation are elements tightly related and difficult to separate. Though, the etiology of COPD and CF are different

Cystic fibrosis

Cystic fibrosis is a chronical life-limiting autosomal recessive pathological condition caused by mutations in the cystic fibrosis transmembrane conductance regulator (CFTR) gene which encode for a cAMP-regulated epithelial chloride channel.[43] CF is one of the most lethal genetic disease affecting white people with an incidence of 1 in 3,000 live births.[44,45] The primary function of the CFTR protein is to facilitate the transport of chloride in and out of cells, but it indirectly regulates also the trafficking of sodium and bicarbonate. Different mutations of the CFTR gene can result either in transcription of dysfunctional protein, or in a reduced amount (sometimes even absence) of the CFTR protein at the cell surface.[44,46,47] The phenotype is characterized by progressive pulmonary disease, loss of pancreatic exocrine functions, occlusion of reproductive ducts in male, and intestinal disorders which results in altered absorption of nutrients and eventually malnutrition.[45]

Even if CF manifests also in pancreas, gastrointestinal tract, sweat glands and vas deferens, the pulmonary disease rests the most difficult problem in the management of cystic fibrosis and airway complications are the main cause of morbidity and mortality.[44,48] In physiological

conditions the airway surface liquid (ASL) supports an environment in which cilia can freely beat. The CFTR-mediated chloride secretion is necessary to regulate the volume of ASL. An impaired secretion in CF leads to dehydration of ASL, resulting in decreased mucus clearance, thick secretion, and obstruction of the airways.[3,49] The clearance deficit promotes bacterial colonization and infection which is a major contributor for progressive lung disease. Moreover, since CFTR play an important role in the pH regulation of the ASL, through bicarbonate secretion, its compromised function results in acidification of the ASL and reduced activity of pH-dependent defensines.[50] A wide variety of bacterial species infect and nourish within CF mucus (Table 2). *Staphylococcus aureus* and *Hemophilus influenzae* are the most common bacteria that can be isolated in the first decade of life. It was proposed that *S. aureus* may be responsible of the pulmonary damage which further pave the way for other pathogens (*i.e.*, *Pseudomonas aeruginosa*).[51] *P. aeruginosa* infect more than 50% of CF patients and it is the most frequently encountered pathogen in the second and third decade of CF patients' life.[52] The mucoid type of *P. aeruginosa* secretes a protective alginate biofilm that covers the bacterial colonies, ensuring protection against the activity of polymorphonuclear leukocytes. The presence of mucoid phenotype has been associated with increased mortality, frequent exacerbations and severe lung inflammation.[53–57]

The impaired mucociliary clearance and mucus' altered physicochemical properties sustains chronic infections and a permanent inflammatory milieu. Over time CF patients develop a progressive destruction of the pulmonary parenchyma, evolving then in bronchiectasis and chronic respiratory failure that cause ~90% of deaths in CF patients (Figure 2-2).[58,59]

Table 2. Most frequently encountered pulmonary bacterial pathogens in cystic fibrosis. Adapted from Coutinho H. *et al.*, (International Archives of Medicine 2008)[60]

Bacterial pathogens associated with pulmonary risk	
Major pathogens	Minor pathogens
Mycobacterium sp.	*Achromobacter xylosoxidans*
Staphylococcus aureus	*Inquilinus limosus*
Pseudomonas aeruginosa	*Ralstonia sp*
Burkholderia ssp.	*Pandoraeapista*
	Streptococcus pneumoniae
	Stenotrophomonos maltophilia
	Haemophilus influenzae
	Bordetella bronchiseptica
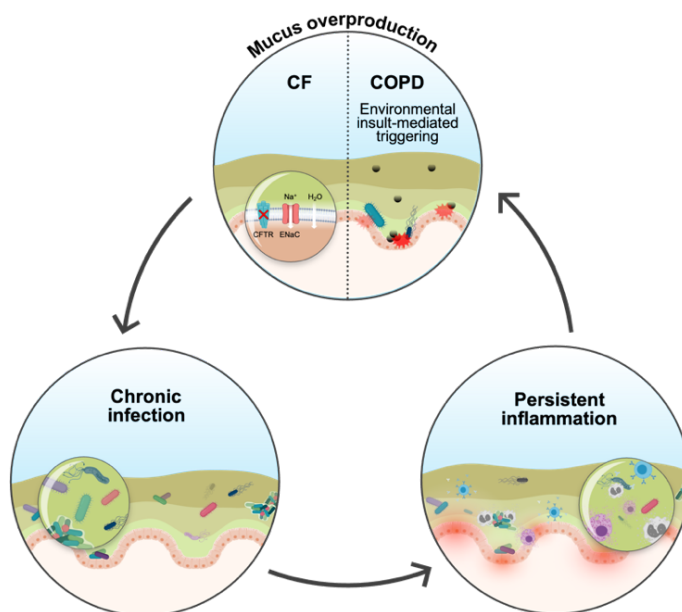
Figure 2-2. Mucus-related pathophysiological vicious cycle. The cystic fibrosis transmembrane conductance regulator (CFTR) dysfunction in cystic fibrosis (CF) and the environmental insult-mediated triggering in chronic obstructive pulmonary disease (COPD) stimulate the overproduction of mucus. Mucus stasis facilitates bacterial colonization which induces the inflammatory response. Chronic inflammation causes damages to lung tissues leading eventually to respiratory failure.

Chronic obstructive pulmonary disease

Chronic obstructive pulmonary disease (COPD) is a chronic inflammatory lung disease that causes obstructed airflow from the lungs. With more than 3 millions deaths per year, COPD is now the third cause of death globally.[61] It is characterized by persistent respiratory symptoms and airflow limitations that is due to airway and/or alveolar abnormalities, usually caused by long-term cumulative exposure to noxious particles (*i.e.*, cigarette smoke) or gases.[62]

Emphysema and chronic bronchitis are the two most common conditions that contribute to COPD phenotype. Chronic bronchitis is characterized by mucus hypersecretion and persistent cough that persist for at least three months, for two consecutive years. The primary mechanism responsible for mucus accumulation is the hypersecretion by goblet cells in response to external stress, and the decreased turnover.[63] Similarly to what happens in CF, also COPD is characterized by

dysfunctional mucociliary clearance, that leads to mucus accumulation and stasis in the airways. The vicious cycle of persistent epithelial stress, mucus overproduction, chronic infection and inflammation eventually produce permanent damage of the lung tissue (*i.e.*, emphysema). In particular, the alveolar walls are gradually and irreversibly destroyed creating larger air sacs, thus a reduced lung surface area (Figure 2-2).[64]

2.3. MUCUS MODELS

In the last decades the interest on mucins and mucus has rapidly grown. The rising interest was fostered on one hand by the understanding of the huge potential that mucin and mucus-like materials have in terms of filtering activity, rheological and tribological properties; on the other hand, new evidence suggested that mucins and mucus play key roles in numerous disorders (*e.g.*, respiratory diseases, peptic ulcer, inflammatory bowel disease, and even cancer). Moreover, the experimental evidence of the interconnection between the microbiota harbored within intestinal mucus and brain (*i.e.*, gut-brain-axis) has evolved from simple theory to a concrete branch of neuroscience.[65] The increased demand, however, was not necessarily satisfied by an increased availability of mucus. This because manipulating and handling native human mucus has several drawbacks, being the intrinsic availability (*i.e.*, difficult to collect), the associated biological risk, and the wide variability among patients in terms of composition. Therefore, the need for realistic mucus models became more and more stronger. The ideal model should mimic the composition and tridimensional structure of native mucus to the greatest extent possible,[66] yet being easy to produce, economic and reproducible.

Developing *in vitro* mucus models that mimics both the functions and biological structure of native mucus is extremely important in the drug discovery context, where the failure rate of novel drug candidates addressing intestinal or pulmonary diseases is ~85%.[67,68] In the last decades several mucus models have been developed, including native collected mucus, purified mucin preparations, *in vitro* cell cultures, and intact mucosal tissues (Figure 2-3).

The more complex mucus models used to assess the impact of mucus on the diffusion of drugs rely on *in vivo* and *ex vivo* models. The *in vivo* gold standard model is Loc-I-Gut™ consisting of a jejunal perfusion technique,[69] while similarly, the everted intestinal ring is the only *ex vivo* model proposed.[70] The results that can be obtained using these methods are certainly the most realistic, as the entire complexity of the *in vivo* scenario is maintained. However, the intricate setup, high cost, animal sacrifice, and high variability very often are not worth the hassle.
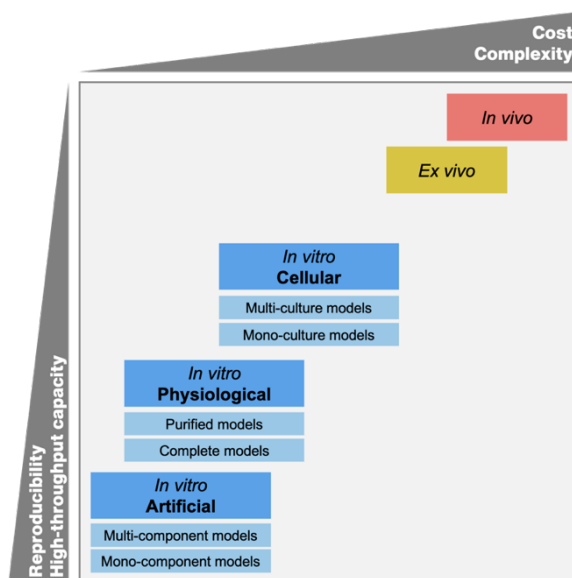
Figure 2-3. Classification of *in vivo*, *ex vivo*, and *in vitro* mucus models based on biological complexity, cost, reproducibility and high-throughput capacity. Adapted from Sardelli L. *et al.*, (*RSC Adv. 2019*).[65]

To overcome these limitations, efforts have been made to develop many more *in vitro* models.[65,66,71] The in vitro models can be classified according to their complexity. The most basic models include mucins or mucin-like polymers suspended in buffers.[72] To these suspensions other components such as lipids, DNA, and proteins, can be added to increase the system complexity, creating mixtures that mimic mucus-specific districts.[73–75] Thanks to the availability of commercial mucins, mono- and multi-component mucus models can provide versatility, repeatability, and high-throughput capacity, even though they fail to reproduce the tridimensional and dynamic architecture of native mucus and its interactional filtering ability. Physiological mucus models are the most representative models since they are extracted directly from humans or animals.[76] However, the difficulty to obtain large volumes, and the high inter/intra variability (*e.g.*, different site of extraction, different organism, fed-fast condition) are the main limitations of these models. Several cellular-based mucus models have been also developed. These include cell lines able to secrete mucus such as Calu-3, a model used to model the airway epithelium, and HT29-MTX derived from human colon.[77–79] Cell-based mucus models are often used coupled with non-cell-based models, since the latter does not take into account active transport mechanism but only the passive diffusion of molecules.

Despite all the mucus models developed so far, yet no standard protocols have been assessed for studying the impact of mucus on drug diffusion. The selection of a model system may be limited by the ease of use, reproducibility, and ability to obtain specific measurements.[65]

2.3.1.　*A mucus model as a fast-screening tool for early drug discovery*

As discussed so far, mucus can have a significant impact over the absorption of potential drug candidates. Using mucin as a model to mimic mucus could be useful to obtain information about the interactional filtering exerted by mucus. Yet, mucin-based solutions are not realistic models of mucus because they fail to model the tridimensional framework, thus the steric barrier of mucus. In pathological contexts (*e.g.*, cystic fibrosis) the barrier activity of mucus is even more pronounced. Despite its important role, so far there are no standard mucus models suitable for high throughput screening (HTS) purposes that can be used in the early drug discovery processes.

Disassembling the complexity of mucus barriers to develop a fast screening tool for early drug discovery – overview

«The work presented in this section was published in the journal Journal of Materials Chemistry B *and it is attached as full article in Appendix B»*

Since mucin-based suspensions are limited models of CF mucus, and because there is a real need of realistic mucus models, the next step of this thesis consisted of engineering a mucus model that simplifies the complexity of CF mucus by mimicking its chemical composition, structural features and viscoelastic properties.

The result is a mucus model composed mainly of mucin and alginate, both key components of CF mucus (for experimental details, the reader is invited to consult Appendix B). The model relies on commercially available products offering interlaboratory reproducibility without requesting specific or complicated experimental set-ups (Figure 2-4, A). The rheological properties were recreated by taking advantage of the internal crosslinking of alginate mediated by calcium ions. Alginate was used since it is an extracellular exopolysaccharide formed by repetition of 1,4-β-D-mannuronate (M) units and α-L-glucuronate (G) residues produced by mucoid *Pseudomonas aeruginosa* (a hallmark of CF infections), in response to environmental conditions. Owing to the presence of carboxyl groups, alginate is able to crosslink in the presence of divalent cations, such as Ca^{2+} ions, at neutral pH, generating a hydrogel whose resultant viscoelastic properties depend on the M/G

ratio and molecular weight. Given this, extensive rheological characterization was conducted to assess storage (G', Pa) and loss components (G'', Pa), of the complex modulus (G^*, Pa), $\tan\delta$, as well as complex viscosity (η^*, Pa s), and further compared to the viscoelastic characterization reported by Yuan *et al.* for CF sputum (Figure 2-4, B-C).[80] Different concentrations of alginate were tested to find the best representative of pathological mucus.

The chemical composition was tuned by including mucin, alginate, sodium chloride and calcium. The viscoelastic properties of the hydrogels were investigated through rheological analysis, and their mesh size was calculated using the Generalized Maxwell Model. CF mucus exhibits gel-like behaviour with a predominant elastic component ($\tan\delta$ <1), which means that the ciliary beating stretches the mucus rather than making it flow, resulting in mucus accumulation in the airways. Like CF mucus, all developed hydrogels exhibit $\tan\delta$ <1, and therefore predominant elastic behaviour. The estimated mesh size varied according to the alginate concentration and the presence or absence of mucin; mesh size decreased with increasing alginate concentration while no significant variations were detected after addition of mucin. The estimated mesh size of the optimized hydrogel (*i.e.*, containing 3 mg/mL alginate) is ~50 nm, that is in good agreement with what reported in the literature for pathological mucus.[39] Stability in terms of thickness and weight variation were investigated in different media over a period of 6h (Figure 2-4, D-E). The optimized hydrogel model proved to be stable since the thickness variation was below 10%. Because in the early drug discovery promising drug candidates are screened according to their ability to diffuse mucosal barriers, the optimized mucus model was coupled to a drug diffusion platform consisting of two compartments separated by a membrane precoated with structured layers of phospholipids. The passive diffusion of three model drugs was then investigated (Figure 2-4, F-G). The mucus model was able to identify compounds known to interact with mucin by reducing their diffusion profiles.

The developed mucus model is easy to produce and it is fully tunable with other components (*e.g.*, albumin, DNA, lipids) in a modular approach, that allows to further increase resemblance with the real pathological mucus. Recently, a more sophisticated version of the herein presented model, called Bac3Gel™, was developed and patented (Patent WO2020128965A1).[81] Bac3Gel™ is a three-dimensional support for bacteria growth that recreates different environmental conditions of bacterial niches. Its internal structure exhibits non-homogeneous viscoelastic properties, with gradients of crosslinking density, oxygen tension, nutrient content and drug penetration in which bacteria can gradually distribute themselves accordingly to the environment that

suits them better (manuscript in preparation). Bac3Gel technology allows the production of mucus-based products, which properties and chemistry match those of the lung, intestinal, vaginal and stomach mucus.
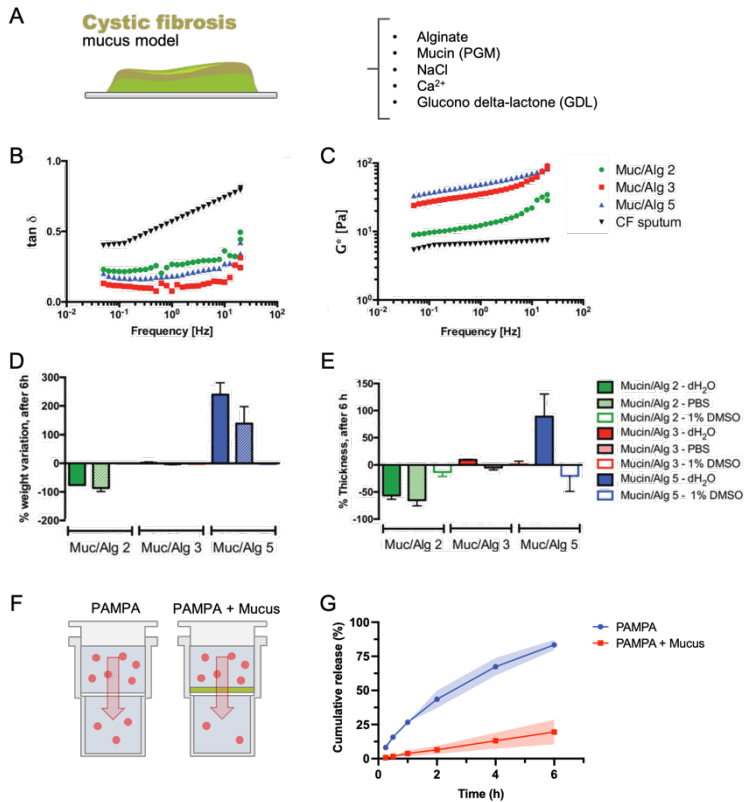
Figure 2-4. The cystic fibrosis (CF) mucus model proposed to specifically model the chemical-physical properties of CF mucus. (A) The chemical composition of the mucus model . Rheological characterization in frequency sweep mode of the hydrogels at different concentrations of alginate, and compared with CF sputum. (B) The variation of loss factor (tand), and (C) complex modulus. Stability of the different hydrogels was assessed in different media, and alterations were measured in terms of weight (D) and thickness (E) variations. The superior stability combined with their ability to model the viscoelastic properties of pathological airway mucus makes Muc/Alg 3 (optimized mucus model, alginate concentration 3 mg/mL) hydrogel the preferred candidate to serve as a platform for drug diffusion studies. (F) experimental setup of the drug diffusion study, and (G) the cumulative release of cephalexin through PAMPA and PAMPA coupled to the optimized mucus model.

MUCUS

3 OVERCOMING THE MUCOSAL BARRIER

3.1. PERMEABILITY PRINCIPLES

Drug absorption is defined as the movement of a drug into the bloodstream. Many factors influence this process, including a drug's physicochemical properties, formulation, and route of administration. Independently of the administration route, drugs must be solubilized and absorbed in order to achieve the therapeutic effects.

The permeability of compounds across cell membranes is a critical characteristic that determines the rate and extent of human absorption and ultimately affects the bioavailability of a drug candidate. This is because if a drug wants to reach the systemic circulation, it needs to cross several semipermeable cell membranes firstly.[82] Drugs may cross cell membranes by passive diffusion, facilitated passive diffusion, active transport, and pinocytosis. The drug's physicochemical properties (*e.g.*, size and lipophilicity), as well as membrane-based efflux mechanisms, can lead to poor permeability. Since passive diffusion is often the primary mechanism of membrane permeation, the permeability is a key property to consider during the drug design process, and particularly vital when dealing with small molecules that have intracellular targets as their efficacy highly depends on their ability to cross the membrane.[83] Compounds with poor permeability are more likely to have poor absorption, distribution, metabolism, excretion (ADME) and pharmacokinetics (PK) properties.

Permeability can be viewed as a property of membrane barriers. As such, it refers to the degree to which a membrane separating two aqueous solutions allows the passage of solute from one side to the other, commonly by passive diffusion as a result of transmembrane concentration gradient of the "permeating" substance.[84] Therefore, given its biological and pharmaceutical importance, approaches for quantitative measurement of membrane permeability have been the topics of research for decades, resulting in sophisticated biomimetic systems coupled with advanced techniques.[85] Cell-free permeation systems are gaining interest in drug discovery and development as tools to obtain a reliable prediction of passive absorption without the

disadvantages associated with cell- or tissue-based permeability profiling.[86] Since Kansy *et al*. introduced it in 1998, parallel artificial membrane permeability assay (PAMPA) become the state-of-the-art method for studying membrane permeability.[87] PAMPA is a classic 96-well plate where each well consists of a donor and an acceptor compartments separated by a filter precoated with phospholipids. At the start of the experiment, the drug solution is introduced into the donor compartment, then, following the permeation period, the concentration of drug is quantified in both compartments. Conceptually similar to PAMPA, other cell-free permeation systems have been developed; these include the phospholipid vesicle-based permeation assay (PVPA) and PermeaPad®, relying on artificial liposome-based and spheroid phospholipids vesicles, respectively.[88,89] Since the artificial membranes have no active transport systems neither metabolizing enzymes, these assays would not be expected to model actively transported molecules. In other words, with cell-free permeation systems only passive diffusion can be measured, which is extremely useful especially in the first stages of drug discovery to classify poorly from highly permeable drug candidates. In the case that active transport has to be taken into account too, then the cell-based methods should necessarily be adopted. Thus, one of the most common cell-based model systems consists of a monolayer of cultured colorectal adenocarcinoma-derived cells, called Caco-2, or alternatively, the Madin-Darby canine kidney (MDCK) cell line.[90–93] However, because cell-based models intrinsically contain endogenous transporters and efflux systems, data interpretation and reproducibility can often be challenging. It is worth mentioning also that cell-based methods are much more time-consuming than non-cell based methods, since the former requires up to 30 days for the preparation of stable cell monolayers, making it poorly suitable for high throughput purposes.[85]

During early drug discovery process, a huge number of potential drug candidates requires a fast validation to assess their capacity to pass the cellular membrane. Among the potential candidates, many are supposed to cross the mucosal membranes in order to reach their biological target. However, mucus, which covers all the wet epithelia of the human body, can represent a strong barrier to tackle even for drugs, especially in those pathological conditions where mucus is overproduced. Despite its important role on drug absorption, nowadays mucus is not considered when screening drug candidates. This happens because there is a lack of *in vitro* standardized protocols that can be applied to assess the effect of mucus over the absorption of drugs. In fact, all the above-mentioned methods, routinely used to measure the permeability of molecules, do not take into account the effect that mucus might induce on permeability.

3.2. AN *IN VITRO* MUCOSAL PLATFORM TO INVESTIGATE DRUG PERMEABILITY

As discussed in the previous section, the current methods adopted to investigate the permeability of drugs neglect to model the mucus layer that the oral, pulmonary or rectal administered drugs face before being absorbed. Overlooking the activity of mucus over the passive diffusion of drugs might underestimate the *in vivo* permeability behaviour of pharmaceuticals, especially in mucus-related disorders.

Cystic fibrosis mucus model to design more efficient drug therapies – overview

«*The work presented in this section was published in the journal* Molecular Pharmaceutics *and it is attached as full article in Appendix C*»

We identified the need for an *in vitro* tool to measure the permeability of drugs and drug candidates that takes into account the barrier effect of mucus, and that is suitable for high throughput screening applications (Figure 3-1, A). As described in the previous section "*A mucus model as a fast-screening tool for early drug discovery*" (Appendix B), we have developed a CF mucus model that reproduces both the composition and the architecture of the pathological mucus.[94] As a proof of concept, the diffusion of three model drugs was tested across the CF mucus model. In the next step, we wanted to expand the applicability of our model in relation also to sputum from CF patients (for experimental details, the reader is invited to consult Appendix C).

At first, focus was set on a number of anti-inflammatory and antibacterial drugs commonly employed in the CF therapy regimes. In order to properly evaluate the performances of the CF mucus model, the data set was expanded up to 45 compounds considering it a reasonable number of drugs to be investigated, with good variability in terms of chemical properties. Indeed, a good chemical heterogeneity was achieved as the investigated data set was well distributed within the chemical space of DrugBank's database of approved drugs (Figure 3-1, B).[95]

Prior to assess the effect of mucus on drug permeability, benchmark permeability values were measured in the absence of mucus across the structured layer of phospholipids of PAMPA (Figure 3-1, C top). Such step was crucial to validate and assess the physicochemical determinants of the permeability behaviour since the experimental set up embedding mucus is different than the standard PAMPA protocol. By computing a correlation matrix between apparent permeability (P_{app}) and several

molecular descriptors, it was found that the topological polar surface area (TPSA) is the physicochemical property that better correlates with drugs' permeability. Hence, evidence was provided about the ability to distinguish high from low permeable compounds according to TPSA. It was found that almost 80% of the tested drugs has the permeability correctly predicted based on the calculated TPSA.

In the next step, the CF mucus model was coupled to PAMPA, recreating *in vitro* a model of CF airway mucosal surface, and the permeability of the investigated dataset was measured. The effect of mucus was measured in terms of variations of permeability (statistical significance set at p-value < 0.05). Three kinds of mucus induced effects were observed (Figure 3-1, C bottom): (*a*) in the presence of mucus 44% of drugs showed a decreased permeability, (*b*) 38% had no statistically significant variation, (*c*) 18% had an increased permeability. According to the observed variation of P_{app}, it is clear that mucus is not just a physical barrier but it behaves as a dynamic filter. No correlation was found between the effect of mucus with any of the molecular descriptors considered. If without mucus, TPSA was found to be the physicochemical property better explaining permeability, in the presence of mucus this correlation is not true anymore; when mucus is present, only 53% of the molecules have the permeability correctly predicted based on the calculated TPSA. These observations demonstrate that the pathologic mucus can strongly influence the passive diffusion of drugs.

Interestingly, it was found that the permeability of a series of molecules sharing some common physicochemical features (*i.e.*, similar MW, total surface area, lipophilicity, polarity, and negative charge) is increased in the presence of mucus. We demonstrate that the reason behind the increased-permeability phenomenon is the formation of drug-calcium salts. The hypothesized scenario relies on an ion pairing effect produced by calcium which is used to crosslink alginate, and thus recreate the viscoelastic properties of pathological mucus. When forming complexes with calcium, the anionic drugs are neutralized; they shift from a negatively charged form to exhibiting no relative charge. The neutralization implies a decrease of polarity in favour of lipophilicity, which could actually favour the diffusion through the artificial phospholipid membrane of PAMPA (Figure 3-1, D). The calcium-induced effect on permeability was confirmed also when CF sputum was used, instead of the CF mucus model, as a rough *ex-vivo* model of CF mucus.
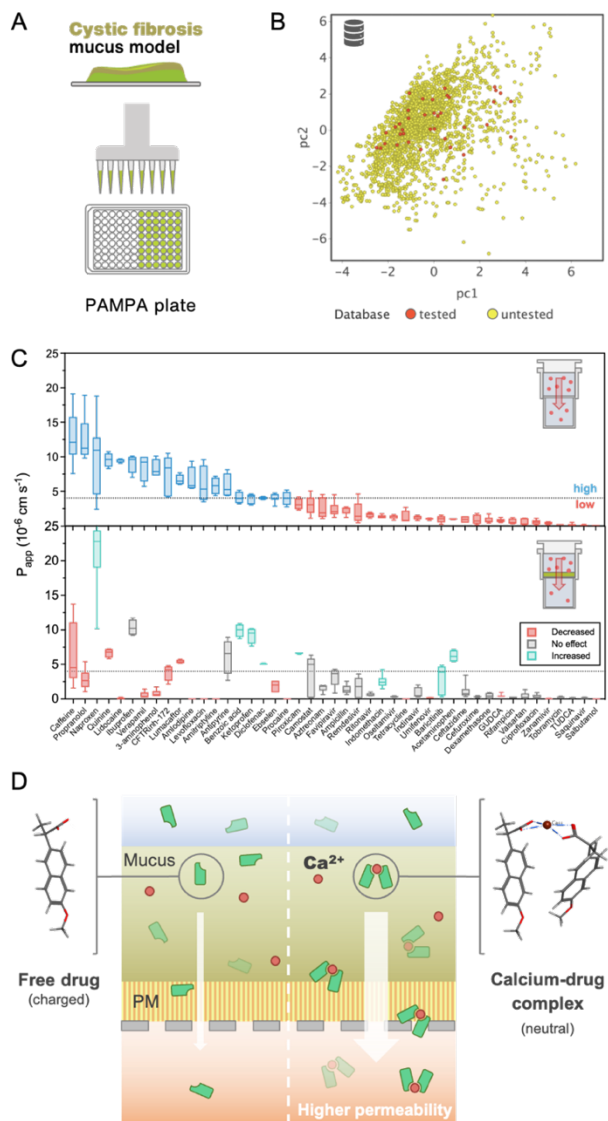
Figure 3-1. The cystic fibrosis (CF) mucus model is a useful tool to assess the effect of mucus on drug's permeability. (A) Mucus is coupled to a 96-well permeable support precoated with structured layers of phospholipids (PAMPA), ensuring a high throughput set up. (B) The drugs tested have been *ad hoc* selected; they are well distributed within the chemical space of the approved drugs, therefore physicochemical variability within the data set is maximized. (C) Mucus is not a mere physical barrier but it behaves as an interactive filter; in nearly one-

half of the investigated compounds, the diffusion was reduced by mucus, while other drugs were not sensitive to the mucus barrier, for some the permeability was even increased. On top and the bottom of B the permeability without mucus and with mucus, respectively. (D) The increased-permeability effect originates from the formation of drug-calcium salts which hydrophilic-lipophilic balance enhances the permeability. This result was confirmed also with CF sputum as a rough *ex vivo* model of CF mucus.

These findings highlight the important, and yet neglected, effect that mucus can exert on passive drug diffusion, thus the importance of *in vitro* mucus models when screening potential drugs, especially in mucus diseases. Since the drug development is characterized by a high rate of failure, the developed mucus platform could help to reduce the number of non-effective drugs that reach the preclinical trials. Moreover, evidence was established indicating that some drugs can form calcium salts which have higher permeabilities than the free drugs. From the formulation point of view, active pharmaceutical ingredients formulated as calcium salts might achieve higher permeabilities, thus better biological activities.

3.2.1. *Application of the mucosal platform in the pipeline development of a PI3Kγ mimetic peptide*

Obstructive airway diseases, including asthma, chronic obstructive pulmonary disease (COPD) and the genetic disorder cystic fibrosis (CF), represent a major health burden worldwide. Cyclic AMP (cAMP) elevating agents, like β2-adrenergic receptor (β2-AR) agonists and phosphodiesterase (PDE) inhibitors, remain a mainstay in the treatment of obstructive respiratory diseases. PI3Kγ is an enzyme that has two functions: on one hand it works as a kinase, amplifying extracellular signals inside the cell and controlling metabolism and proliferation, but on the other hand it works as the "scaffold" of a series of partners controlling the cAMP signaling axis. Therefore, PI3Kγ integrates two different signal transduction pathways: the classical PI3K pathway and the cAMP pathway.[96] Moreover, PI3Kγ binds another kinase called PKA and restricts its function via a negative feedback loop involving type 3 and 4 phosphodiesterase (PDE3/4). The loss of the scaffold function of PI3Kγ lead to decreased PDE3/4 activity and subsequent increased cAMP, which in lungs results in bronchodilation and anti-inflammatory effects.

«The work presented in this section is part of the article "A PI3Kγ mimetic peptide triggers CFTR gating, bronchodilation and reduced inflammation in obstructive airway disease" which was published in the journal Science Translational Medicine»

KITHER biotech developed a cell-permeable peptide containing the PI3Kγ sequence allowing the association with PKA.[97] It was observed that inhalation of the PI3Kγ mimetic peptide (PI3Kγ MP) increases cAMP and, leads to the phosphorylation and opening of the chloride channel CFTR. Therefore, PI3Kγ MP shares three useful pharmacological properties with high potential in obstructive airway diseases: it works as a bronchodilator, as an anti-inflammatory agent and as a CFTR opener.

As part of this thesis, it was proved that PI3Kγ MP binds the recombinant RIIα subunit of its target protein, the PKA, with a measured dissociation constant (K_d) of 7.5 μM. Experimentally the interaction was investigated by fluorescence spectroscopy. In particular a constant concentration of PKA was titrated with increasing concentration of PI3Kγ MP and their steady-state fluorescence spectra was recorded (Figure 3-2, A-B). The kinetics of the binding was investigated too by stopped-flow fluorescence spectroscopy, which results corroborates with the K_d obtained in steady-state mode (data not reported in the main manuscript).

Since PI3Kγ MP represents a potential drug candidate and it is ready to enter phase one clinical trials, it was really important to know how it behaves within a mucus environment. This because patients suffering of obstructive airway diseases have an overproduction of thick and sticky mucus which hamper the absorption of inhaled drugs. And because PI3Kγ MP is supposed to be administered by pulmonary inhalation, it is crucial to understand its permeability behavior. In order to obtain such information, the permeability of PI3Kγ MP was measured using the mucosal platform presented in section 3.2 and results were compared with permeability recorded through cystic fibrosis sputum (Figure 3-2, C). It was found that the diffusion rate of PI3Kγ MP in the presence of the CF mucus model is reduced and the result is comparable to what observed in the presence of CF sputum (manuscript in preparation).

In addition to obtaining useful information about the optimal dose to administer *in vivo*, these results confirm the potential of the mucus platform for drug development purposes.
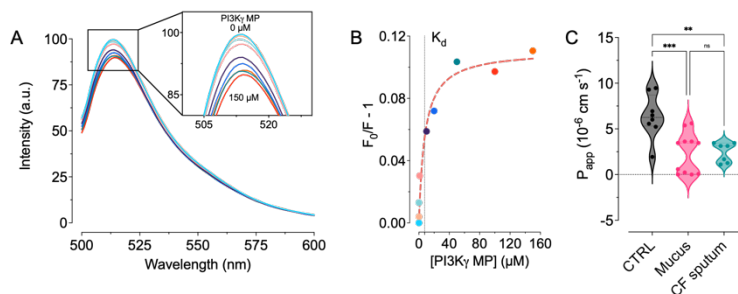
Figure 3-2. (A) Steady-state emission spectra of recombinant RIIα subunit of PKA biolabeled with fluorescein-5-maleimide in the presence of increasing concentrations of PI3Kγ MP (0-150 μM), (B) revealing a dissociation constant for the PI3Kγ MP/PKA interaction of 7.5 μM. (C) Permeability of PI3Kγ MP measured on PAMPA, without (CTRL) and with mucus and cystic fibrosis sputum.

3.2.2.   *Integration of the cystic fibrosis mucus model on PermeaPad*

The cystic fibrosis (CF) mucus model described in section 2.3.1 coupled to permeability platforms, as described in section 3.2, could be a valuable tool in the early drug discovery to assess the effect of mucus on the permeability of promising drug candidates. In addition to PAMPA, another permeability platform, namely PermeaPad® plate, was took into account, in order to expand the applicability of the mucus model (manuscript under preparation).

PermeaPad® is an innovative 96-well plate integrating a lipid bio-mimetic barrier. In contrast to the PAMPA barrier, which is based on a lipid-oil-lipid tri-layer structure, the PermeaPad® barrier is constructed as a sandwich of two cellulose-hydrate membranes enclosing a layer of dry phospholipids between them. In wet conditions the PermeaPad® barrier can be considered as a vesicular phospholipid gel constrained within the two cellulose-based support sheets.[98] Because of this conformation, in contrast to PAMPA, the PermeaPad® barrier may, to some extent, allow paracellular permeation along water channels across the barrier.

The same experimental approach used for PAMPA, was followed to integrate the CF mucus model on PermeaPad® plates. Preliminary results indicate that the PermeaPad® barrier is stronger than that of PAMPA since the permeability of gold standard molecules on PermeaPad®, measured in the same experimental conditions used on PAMPA, is lower (Figure 3-3). This observation deserves further investigation and experiments are still ongoing (manuscript in preparation).
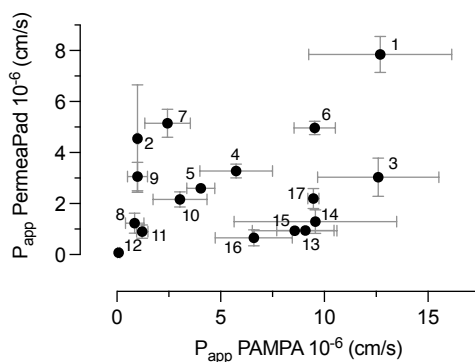
Figure 3-3. The barrier properties of PermeaPad membranes are stronger than that of PAMPA. Comparison of the permeability of 17 compounds measured on PermeaPad and PAMPA plates. 1. Caffeine, 2. Acetaminophen, 3. Propranolol, 4. Antipyrine, 5. Ketoprofen, 6. Quinine, 7. Favipiravir, 8. Dexamethasone, 9. Baricitinib, 10. Camostat, 11. Indinavir, 12. Saquinavir, 13. Ibuprofen, 14. Naproxen, 15. Verapamil, 16. Amlodipine, 17. Lidocaine.

3.3. STRATEGIES TO INCREASE DIFFUSION THROUGH MUCUS

In order to facilitate transport through mucus of drugs with unfavorable permeability profiles (*i.e.*, lipophilic, positively charged, high molecular weight), recent trends are focusing on how to bypass mucus either by modulating its native properties, or by reducing interactions with its components. In contrast, in some cases, it is desired to increase drugs' residence time at the mucosal surface, therefore strategies to enhance retention are pursued as well (Figure 3-4).

3.3.1. *Mucolytics*

Mucolytics, or mucus-thinner agents, reduce mucus viscosity by affecting the tridimensional mesh structure of mucus. Most of the time mucolytics are used before or during airway clearance technique to manage the thick pathological mucus in mucus-related disorders. Generally, they can be divided in three classes based on their mechanism of action: (I) proteases and deoxyribonucleases able to cleave the amino acid sequence of mucin glycoproteins and DNA, respectively (*e.g.*, papain, dornase alfa); (III) disulfide-reducing agents which reduce the sulfide bond (S—S) into sulfhydryl bonds (-SH) (*e.g.*, *N*-acetylcysteine, NAC); (III) detergents affecting the non-covalent linkages of mucus (*e.g.*,

saponins).[21] Mucolytics are considered safe and associated with a low risk of adverse events.

3.3.2.   *Increased mucopenetration*

Particles able to freely diffuse through mucus share some general physicochemical properties: (a) they are relatively small with respect to the mucins mesh, (b) have a neutral surface, and (c) have an overall high hydrophilicity. Substances that can favor one of these physicochemical features, will eventually increase the ability to penetrate mucus. The interest on mucus-penetrating drug delivery systems has exponentially grown. One of the most frequently adopted strategies is to covalently coat the surface of particles with PEG in order to increase hydrophilicity and thus, the adhesiveness for mucus.[35] For example, a 40% reduction of the PEG density on the surface of polystyrene nanoparticles reduced by ~700-fold the diffusiveness of the particles.[99] Recently a number of other polymers were explored as alternatives to PEGylation, including poly(2-alkyl-2-oxazolines), polysarcosine, poly(vinyl alcohol), and zwitterionic polymers (*i.e.*, polybetaines).[100] However, enhanced mucus penetration does not directly lead to increased cell uptake. In fact, the hydrophilic coat produced by PEG limits the diffusion across the lipophilic environment of cellular membranes.

In addition to a favorable hydrophilic/lipophilic balance, also the particles' charge plays a key role upon the interaction with mucus. It has been proved that positively charged molecules strongly bind the negatively charged glycans of mucins.[21] Therefore, for the sake of mucus-penetration, negatively charged particles could have better performances. However, zwitterion molecules (*i.e.*, overall neutral charge) have to be preferred, since they have a better cellular uptake. Shan *et al.*, proved that nanoparticles coated with a zwitterionic surfactant achieved better mucus penetration and cellular uptake compared to PEGylated nanoparticles.[101]

3.3.3.   *Increased mucoadhesion*

In several pathological conditions a prolonged and localized effect of the active ingredient is required at, and within, the mucus layer. One of the strategies pursued to improve performance of pharmaceutical drug formulation consists of adoption of mucoadhesive drug delivery systems. Adhesion of chemicals to mucous membranes or a mucus-covered surface prolongs the contact with the adsorption site, overcoming the challenge of short retention time.[102] Over the years, several mucoadhesive polymers for drug delivery applications have

been investigated, including natural polymers as alginates[103] and chitosan[104], but also synthetic as poly(acrylic acid)[105], and poly vinyl pyrrolidone[106].
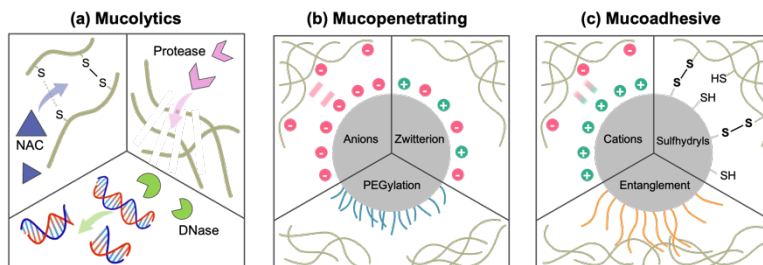
Figure 3-4. Strategies adopted to improve drug diffusion through mucus. (a) Mucolytic agents are used to disrupt the tridimensional structure of mucus. Disulfide-reducing agents as *N*-acetylcysteine (NAC), protease or DNase are used to thin mucus by breaking the structure of mucin and DNA within mucus. (b) Mucopenetrating agents are used to facilitate diffusion through mucus. Negatively charged particles avoid contact with mucins by electrostatic repulsion, while zwitterion particles, in addition of being inert to mucins, are also able to penetrate the cellular membrane. PEGylation is used to increase surface hydrophilicity. (c) Mucoadhesive strategies are used to increase the residence time at mucosal level. Positively charged particles can bind mucins by electrostatic interactions. Surface thiolation can favor the formation of disulfide bonds with the cysteine rich domains of mucins, while functionalization with mucoadhesive polymers is exploited to attach the mucin fibers, thus to prolong retention.

3.4.   MUCOSOMES AS DRUG DELIVERY PLATFORM

Strategies addressing mucus-related diseases have taken central stage, especially after the blow of COVID-19 pandemic. There is the need to reinvent the way in which current drugs are delivered, focusing on different mechanisms of action and improving the efficiency of delivery systems to make them more selective for the specific body district and the type of targeted environment. Nanoformulations with mucoadhesive properties represent an attractive option for targeted drug delivery on mucosal surfaces.

«The work presented in this section was submitted to the journal Advanced Healthcare Materials *and it is attached as full manuscript in Appendix D. At the time of writing this thesis (March 2022), the manuscript is under peer-reviewing»*

We identified the need to design drug delivery systems specifically targeting mucus and able to carry active pharmaceutical ingredients, avoiding though successive functionalization steps. Inspired by the unique properties of mucus, which is our first-line of defense, a cutting-edge technology that exploits the mucus' natural mucoadhesive and binding capacity, was developed. Here we present a novel class of intrinsically mucoadhesive and glycosylated mucin-based nanoparticles that have been named *mucosomes*.

Similarly to other proteins, mucin is also described to form nanostructures through a glycerol-mediated condensation.[107] Building up from the state-of-the-art knowledge, it was engineered a lean synthetic method where the synthesis of nanoparticles, the functionalization with glycans, and the loading with the active compound, occur in one single reaction pot (Figure 3-5, A).[108] For experimental details, the reader is invited to consult Appendix D. The agile synthesis overcomes the limits (*i.e.*, in terms of time and costs), of classic procedures where successive steps are usually required for surface functionalization. It is worth mentioning that mucosomes are synthesized starting from commercially available porcine gastric mucin. The advantages of using the commercial protein are multiple in terms of scalability, availability and production costs.

Evidence of mucosomes' morphological characteristics regarding the size, shape, mucoadhesive properties, and surface glycosylation was produced. In particular, it is shown that mucosomes are protein nanoparticles of ~200 nm diameter, of spherical shape, and constituted largely of C, O, N and S. Mucosomes' mucoadhesive properties were demonstrated *in vitro* testing their ability to attach and stick to a mucin layer (Figure 3-5, B), and also investigating their ability to diffuse through the *in vitro* cystic fibrosis (CF) mucus model, presented in 2.3.1 above. The attached *O-* and *N*-linked glycans on mucin are important binding sites since engage bacterial and viral glycoproteins (*e.g.*, lectins). It was proved that after the desolvation of mucin into mucosomes, the glycosylation is preserved and sugars maintain their functionality. Tests on HeLa cells showed that mucosomes can reach the intracellular compartment without toxic effects for cells. Comparison with a known inflammatory agent (*i.e.*, LPS) suggested low immunogenicity of mucosomes, as a low production of cytokines (*i.e.*, IL-1β, IL-6, TNFα) was induced on macrophages. Addition of mucosomes to blood samples did not alter the coagulation cascade, implying that the intravenous

administration could be pursued as a possible administration route. It could be argued that commercial mucins are of scarce quality compared to laboratory purified protein since it contains impurities resultant from the extraction procedure. This might be true, however encouraging results were obtained from the *in vivo* toxicity tests since, following intravenous administration of mucosomes into mice, the animals remained healthy during the follow-up period (*i.e.*, 14 days), without significant weight variations or any other relevant clinical sign. Interestingly, the main distribution sites were the lungs, suggesting that mucosomes may have a natural trophism for mucosal districts, even when intravenously administered. Within the main distribution organs, a gradual decrease of mucosomes' concentration was observed, implying absence of accumulation, phenomenon that might induce organ-specific toxicity. Moreover, mucosomes showed to have an outstanding ability to encapsulate compounds spanning a wide range of physicochemical properties (Figure 3-5, B), including small molecules (*i.e.*, fluorescein isothiocyanate, cyanine 5.5, ceftazidime, dexamethasone, oseltamivir, MW < 1 kDa), oligonucleotide (*i.e.*, peptide nucleic acid, PNA, MW < 10 kDa), and even proteins (*i.e.*, albumin, MW < 100 kDa). It is also shown that mucosomes withstand freeze drying process, allowing to obtain stable formulations in time. Given their mucoadhesive properties, tests have been conducted in order to investigate resistance to nebulization through a spray pump device, which revealed that the nanoparticles maintain their shape integrity.

Overall, these results suggest that mucosomes are a biocompatible nanosystem, able to encapsulate drugs, intrinsically glycosylated and mucoadhesive. Given these unique features, mucosomes represent an attractive nanocarrier for mucosal delivery, in particular in the context of respiratory diseases. The administration of therapeutics aimed at managing respiratory diseases aids from the pulmonary delivery route because of the large surface area which ensure rapid adsorption into systemic circulation and for achieve quick local effect at the target area.[109]

The mucosomes technology steamed the rising of a new project called NanoMuG.[110] The NanoMuG project was awarded with two grants under the *Switch2Product Innovation Challenge* (S2P 2020) run by PoliHub (World Top 5 University Business Incubator), the Technology Transfer Office at Politecnico di Milano, and Officine Innovazione at Deloitte. NanoMuG is currently a living project developed by a multidisciplinary team and supported by three technology transfer offices (University of Turin, Politecnico di Milano, University of Pavia).
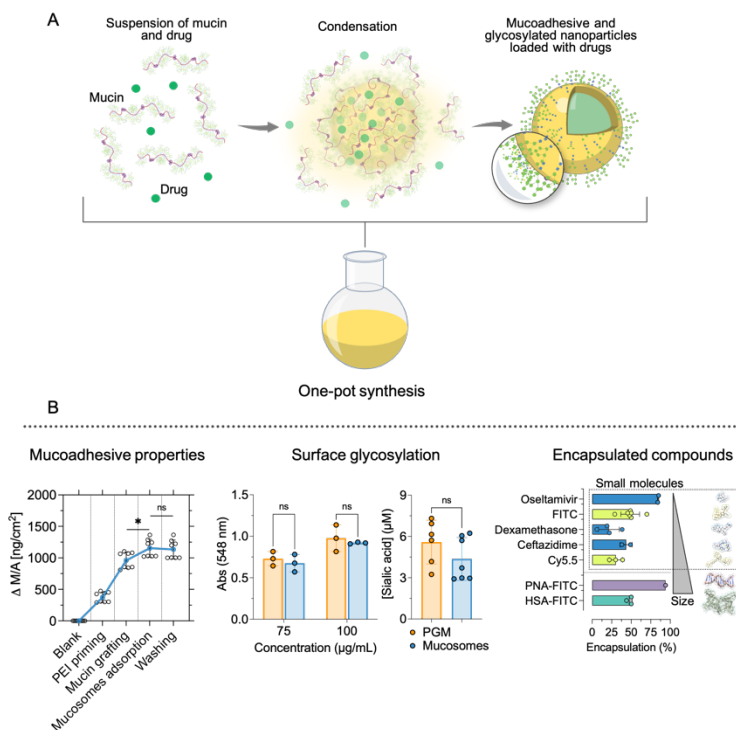
Figure 3-5. Summary of the distinctive features of mucosomes nanoparticles. (A) Schematic representation of the one-pot synthesis. A suspension of mucin is condensed with organic solvent and crosslinked with glutaraldehyde into mucin nanoparticles. In the first step of the reaction, pharmaceuticals can be suspended within the reaction pot, obtaining loaded mucosomes. (B) A brief overview of experimental results regarding the mucoadhesive properties, surface glycosylation, and encapsulated compounds. The sensogram shows the output of QCM analysis which depicts the ability of mucosomes to attach to a layer of mucin. Using the period-acid Schiff staining it was possible to appreciate that the amount of glycans present on mucosomes is comparable to that of the extended protein. Similarly, the concentration of sialic acid is similar between mucosomes and mucin. Mucosomes can be loaded with compounds spanning a wide range of molecular weights and physicochemical properties.

4 MUCINS IN CANCER

Up to this point it was discussed only about the implication of mucins and mucus in obstructive airway diseases such as cystic fibrosis, chronic obstructive pulmonary disease and asthma. However, in addition to these well documented disorders, in the last years great attention was addressed to the implication of mucins in cancer.[111–114] In physiological conditions, epithelial cells express mucins in response to particularly harsh environments, such as the low pH in the stomach, the exposure to air in the lungs and on eyes, and the tough environment of the intestine. It has been proposed that overexpression of mucins in cancer cells could have a similar reason, namely, favoring growth and proliferation in inhospitable conditions. Mucin can provide a tumor-friendly environment by reducing hypoxia, acidic conditions, and avoiding the immune and chemotherapy response.[114]

Large amounts of transmembrane mucins can be expressed by mucosal epithelial cancer, or adenocarcinomas, associated with poor survival rate. MUC1 is so deeply intertwined with cancer development that it has been even proposed as an oncogene implicated in invasion, angiogenesis and metastasis.[115] In pancreatic cancer, which is the third most deathly type of cancer globally, mucins have been proposed as a promising biomarker for diagnosis, prognosis and therapy.[116]

The advantages tumor cells acquire by coating themselves with mucins is multifaced, and is reflected on the control of the local microenvironment. The aberrant expression of transmembrane mucins enables cancer cells to mimic the normal epithelial cells and mask tumor-specific antigens. Tumor cells expressing mucins are able to elude the immune surveillance. Moreover, thanks to sialyl-Tn (sTn) antigen, mucins are able to engage a wide number of receptors present on macrophages, dendritic cells, and natural kill cells, thus competing with their natural ligands and determining an overall immunosuppression effect.[113,117] Because of the high binding capacity characteristic of mucins, malignant cells expressing mucins are able to capture growth factors and cytokines, which might contribute to tumoral proliferation. Exploiting the same adhesive properties of mucins, tumor cells engage leukocytes and platelets in the tumor microenvironment to facilitate their spreading at distant sites and promoting metastasis. Dissemination is favored also by overexpression of sialic acid on the membrane surface which

increases electrostatic repulsion between adjacent cells facilitating the entrance of the tumor cell into the bloodstream.[118,119]

Given the important role played by mucins in cancer proliferation and metastasis, great efforts are being made to develop therapies addressing mucins. Several approaches including antibody-drug conjugate targeting cell surface, vaccine based on mucin specific epitopes, and MUC1-specific chimeric antigen receptor T-Cell (CAR-T cell)-based therapeutics have been already proposed as successful strategies to tackle cancer.[113]
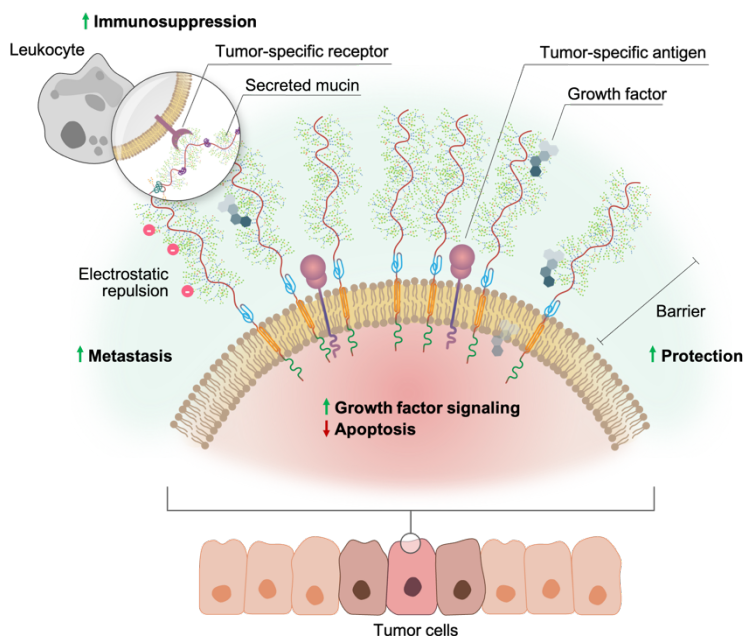
Figure 4-1. Influence of the overexpression of mucins on the surface of cells.

4.1. FLUOROMETRIC DETECTION OF MUCIN

Mucins overexpression and aberrant glycosylation in several malignancies facilitates oncogenesis from initial to metastatic events.[113] In pancreatic cancer mucins have been proposed as a diagnostic and prognostic biomarker. In cancer, more than other diseases, the early diagnosis is a key factor for the outcomes and effective treatments. Nowadays, among the most interesting diagnostic methods is the fluorescence detection mediated by fluorescence probes. The

fluorescence approach is attractive because of the extremally high sensitivity and relative simplicity. Amid relevant biological fluorescent probes, squaraine dyes (SQ) are characterized by high absorption coefficients and emission in the visible up to the NIR region and, for this reason, they have been investigated for a plethora of purposes. In organic solvents SQ are characterized by sharp absorption and high fluorescence intensities. However, their main drawback resides in formation of insoluble aggregates which fluorescence is almost completely quenched. Yet, it is known that SQ aggregates can turn-on their fluorescence upon interaction with specific proteins (Figure 4-2, B). In our previous work we have observed that the fluorescence of four in-house synthesized squaraines (Figure 4-2, A) can be turned on by albumin, empowering SQ as potential probes suitable to detect albumin.[120]

Squaraine dyes as fluorescent turn-on sensors for the detection of porcine gastric mucin: a spectroscopic and kinetic study - overview

«The work presented in this section was published in the journal Journal of Photochemistry and Photobiology B: Biology *and it is attached as full article in Appendix E»*

The aim pursued in this work is to identify and develop a robust, convenient and sensitive fluorescent probe based on SQ to detect secreted mucins at serum level. Such an ideal probe would allow to develop a fast screening-test able to detect and discriminate healthy from people at risk of pancreatic cancer.

Following the method developed to study the response to albumin, here, we studied the interaction between the same four in-house synthesized SQ with porcine gastric mucin (for experimental details, the reader is invited to consult Appendix E). It is shown that similarly to what observed with albumin, PGM too is able to turn-on the fluorescence of squaraines, resulting in increases of fluorescence intensity up to 45-fold (Figure 4-2, C). It was observed a structure activity relationship between squaraines' structure and the turn-on response, namely the higher the squaraines' lipophilicity the stronger the increase of fluorescence. By absorption spectroscopy it was observed that increasing the concentration of mucin results in an increase of the band corresponding to the monomeric form of the SQ (Figure 4-2, D). Taken together these results, it was hypothesized that the driving force behind the interaction between SQ aggregates and mucin might be ruled by hydrophobic interactions; namely the lipophilic domains of mucin could aid the dissolution of the aggregate, resulting in an increase of fluorescence and quantum yield. This hypothesis is supported by the

measured thermodynamic parameters (*i.e.*, $\Delta H°$, $\Delta S°$) which indicated hydrophobic forces as the major player in the interaction of SQ with the protein. Moreover, in our last publication we further investigated this hypothesis by studying the turn-on effect in response to different proteins.[121] It was found that the increase of fluorescence is, for some extent, proportional to protein's surface hydrophobicity (expressed as molecular lipophilicity potential). Yet, this is true only for squaraines with short alkyl chains.

Next, affinity constants (*i.e.*, K_A and K_D) toward mucin have been calculated. In addition, in order to investigate the application of SQ as probes to detect mucin, tests have been performed in deproteinized serum samples spiked with known concentrations of mucin. Here, good protein recoveries have been achieved (*i.e.*, 94.9 – 116.2%).

The obtained results appoint SQ as potential biosensors able to sense mucin. The fluorometric detection could represent a simple, robust, and cost-efficient method to identify mucin, thus paving the way for numerous biological applications (*e.g.*, staining, diagnostics). Further studies should be conducted to decipher the turn-on mechanism in order to develop a selective SQ probe responsive only to mucins.
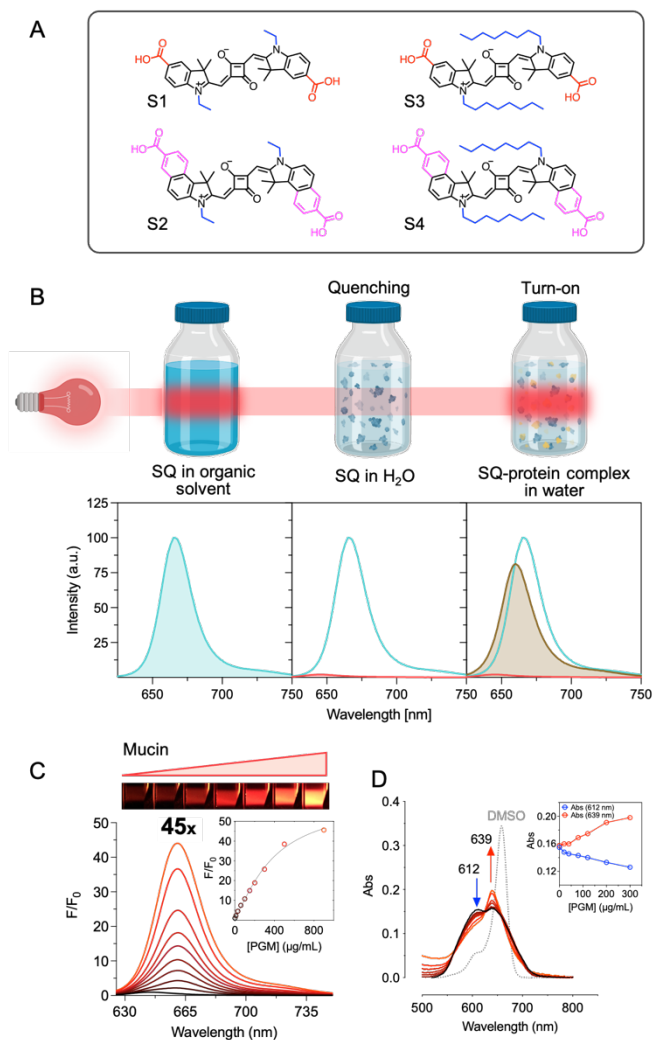
Figure 4-2. Mucin can turn-on the fluorescence of squaraines (SQ). (A) The molecular structures of the 4 squaraines investigated. (B) The fluorescence spectra of SQ in different solvents. In organic solvents SQ have sharp and intense fluorescence; in water they form insoluble aggregates losing their fluorescence properties, while interaction with specific proteins can restore their fluorescence. (C) Increase of fluorescence induced by different concentrations of mucin. (D) Absorption spectrum of SQ in the presence of mucin. Mucin might act as a desolvating agent favoring the solubilization of SQ aggregates.

5 CONCLUSIONS AND FUTURE OUTLOOK

In this thesis, multiple approaches were adopted to analyze questions regarding to the binding, selective permeability and pathological implications of mucins and mucus.

In the paper presented in Appendix A, focus was set on binding of drugs of interest in cystic fibrosis (CF) to porcine gastric mucin (PGM). Spectroscopic methods (*i.e.*, UV-Vis, steady-state fluorescence) were used to decipher the binding mechanism. It is shown that some drugs are able to interact with mucin by moderate binding that is mainly governed by hydrophobic interactions. No interaction was observed with the aminoglycoside antibiotic tobramycin, though there is evidence of strong binding of this polycationic drug to mucin. This result highlights the limitation of fluorescence studies where the binding on the protein can be monitored only in the proximity of fluorescent amino acids (*i.e.*, tryptophan, phenylalanine, tyrosine, histidine). In the case of a complex protein such as mucin, fluorescence-based studies can underestimate the real extent of interactions that mucin can undertake; binding in proximity of non-fluorescent amino acids, as well as on the carbohydrate chains, which are non-fluorescent, might not be detected. Moreover, adoption of mucin as a model to mimic mucus might be a too simplistic model as mucin fails to recreate the complex architecture of mucus and it only partially model its chemical composition.

Because of the aforementioned limitations, more realistic *in vitro* models are necessary when aiming to elucidate the binding of drugs to mucus. For this reason, in the paper presented in Appendix B it is shown how an *in vitro* CF mucus model that recapitulates both the composition and the rheological properties of CF mucus, was developed using a modular approach. We propose the model as an *in vitro* tool for early drug discovery, representing a step forward on modeling the mucus layer that is often neglected when assessing drug permeability. The mucus hydrogel is easy to produce and easy to use, and it can be easily tied to drug diffusion platforms for high-throughput analysis. Following this concept, the CF mucus model was coupled to the state-of-the-art drug diffusion platform (parallel artificial membrane permeability assay, PAMPA), consisting of structured layers of phospholipids, recreating *in vitro* the mucosal surface. As it was discussed in Appendix C, such a

mucosal platform can be used as a drug screening tool for a large dataset of molecules. It was found that diffusion of drugs is affected to different extents, either being slowed down or not being affected at all. Results suggest that the effect of mucus on drugs' permeability is not correlated with any molecular property (*i.e.*, charge, lipophilicity, size, polarity), meaning that its effect depends on a multiplicity of chemical-physical properties rather than a single chemical descriptor. These findings represent an additional proof of the need for *in vitro* mucus models to be used for drug screening. In particular, in mucus-related disorders, administration of standard therapeutic regimes could result in treatment failure because of drugs' inability to overcome the mucus barrier. Treatment with poorly permeable drugs could be avoided if a mucus-containing screening platform (as the one herein described) would be available to experimentally screen and quickly determine the most effective drug *ex-ante* starting the therapy. Furthermore, while only pathological respiratory mucus was discussed so far in this dissertation, similar considerations about mucus binding and permeability apply to other mucus from different districts of the human body (*i.e.*, gastric, intestinal, cervical). In addition, a modified version of the herein present CF mucus model was developed as an *in vitro* 3D platform to assess antimicrobial susceptibility (data not shown, manuscript in preparation). In particular, it was found that bacteria cultured within the modified CF mucus model exhibited many pathophysiological features, as these not only were able to colonize the mucus model, but also generate microcolony aggregates characteristic of CF mucus. The interplay of all these features resulted in similar barrier to antimicrobial treatment and, in some cases, was able to reproduce the mismatch between planktonically cultured bacteria and human patients.

One important output highlighted in the paper reported in Appendix C is the ability of calcium ions to increase the permeability of several negatively charged drugs by formation of drug-calcium complexes. The same behavior was observed also when CF sputum was used instead of the CF mucus model, confirming the calcium-induced effect. From the pharmaceutical point of view, formulation as calcium salts should be considered when developing new drugs supposed to be administered by oral or inhalation routes. Moreover, calcium formulations would offer new possibilities also for the repositioning of current pharmaceuticals that might suffer of poor permeability. On the contrary, thanks to these findings it was possible to point out one limitation of the developed CF mucus model, namely the high concentration of contained calcium (~10x higher than CF sputum). Such high concentration is necessary to crosslink alginate and recreate the gel-like properties of CF mucus, that otherwise would not be possible to reproduce through the only use of mucin. In fact, commercial mucins fail to form hydrogels at high

concentrations and low pH. The clear next steps for this project centers around improving the similarity to "real" mucus, thus one of the first identified steps is the reduction of calcium concentrations. For this purpose, adoption of lab-purified mucins is supposed to result in a double advantage: on one hand, the viscoelastic properties of CF mucus could be naturally obtained because lab-purified mucins are able to form gels, hence they are qualitatively superior to commercial mucins; on the other hand, calcium concentration could be reduced, as relying on gel-forming properties of alginate would be less fundamental to recreate the viscoelastic properties of mucus.

Because drug delivery is equally important as drug permeation of mucosal surfaces, in the manuscript reported in Appendix D a novel intrinsically mucoadhesive glycosylated mucin nanoparticles as multi drug delivery platform is presented and discussed. Bioinspired from mucus, the nanoparticles have been called *mucosomes*. Evidence about the morphological characterization, *in vitro* and *in vivo* safety, as well as the ability to be loaded with different compounds support the hypothesis of mucosomes as promising drug carrier. Following this proof of concept, the possibility to deliver active ingredients using mucosomes may offer several advantages over conventional systems in terms of increased residence time and targeted delivery. The mucoadhesive property would ensure permanence of the encapsulated drug within the mucus layer, while the presence of surface glycans would mediate the engagement of glycoproteins expressed by pathogens such as bacteria and viruses. Drugs would be released more closely to pathogens, limiting the adverse effects and maximizing the effectiveness.

Of utmost interest in biomedicine is the development of selective fluorescent probes to detect disease-associated biomarkers in biological fluids. This topic was addressed in the paper reported in Appendix E. Here the application of squaraine dyes (SQ) as fluorescent turn-on probes to detect mucin was investigated. The development of specific and selective probes targeting secreted mucins could pave the way for rapid and effective approach to screen people at risk of cancer. Although the investigated SQ are responsive to mucin, they still are not sufficiently selective for mucin since the turn-on response induced by albumin, which is the most abundant protein at serum level, is higher compared to mucin (data not shown).[120] Given the structural complexity of mucins it would be challenging but scientifically rewarding to develop a squaraine that binds mucin but not all the other interfering serum proteins. For this purpose, an accurate definition of the structure-response relationship of a dataset of fluorescent dyes could help to identify the physicochemical characteristics that favours the response toward mucin. Subsequently, *in vitro* testing of libraries designed on

rational basis could help determine new and better fluorescent turn-on probes.

"What do you think it takes to be a good scientist?"

« I think what is really, really important when I look back at my own career, and by the early days when I was a kid, or when I was a student, I think it was curiosity. *Being eager to learn and to get inspiration from Mother Nature, or from all the questions you know you can think of, or the beauty around you (…). I think the most beautiful thing of being a scientist is there to have a family, a family of colleagues all around the world, being it young and old, junior and senior (…). Everywhere we met scientists that share a common passion, a passion to learn and to discover. And I think this is one of the most beautiful things of being a scientist (…).*

"What makes a good scientist?" As I mentioned already, it's difficult to say, but definitely the sense of wanting to know, to learn and to go a bit into unknown territory. Because what you want to do as a scientist is not only thinking about things we know already, but in particular about things, the questions, what we don't know. And it is a bit daring. It needs also to be a bit brave because you go in an unknown territory and often, I tell you, you hit your head because you don't know what you can expect. You can be in a completely dead alley. The beauty of Science is that are always these fantastic questions and sometimes these great discoveries are insights and that keeps us going (…).

I think there is a few other things. One is of course creativity. *Try to think a little bit out of the box. Try to think about what are important problems or important questions. And I think also two other things which are important, and that is* integrity *and* ethical aspects. *I think it's really important that we have high standards. You know, the scientific process that you come up with good data. Of course our explanations sometimes might fail, because the new insights a year later might we have to change our mind about certain theories and explanations. But the data should be solid and the Science we do should have high ethical standards with respect to what we do, how we are going to use it and present it. Integrity and high ethical standards are crucial for scientists. Why? Because I want to emphasize that all scientists are role models. Role models for others in society and this is an important, and even more important than ever I would say in current society, where we keep high standards and we act as role models, knowledge, insight and the truth, as far as we can tell from scientific insights and data (…)*

People say always, "Oh the Science is beautiful, you make a discovery or whatever". But you don't make discoveries too many. Of course there are these beautiful moments, these real "Eureka"

moments, but you don't have them every day. The reality is that you work hard, and you have to show perseverance. *I tell always people, "if you want to become a scientist, you have to stand failures and disappointments", because often you are in a dead alley, or you are simply not smart enough (…). There are so difficult questions, and difficult problems, and of course you might go to the left and the answer might be to the right, and we have seen this so many times. But don't get distracted by that! Take inspiration and a positive attitude from the small successes you get. These steps bring Science forward, and then sometimes, you have a breakthrough.[1]»*

Ben Feringa,
Nobel prize in Chemistry 2016

---

[1] Speech excerpt from Youtube video "Nobel prize laureate Ben Feringa talks with students. United by Science event"

6 REFERENCES

(1)   Brown, R. B.; Hollingsworth, M. A. Mucin Family of Glycoproteins. *Encycl. Biol. Chem. Second Ed.* **2013**, *2*, 200–204. https://doi.org/10.1016/B978-0-12-378630-2.00670-8.

(2)   Ma, J.; Rubin, B. K.; Voynow, J. A. Mucins, Mucus, and Goblet Cells. *Chest* **2018**, *154* (1), 169–176. https://doi.org/10.1016/j.chest.2017.11.008.

(3)   Hansson, G. C. Mucus and Mucins in Diseases of the Intestinal and Respiratory Tracts. *J. Intern. Med.* **2019**, *285*, 479–490.

(4)   Petrou, G.; Crouzier, T. Mucins as Multifunctional Building Blocks of Biomaterials. *Biomater. Sci.* **2018**, *6* (9), 2282–2297. https://doi.org/10.1039/c8bm00471d.

(5)   Van Putten, J. P. M.; Strijbis, K. Transmembrane Mucins: Signaling Receptors at the Intersection of Inflammation and Cancer. *J. Innate Immun.* **2017**, *9* (3), 281–299. https://doi.org/10.1159/000453594.

(6)   Hansson, G. C. Mucins and the Microbiome. *Annu. Rev. Biochem.* **2020**, *89*, 769–793. https://doi.org/10.1146/annurev-biochem-011520-105053.

(7)   Demouveaux, B.; Gouyer, V.; Gottrand, F.; Narita, T.; Desseyn, J.-L. Gel-Forming Mucin Interactome Drives Mucus Viscoelasticity. *Adv. Colloid Interface Sci.* **2018**, *252*, 69–82. https://doi.org/10.1016/j.cis.2017.12.005.

(8)   Ferez-Vilar, J.; Hill, R. L. The Structure and Assembly of Secreted Mucins. *J. Biol. Chem.* **1999**, *274* (45), 31751–31754. https://doi.org/10.1074/jbc.274.45.31751.

(9)   Bansil, R.; Turner, B. S. Mucin Structure, Aggregation, Physiological Functions and Biomedical Applications. *Curr. Opin. Colloid Interface Sci.* **2006**, *11*, 164–170. https://doi.org/10.1016/j.cocis.2005.11.001.

(10)   Bergstrom, K. S. B.; Xia, L. Mucin-Type O-Glycans and Their Roles in Intestinal Homeostasis. *Glycobiology* **2013**, *23* (9), 1026–1037. https://doi.org/10.1093/glycob/cwt045.

(11)   Jin, C.; Kenny, D. T.; Skoog, E. C.; Padra, M.; Adamczyk, B.; Vitizeva, V.; Thorell, A.; Venkatakrishnan, V.; Lindén, S. K.; Karlsson, N. G. Structural Diversity of Human Gastric Mucin Glycans. *Mol. Cell. Proteomics* **2017**, *16* (5), 743–758. https://doi.org/10.1074/mcp.M117.067983.

(12)   Lee, H. J.; Zheng, J. J. PDZ Domains and Their Binding Partners: Structure, Specificity, and Modification. *Cell Commun. Signal.* **2010**, *8*, 1–18. https://doi.org/10.1186/1478-811X-8-8.

(13)   Pelaseyed, T.; Zäch, M.; Petersson, Å. C.; Svensson, F.;

Johansson, D. G. A.; Hansson, G. C. Unfolding Dynamics of the Mucin SEA Domain Probed by Force Spectroscopy Suggest That It Acts as a Cell-Protective Device. *FEBS J.* **2013**, *280* (6), 1491–1501. https://doi.org/10.1111/febs.12144.

(14)   Macao, B.; Johansson, D. G. A.; Hansson, G. C.; Härd, T. Autoproteolysis Coupled to Protein Folding in the SEA Domain of the Membrane-Bound MUC1 Mucin. *Nat. Struct. Mol. Biol.* **2006**, *13* (1), 71–76. https://doi.org/10.1038/nsmb1035.

(15)   Javitt, G.; Khmelnitsky, L.; Albert, L.; Bigman, L. S.; Elad, N.; Morgenstern, D.; Ilani, T.; Levy, Y.; Diskin, R.; Fass, D. Assembly Mechanism of Mucin and von Willebrand Factor Polymers. *Cell* **2020**, *183* (3), 717-729.e16. https://doi.org/10.1016/j.cell.2020.09.021.

(16)   McKinnon, T. A. J.; Goode, E. C.; Birdsey, G. M.; Nowak, A. A.; Chan, A. C. K.; Lane, D. A.; Laffan, M. A. Specific N-Linked Glycosylation Sites Modulate Synthesis and Secretion of von Willebrand Factor. *Blood* **2010**, *116* (4), 640–648. https://doi.org/10.1182/blood-2010-02-267450.

(17)   Baos, S. C.; Phillips, D. B.; Wildling, L.; McMaster, T. J.; Berry, M. Distribution of Sialic Acids on Mucins and Gels: A Defense Mechanism. *Biophys. J.* **2012**, *102* (1), 176–184. https://doi.org/https://doi.org/10.1016/j.bpj.2011.08.058.

(18)   Kim, J.; Lee, B.; Lee, J.; Ji, M.; Park, C. S.; Lee, J.; Kang, M.; Kim, J.; Jin, M.; Kim, H. H. N-Glycan Modifications with Negative Charge in a Natural Polymer Mucin from Bovine Submaxillary Glands, and Their Structural Role. *Polymers* . 2021. https://doi.org/10.3390/polym13010103.

(19)   Falavigna, M.; Stein, P. C.; Flaten, G. E.; di Cagno, M. P. Impact of Mucin on Drug Diffusion: Development of a Straightforward In Vitro Method for the Determination of Drug Diffusivity in the Presence of Mucin. *Pharmaceutics* . 2020. https://doi.org/10.3390/pharmaceutics12020168.

(20)   Xu, Q.; Ensign, L. M.; Boylan, N. J.; Schön, A.; Gong, X.; Yang, J.-C.; Lamb, N. W.; Cai, S.; Yu, T.; Freire, E.; Hanes, J. Impact of Surface Polyethylene Glycol (PEG) Density on Biodegradable Nanoparticle Transport in Mucus Ex Vivo and Distribution in Vivo. *ACS Nano* **2015**, *9* (9), 9217–9227. https://doi.org/10.1021/acsnano.5b03876.

(21)   Huang, J. X.; Blaskovich, M. A. T.; Pelingon, R.; Ramu, S.; Kavanagh, A.; Elliott, A. G.; Butler, M. S.; Montgomery, A. B.; Cooper, M. A. Mucin Binding Reduces Colistin Antimicrobial Activity. *Antimicrob. Agents Chemother.* **2015**, *59* (10), 5925–5931. https://doi.org/10.1128/AAC.00808-15.

(22)   Pontremoli, C.; Barbero, N.; Viscardi, G.; Visentin, S. Mucin-Drugs Interaction: The Case of Theophylline, Prednisolone and Cephalexin. *Bioorganic Med. Chem.* **2015**, *23* (20), 6581–6586. https://doi.org/10.1016/j.bmc.2015.09.021.

(23)   Paone, P.; Cani, P. D. Mucus Barrier, Mucins and Gut Microbiota: The Expected Slimy Partners? *Gut* **2020**, *69* (12), 2232–2243. https://doi.org/10.1136/gutjnl-2020-322260.

(24)   Meldrum, O. W.; Chotirmall, S. H. Mucus, Microbiomes and

Pulmonary Disease. *Biomedicines* **2021**, *9* (6), 675. https://doi.org/10.3390/biomedicines9060675.

(25) Leal, J.; Smyth, H. D. C.; Ghosh, D. Physicochemical Properties of Mucus and Their Impact on Transmucosal Drug Delivery. *Int. J. Pharm.* **2017**, *532* (1), 555–572. https://doi.org/10.1016/j.ijpharm.2017.09.018.

(26) McGuckin, M. A.; Lindén, S. K.; Sutton, P.; Florin, T. H. Mucin Dynamics and Enteric Pathogens. *Nat. Rev. Microbiol.* **2011**, *9* (4), 265–278. https://doi.org/10.1038/nrmicro2538.

(27) Miyake, K.; Tanaka, T.; McNeil, P. L. Disruption-Induced Mucus Secretion: Repair and Protection. *PLoS Biol.* **2006**, *4* (9), 1525–1531. https://doi.org/10.1371/journal.pbio.0040276.

(28) Davis, C. W.; Dickey, B. F. Regulated Airway Goblet Cell Mucin Secretion. *Annu. Rev. Physiol.* **2008**, *70*, 487–512. https://doi.org/10.1146/annurev.physiol.70.113006.100638.

(29) Cone, R. A. *Mucosal Immunology: Chapter 4 – Mucus*, 3rd ed.; 2005.

(30) Atuma, C.; Strugala, V.; Allen, A.; Holm, L. The Adherent Gastrointestinal Mucus Gel Layer: Thickness and Physical State in Vivo. *Am. J. Physiol. Liver Physiol.* **2001**, *280* (5), G922–G929. https://doi.org/10.1152/ajpgi.2001.280.5.G922.

(31) Bansil, R.; Turner, B. S. The Biology of Mucus: Composition, Synthesis and Organization. *Adv. Drug Deliv. Rev.* **2017**, *124*, 3–15. https://doi.org/10.1016/j.addr.2017.09.023.

(32) Creeth, J. M. Constituents of Mucus and Their Separation. *Br. Med. Bull.* **1978**, *34* (1), 17–24. https://doi.org/10.1093/oxfordjournals.bmb.a071454.

(33) Sahu, S.; Lynn, W. S. Lipid Composition of Airway Secretions from Patients with Asthma and Patients with Ystic Fibrosis. *Am. Rev. Respir. Dis.* **1977**, *115* (9), 233–239.

(34) Robinson, N. P.; Kyle, H.; Webber, S. E.; Widdicombe, J. G. Electrolyte and Other Chemical Concentrations in Tracheal Airway Surface Liquid and Mucus. *J. Appl. Physiol.* **1989**, *66* (5), 2129–2135. https://doi.org/10.1152/jappl.1989.66.5.2129.

(35) Huckaby, J. T.; Lai, S. K. PEGylation for Enhancing Nanoparticle Diffusion in Mucus. *Adv. Drug Deliv. Rev.* **2018**, *124*, 125–139. https://doi.org/10.1016/j.addr.2017.08.010.

(36) Lai, S. K.; Wang, Y. Y.; Hida, K.; Cone, R.; Hanes, J. Nanoparticles Reveal That Human Cervicovaginal Mucus Is Riddled with Pores Larger than Viruses. *Proc. Natl. Acad. Sci. U. S. A.* **2011**, *108* (34), 14371. https://doi.org/10.1073/pnas.1111693108.

(37) Yildiz, H. M.; McKelvey, C. A.; Marsac, P. J.; Carrier, R. L. Size Selectivity of Intestinal Mucus to Diffusing Particulates Is Dependent on Surface Chemistry and Exposure to Lipids. *J. Drug Target.* **2015**, *23* (7–8), 768–774. https://doi.org/10.3109/1061186X.2015.1086359.

(38) Schuster, B. S.; Suk, J. S.; Woodworth, G. F.; Hanes, J. Nanoparticle Diffusion in Respiratory Mucus from Humans without Lung Disease. *Biomaterials* **2013**, *34* (13), 3439–3446. https://doi.org/10.1016/j.biomaterials.2013.01.064.

(39) Suk, J. S.; Lai, S. K.; Wang, Y.-Y.; Ensign, L. M.; Zeitlin, P. L.; Boyle, M. P.; Hanes, J. The Penetration of Fresh Undiluted

Sputum Expectorated by Cystic Fibrosis Patients by Non-Adhesive Polymer Nanoparticles. *Biomaterials* **2009**, *30* (13), 2591–2597. https://doi.org/10.1016/j.biomaterials.2008.12.076.

(40)   J.S., S.; S.K., L.; N.J., B.; M.R., D.; M.P., B.; J., H. Rapid Transport of Muco-Inert Nanoparticles in Cystic Fibrosis Sputum Treated with N-Acetyl Cysteine. *Nanomedicine* **2011**, *6* (2), 365–375.

(41)   Smith-Dupont, K. B.; Wagner, C. E.; Witten, J.; Conroy, K.; Rudoltz, H.; Pagidas, K.; Snegovskikh, V.; House, M.; Ribbeck, K. Probing the Potential of Mucus Permeability to Signify Preterm Birth Risk. *Sci. Rep.* **2017**, *7* (1), 1–14. https://doi.org/10.1038/s41598-017-08057-z.

(42)   Behera, S. K.; Praharaj, A. B.; Dehury, B.; Negi, S. *Exploring the Role and Diversity of Mucins in Health and Disease with Special Insight into Non-Communicable Diseases*; 2015; Vol. 32. https://doi.org/10.1007/s10719-015-9606-6.

(43)   Robbins Basic Pathology; 2018; pp 250–254. https://doi.org/10.1017/CBO9781107415324.004.

(44)   Ratjen, F.; Bell, S. C.; Rowe, S. M.; Goss, C. H.; Quittner, A. L.; Bush, A. Cystic Fibrosis. *Nat. Rev. Dis. Prim.* **2015**, *1* (May), 15010. https://doi.org/10.1038/nrdp.2015.10.

(45)   Shteinberg, M.; Haq, I. J.; Polineni, D.; Davies, J. C. Cystic Fibrosis. *Lancet* **2021**, *397* (10290), 2195–2211. https://doi.org/10.1016/S0140-6736(20)32542-3.

(46)   Boeck, D.; Amaral, M. Classification of CFTR Mutation Classes. *Www.Thelancet.Com* **2016**, *4* (August), 37–38. https://doi.org/10.1016/S2213-2600(16)30188-6.

(47)   Fanen, P.; Wohlhuter-Haddad, A.; Hinzpeter, A. Genetics of Cystic Fibrosis: CFTR Mutation Classifications toward Genotype-Based CF Therapies. *Int. J. Biochem. Cell Biol.* **2014**, *52*, 94–102. https://doi.org/10.1016/j.biocel.2014.02.023.

(48)   Cohen, T. S.; Prince, A. Cystic Fibrosis: A Mucosal Immunodeficiency Syndrome. *Nat. Med.* **2012**, *18* (4), 509–519. https://doi.org/10.1038/nm.2715.

(49)   Knowles, M. R.; Boucher, R. C. Mucus Clearance as a Primary Innate Defense Mechanism for Mammalian Airways. *J. Clin. Invest.* **2002**, *109* (5), 571–577. https://doi.org/10.1172/JCI200215217.The.

(50)   Pezzulo, A. A. et al. Reduced Airway Surface PH Impairs Bacterial Killing in the Porcine Cystic Fibrosis Lung. *Nature* **2012**, *487*, 109–113. https://doi.org/10.1038/nature11130.Reduced.

(51)   Kahl, B. C. Staphylococcus Aureus and Pseudomonas Aeruginosa Respiratory Tract Coinfection - What Can We Learn from Animal Models? *J. Infect. Dis.* **2018**, *217* (6), 854–856. https://doi.org/10.1093/infdis/jix624.

(52)   Vonberg, R.; Gastmeier, P. Isolation of Infectious Cystic Fibrosis Patients: Results of a Systematic Review. *Infect. Control Hosp. Epidemiol.* **2005**, *26* (4), 401–409.

(53)   Govan, J. R. W.; Deretic, V. Microbial pathogenesis in cystic fibrosis: mucoid Pseudomonas aeruginosa and Burkholderia cepacia. https://doi.org/10.1111/j.1365-2672.2007.03706.x.

(54)   Bjarnsholt, T.; Jensen, P. Ø.; Fiandaca, M. J.; Pedersen, J.; Hansen,

C. R.; Andersen, C. B.; Pressler, T.; Givskov, M.; Høiby, N. Pseudomonas Aeruginosa Biofilms in the Respiratory Tract of Cystic Fibrosis Patients. *Pediatr. Pulmonol.* **2009**, *44* (6), 547–558. https://doi.org/10.1002/ppul.21011.

(55)   McCaslin, C. A.; Petrusca, D. N.; Poirier, C.; Serban, K. A.; Anderson, G. G.; Petrache, I. Impact of Alginate-Producing Pseudomonas Aeruginosa on Alveolar Macrophage Apoptotic Cell Clearance. *J. Cyst. Fibros.* **2015**, *14* (1), 70–77. https://doi.org/10.1016/j.jcf.2014.06.009.

(56)   Leid, J. G.; Willson, C. J.; Shirtliff, M. E.; Hassett, D. J.; Parsek, M. R.; Jeffers, A. K. The Exopolysaccharide Alginate Protects Pseudomonas Aeruginosa Biofilm Bacteria from IFN-γ-Mediated Macrophage Killing . *J. Immunol.* **2005**, *175* (11), 7512–7518. https://doi.org/10.4049/jimmunol.175.11.7512.

(57)   Hentzer, M.; Teitzel, G. M.; Balzer, G. J.; Heydorn, A.; Molin, S.; Givskov, M.; Parsek, M. R. Alginate Overproduction Affects Pseudomonas Aeruginosa Biofilm Structure and Function. *J. Bacteriol.* **2001**, *183* (18), 5395–5401. https://doi.org/10.1128/JB.183.18.5395-5401.2001.

(58)   Flume, P. A. Pulmonary Complications of Cystic Fibrosis. *Respir Care* **2009**, *54* (5), 618–627. https://doi.org/10.1016/j.crad.2013.10.023.

(59)   Barley, M.; Mcnally, J.; Marshall, B.; Faro, A.; Elbert, A.; Fink, A.; Sewall, A.; Loeffler, D.; Petren, K.; O'Neil, T.; Rizvi, S. Annual Data Report 2016 Cystic Fibrosis Foundation Patient Registry. *Cyst. Fibros. Found. Patient Regist.* **2016**, 1–94.

(60)   Coutinho, H.; Falcão-Silva, V. S.; Gonçalves, G. Pulmonary Bacterial Pathogens in Cystic Fibrosis Patients and Antibiotic Therapy: A Tool for the Health Workers. *Int. Arch. Med.* **2008**, *1* (1), 24. https://doi.org/10.1186/1755-7682-1-24.

(61)   World Health Organization - The top 10 causes of death.

(62)   Global Strategy for Prevention, Diagnosis and Management of Chronic Obstructive Pulmonnary Disease - 2022 Report. 2022.

(63)   Osadnik, C. R.; McDonald, C. F.; Holland, A. E. Clinical Issues of Mucus Accumulation in COPD. *Int. J. COPD* **2014**, *9*, 301–302. https://doi.org/10.2147/COPD.S61797.

(64)   Hogg, J. C. Pathophysiology of Airflow Limitation in Chronic Obstructive Pulmonary Disease. *Lancet* **2004**, *364* (9435), 709–721. https://doi.org/10.1016/S0140-6736(04)16900-6.

(65)   Sardelli, L.; Pacheco, D. P.; Ziccarelli, A.; Tunesi, M.; Caspani, O.; Fusari, A.; Briatico Vangosa, F.; Giordano, C.; Petrini, P. Towards Bioinspired: In Vitro Models of Intestinal Mucus. *RSC Adv.* **2019**, *9* (28), 15887–15899. https://doi.org/10.1039/c9ra02368b.

(66)   Lock, J. Y.; Carlson, T. L.; Carrier, R. L. Mucus Models to Evaluate the Diffusion of Drugs and Particles. *Adv. Drug Deliv. Rev.* **2018**, *124*, 34–49. https://doi.org/10.1016/j.addr.2017.11.001.

(67)   Barnes, P. J.; Bonini, S.; Seeger, W.; Belvisi, M. G.; Ward, B.; Holmes, A. Barriers to New Drug Development in Respiratory Disease. *Eur. Respir. J.* **2015**, *45* (5), 1197–1207. https://doi.org/10.1183/09031936.00007915.

(68)   Parker, J. L.; Kohler, J. C. The Success Rate of New Drug Development in Clinical Trials: Crohn's Disease. *J. Pharm. Pharm. Sci.* **2010**, *13* (2), 191–197. https://doi.org/10.18433/j39014.

(69)   Petri, N.; Tannergren, C.; Holst, B.; Mellon, F. A.; Bao, Y.; Plumb, G. W.; Bacon, J.; O'Leary, K. A.; Kroon, P. A.; Knutson, L.; Forsell, P.; Eriksson, T.; Lennernas, H.; Williamson, G. Absorption/Metabolism of Sulforaphane and Quercetin, and Regulation of Phase II Enzymes, in Human Jejunum in Vivo. *Drug Metab. Dispos.* **2003**, *31* (6), 805–813. https://doi.org/10.1124/dmd.31.6.805.

(70)   Fix, A. J.; Leppert, P. S. Use of Everted Intestinal Rings for in Vitro Examination of Oral Absorption Potential. *J. Pharm. Sci.* **1994**, *83* (7), 4–9.

(71)   Liu, L.; Tian, C.; Dong, B.; Xia, M.; Cai, Y.; Hu, R.; Chu, X. Models to Evaluate the Barrier Properties of Mucus during Drug Diffusion. *Int. J. Pharm.* **2021**, *599* (1), 120415. https://doi.org/10.1016/j.ijpharm.2021.120415.

(72)   Norris, D. A.; Sinko, P. J. Effect of Size, Surface Charge, and Hydrophobicity on the Translocation of Polystyrene Microspheres through Gastrointestinal Mucin. *J. Appl. Polym. Sci.* **1997**, *63* (11), 1481–1492. https://doi.org/10.1002/(SICI)1097-4628(19970314)63:11<1481::AID-APP10>3.0.CO;2-5.

(73)   Dawson, M.; Krauland, E.; Wirtz, D.; Hanes, J. Transport of Polymeric Nanoparticle Gene Carriers in Gastric Mucus. *Biotechnol. Prog.* **2004**, *20* (3), 851–857. https://doi.org/10.1021/bp0342553.

(74)   Bhat, P. G.; Flanagan, D. R.; Donovan, M. D. Drug Diffusion through Cystic Fibrotic Mucus: Steady-State Permeation, Rheologic Properties, and Glycoprotein Morphology. *J. Pharm. Sci.* **1996**, *85* (6), 624–630. https://doi.org/10.1021/js950381s.

(75)   Boegh, M.; Baldursdóttir, S. G.; Müllertz, A.; Nielsen, H. M. Property Profiling of Biosimilar Mucus in a Novel Mucus-Containing in Vitro Model for Assessment of Intestinal Drug Absorption. *Eur. J. Pharm. Biopharm.* **2014**, *87* (2), 227–235. https://doi.org/10.1016/j.ejpb.2014.01.001.

(76)   Bhattacharjee, S.; Mahon, E.; Harrison, S. M.; McGetrick, J.; Muniyappa, M.; Carrington, S. D.; Brayden, D. J. Nanoparticle Passage through Porcine Jejunal Mucus: Microfluidics and Rheology. *Nanomedicine Nanotechnology, Biol. Med.* **2017**, *13* (3), 863–873. https://doi.org/10.1016/j.nano.2016.11.017.

(77)   Grainger, C. I.; Greenwell, L. L.; Lockley, D. J.; Martin, G. P.; Forbes, B. Culture of Calu-3 Cells at the Air Interface Provides a Representative Model of the Airway Epithelial Barrier. *Pharm. Res.* **2006**, *23* (7), 1482–1490. https://doi.org/10.1007/s11095-006-0255-0.

(78)   Florea, B. I.; Cassara, M. L.; Junginger, H. E.; Borchard, G. Drug Transport and Metabolism Characteristics of the Human Airway Epithelial Cell Line Calu-3. *J. Control. Release* **2003**, *87* (1–3), 131–138. https://doi.org/10.1016/S0168-3659(02)00356-5.

(79)   Navabi, N.; McGuckin, M. A.; Lindén, S. K. Gastrointestinal Cell

Lines Form Polarized Epithelia with an Adherent Mucus Layer When Cultured in Semi-Wet Interfaces with Mechanical Stimulation. *PLoS One* **2013**, *8* (7). https://doi.org/10.1371/journal.pone.0068761.

(80)   Yuan, S.; Hollinger, M.; Lachowicz-Scroggins, M. E.; Kerr, S. C.; Dunican, E. M.; Daniel, B. M.; Ghosh, S.; Erzurum, S. C.; Willard, B.; Hazen, S. L.; Huang, X.; Carrington, S. D.; Oscarson, S.; Fahy, J. V. Oxidation Increases Mucin Polymer Cross-Links to Stiffen Airway Mucus Gels. *Sci. Transl. Med.* **2015**, *7* (276), 276ra27-276ra27. https://doi.org/10.1126/scitranslmed.3010525.

(81)   Bac3Gel https://bac3gel.com/.

(82)   Sugano, K.; Kansy, M.; Artursson, P.; Avdeef, A.; Bendels, S.; Di, L.; Ecker, G. F.; Faller, B.; Fischer, H.; Gerebtzoff, G.; Lennernaes, H.; Senner, F. Coexistence of Passive and Carrier-Mediated Processes in Drug Transport. *Nat. Rev. Drug Discov.* **2010**, *9* (8), 597–614. https://doi.org/10.1038/nrd3187.

(83)   Bennion, B. J.; Be, N. A.; McNerney, M. W.; Lao, V.; Carlson, E. M.; Valdez, C. A.; Malfatti, M. A.; Enright, H. A.; Nguyen, T. H.; Lightstone, F. C.; Carpenter, T. S. Predicting a Drug's Membrane Permeability: A Computational Model Validated with in Vitro Permeability Assay Data. *J. Phys. Chem. B* **2017**, *121* (20), 5228–5237. https://doi.org/10.1021/acs.jpcb.7b02914.

(84)   Avdeef, A. Permeability—PAMPA. In *Absorption and Drug Development*; John Wiley & Sons, Ltd, 2012; pp 319–498. https://doi.org/https://doi.org/10.1002/9781118286067.ch7.

(85)   Sharifian Gh., M. Recent Experimental Developments in Studying Passive Membrane Transport of Drug Molecules. *Mol. Pharm.* **2021**, *18*, 2122–2141. https://doi.org/10.1021/acs.molpharmaceut.1c00009.

(86)   Berben, P.; Bauer-Brandl, A.; Brandl, M.; Faller, B.; Flaten, G. E.; Jacobsen, A.-C.; Brouwers, J.; Augustijns, P. Drug Permeability Profiling Using Cell-Free Permeation Tools: Overview and Applications. *Eur. J. Pharm. Sci.* **2018**, *119*, 219–233. https://doi.org/https://doi.org/10.1016/j.ejps.2018.04.016.

(87)   Kansy, M.; Senner, F.; Gubernator, K. Parallel Artificial Membrane Permeation Assay in the Description of Passive Absorption Processes. *J. Med. Chem.* **1998**, *41* (7), 1007–1010.

(88)   Flaten, G. E.; Dhanikula, A. B.; Luthman, K.; Brandl, M. Drug Permeability across a Phospholipid Vesicle Based Barrier: A Novel Approach for Studying Passive Diffusion. *Eur. J. Pharm. Sci.* **2006**, *27* (1), 80–90. https://doi.org/https://doi.org/10.1016/j.ejps.2005.08.007.

(89)   Di Cagno, M.; Bibi, H. A.; Bauer-Brandl, A. New Biomimetic Barrier Permeapad™ for Efficient Investigation of Passive Permeability of Drugs. *Eur. J. Pharm. Sci.* **2015**, *73*, 29–34. https://doi.org/10.1016/j.ejps.2015.03.019.

(90)   Hidalgo, I. J.; Raub, T. J.; Borchardt, R. T. Characterization of the Human Colon Carcinoma Cell Line (Caco-2) as a Model System for Intestinal Epithelial Permeability. *Gastroenterology* **1989**, *96* (2, Part 2), 736–749. https://doi.org/https://doi.org/10.1016/S0016-

5085(89)80072-1.

(91)   Artursson, P.; Palm, K.; Luthman, K. Caco-2 Monolayers in Experimental and Theoretical Predictions of Drug Transport. *Adv. Drug Deliv. Rev.* **2012**, *64* (SUPPL.), 280–289. https://doi.org/10.1016/j.addr.2012.09.005.

(92)   Irvine, J. D.; Takahashi, L.; Lockhart, K.; Cheong, J.; Tolan, J. W.; Selick, H. E.; Grove, J. R.; Rove, J. R. U. G. MDCK (Madin − Darby Canine Kidney) Cells: A Tool for Membrane Permeability Screening. *J. Pharm. Sci.* **1999**, *88* (1), 28–33. https://doi.org/10.1021/js9803205.

(93)   VOLPE, D. A. Variability in Caco-2 and MDCK Cell-Based Intestinal Permeability Assays. *J. Pharm. Sci.* **2008**, *97* (2), 26–33. https://doi.org/10.1002/jps.

(94)   Pacheco, D. P.; Butnarasu, C. S.; Briatico Vangosa, F.; Pastorino, L.; Visai, L.; Visentin, S.; Petrini, P. Disassembling the Complexity of Mucus Barriers to Develop a Fast Screening Tool for Early Drug Discovery. *J. Mater. Chem. B* **2019**, *7* (32), 4940–4952. https://doi.org/10.1039/C9TB00957D.

(95)   Wishart, D. S.; Knox, C.; Guo, A. C.; Shrivastava, S.; Hassanali, M.; Stothard, P.; Chang, Z.; Woolsey, J. DrugBank: A Comprehensive Resource for in Silico Drug Discovery and Exploration. *Nucleic Acids Res.* **2006**, *34* (Database issue), 668–672. https://doi.org/10.1093/nar/gkj067.

(96)   Perino, A.; Ghigo, A.; Ferrero, E.; Morello, F.; Santulli, G.; Baillie, G. S.; Damilano, F.; Dunlop, A. J.; Pawson, C.; Walser, R.; Levi, R.; Altruda, F.; Silengo, L.; Langeberg, L. K.; Neubauer, G.; Heymans, S.; Lembo, G.; Wymann, M. P.; Wetzker, R.; Houslay, M. D.; Iaccarino, G.; Scott, J. D.; Hirsch, E. Integrating Cardiac PIP$_3$ and CAMP Signaling through a PKA Anchoring Function of P110γ *Mol. Cell* **2011**, *42* (1), 84–95. https://doi.org/10.1016/j.molcel.2011.01.030.

(97)   Emilio, H.; Alessandra, G. WO2016103176 - Novel Pi3K Gama Inhibitor Peptide for Treatment of Respiratory System Diseases, 2016.

(98)   Jacobsen, A.-C.; Nielsen, S.; Brandl, M.; Bauer-Brandl, A. Drug Permeability Profiling Using the Novel Permeapad® 96-Well Plate. *Pharm. Res.* **2020**, *37* (6), 93. https://doi.org/10.1007/s11095-020-02807-x.

(99)   Lai, S. K.; O'Hanlon, D. E.; Harrold, S.; Man, S. T.; Wang, Y. Y.; Cone, R.; Hanes, J. Rapid Transport of Large Polymeric Nanoparticles in Fresh Undiluted Human Mucus. *Proc. Natl. Acad. Sci. U. S. A.* **2007**, *104* (5), 1482–1487. https://doi.org/10.1073/pnas.0608611104.

(100)   Khutoryanskiy, V. V. Beyond PEGylation: Alternative Surface-Modification of Nanoparticles with Mucus-Inert Biomaterials. *Adv. Drug Deliv. Rev.* **2018**, *124*, 140–149. https://doi.org/10.1016/j.addr.2017.07.015.

(101)   Shan, W.; Zhu, X.; Tao, W.; Cui, Y.; Liu, M.; Wu, L.; Li, L.; Zheng, Y.; Huang, Y. Enhanced Oral Delivery of Protein Drugs Using Zwitterion-Functionalized Nanoparticles to Overcome Both the Diffusion and Absorption Barriers. *ACS Appl. Mater. Interfaces*

2016, *8* (38), 25444–25453. https://doi.org/10.1021/acsami.6b08183.

(102) Dat Pham, Q.; Nöjd, S.; Edman, M.; Lindell, K.; Topgaard, D.; Wahlgren, M. Mucoadhesion: Mucin-Polymer Molecular Interactions. *Int. J. Pharm.* **2021**, *610* (October), 121245. https://doi.org/10.1016/j.ijpharm.2021.121245.

(103) Shtenberg, Y.; Goldfeder, M.; Prinz, H.; Shainsky, J.; Ghantous, Y.; Abu El-Naaj, I.; Schroeder, A.; Bianco-Peled, H. Mucoadhesive Alginate Pastes with Embedded Liposomes for Local Oral Drug Delivery. *Int. J. Biol. Macromol.* **2018**, *111*, 62–69. https://doi.org/10.1016/j.ijbiomac.2017.12.137.

(104) Sogias, I. A.; Williams, A. C.; Khutoryanskiy, V. V. Why Is Chitosan Mucoadhesive? *Biomacromolecules* **2008**, *9* (7), 1837–1842. https://doi.org/10.1021/bm800276d.

(105) Park, H.; Robinson, J. R. Mechanisms of Mucoadhesion of Poly(Acrylic Acid) Hydrogels. *Pharmaceutical Research: An Official Journal of the American Association of Pharmaceutical Scientists*. 1987, pp 457–464. https://doi.org/10.1023/A:1016467219657.

(106) Jaipakdee, N.; Pongjanyakul, T.; Limpongsa, E. Preparation and Characterization of Poly (Vinyl Alcohol)-Poly (Vinyl Pyrrolidone) Mucoadhesive Buccal Patches for Delivery of Lidocaine HCL. *Int. J. Appl. Pharm.* **2018**, *10* (1), 115–123. https://doi.org/10.22159/ijap.2018v10i1.23208.

(107) Yan, H.; Chircov, C.; Zhong, X.; Winkeljann, B.; Dobryden, I.; Nilsson, H. E.; Lieleg, O.; Claesson, P. M.; Hedberg, Y.; Crouzier, T. Reversible Condensation of Mucins into Nanoparticles. *Langmuir* **2018**, *34* (45), 13615–13625. https://doi.org/10.1021/acs.langmuir.8b02190.

(108) Sonia, V.; Francesco, B.; Paola, P.; Livia, V. WO2021260525A3 - Covalently Cross-Linked Glycosylated Mucin Nanoparticles as Systems for the Delivery and Release of Active Ingredients and Biomolecules, 2022.

(109) Prasher, P.; Sharma, M. Mucoadhesive Nanoformulations and Their Potential for Combating COVID-19. *Nanomedicine* **2021**, *16* (28), 2497–2501. https://doi.org/10.2217/nnm-2021-0287.

(110) NanoMuG https://www.nanomug.it/.

(111) Kufe, D. W. Mucins in Cancer: Function, Prognosis and Therapy. *Nat. Rev. Cancer* **2009**, *9* (12), 874–885. https://doi.org/10.1038/nrc2761.

(112) Hollingsworth, M. A.; Swanson, B. J. Mucins in Cancer: Protection and Control of the Cell Surface. *Nat. Rev. Cancer* **2004**, *4* (1), 45–60. https://doi.org/10.1038/nrc1251.

(113) Bhatia, R.; Gautam, S. K.; Cannon, A.; Thompson, C.; Hall, B. R.; Aithal, A.; Banerjee, K.; Jain, M.; Solheim, J. C.; Kumar, S.; Batra, S. K. Cancer-Associated Mucins: Role in Immune Modulation and Metastasis. *Cancer Metastasis Rev.* **2019**, *38* (1–2), 223–236. https://doi.org/10.1007/s10555-018-09775-0.

(114) Wi, D. H.; Cha, J. H.; Jung, Y. S. Mucin in Cancer: A Stealth Cloak for Cancer Cells. *BMB Rep.* **2021**, *54* (7), 344–355. https://doi.org/10.5483/BMBRep.2021.54.7.064.

(115)   Behrens, M. E.; Grandgenett, P. M.; Bailey, J. M.; Singh, P. K.; Yi, C. H.; Yu, F.; Hollingsworth, M. A. The Reactive Tumor Microenvironment: MUC1 Signaling Directly Reprograms Transcription of CTGF. *Oncogene* **2010**, *29* (42), 5667–5677. https://doi.org/10.1038/onc.2010.327.

(116)   Wang, S.; You, L.; Dai, M.; Zhao, Y. Mucins in Pancreatic Cancer: A Well-Established but Promising Family for Diagnosis, Prognosis and Therapy. *J. Cell. Mol. Med.* **2020**, *24* (18), 10279–10289. https://doi.org/10.1111/jcmm.15684.

(117)   Munkley, J. The Role of Sialyl-Tn in Cancer. *Int. J. Mol. Sci.* **2016**, *17* (3). https://doi.org/10.3390/ijms17030275.

(118)   Chen, J.; Liu, T.; Gao, J.; Gao, L.; Zhou, L.; Cai, M.; Shi, Y.; Xiong, W.; Jiang, J.; Tong, T.; Wang, H. Variation in Carbohydrates between Cancer and Normal Cell Membranes Revealed by Super-Resolution Fluorescence Imaging. *Adv. Sci.* **2016**, *3* (12). https://doi.org/10.1002/advs.201600270.

(119)   Mereiter, S.; Balmaña, M.; Campos, D.; Gomes, J.; Reis, C. A. Glycosylation in the Era of Cancer-Targeted Therapy: Where Are We Heading? *Cancer Cell* **2019**, *36* (1), 6–16. https://doi.org/10.1016/j.ccell.2019.06.006.

(120)   Barbero, N.; Butnarasu, C.; Visentin, S.; Barolo, C. Squaraine Dyes: Interaction with Bovine Serum Albumin to Investigate Supramolecular Adducts with Aggregation-Induced Emission (AIE) Properties. *Chem. - An Asian J.* **2019**, *14* (6), 896–903. https://doi.org/10.1002/asia.201900055.

(121)   Butnarasu, C.; Barbero, N.; Barolo, C.; Visentin, S. Interaction of Squaraine Dyes with Proteins: Looking for More Efficient Fluorescent Turn-on Probes. *Dye. Pigment.* **2021**, *184*, 108873. https://doi.org/10.1016/j.dyepig.2020.108873.

APPENDIX

I.   APPENDIX A

Mucin binding to therapeutic molecules: The case of antimicrobial agents used in cystic fibrosis

The author's contributions to the appended manuscript consist of all the experimental work and manuscript preparation; data interpretation was done together with author's supervisor, Prof. Sonia Visentin.

Mucin binding to therapeutic molecules: The case of antimicrobial agents used in cystic fibrosis

Cosmin Butnarasu[a], Nadia Barbero[b], Daniela Pacheco[c], Paola Petrini[c], Sonja Visentin[a],[*]

[a] Molecular Biotechnology and Health Science Department, University of Torino, Via Gioachino Quarello 15, 10135 Torino, Italy
[b] NIS Interdepartmental and INSTM Reference Centre, Department of Chemistry, University of Torino, Via Pietro Giuria 7, 10125 Torino, Italy
[c] Department of Chemistry, Materials and Chemical Engineering "Giulio Natta", Politecnico di Milano, Piazza Leonardo da Vinci 32, 20133 Milan, Italy

ARTICLE INFO

ABSTRACT

Mucin is a complex glycoprotein consisting of a wide variety of functional groups that can interact with exogenous agents. The binding to mucin plays a crucial role in drug pharmacokinetics especially in diseases, such as cystic fibrosis (CF), where mucin is overexpressed. In this study, we have investigated the interaction between mucin and several drugs used in CF therapy. Protein-drug interaction was carried out by UV–Vis and fluorescence spectroscopy; quenching mechanism, binding constants, number of binding sites, thermodynamic parameters and binding distance of the interaction were obtained.

1. Introduction

Many epithelial surfaces in the human body are covered with a thin mucus layer. The airways, the entire gastrointestinal tract, and the eyes are only few of the sites where mucus can be found. Structurally, the mucus is a semi-permeable viscoelastic hydrogel with heterogeneous composition. Indeed, it consists of about 95% by water and approximately 5% by electrolytes, lipids, fragments of DNA (especially observed in pathological states) and different types of proteins (Murgia et al., 2018). By acting as a barrier, mucus primary function is to protect the underlying epithelium from noxious agents, such as air pollutants or bacteria. The defensive activity of mucus can be principally attributed to mucins, that are the primarily expressed proteins within mucus.

Mucins are described as long polymeric glycoconjugates having high molecular weight (1–40 × 10^6 Da, (Taherali et al., 2017)), consisting of a linear peptide backbone, rich in tandem repeats of proline, threonine and serine (PTS domains). To PTS domains a huge amount of carbohydrate chains (up to 40–80% by weight) are O-linked (García-Díaz et al., 2017; Johansson et al., 2011). The bounds are formed between hydroxylic groups on the peptide backbone, with fragments of fucose, galactose, sialic acids, N-acetylglucosamine (GlcNAc) and N-acetylgalactoseamine (GalNAc) on the polysaccharide chains (Boegh and Nielsen, 2015). Also present, but less abundant, are the N-linked glycans to the N-terminus. The glycosylated and highly hydrophilic domains are separated by "naked" cystine rich and more hydrophobic domains that fold into globules stabilized by multiple internal disulfide

bonds (Cone, 2009). In all the secretory mucins, domains similar to the von Willebrand Factor (vWF) C and D are present at the N-terminal, and likewise, at the C-terminal cysteine knot domains are exposed. Mucins exhibit an overall negative charge due to the free carboxylate (sialic acid) and sulfonate groups present in the glycosylated PTS domains. The overall negative charge increases the stability of the mucin network thanks to repulsive forces.

Due to the wide variety of functional groups present into its structure, mucin can establish many interactions with molecules of hydrophilic or hydrophobic nature, by electrostatic and hydrogen bonding interactions hence hinder the diffusion of drugs (Araújo et al., 2018; Murgia et al., 2018; Sigurdsson et al., 2013; Witten et al., 2000). Conversely, as reported by Yeap et al., mucin has shown to improve the solubility of supersaturated solutions hence increasing the drug absorption (Yeap et al., 2018). Lipophilic molecules can interact either with cystine rich domains or with non-PTS regions. Similarly, drugs provided with sulfhydryl groups are capable to form stronger bonds (covalent bonds) with the cystine-rich domains of the naked portions of the mucin structure (Boegh and Nielsen, 2015), (Zanin et al., 2016) (Fig. 1). The mesh-like structure of mucins, creates a steric and potentially highly adhesive barrier to the transport of drugs to the underlying mucosal surface impairing the distribution of drugs through all the mucosa.

It results clear that the mucin-drug interaction may have a remarkable impact on drug absorption since mucus is the first barrier that drugs must overcome to be adsorbed and gain access to the circulatory

---

[*] Corresponding author.
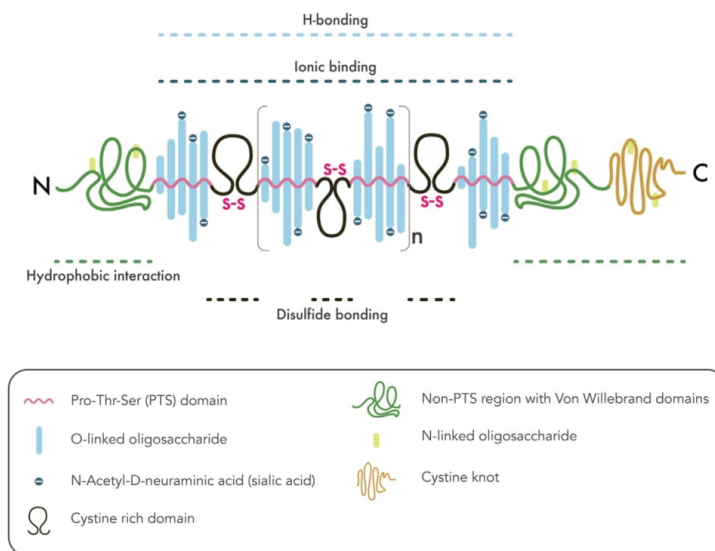*E-mail address:* sonja.visentin@unito.it (S. Visentin).

Fig. 1. Structure of mucin monomer and types of interactions that can be established with drugs.

system and distribution. In early drug discovery, by definition, simple and fast screening tools are needed for filtering the most promising candidates. These screening tools highlight the main intermolecular forces governing the investigated phenomenon. The proof of concept of using mucin to mimic mucus is widely reported in the literature also by Xu and coworkers, who state that reduced mucin-binding in vitro has been shown to correlate with rapid penetration of nanoparticles through mucus (Xu et al., 2016) or to reduce the measured MIC potency of the colistin, as described by Huang et al. (2015). Obviously, the use of mucin to mimic mucus in some way is too simple, but on the other hand this system could give us some useful information about the interaction that occurs between drugs and mucin in the absence of interfering molecule (like DNA, lipids etc.).

In this study we have investigated the interaction between several drugs of interest in cystic fibrosis (CF) and mucin (Fig. 2). Since CF patients are susceptible to concurrent chronic pulmonary infections by bacteria, which gradually destroys lung tissues, one of the major goals of CF therapies involves the maintenance of the pulmonary function (Cystic Fibrosis Foundation [US], 2019). With this purpose, antibiotics are a standard of care for CF patients. Anti-infective therapies are employed to prevent, eradicate and control respiratory infections. By fighting bacterial infections, the antibiotic treatments lead to a reduction of the inflammatory milieu, therefore an improvement of the pulmonary function. One of the most recurrent and aggressive bacteria is *Pseudomonas aeruginosa*. If not detected and treated adequately, infections related to this gram-negative, opportunistic bacterium become chronic, which resultant inflammatory response is closely linked to decreased pulmonary function (Edmondson and Davies, 2016). While *P. aeruginosa* is the most aggressive bacteria for CF patients, other pathogens as *Staphylococcus aureus* or *Burkholderia cepacia* can also infect the airways, therefore different classes of antibiotics are employed in CF therapy. Inhaled tobramycin associated with aztreonam lysine is usually the first line of treatment for early infections.

The affinity of some drugs for mucin has been previously studied using spectroscopic methods by Pontremoli et al. (2015), by chromatographic methods by Gargano et al. (2014), whereas Barbero *et al* have investigated the interactions of both carbon nanotubes (CNTs) and gold nanoparticles (GNPs) with mucin (Barbero et al., 2018, 2016). Starting

from the work of Gargano et al., in our previous paper (Caron et al., 2015) we tried to highlight the balance of the intermolecular forces governing the interaction and we concluded that hydrogen bonding donor (HBD) properties of solutes favor the interaction with mucin. Yet, much needs still to be uncover about mucin-drugs interaction and the physico-chemical parameters that govern the affinity of drugs for mucin. In this work, antibiotics from different anti-infective classes were employed to assess their interaction with mucin, including ceftazidime, and its core chemical structure, 7-aminocephalosporanic acid (7-ACA), aztreonam, ampicillin, tobramycin, levofloxacin and rifampicin. Moreover, a selective and reversible inhibitor of the transmembrane protein CFTR (CFTR(inh)-172) has been tested too (Thiagarajah et al., 2004).

2. Materials and methods

2.1. Materials

Mucin from porcine stomach (PGM type III, bound sialic acid 0.5–1.5%, partially purified powder), aztreonam, CFTR(inh)-172, ampicillin, tobramycin, levofloxacin, 7-ACA and rifampicin were purchased from Sigma Aldrich. Commercial ceftazidime for injection was supplied from Fresenius Kabi. PGM and drugs stock solutions for UV and fluorescence analysis were prepared in PBS (phosphate buffer solution 2 mM, pH = 7.4). PGM itself is a water insoluble material, therefore to facilitate solubility in water and obtain a more homogeneous suspension, samples were sonicated for two minutes at room temperature. When necessary the dissolution of the powder drugs was enhanced by sonication. The CFTR(inh)-172 stock solution was prepared by previously dissolution of the powder into a minimum volume of EtOH. All chemicals were of analytical reagent grade and were used without further purification. Millipore grade water was obtained from an in-house Millipore system (resistivity: 18.2 MΩ cm at 25 °C).

2.2. Methods

2.2.1. UV–Vis absorption spectroscopy

UV–Vis absorption spectra were measured by a UH5300 Hitachi
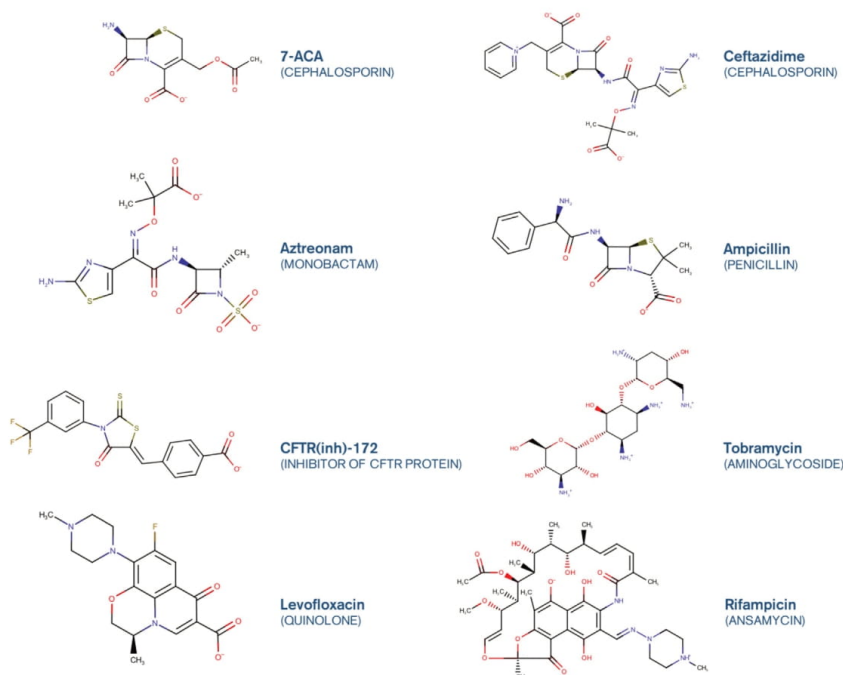
Fig. 2. Chemical structures and pharmaceutical class of the tested molecules. (Marvin 18.28, ChemAxon was used for drawing the chemical structures and predict the major species at pH 7.4 (Marvin 18.28, ChemAxon, n.d.)).

spectrophotometer at room temperature, using quartz cuvettes (1 cm pathway length). The UV measurements were made in the range of 200–400 nm (with the exception of CFTR(inh)-172 where the range was set on 200–500 nm). Spectra of a 0.05 mg/mL mucin solution were recorded in the absence and in the presence of increasing concentrations of drugs (Fig. 3). Drugs concentrations are reported in Table S1 of SI.

2.2.2. Emission spectroscopy

Fluorescence emission spectra in steady state mode were acquired at three temperatures (296, 303 and 310 K) using a Horiba Jobin Yvon Fluorolog 3 TCSPC fluorimeter equipped with a 450-W Xenon lamp and a Hamamatsu R928 photomultiplier.

Fluorescence spectra were recorded in the range of 290–480 nm and the excitation wavelength was fixed on 280 nm. Excitation and emission slit width was set on 6 and 7, respectively. A constant concentration (0.05 mg/mL) of PGM was analysed by successive increasing the concentration of the drugs (Fig. 4). After preparation, samples were left to equilibrate for at least 30 min and only then fluorescence measures were performed.

A significant obstacle to the use of fluorescent methods is the nonlinear dependence of the fluorescence intensity on the concentration of the fluorescent substance. This effect, known as the inner filter effect (IFE), greatly complicates the record of fluorescence emission spectra and the determination of the binding parameters effect often leading to incorrect uses of the method. To minimize the IFE, the concentration of the different drugs was set in order to have absorbance values lower than 0.1. However, as reported by Sharma *et al.*, a change in absorption equal to 0.03 corresponds to a 3% reduction in emission intensity of protein, so it is necessary to correct the observed emission intensity for IFE even for absorption values lower than 0.1 (Sharma et al., 2014). The

IFE correction was done for the fluorescence intensities of mucin and drug using the following equation:

$$F_{corrected} = F_{observed} \cdot 10^{\frac{(A_{ex} + A_{em})}{2}} \tag{1}$$

where $F_{corrected}$ and $F_{observed}$ are the corrected and observed fluorescence intensities, respectively. A_{ex} and A_{em} are the solution absorbance at the excitation and emission wavelengths, respectively.

3. Results and discussion

3.1. UV–Vis absorption studies

UV–Vis absorption spectroscopy is a simple and commonly employed technique for studying the interactions between proteins and small molecules (Sirajuddin et al., 2013; Zhang et al., 2008). By monitoring the changes in the absorption properties of the protein, it is possible to detect the formation of a complex between the protein and the small molecule. It has been assumed that a shift of the maximum peak of the protein in the presence of the ligand is a proof of the formation of a complex between the two species. Mucin has an absorption peak at 257 nm principally due to the presence of the amino acid phenylalanine.

The UV–Vis absorption spectra of mucin were recorded by keeping constant the concentration of protein, while the concentration of drug was varied increasingly (Fig. 3). Except for tobramycin (Fig. 3-F), that have no effect at all upon mucin, the UV absorption intensity was gradually enhanced for PGM following the addition of increasing amounts of drug (hyperchromism). These changes may be explained by the formation of a new mucin-drug complex.
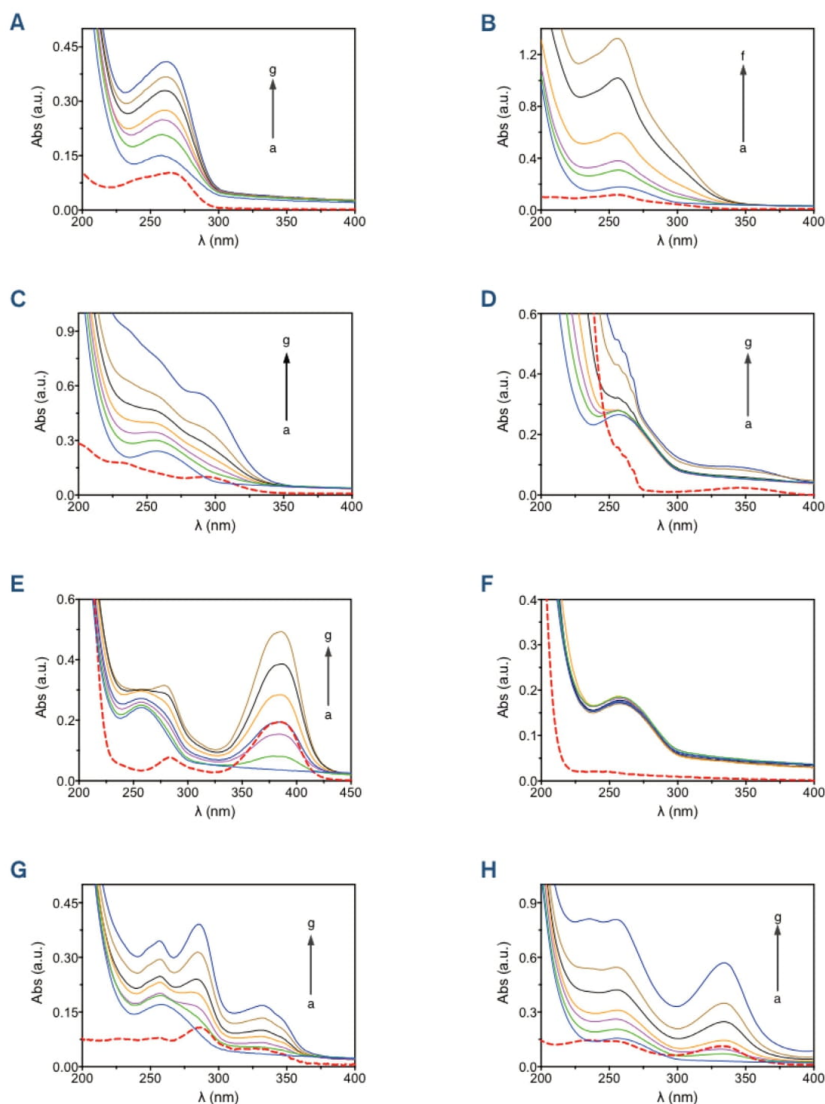
Fig. 3. UV–Vis absorption spectra of mucin (PGM, blue line) in the presence of 7-ACA (A), ceftazidime (B), aztreonam (C), ampicillin (D), CFTR(inh)-172 (E), tobramycin (F), levofloxacin (G), and rifampicin (H). The red dashed lines reports the absorption spectra of the drugs alone at a concentration that gives an absorbance of about 0.1 (7-ACA 12 μM, ceftazidime 6 μM, aztreonam 10 μM, ampicillin 500 μM, CFTR(inh)-172 5 μM, tobramycin 1600 μM, levofloxacin 2 μM, and rifampicin 5 μM). (For interpretation of the references to colour in this figure legend, the reader is referred to the web version of this article.)

3.2. Steady state fluorescence spectroscopy

Fluorescence spectroscopy is probably one of the most commonly technique used to study interaction between small molecules and proteins. Normally, the fluorescence of proteins is caused only by three intrinsic fluorophores present in the protein, i.e. tryptophan, phenylalanine and tyrosine amino acids (Sirajuddin et al., 2013; Zhang et al., 2008). After excitation at 280 nm, PGM shows a strong fluorescence emission at 350 nm due to the presence of tryptophan residues.

Since tryptophan fluorescence intensity is extremely sensitive to the

local environment, in the present work, the interaction between the drugs and the core of PGM was evaluated by measuring the intrinsic fluorescence of the protein before and after addition of increasing concentrations of drug. It was observed that the fluorescence intensities of PGM was gradually reduced with increasing concentrations of ceftazidime, aztreonam, CFTR(inh)-172, and levofloxacin (Fig. 4, graphs B, C, E, and G, respectively). It is possible to assume that during the binding interaction, the aforementioned drugs have altered tryptophan microenvironment. No significative variations of fluorescence intensities were detected in the presence of 7-ACA, ampicillin,
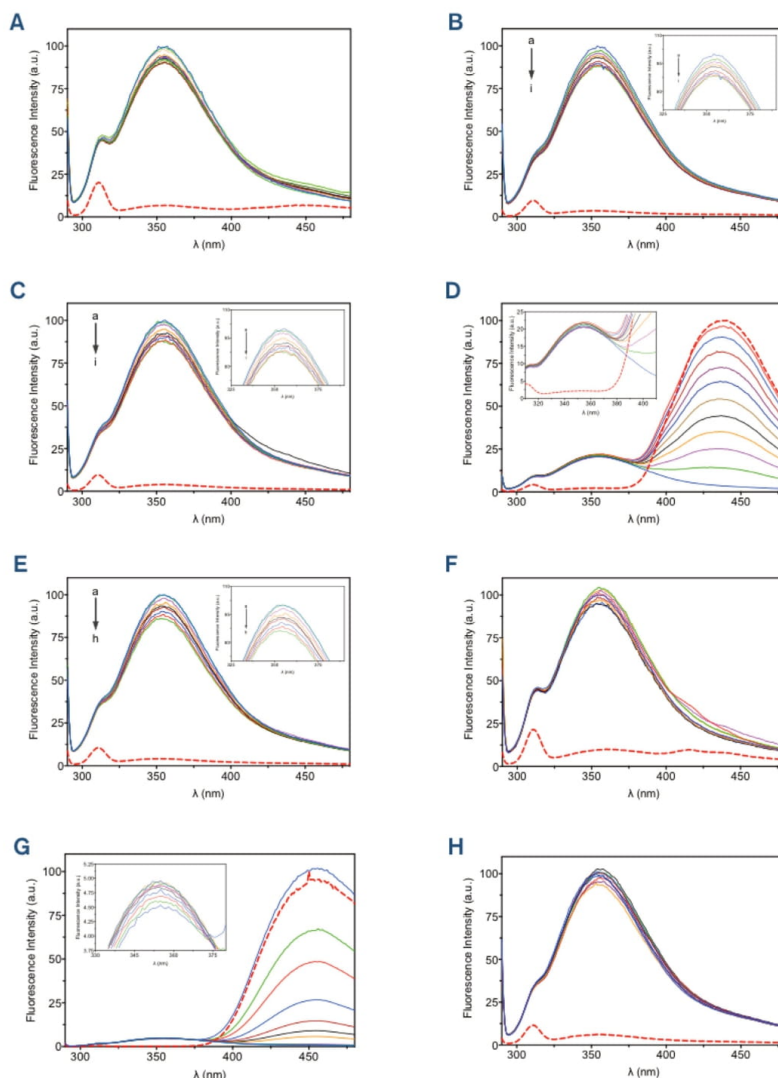
Fig. 4. Steady state fluorescence spectra of mucin (PGM) in the presence of 7-ACA (A), ceftazidime (B), aztreonam (C), ampicillin (D), CFTR(inh)-172 (E), tobramycin (F), levofloxacin (G), and rifampicin (H). The red dashed lines report the fluorescence emission spectra of drug alone at the maximum concentration used. (For interpretation of the references to colour in this figure legend, the reader is referred to the web version of this article.)

tobramycin, and rifampicin (Fig. 4, graphs A, D, F, and H, respectively). Even if tobramycin is charged at pH 7.4, the drug seems to not affect the Trp environment and the interaction that was described by other authors could be ascribed to electrostatic interactions (Huang et al., 2015).

The process that decreases the intensity of the fluorescence emission is known as fluorescence quenching. Several processes can result in quenching, such as excited state reactions, energy transfer, ground-state complex formation (static quenching) and collisional quenching (also called dynamic quenching). Both static and dynamic quenching require molecular contact between the fluorophore (mucin) and the quencher (drug). In the case of dynamic quenching, the quencher diffuses to the

fluorophore and, upon contact, the fluorophore returns to the ground state without emission of a photon. On the other hand, in static quenching a non-fluorescent complex is formed between the fluorophore and the quencher (Lakowicz, 2006).

3.2.1. Quenching mechanism of PGM in the presence of drugs

The fluorescence quenching data were analysed according to Stern-Volmer equation:

$$\frac{F_0}{F} = 1 + K_{SV}[Q] \qquad (2)$$

where F_0 is the fluorescence intensity of mucin alone and F is the

Fig. 5. Stern-Volmer plots of PGM – ceftazidime (B), PGM – aztreonam (C), PGM – CFTR(inh)-172 (E), and PGM – Levofloxacin (G).

fluorescence of mucin in the presence of increasing concentrations of quencher [Q]. K_{SV} is the Stern-Volmer quenching constant. [Q] is the quencher (drug) concentration. Quenching data are presented as plots of F_0/F vs [Q], yielding an intercept of one on the y axis and a slope equal to K_{SV} (Fig. 5).

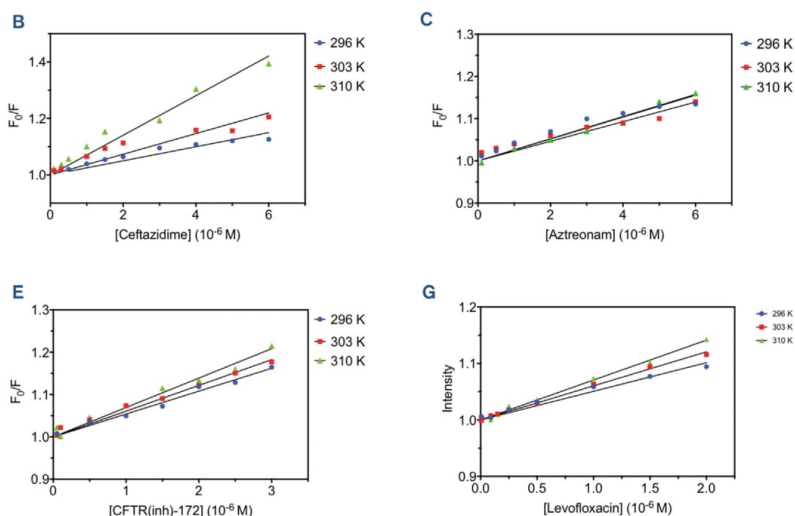Linear Stern-Volmer plots does not prove that collisional quenching of fluorescence has occurred. Static and dynamic quenching can be distinguished by their differing dependence on temperature. Larger amounts of collisional quenching are observed at higher temperatures due to the faster diffusion rates, while smaller amounts of static quenching are observed at higher temperatures since less weakly bound complexes are formed (Lakowicz, 2006).

The K_{SV} of PGM – ceftazidime, PGM – CFTR(inh)-172 and PGM – levofloxacin increases with the increasing of temperature (checked at 296 K, 303 K and 310 K. See Table 1), which implies a dynamic quenching between mucin and the aforementioned drugs. The K_{SV} of PGM – aztreonam is similar with negligible variations upon increasing temperature. In order to take into account the heterogeneous dispersion of the protein, standard deviation (SD) of K_{SV}, n, K_A and K_D was calculated.

3.2.2. Binding parameters

For the determination of the association constant (K_A) and the number of binding sites (n), the double logarithm regression curve (Eq. (3)) was used.

$$log\frac{(F_0 - F)}{F} = logK_A + nlog[Q] \qquad (3)$$

where F_0 and F are the fluorescence intensities in absence and presence

of quencher (drug), K_A denotes the binding constant, n refers to the number of binding sites on the protein, and [Q] is the quencher concentration. Dissociation constant (K_D) was calculated as the reciprocal of K_A. From the plot of $log[(F_0-F)/F]$ vs $log[Q]$ it is possible to calculate n and $logK_A$ as it represents the slope of the line, and its interception on the y axis, respectively. Values of n, K_A and K_D are reported in Table 2.

Based on the values of n almost equal to 1, one binding site on mucin for each drug can be deduced. It was found that the values of K_A for PGM – ceftazidime, PGM – CFTR(inh)-172 and PGM – levofloxacin interactions increased with a rise in temperature, which implies a dynamic quenching. While, for PGM – aztreonam interaction, the rise in temperature does not affect significantly the K_A. The overall low values of K_A reflect the establishment of a weak bound with mucin.

3.2.3. Thermodynamic parameters

A ligand can bind a protein basically through four types of noncovalent interactions: van der Waals forces, hydrogen bond, hydrophobic and electrostatic interactions. The thermodynamic parameters, enthalpy (ΔH°) and entropy (ΔS°), are used as evidence for the nature of

Table 2

Values of the number of binding sites on mucin for each mucin-drug complex (n), association (K_A) and dissociation constant (K_D).

	n	K_A (M^{-1}) 10^3	K_D (M) 10^{-4}
Ceftazidime			
296 K	0.74 (± 0.040)	1.1 (± 0.081)	9.14 (± 0.68)
303 K	0.73 (± 0.064)	1.3 (± 0.15)	7.62 (± 0.90)
310 K	0.78 (± 0.039)	4.6 (± 0.29)	2.16 (± 0.13)
Aztreonam			
296 K	0.64 (± 0.035)	0.32 (± 0.026)	32 (± 2.6)
303 K	0.63 (± 0.064)	0.26 (± 0.038)	39 (± 5.8)
310 K	0.64 (± 0.11)	0.30 (± 0.076)	34 (± 8.7)
CFTR(inh)-172			
296 K	0.72 (± 0.049)	1.3 (± 0.12)	7.8 (± 0.74)
303 K	0.81 (± 0.032)	5.0 (± 0.25)	2.0 (± 0.1)
310 K	0.93 (± 0.045)	24 (± 1.5)	0.41 (± 0.024)
Levofloxacin			
296 K	0.85 (± 0.14)	7.6 (± 1.8)	1.3 (± 0.31)
303 K	0.91 (± 0.024)	17.9 (± 0.63)	0.56 (± 0.020)
310 K	0.97 (± 0.070)	46.5 (± 4.4)	0.22 (± 0.021)

Table 1

The quenching constants of mucin (PGM) and drugs at different temperatures.

	K_{SV} (M^{-1}) 10^4		
	296 K	303 K	310 K
Ceftazidime	2.5 (± 0.17)	3.7 (± 0.30)	7.0 (± 0.36)
Aztreonam	2.6 (± 0.17)	2.3 (± 0.15)	2.5 (± 0.09)
CFTR(inh)-172	5.4 (± 0.16)	6.1 (± 0.19)	6.9 (± 0.24)
Levofloxacin	5.1 (± 0.22)	6.0 (± 0.11)	7.1 (± 0.16)

Table 3
Thermodynamic parameters for mucin-drug complexes at different temperatures.

	ΔG (kJ mol^{-1})	$\Delta H°$ (kJ mol^{-1})	$\Delta S°$ (J mol^{-1} K^{-1})	Type of interaction
Ceftazidime				
296 K	−24.92	56.22	273.7	Hydrophobic
303 K	−26.47			
310 K	−28.76			
Aztreonam				
296 K	−25.04	−0.74	81.77	Hydrophobic/
303 K	−25.32			Electrostatic
310 K	−26.20			
CFTR(inh)-172				
296 K	−26.82	13.66	136.7	Hydrophobic
303 K	−27.75			
310 K	−28.73			
Levofloxacin				
296 K	−26.66	18.08	151.2	Hydrophobic
303 K	−27.73			
310 K	−28.78			

the acting forces (Chaves et al., 2017). According to the data of enthalpy and entropy changes, the model of protein-drug interaction can be summarized as (Pontremoli et al., 2015): (i) $\Delta H° > 0$ and $\Delta S° > 0$ are indicative of binding driven by hydrophobic forces; (ii) $\Delta H° < 0$ and $\Delta S° < 0$ interactions through van der Waals interactions and hydrogen bonds; (iii) $\Delta H° < 0$ and $\Delta S° > 0$ are indicative of electrostatic interactions. The thermodynamic parameters were calculated through Van't Hoff equations:

$$\int K_A = -\frac{\Delta H°}{RT} + \frac{\Delta S°}{R} \tag{4}$$

$$\Delta G° = -RT \ln K_A \tag{5}$$

$$\Delta S° = \frac{\Delta H° - \Delta G°}{T} \tag{6}$$

where K_A is the binding constant, R is the gas constant (8.31447 J mol^{-1} K^{-1}), T are the experimental temperatures (296 K, 303 K, 310 K) and $\Delta G°$ corresponds to the Gibbs free energy variation. Values of $\Delta H°$, $\Delta S°$ and $\Delta G°$ are summarized in Table 3. As it can be observed from Table 3, for mucin – ceftazidime, mucin – CFTR(inh)-172 and mucin – levofloxacin complexes both $\Delta H°$ and $\Delta S°$ are positive, therefore hydrophobic interactions are the predominant driving forces for the formation of these protein-drug complexes. On the other hand, a negative (even if almost near to zero) and positive value of $\Delta H°$ and $\Delta S°$ respectively, have been found for mucin – aztreonam complex, so this implies that mostly electrostatic forces occur between mucin and drug. The binding process is assumed to be spontaneous as $\Delta G°$ values are negative for all interactions.

It seems that an undefined relation exists between drug lipophilicity and interaction with mucin, particularly, hydrophobic drugs tend to interact more with mucin. As reported in Fig. 6, the greater the $logD_{7.4}$ is, the greater the K_{SV}. Indeed, CFTR(inh)-172 that is the more lipophilic molecule at pH 7.4 has the greater value of K_{SV}, followed by levofloxacin with a lower value of $logD_{7.4}$; aztreonam and ceftazidime, which are the more hydrophilic drugs at pH 7.4, have the lowest values of K_{SV}.

3.2.4. Resonance energy transfer

One important process that can occur in the excited state is the resonance energy transfer, RET (also called fluorescence, or Förster, energy transfer, FRET). This process takes place whenever the emission spectrum of a fluorophore, called the donor, overlaps with the absorption spectrum of another molecule, called the acceptor. The distance between donor and acceptor, as well as the extent of spectral
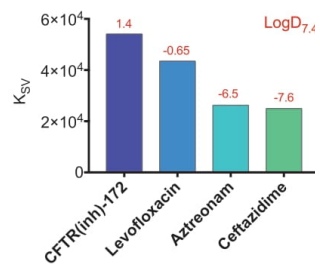
Fig. 6. Histogram of the Stern-Volmer constants (K_{SV}) and values of $logD_{7.4}$ of drugs. Values of $logD_{7.4}$ are predicted by means of ChemAxon.

overlap, determine the amount of energy transfer (Lakowicz, 2006). The efficiency of energy transfer can be calculated according to Eq. (7):

$$E = 1 - \left(\frac{F}{F_0}\right) = \frac{R_0^6}{R_0^6 + r^6} \tag{7}$$

where E can be determined experimentally from the donor (mucin) emission in the absence (F_0) and presence of acceptor (F); r is the distance between the donor and the acceptor (drug); R_0 is the critical distance when the efficiency of transfer is 50%. R_0 can be obtained with the Eq. (8):

$$R_0^6 = 8.79 * 10^{-5}[k^2 n^4 \varphi J(\lambda)] \tag{8}$$

where k^2 is the orientation factor, n is the refractive index of the medium, φ is the fluorescence quantum yield of the donor, and J is the overlap integral between the fluorescence emission spectrum of donor and the absorption spectrum of the acceptor, and it can be obtained according to Eq. (9):

$$J = \frac{F(\lambda)\varepsilon(\lambda)\lambda^4\Delta\lambda}{\sum F(\lambda)\Delta\lambda} \tag{9}$$

where $F(\lambda)$ is the fluorescence intensity of the donor at wavelength λ and $\varepsilon(\lambda)$ is the molar absorption coefficient of the acceptor at wavelength λ. In this case $k^2 = 2/3$, $n = 1.336$ and $\varphi = 0.118$ (Pontremoli et al., 2015).

An example, the overlaps of emission spectra of mucin and absorption spectra of aztreonam and tobramycin are presented in Fig. 7 (The remaining spectra are reported in Fig. S1 of SI). Values of J, E, R_0 and r were determined for every interaction and are reported in Table 4.

Data obtained according to the FRET theory confirm that ceftazidime, aztreonam, CFTR(inh)-172 and levofloxacin interact with mucin, whereas the other drugs do not form any complex with the protein. However, the efficiency of energy transfer (E) for the drugs able to form a mucin-drug complex is quite low (0.1–0.3%), while in the other cases E is almost zero. Even if resonance energy transfer (RET) can occur across a distance below 10 nm (Ray et al., 2014), it does not mean that a value of donor-to-acceptor smaller than 10 nm results in RET. Indeed, as for 7-ACA, ampicillin, tobramycin and rifampicin, the donor-to-acceptor value is even more than two-fold the Förster distance (R_0), that is the distance at which the RET is efficient at 50%. Even if rifampicin has a high value of spectra overlap, no interaction is established as the efficiency of energy transfer is zero.

4. Conclusions

In the present work, the interaction of mucin with some antibiotics of interest in cystic fibrosis was investigated at three different temperatures by two spectroscopic methods. Fluorescence quenching data indicate that ceftazidime, aztreonam, CFTR(inh)-172 and levofloxacin binds mucin, whereas no interaction is observed for 7-ACA, ampicillin, tobramycin and rifampicin. The increasing quenching upon increasing
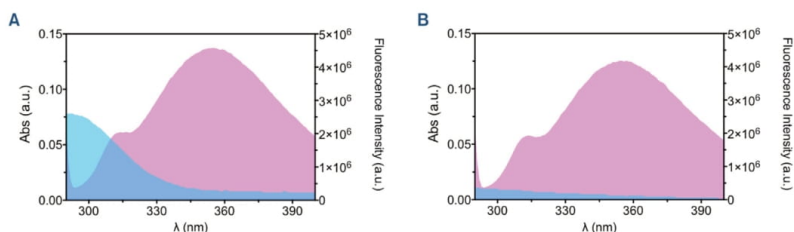
Fig. 7. The overlaps of emission spectra of mucin and the absorption spectra of aztreonam (A) and tobramycin (B).

Table 4
Values of J, E, R_0 and r of mucin-drug complexes determined according to Eqs. (3)–(5).

		J (cm^3 L mol^{-1})	E (%)	R_0 (nm)	r (nm)
A	7-ACA	$3.82 \cdot 10^{12}$	0.01	3.74	8.56
B	Ceftazidime	$2.99 \cdot 10^{13}$	0.18	5.27	6.75
C	Aztronam	$3.54 \cdot 10^{13}$	0.20	5.41	6.80
D	Ampicillin	$3.36 \cdot 10^{11}$	0.00	2.40	9.07
E	CFTR(inh)-172	$3.24 \cdot 10^{14}$	0.22	7.83	9.69
F	Tobramycin	$3.92 \cdot 10^{10}$	0.00	1.74	4.12
G	Levofloxacin	$1.76 \cdot 10^{14}$	0.13	7.07	9.77
H	Rifampicin	$1.52 \cdot 10^{14}$	0.00	6.90	17.9

temperature for ceftazidime, CFTR(inh)-172 and levofloxacin indicate a dynamic quenching process. The K_A and n values indicate that ceftazidime, aztreonam, CFTR(inh)-172 and levofloxacin moderately binds to mucin and there is only one principal site of binding for this association. The low affinity, or absence of it, as for tobramycin, toward mucin could in part explain why these antibiotics are widely used in CF therapies. Contrary to what was expected, the charge of the molecule seems to not play a fundamental role over mucin-drug interaction in our experimental setup, in fact positively charged molecules at pH 7.4, such as tobramycin, have no interaction, whereas negatively charged drugs such as CFTR(inh)-172 or aztreonam can complex the protein. These results denote, as reported by Witten et al. (2000) that the net charge is not necessarily a reliable predictor for mucus binding since other types of interaction could occur (hydrogen bonding, hydrophobic interactions). In our case, the thermodynamic parameters ($\Delta H°$ and $\Delta S° > 0$) suggest that hydrophobic forces played the major role in the binding process between mucin and ceftazidime, CFTR(inh)-172 and levofloxacin, while both hydrophobic and electrostatic forces may play a major role for mucin – aztreonam interaction. The negative values of $\Delta G°$ that we obtained for all the compounds implies a spontaneous binding. In our previous work (Pontremoli et al., 2015) we evidenced that still the hydrophobic forces favour the interaction of a methylxanthine with mucin, but also hydrogen bonds and van der Waals forces played significant roles in stabilizing the mucin complexes with other drugs.

The distance between donor and acceptor was calculated according to FRET theory and resonance energy transfer was confirmed for ceftazidime, aztreonam, CFTR(inh)-172 and levofloxacin.

The results herein reported may improve the knowledge about drug pharmacokinetics (absorption and distribution process) for drugs administered in CF therapy. However, the real mechanism of interaction between drugs and mucus rest still poorly understood, but it is clear that the net charge is not necessarily the only reliable predictor for mucus binding. In fact, electrostatic interactions play a crucial role for some net charged drugs like colistin, but most small molecules are less charged, and the effect of the electrostatic interactions are weaker and sometimes almost inexistent. Monitoring the tryptophan environment of the protein during the interaction, could clarify some aspects of the binding between mucin and drugs.

In order to find a relation between the molecular structure and affinity towards mucin, further studies should be conducted, and a broader dataset of drugs should be investigated. Moreover, as investigated by Pontier and coworkers, it would be interesting to study whether the results obtained in this study correlate with the diffusion through mucus models as well mucus from cystic fibrosis patients (Pontier et al., 2001).

Appendix A. Supplementary data

Supplementary data to this article can be found online at https://doi.org/10.1016/j.ijpharm.2019.04.032.

References

Araújo, F., Martins, C., Azevedo, C., Sarmento, B., 2018. Chemical modi fi cation of drug molecules as strategy to reduce interactions with mucus. Adv. Drug Deliv. Rev. 124, 98–106. https://doi.org/10.1016/j.addr.2017.09.020.
Barbero, N., Coletti, M., Catalano, F., Visentin, S., 2018. Exploring gold nanoparticles interaction with mucins: a spectroscopic-based study. Int. J. Pharm. 535, 438–443. https://doi.org/10.1016/j.ijpharm.2017.11.026.
Barbero, N., Marenchino, M., Campos-Olivas, R., Oliaro-Bosso, S., Bonandini, L., Baskovic, J., Viscardi, G., Visentin, S., 2016. Nanomaterial – protein interactions: the case of pristine and functionalized carbon nanotubes and porcine gastric mucin. J. Nanoparticle Res. 18, 179–185. https://doi.org/10.1007/s11051-016-3388-z.
Boegh, M., Nielsen, H.M., 2015. Mucus as a barrier to drug delivery – understanding and mimicking the barrier properties. Basic Clin. Pharmacol. Toxicol. 116, 179–186. https://doi.org/10.1111/bcpt.12342.
Caron, G., Visentin, S., Pontremoli, C., Ermondi, G., 2015. Profile of the intermolecular forces governing the interaction of drugs with mucin. Int. J. Pharm. 488, 67–69. https://doi.org/10.1016/j.ijpharm.2015.04.058.
Chaves, O.A., da Silva, V.A., Sant'Anna, C.M.R., Ferreira, A.B.B., Ribeiro, T.A.N., de Carvalho, M.G., Cesarin-Sobrinho, D., Netto-Ferreira, J.C., 2017. Binding studies of lophirone B with bovine serum albumin (BSA): Combination of spectroscopic and molecular docking techniques. J. Mol. Struct. 1128, 606–611. https://doi.org/10.1016/j.molstruc.2016.09.036.
Cone, R.A., 2009. Barrier properties of mucus. Adv. Drug Deliv. Rev. 61, 75–85. https://doi.org/10.1016/j.addr.2008.09.008.
Cystic Fibrosis Foundation [US] [WWW Document], 2019. URL https://www.cff.org/Research/Research-Into-the-Disease/Research-into-CF-Complications/Infections/.
Edmondson, C., Davies, J.C., 2016. Current and future treatment options for cystic fibrosis lung disease: latest evidence and clinical implications. Ther. Adv. Chronic Dis. Rev. 7, 170–183. https://doi.org/10.1177/2040622316641352.
García-Díaz, M., Birch, D., Wan, F., Nielsen, H.M., 2017. The role of mucus as an invisible cloak to transepithelial drug delivery by nanoparticles. Adv. Drug Deliv. Rev. 124, 107–124. https://doi.org/10.1016/j.addr.2017.11.002.
Gargano, A.F.G., Lämmerhofer, M., Lönn, H., Schoenmakers, P.J., Leek, T., 2014. Mucin-based stationary phases as tool for the characterization of drug-mucus interaction. J. Chromatogr. A 1351, 70–81. https://doi.org/10.1016/j.chroma.2014.05.031.
Huang, J.X., Blaskovich, M.A.T., Pelingon, R., Ramu, S., Kavanagh, A., Elliott, A.G., Butler, M.S., Montgomery, A.B., Cooper, M.A., 2015. Mucin binding reduces colistin antimicrobial activity. Antimicrob. Agents Chemother. 59, 5925–5931. https://doi.org/10.1128/AAC.00808-15.
Johansson, M.E.V., Ambort, D., Pelaseyed, T., Schutte, A., Gustafsson, J.K., Ermund, A., Subramani, D.B., Holmèn-Larsson, J.M., Thomsson, K.A., Bergstrom, J.H., Van Der Post, S., Rodriguez-Pineiro, A.M., Sjovall, H., Backstrom, M., Hansson, G.C., 2011.

Composition and functional role of the mucus layers in the intestine. Cell. Mol. Life Sci. 68, 3635–3641. https://doi.org/10.1007/s00018-011-0822-3.

Lakowicz, J.R., 2006. Principles of Fluorescence Spectroscopy Principles of Fluorescence Spectroscopy, Principles of fluorescence spectroscopy, 3rd ed. Springer, New York, USA https://doi.org/10.1007/978-0-387-46312-4.

Marvin 18.28, ChemAxon [WWW Document], n.d. URL https://chemaxon.com/.

Murgia, X., Loretz, B., Hartwig, O., Hittinger, M., Lehr, C., 2018. The role of mucus on drug transport and its potential to affect therapeutic outcomes. Adv. Drug Deliv. Rev. 124, 82–97. https://doi.org/10.1016/j.addr.2017.10.009.

Pontier, C., Pachot, J., Botham, R., Lenfant, B., Arnaud, P., 2001. HT29-MTX and Caco-2/ TC7 Monolayers as Predictive Models for Human Intestinal Absorption : Role of the Mucus Layer 90, pp. 1608–1619.

Pontremoli, C., Barbero, N., Viscardi, G., Visentin, S., 2015. Mucin-drugs interaction: the case of theophylline, prednisolone and cephalexin. Bioorganic Med. Chem. 23, 6581–6586. https://doi.org/10.1016/j.bmc.2015.09.021.

Ray, P.C., Fan, Z., Crouch, R.A., Sinha, S.S., Pramanik, A., 2014. Nanoscopic optical rulers beyond the FRET distance limit: fundamentals and applications. Chem. Soc. Rev. 43, 6370–6404. https://doi.org/10.1039/c3cs60476d.

Sharma, A.S., Anandakumar, S., Ilanchelian, M., 2014. In vitro investigation of domain specific interactions of phenothiazine dye with serum proteins by spectroscopic and molecular docking approaches. RSC Adv. 4, 36267–36281. https://doi.org/10.1039/c4ra04630g.

Sigurdsson, H.H., Kirch, J., Lehr, C.M., 2013. Mucus as a barrier to lipophilic drugs. Int. J. Pharm. 453, 56–64. https://doi.org/10.1016/j.ijpharm.2013.05.040.

Sirajuddin, M., Ali, S., Badshah, A., 2013. Drug-DNA interactions and their study by UV-Visible, fluorescence spectroscopies and cyclic voltametry. J. Photochem. Photobiol. B Biol. 124, 1–19. https://doi.org/10.1016/j.jphotobiol.2013.03.013.

Taherali, F., Varum, F., Basit, A.W., 2017. A slippery slope: on the origin, role and physiology of mucus. Adv. Drug Deliv. Rev. 124, 16–33. https://doi.org/10.1016/j.addr.2017.10.014.

Thiagarajah, J.R., Song, Y., Haggie, P.M., Verkman, A.S., 2004. A small molecule CFTR inhibitor produces cystic fibrosis-like submucosal gland fluid secretions in normal airways. FASEB J. 18, 875–877. https://doi.org/10.1096/fj.03-1248fje.

Witten, J., Samad, T., Ribbeck, K., 2000. ScienceDirect selective permeability of mucus barriers. Curr. Opin. Biotechnol. 52, 124–133. https://doi.org/10.1016/j.copbio.2018.03.010.

Xu, Q., Ensign, L.M., Boylan, N.J., Yang, J., Lamb, N.W., Cai, S., Yu, T., Hanes, J., Sciences, M., 2016. HHS public access. ACS Nano 9, 9217–9227. https://doi.org/10.1021/acsnano.5b03876.Impact.

Yeap, Y.Y., Lock, J., Lerkvikarn, S., Semin, T., Nguyen, N., Carrier, R.L., 2018. Intestinal mucus is capable of stabilizing supersaturation of poorly water-soluble drugs. J. Control. Release 107–113. https://doi.org/10.1016/j.jconrel.2018.11.023.

Zanin, M., Baviskar, P., Webster, R., Webby, R., 2016. The interaction between respiratory pathogens and mucus. Cell Host Microbe 19, 159–168. https://doi.org/10.1016/j.chom.2016.01.001.

Zhang, G., Que, Q., Pan, J., Guo, J., 2008. Study of the interaction between icariin and human serum albumin by fluorescence spectroscopy. J. Mol. Struct. 881, 132–138. https://doi.org/10.1016/j.molstruc.2007.09.002.

69

II.   APPENDIX B

Disassembling the complexity of mucus barriers to develop a fast screening tool for early drug discovery

The author's contribution to the appended manuscript consists of planning and execution of drug diffusion experiment; design of graphical abstract; participation to prepare the manuscript.

PAPER

Disassembling the complexity of mucus barriers to develop a fast screening tool for early drug discovery†

Daniela Peneda Pacheco, [ID] [a] Cosmin Stefan Butnarasu, [ID] [b]
Francesco Briatico Vangosa, [ID] [a] Laura Pastorino, [ID] [c] Livia Visai, [ID] [de]
Sonja Visentin [ID] *[b] and Paola Petrini [ID] *[a]

Mucus is a natural barrier with a protective role that hinders drug diffusion, representing a steric and interactive barrier to overcome for an effective drug delivery to target sites. In diseases like cystic fibrosis (CF), pulmonary mucus exhibits altered features, which hamper clearance mechanisms and drug diffusion, ultimately leading to lung failure. Effectively modelling the passage through mucus still represents an unmet challenge. An airway CF mucus model is herein proposed to disassemble the complexity of the mucus barrier following a modular approach. A hydrogel, mainly composed of mucin in an alginate (Alg) network, is proposed to specifically model the chemical–physical properties of CF mucus. The steric retention of pathological mucus was reproduced by targeting its mesh size (approximately 50 nm) and viscoelastic properties. The interactive barrier was reproduced by a composition inspired from the CF mucus. Optimized mucus models, composed of 3 mg ml^{-1} Alg and 25 mg ml^{-1} mucin, exhibited a G' increasing from $\sim$21.2 to 55.2 Pa and a G'' ranging from $\sim$5.26 to 28.8 Pa in the frequency range of 0.1 to 20 Hz. Drug diffusion was tested using three model drugs. The proposed mucus model was able to discriminate between the mucin–drug interaction and the steric barrier of a mucus layer with respect to the parallel artificial membrane permeability (PAMPA) that models the phospholipidic cell membrane, the state-of-the-art screening tool for passive drug diffusion. The mucus model can be proposed as an *in vitro* tool for early drug discovery, representing a step forward to model the mucus layer. Additionally, the proposed methodology allows to easily include other molecules present within mucus, as relevant proteins, lipids and DNA.

1 Introduction

Mucus is a protective barrier that selectively filters the passage of gases, pathogens, pollutants, and nutrients, and also a barrier for drug products.[1] An effective pharmacological treatment requires that drug products freely diffuse through mucus, otherwise these are eliminated before playing their roles. Drug diffusion through mucus is dependent on its chemical composition, ionic strength, structure and viscoelastic properties, as well as the net charge and concentration of drugs and particles (Fig. 1).[2] Despite its complex and important role as a barrier, there are no standard protocols that model the mucus barrier. Instead, drug screening platforms typically rely on 2D cell cultures and parallel artificial membrane permeability (PAMPA) assay. The latter has been adopted to study the permeability of drug products across a lipid-infused artificial membrane. Thus, poor information of possible chemical and steric interactions with mucus has been obtained at the *in vitro* screening stage.[3] This largely affects drug discovery, a long and complex process of about 10 years that includes many stages, the first of which is often called early drug discovery.[4] At this stage, a number of hits requires a fast validation through virtual screening and/or high throughput screening (HTS) to assess possible chemical and structural interactions that determine the efficacy and biological performance, and therefore to unveil potential drug candidates.[4,5] Often, drug candidates, independently of their target, are compounds expected to pass the mucus.[3] Mimicking the whole

[a] Department of Chemistry, Materials and Chemical Engineering "Giulio Natta" at Politecnico di Milano, Milan, Italy. E-mail: paola.petrini@polimi.it

[b] Molecular Biotechnology and Health Sciences Department, University of Torino, Torino, Italy. E-mail: sonja.visentin@unito.it

[c] Department of Informatics, Bioengineering, Robotics and Systems Engineering, University of Genova, Genova, Italy

[d] Molecular Medicine Department (DMM), Center for Health Technologies (CHT), UdR INSTM, University of Pavia, Pavia, Italy

[e] Department of Occupational Medicine, Toxicology and Environmental Risks, Istituti Clinici Scientifici (ICS) Maugeri, IRCCS, Pavia, Italy

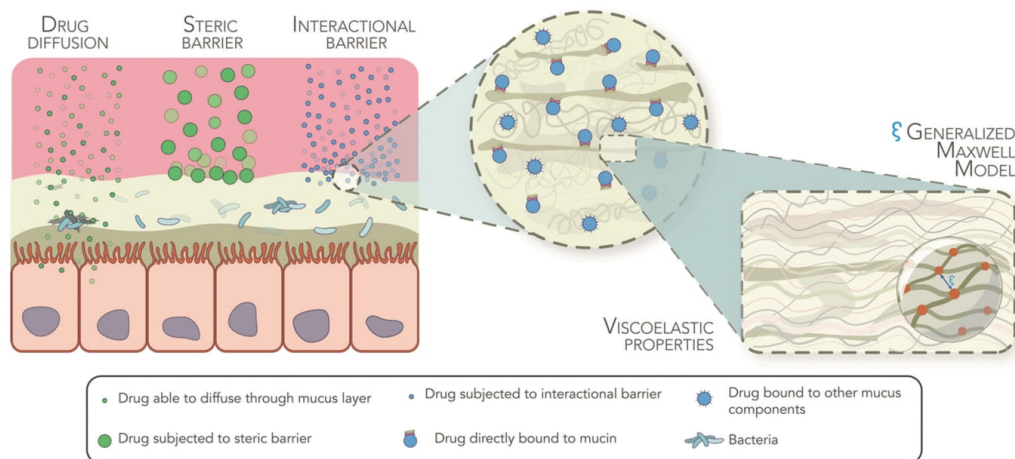† Electronic supplementary information (ESI) available. See DOI: 10.1039/c9tb00957d

4940 | *J. Mater. Chem. B*, 2019, **7**, 4940–4952

This journal is © The Royal Society of Chemistry 2019

71

Fig. 1 Steric and interactive barriers of airway mucus. Particles able to entangle with mucus components are subjected to the interactional barrier of mucus (blue circles, right); diffusion of particles bigger than the size of the mesh between mucin fibbers is hampered by the steric barrier of mucus (green circles, centre); particles not subjected to any of the barriers imposed by mucus freely diffuse through the mucus layer (green circles, left).

complexity of the *in vivo* scenario is a challenge far from being met. Yet, it is now time to provide pharmaceutical companies with a standard protocol for the production of relevant mucus models for early drug discovery.

Mucus hypersecretion with altered chemical and structural features has been observed in many diseases such as bronchial asthma, chronic obstructive pulmonary disease (COPD), bronchiectasis and cystic fibrosis (CF), in which patients suffer from chronic lung inflammation.[6] CF is a genetic disease that results in the production of thick and viscous mucus secretions in multiple organs. Due to abnormal chloride and HCO_3^- transport and chronic inflammatory states, the CF mucus composition entails a polymeric network made of mucin,[7] albumin[8] and extracellular DNA,[7] increased concentration of calcium (Ca^{2+}) ions,[9] and the presence of alginate produced by *Pseudomonas aeruginosa*.[10,11] At the structural level, this pathological chemical cocktail is translated in the presence of a thick (50–400 μm)[9] gel-like structure with significantly smaller mesh size (90–190 nm)[12] with respect to physiological mucus (497–503 nm).[13] These molecular interactions generate CF mucus exhibiting shear-thinning behaviour with increased viscosity, storage (G') and loss moduli (G'') compared to physiological mucus.[14] Ultimately, drug diffusion and mucus clearance mechanisms are hampered and bacteria find a suitable environment to establish and proliferate that results in lung failure. Different studies have reported chemical binding of different entities to mucin that has a direct influence over nanoparticle penetration[15,16] and reduced antibacterial potential of colistin,[17] among others.[18] Sputum – expectorated mass that contains mucus, blood, saliva, among others – is often considered as a first rough *ex vivo* model of CF mucus due to the low invasiveness to retrieve it when compared to physiological mucus. However, CF sputum contains contaminants, and exhibits low reproducibility, low stability and time-dependent

properties due to both degradation by enzymes present on saliva and molecular disruption by the employed extraction procedure.[19]

Current *in vitro* mucus models used, at the research level, during drug screening either rely on mucin-based solutions or mucin-based structures. Some examples include viscous solutions, such as pseudogels, of commercial mucins,[20] mucin solutions mixed with bovine serum albumin[21] and calf thymus DNA,[9] linoleic acid, cholesterol, phosphatidylcholine and pig serum albumin,[22] polyacrylic acid (PAA) gels,[23,24] locust bean gum,[25] and complex mixtures of salmon DNA, egg yolk emulsion, mucin and salts.[26] Another model proposes *N*-acryloyl-D-glucosamine, a glycopolymer, to model the glycoproteins that are prevalent in mucus–mucins, and 2-hydroxyethylmethacrylate.[27] Yet, mucus-based solutions fail to model the steric barrier of CF mucus, dependent on its mesh size and viscoelastic properties, while those models that reproduce the viscoelastic properties of CF mucus include exogenous compounds that can induce false chemical–physical interactions with drugs and other substances (Table S1, ESI†).

In our *in vitro* mucus models, we aim to disassemble the complex situation by adopting a modular approach that, when put together, gives more realistic information of drug diffusion through mucus. With this in mind, a mucus model was developed that simplifies the complexity by mimicking the chemical composition, structural features and viscoelastic properties of CF mucus and their impact on drug diffusion was further studied. In this way, a hydrogel composed of mucin and alginate (Alg) – components present in CF mucus – was developed. The viscoelastic properties were modelled by controlling the degree of crosslinking of Alg using Ca^{2+} ions, while the chemical composition was tuned by including mucin, Alg, sodium chloride (NaCl) and Ca^{2+} ions within the range of concentrations reported for CF mucus. The ability of the mucin/Alg hydrogels to model the viscoelastic

This journal is © The Royal Society of Chemistry 2019

J. Mater. Chem. B, 2019, **7**, 4940–4952 | **4941**

72

properties was studied through rheological analysis, whose results were further fitted within the Generalized Maxwell Model (GMM) aiming at estimating the mesh size of the hydrogels. The mucus model was further coupled to a PAMPA membrane, and its interactive and steric barrier ability was investigated by testing different drugs with different solubilities, sizes, charges at pH 7.4 and reported degrees of interaction with mucin.

2 Materials and methods

2.1 Materials

Mucin from porcine stomach type III (M1778, lot 84082-64-4), sodium salt of alginic acid (Alg, 180947, lot MKBJ0727V), calcium carbonate ($CaCO_3$), D-(+)-gluconic acid δ-lactone $\geq 99.0\%$ (GDL) and NaCl used to develop the airway mucus model were all purchased from Merck (Germany). All aqueous solutions and suspensions were prepared using distilled water (dH_2O). Potassium phosphate dibasic (K_2HPO_4), potassium phosphate monobasic (KH_2PO_4), and dimethyl sulfoxide (DMSO) were also supplied by Merck to produce the different stability media. Drug diffusion tests were performed using acetylsalicylic acid (CAS# 50-78-2), cephalexin (CAS# 23325-78-2) and epirubicin hydrochloride (CAS# 56390-09-1), which were supplied by Merck.

2.2 Development of an airway pathological mucus model

Mucin/Alg hydrogels were developed by taking advantage of the internal gelation of Alg by Ca^{2+} ions, in a three-step process. In this way, sodium salt of alginic acid was dissolved at different concentrations (14, 21 and 35 mg ml^{-1}) in NaCl solution (16.3 mg ml^{-1}), under slow magnetic agitation for 12 hours. In parallel, a mucin solution (43.75 mg ml^{-1}) was prepared in dH_2O and left under slow agitation for 12 hours. Both Alg and mucin solutions were mixed at a 1:4 proportion using the double syringe method (step 1). A suspension made of $CaCO_3$ (7 mg ml^{-1}) in NaCl solution (16.3 mg ml^{-1}) was sonicated (UP200S, Ultrasonic Processor, Hielscher, Ultrasound Technology) for 5 min, centrifuged (Vortex IKA MS3 Orbital Shaker 100–240 V) at 3500 rpm for 1 min, and further mixed with the solution prepared in step 1 in a 1:5 proportion (step 2). Finally, a GDL solution (10 mg ml^{-1}) was prepared in NaCl (16.3 mg ml^{-1}) and mixed with the solution prepared in step 2 in a proportion of 1:6.

Alg hydrogels were also prepared by substituting the mucin solution by the same volume of dH_2O in step 1, and these formulations served as the basis to tailor viscoelastic properties to match those of CF sputum, as well as controls in the drug diffusion studies to discriminate between mucin–drug and possible Alg–drug interactions.

2.3 Physiochemical characterization

2.3.1 Rheological characterization. Rheological measurements were performed using a rotational rheometer (AR-1500 TA Instruments, UK) coupled to a cone-plate geometry (diameter: 20 mm, cone angle: 1.023°, truncation 32 μm), at 25 °C. First, the linear viscoelastic region of Alg hydrogels was determined by

a strain sweep test ranging from 0.1 to 1000%, at an oscillatory frequency of 1 Hz ($\omega = 2\pi f = 6.28$ rad s^{-1}) and was found to be 0.1–10%. The storage component (G', Pa) and loss component (G'', Pa) of the complex modulus (G^*, Pa), complex viscosity (η^*, Pa s) and tan δ (G''/G') of both Alg and mucin/Alg hydrogels were determined through oscillatory frequency sweep measurements. The frequency sweep was performed at a strain amplitude of 1% (accordingly to LVR results), with a logarithmic increasing of frequency set between 0.05 ($\omega = 0.314$ rad s^{-1}) and 20 Hz ($\omega = 125.7$ rad s^{-1}), to include the ciliary beat frequency (10–15 Hz) and breathing rate (0.5 Hz).[28–30] All rheological tests were conducted in triplicate, and Trios Software v3.3 TA Instruments was used for data acquisition and analysis.

2.3.2 Stability assay. Hydrogels with a diameter of 12 mm and thickness of 0.5 mm of each formulation were immersed in different media (4 ml), including dH_2O, 1% DMSO, and phosphate buffered saline (PBS, 7.4, composed of 244 g ml^{-1} of K_2HPO_4 and 76 g ml^{-1} of KH_2PO_4). After 24 hours of preparation, stability assessment took place at 25 °C. At pre-determined time points, namely 0.25, 0.5, 1, 2, 4 and 6 hours, each sample was weighed (analytical balance A&D HR-60, USA) and photographed. The weight variation $w(\%)$ was evaluated as:

$$w(\%) = \frac{w(t) - w(0)}{w(0)} \times 100 \tag{1}$$

where $w(t)$ is the weight of the hydrated sample evaluated after time (t) of immersion, and $w(0)$ is the initial weight of the respective sample. The photographic images were further processed with ImageJ (32bit) to evaluate the variation in thickness of the sample due to contact with the media. The change of the thickness (h) was determined as:

$$h(\%) = \frac{h(t) - h(0)}{h(0)} \times 100 \tag{2}$$

where $h(t)$ is the thickness of the sample immersed in the medium after time (t) and $h(0)$ is the initial thickness prior to immersion.

2.3.3 Drug diffusion through the airway mucus model. Upon optimization of chemical composition and viscoelastic properties, a mucin/Alg hydrogel (Muc/Alg 3) composed of mucin (25 mg ml^{-1}) and Alg (3 mg ml^{-1}) exhibited superior ability to model the chemical–physical interactions and viscoelastic properties of CF mucus, and therefore was selected as an airway mucus model to proceed to the drug diffusion studies. Drug diffusion studies were conducted following the parallel artificial membrane permeability assay (PAMPA; Corning® Gentest™ Pre-coated PAMPA, 353015, USA), with a porosity of 0.45 μm and inner diameter equal to 7.1 mm, and the PAMPA membranes were considered as controls to discriminate between possible drug–mucus model interactions. Different drugs were tested, including acetylsalicylic acid, cephalexin, and epirubicin. To do so, solutions of acetylsalicylic acid (20 mM), cephalexin (20 mM) and epirubicin (1 mM) were prepared by dissolving the powder in DMSO and subsequently diluting with 2 mM PBS.

Prior to drug diffusion tests, the airway mucus models were prepared over the PAMPA membrane, producing a hydrogel of

4942 | J. Mater. Chem. B, 2019, **7**, 4940–4952

This journal is © The Royal Society of Chemistry 2019

approximately 500 μm thickness, and left to crosslink for 24 hours. The donor compartment was then filled with the relevant drug solution (200 μl) and its diffusion was evaluated for up to 6 hours. At defined time points, all release media were collected, and an equivalent amount of fresh PBS was added. Optical densities of acetylsalicylic acid, cephalexin and epirubicin were measured at 267, 261, and 483 nm, respectively, by UV-vis spectroscopy (Double Beam Spectrophotometer Hitachi UH5300, Japan) and quantified using their relevant calibration curves. The amount of drug released was calculated as follows:

$$\%\text{Drug released} = \frac{C(t)}{C(0)} \times 100 \qquad (3)$$

where $C(t)$ denotes the concentration of drug released at time t and $C(0)$ represents the initial concentration introduced into the donor compartment.

The apparent permeability coefficient (Papp) was also calculated according to eqn (4), where dC/dt is the drug permeation rate, V is the volume of drug introduced into the donor compartment, A is the surface area and $C(0)$ represents the initial concentration introduced into the donor compartment.

$$P_{\text{app}} = \frac{dC}{dt} \times \frac{V}{A \times C_0} \qquad (4)$$

2.4 Statistical analysis

The results of at least three independent experiments are presented as mean $\pm$ standard deviation (SD). Statistical analysis was performed using the Student's t-test and ANOVA calculated using GraphPad Prism version 6 (GraphPad Software, USA). Significance differences were set for $*P < 0.05$.

3 Results and discussion

Mucus confers a protective barrier that is selective towards molecules, gases and bacteria. Yet, diseases like bronchial asthma, COPD, bronchiectasis and CF lead to altered visco-elastic properties and chemical compositions, which produce an even stronger barrier towards the diffusion of drugs and particles, and therefore unsuccessful pharmacological treatment. The need to characterize drug behaviour in pathological mucus during drug formulation, design and optimization has urged the development of mucus models. A mucin/Alg-based airway mucus model that reproduces the chemical–physical properties of CF mucus was developed, envisioned as a fast, simple and reproducible tool for pharmacological screening. In this regard, commercial mucin from porcine stomach was selected owing to its structural similarity to tracheobronchial mucins,[31] although some differences are present.[32] Commercial mucins are cheaper, easily available, and exhibit higher standardization with respect to laboratory isolated mucins. Owing to the extraction/purification process, commercial mucins are not able to form gels at physiological pH, because they lose their ability to form disulphide bonds.[33] Yet, it has also been reported that *P. aeruginosa* exhibits sulfatase activity, which upon infection enables it to degrade mucins present in CF mucus and further use its by-products as

carbon and sulphur sources for growth.[34,35] Therefore, degraded mucins, such as commercial mucins, possibly represent a step forward on modelling the inflammatory situation encountered in pathological conditions, while offering a consistent source to develop mucus models. The concentration of mucin within the mucus model was set at 25 mg ml^{-1}, since its concentration in CF mucus has been reported from 11 to 27 mg ml^{-1}.[36,37] Taking into consideration the composition of CF mucus, Alg (present in the mucus at a concentration of 0.2–2.5 mg ml^{-1} due to *P. aeruginosa* infections[10,11]) was used as the base material to tailor the visco-elastic properties of the pathological mucus model. At a first stage, Alg hydrogels were produced by varying the concentration of both Alg and Ca^{2+} ions until comparable viscoelastic properties were attained. Afterwards, mucin was added to the formulation of Alg hydrogels aiming at enhancing its similarity to CF mucus composition. All formulations were prepared within a saline environment (NaCl), for which the final concentration was set at 7.07 mg ml^{-1} as reported in the literature for CF mucus.[38]

3.1 Alginate hydrogels

Alginate (Alg) hydrogels have long been proposed for drug delivery[39,40] and tissue engineering applications,[41,42] as well as bioinks.[43,44] Alg and mucin have been previously mixed to disclose the mechanism of interaction relevant in CF.[45,46] On the basis of this knowledge, we propose the combination of mucin and Alg in a hydrogel to produce models of CF mucus. Alg is a linear anionic polysaccharide formed by the repetition of 1,4-β-D-mannuronate (M) units and α-L-glucuronate (G) residues.[47] Owing to the presence of carboxyl groups, Alg is able to crosslink in the presence of divalent cations, such as Ca^{2+} ions, at neutral pH, generating a hydrogel whose resultant viscoelastic properties depend on the M/G ratio and molecular weight.[47,48] It is well-known that the presence of alginate within CF mucus increases both storage and loss moduli, and viscosity, which can be partly justified by the high content of Ca^{2+} ions within CF mucus that can further interact with Alg and increase the final viscoelastic properties.[49] Similarly, the concentration of Alg plays a crucial role in the final viscoelastic properties of the mucus model, since its formation is based on the ability of Alg to crosslink in the presence of Ca^{2+} ions.[48] With this in mind, extensive rheological characterization was conducted to assess storage (G', Pa) and loss components (G'', Pa), of the complex modulus (G^*, Pa), $\tan\delta$, as well as complex viscosity (η^*, Pa s), and further compared to the viscoelastic characterization reported by Yuan *et al.* for CF sputum.[14] Different concentrations of Alg were tested and denominated as Alg 2, Alg 3 and Alg 5, for the sake of simplicity, which correspond to a final Alg concentration of 2, 3 and 5 mg ml^{-1}, respectively.

3.1.1 Rheological characterization. Rheological characterization of hydrogels gives important insights into property–structure relationships, which can be useful to predict and correlate diffusion mechanisms of different molecules, as well as to foresee their impact over clearance mechanisms. The viscoelastic behaviour of a material can be investigated by $\tan\delta$, which is defined as the ratio of G''/G'. If $\tan\delta > 1$, the material has predominant viscous behaviour, while materials with $\tan\delta < 1$

This journal is © The Royal Society of Chemistry 2019

J. Mater. Chem. B, 2019, 7, 4940–4952 | 4943

74

predominantly exhibit elastic behaviour.[50] CF mucus exhibits gel-like behaviour with a predominant elastic component ($\tan\delta < 1$) (Fig. 2a), which means that the ciliary beating stretches the mucus rather than making it flow, resulting in mucus accumulation in the airways.[9] Like CF mucus, all developed Alg hydrogels exhibit $\tan\delta < 1$, and therefore predominant elastic behaviour (Fig. 2a) possibly associated with both crosslinking sites and entrapped entanglements.[51]

CF mucus displays a shear-thinning behaviour, meaning that its complex viscosity decreases with increased frequency.[14] All Alg hydrogels showed comparable viscoelastic behaviour with a complex viscosity decreasing with frequency (Fig. 2c and d). The complex viscosity exhibited dependency on Alg concentration. Still, no significant differences were observed between the complex viscosity of Alg 2 and Alg 3 hydrogels and CF sputum at all investigated frequencies (Fig. 2c and d). The variation of G' and G'' with frequency is recognized as the "mechanical spectrum" of the structure. In Alg hydrogels, G' is dependent on the balance between Alg and Ca^{2+} ion concentration and the amount of water retained in the mesh, while G'' depends on the sliding of Alg chains over each other.[52,53] A closer examination at both breathing (~ 0.5 Hz) and ciliary beating frequencies (~ 10 Hz) revealed that both Alg 2 and Alg 3 hydrogels better model the viscoelastic features of CF sputum (Fig. 2c and d).[14,28–30,54]

Both storage and loss components of the complex modulus were of the same order of magnitude as those reported by Fernández Farréz and co-workers, for Alg hydrogels made of 10 mg ml^{-1} Alg, whose G' ranged from 93.5 to 158 Pa, while G'' oscillated from approximately 19.5 to 51.9 Pa.[55] Yet, all the developed Alg hydrogels showed a higher value for the complex modulus, G^*, and were therefore stiffer than the CF sputum. This is especially true for Alg 5 hydrogels, which also fail to model η^* and G' at the breathing rate frequency, as well as G' at the ciliary beating frequency (Fig. 2c and d).

3.1.2 Stability assay. The airway mucus model is expected to incorporate a high content of water, between 90–99%, owing to the interaction of Alg with Ca^{2+} ions that enables both its crosslinking and swelling. Considering that during drug screening, drugs can be dissolved in different media, the stability of the different Alg hydrogels was assessed at 25 °C in dH_2O, PBS and 1% DMSO over a period of 6 hours (Fig. 3). Stability was assessed regarding weight and thickness variations, as these are crucial features to guarantee suitable drug testing. After 6 hours, the percentage of weight variation exhibited three distinct behaviours according to the Alg hydrogel composition. When in contact with dH_2O, PBS or 1% DMSO, Alg hydrogels showed that the swelling degree depends on Alg concentration, which not only affects the viscoelastic properties, but also the

Fig. 2 Rheological characterization in frequency sweep mode of Alg hydrogels and CF sputum. (a) $\tan\delta$; and (b) complex modulus (G^*, Pa s).[9,14] η^* (Pa s), G' (Pa) and G'' (Pa) at (c) breathing frequency (~ 0.5 Hz); and (d) ciliary beating frequency (~ 10 Hz). Significant differences were set for *$p < 0.05$; **$p < 0.01$; ***$p < 0.001$; ****$p < 0.0001$. Alg 2, Alg 3 and Alg 5 hydrogels are depicted in green, red and blue, respectively, while CF sputum corresponds to black.

4944 | J. Mater. Chem. B, 2019, 7, 4940–4952

This journal is © The Royal Society of Chemistry 2019

75

Fig. 3 Stability assessment of different Alg hydrogels. (a) Percentage of weight variation w(%); (b) percentage of thickness variation h (%); and (c) G' (Pa) on dH_2O, PBS and 1% DMSO, after 6 hours of incubation, at 25 °C. Significant differences were set for *$p < 0.05$; **$p < 0.01$; ***$p < 0.001$; ****$p < 0.0001$. Alg 2, Alg 3 and Alg 5 hydrogels are depicted in green, red and blue, respectively.

hydrogel stability. The decreased percentage of weight and thickness of Alg 2 hydrogels might be related to the loss of material up to 6 hours of incubation, which was also observed on Alg 5 hydrogels immersed in 1% DMSO (Fig. 3a). On the other hand, Alg 5 hydrogels showed increased percentage of weight and thickness when incubated in dH_2O and PBS, possibly associated with swelling phenomena. Alg 3 hydrogels exhibited superior stability in all media in terms of weight and thickness, when compared to the other Alg hydrogels (Fig. 3).

Increased concentrations of Alg led to an increase of the solid-like characteristic over the viscous behaviour (Fig. 2c) indicating increased crosslinking degree with increased Alg concentrations. By further increasing the concentration of Alg (Fig. S1, ESI†) this trend is clearly observable. Thus, the hydrogel containing the lowest concentration of alginate was the least stable in all the studied media, with a significant decrease of weight and thickness, indicating mass loss, concomitant with a significant decrease of G', indicating the weakening of the structure. This result is consistent with Alg 2 being the least crosslinked hydrogel (tan δ = 0.165 with respect to 0.123 and 0.103 of Alg 3 and Alg 5 hydrogels, respectively; Fig. 2a).

Minimal variations were observed for the intermediate concentrations with a nonsignificant effect on the rheological properties, thus indicating a slight mass loss while retaining the bulk properties (Fig. 3c). A complex situation is observed for Alg 5. Different phenomena may occur during immersion of this hydrogel: the weight and the thickness increase due to the swelling of the hydrogels. The swelling of the hydrogels in water and PBS differs accounting for the different ionic strengths which equilibrates with the salt contents within the hydrogel. Surprisingly, the G' of the hydrogels is not affected by the increased water content (Fig. 3c).

3.2 Mucin/alginate hydrogels

3.2.1 Rheological characterization. Aiming at closely modelling the chemical composition of CF mucus, mucin was added to Alg 2, Alg 3 and Alg 5 hydrogels, at a final concentration of 25 mg ml^{-1}. The addition of mucin (Muc/Alg 2, Muc/Alg 3 and Muc/Alg 5 hydrogels) was followed by rheological characterization to analyse possible structural changes (Fig. 4). The tan δ of the Muc/Alg hydrogels better represented those of CF sputum than that of Alg hydrogels alone, independently of Alg content (Fig. 4a).[50] The addition of mucin differently impacted the final viscoelastic properties of Muc/Alg hydrogels. The viscoelastic properties of Muc/Alg 2 hydrogels were barely affected by the presence of mucin. Yet, the presence of mucin within Muc/Alg 3 hydrogels resulted in greater G'' (Fig. 4c and d). Finally, Muc/Alg 5 hydrogels presented decreased $G*$, $\eta*$ and G', which can hint some degree of interaction between mucin and Alg (Fig. 4b–d). In Muc/Alg hydrogels, in which the concentration of Alg is 2 or 3 mg ml^{-1}, mucin seems to be homogeneously distributed and non-interacting so that, when submitted to deformation, it slides on the crosslinked Alg chains. Nevertheless, for Muc/Alg 5 hydrogels, possible electrostatic interactions might have occurred between mucin and Alg.[45,49] It has been shown that mucin interactions with the carboxyl groups of Alg are promoted by the presence of NaCl, while possible hydrogen bonds and van der Waals interactions associated with the mannuronic acid unit of the Alg backbone might occur.[45,46,49,56] This is in accordance with the adhesion studies between alginate and commercial mucins reported by Popeski-Dimovski.[46] Previous studies have also shown that mucin and alginate are able to interact when in solution to form gels. Yet, these studies employ purified mucins, instead of commercial mucins, which retain their ability to interact under physiological conditions.[45,49] However, as previously mentioned, purified mucins are harder to obtain and present interindividual variability that results in varied chemical compositions and viscoelastic properties, and therefore they are not suitable for the development of standard mucus models to be routinely adopted by pharmaceutical companies for drug diffusion studies.

Mucus models with viscoelastic properties that match those of pathological mucus were obtained by mimicking the constituents of CF mucus, which include Alg, mucin, NaCl and Ca^{2+} ions. From the viscoelastic point of view, both Muc/Alg 2 and Muc/Alg 3 hydrogels provide viscoelastic properties that match those of CF sputum (Fig. 4). Additionally, the viscoelastic
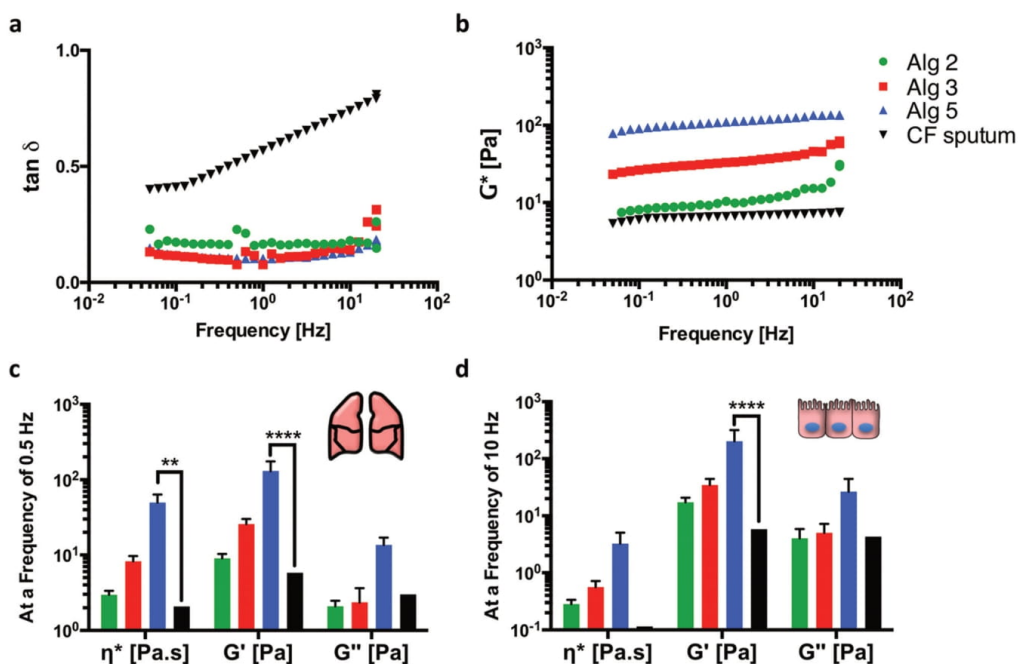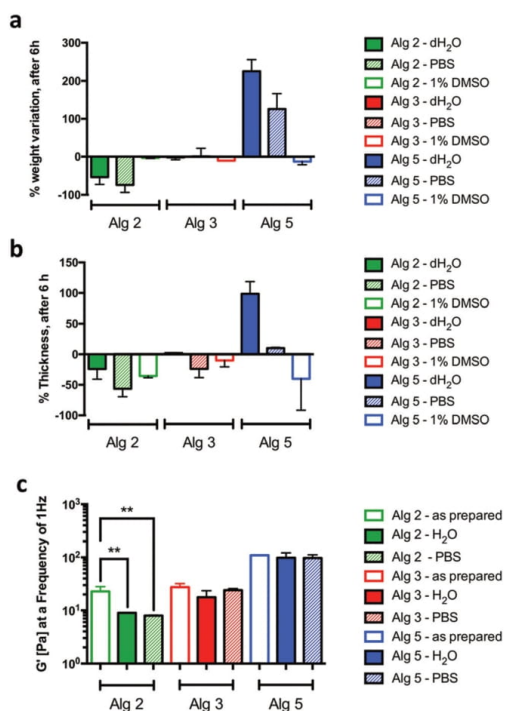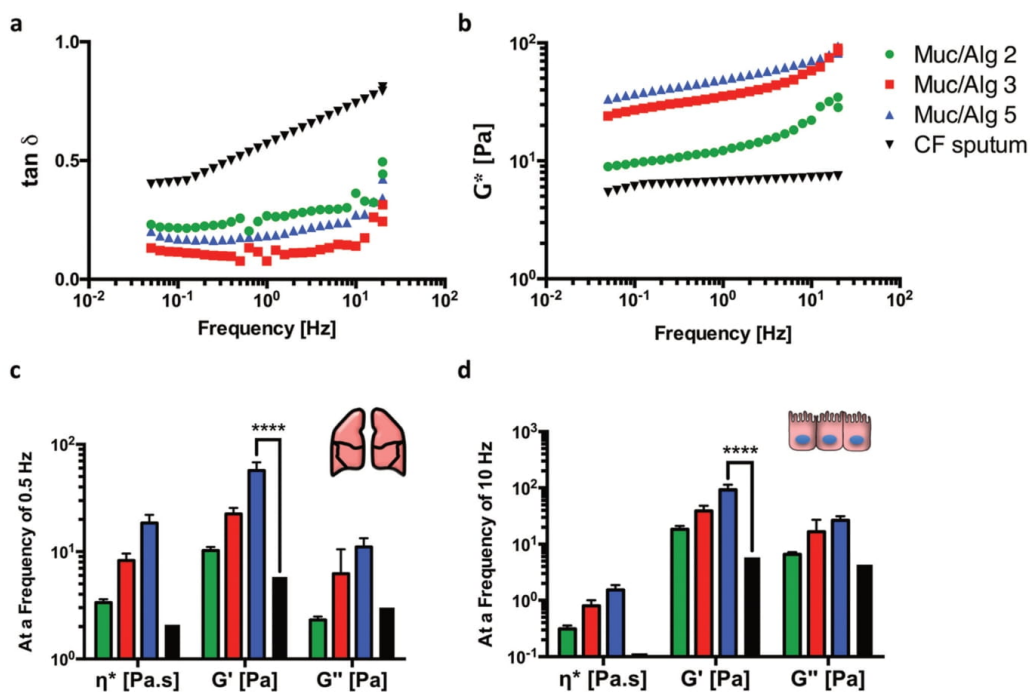
Fig. 4 Rheological characterization in frequency sweep mode of Muc/Alg hydrogels, Alg hydrogels and CF sputum. (a) tan δ; and (b) complex modulus (G^*, Pa s).[9,14] η^* (Pa s), G' (Pa) and G'' (Pa) at (c) breathing frequency (~0.5 Hz); and (d) ciliary beating frequency (~10 Hz). Significant differences were set for $*p < 0.05$; $**p < 0.01$; $***p < 0.001$; $****p < 0.0001$. Muc/Alg 2, Muc/Alg 3 and Muc/Alg 5 hydrogels are depicted in green, red and blue, respectively, while CF sputum corresponds to black.

properties of the airway mucus of COPD and asthma patients are comparable to those of CF sputum, and therefore the developed platforms can find a wider spectrum of applications.[12] Previously, purified pig gastric mucin, DNA and bovine serum albumin were exploited as CF mucus models, though their properties differed in terms of viscoelastic behaviour and magnitude.[9]

Previously developed mucus models rely on the addition of synthetic compounds to tailor the viscoelastic properties to match those of CF sputum. A mixture of autoclaved mucin, albumin, DNA, amino acids and pentetic acid showed a similar storage modulus to both Muc/Alg 2 and Muc/Alg 3 hydrogels.[26] Pentetic acid is a highly interactive molecule that possesses many available interaction sites and is not present in CF sputum. Additionally, no information regarding η^* and G'' is given, which are important parameters to evaluate the diffusion and clearance of mucus. Boegh et al. have also proposed a mucus model composed of PAA, mucin and a lipid/protein mixture, whose rheological properties match the viscoelastic properties of porcine intestinal mucus.[23] Similar results were obtained using locust bean gum as the base material to tailor the viscoelastic properties,[25] but neither locust bean gum nor PAA is present in the pathological or physiological mucus, which limits their application since these can also contribute to the final steric barrier.

3.2.2 Determination of mesh size by applying the generalized Maxwell model (GMM). The viscoelastic features are associated with crosslinking and entanglement degrees, as well as chemical interactions between the different components present in the structure. Consequently, rheological data can be employed to get information on the mesh size associated with the viscoelastic properties of hydrogels, which can be further correlated with steric hindrance during diffusion processes. The mesh size is defined as the linear distance between two crosslinking sites. The results of the frequency sweep analysis of the mucus models were further interpreted in terms of the GMM, which describes the viscoelastic response of the hydrogel as a combination of a series of (elastic) springs and (viscous) dashpots in parallel with an additional spring, as previously described by Turco et al.[57] Both G' and G'' can be modelled as a function of the frequency according to the following equations:

$$G' = G_e + \sum_{i=1}^{n} G_i \frac{(\lambda_i \omega)^2}{1 + (\lambda_i \omega)^2}; \, G_i = \frac{\eta_i}{\lambda_i} \qquad (5)$$

$$G'' = \sum_{i=1}^{n} G_i \frac{\lambda_i \omega}{1 + (\lambda_i \omega)^2}; \, G_i = \frac{\eta_i}{\lambda_i} \qquad (6)$$

where n is the number of Maxwell elements considered, G_i, η_i and λ_i represent the spring constant, the dashpot viscosity, and the relaxation time of the i-th Maxwell element, respectively. G_e is the spring constant of the additional spring element. In order to decrease the complexity of fitting, the number of fitting parameters was reduced by imposing the condition that the relaxation time of each subsequent parallel element was 10 times smaller than that of the preceding one, in agreement with the proposal of Turco $et\ al.$[57] Therefore, the parameters of the model are G_e, G_i, and λ_1. The GMM was applied to fit the experimental data using five elements ($i = 5$), which minimized the error defined as:

$$\text{err} = \sum \left[\left(G_{\text{exp}}' - G_{\text{model}}' \right)^2 \right] \qquad (7)$$

The adoption of GMM allows determining the materials' shear modulus after relaxation (G_∞) as:

$$G_\infty = G_e + \sum_i^n G_i \qquad (8)$$

This corresponds to the shear modulus of a rubbery material and hence, from the Rubber Elasticity Theory, it can be related to the average mesh size (ξ)[57,58] according to the following equation:

$$\xi = \sqrt[3]{\frac{6\beta RT}{\pi N_A G}} \qquad (9)$$

where β is the front factor (equal to 1 assuming an ideal rubber model), R is the universal gas constant, T is the absolute temperature, and N_A is the Avogadro constant. The obtained G_∞ and ξ are presented in Table 1 (Fig. S3, ESI†).

The estimated mesh size by applying the GMM varied according to the Alg concentration and the presence or absence of mucin (Table 1 and Fig. S3, ESI†). The estimated mesh size decreased with increasing Alg concentration. Upon addition of mucin, no significant differences in mesh size were detected for Muc/Alg 3 and Muc/Alg 5 hydrogels, yet Muc/Alg 2 presented a larger mesh size upon addition of mucin (Table 1). The shear modulus was found to increase with the concentration of Alg in the presence or absence of mucin ($G_\infty \propto$ Alg concentration$^{0.812}$ and $G_\infty \propto$ Muc/Alg concentration$^{1.89}$), which was also observed for the estimated mesh size ($\xi \propto$ Alg concentration$^{-0.249}$ and $\xi \propto$ Muc/Alg concentration$^{-0.630}$). The obtained magnitudes for the dependency of both shear modulus and mesh size corroborated those reported by Turco $et\ al.$[57] The Alg hydrogels developed by Turco $et\ al.$ displayed different viscoelastic properties than those presented here, and consequently a different mesh size. These differences may be related to a higher concentration of Alg and Ca^{2+} ions, as well as the presence of other ions (such as divalent ions present in HEPES), which can possibly interact with

the Alg backbone and increase the crosslinking density, and consequently result in a smaller mesh size (ranging from 3.3 to 5.1 nm dependent on Alg concentration). By applying the described method, Grassi and co-workers estimated that the mesh size of Alg hydrogels ranged from 7.70 to 22.0 nm, according to the Alg concentration.[58] Interestingly, Alg 5 hydrogels exhibited a mesh size of about 22.0 nm, which is not far from the size of the Alg 5 hydrogels developed here (~ 42.9 nm) (Fig. 4). The differences might be explained by the higher Ca^{2+} concentration that the authors employed and therefore higher probability of crosslinking. In a similar fashion, Alg hydrogels produced using 60 mg ml^{-1} of CaCl$_2$ displayed an estimated mesh size that ranged from 1 to 13 nm, from higher (120 mg ml^{-1}) to lower (10 mg ml^{-1}) Alg concentrations.[59] The smaller mesh size is probably related to high Ca^{2+} concentration and other ions that can be involved in the crosslinking.[57] Additionally, the mesh sizes estimated for the mucus models developed here were similar to those reported in the literature for pathological mucus (60–300 nm with an average between 90 and 190 nm).[12]

3.2.3 Stability assay.
The stability of Muc/Alg hydrogels was studied at 25 °C in dH$_2$O, PBS and 1% DMSO (Fig. 5). Like Alg 2 hydrogels, Muc/Alg 2 hydrogels present a decreased percentage of both weight and thickness variation either in dH$_2$O or PBS, while Muc/Alg 5 hydrogels showed an increased percentage of weight variation as observed for Alg 5 hydrogels (Fig. 3a and 5a). Similarly, Muc/Alg 3 hydrogels demonstrated greater stability with respect to weight and thickness variation (Fig. 5), and have therefore proven their applicability at least within 6 hours of experiment.

Rheological analyses were also performed at the end of the 6 hours for the Muc/Alg hydrogels to assess possible degradation (Fig. 5c). As previously observed for Alg 2 hydrogels (Fig. 3c), Muc/Alg 2 hydrogels were also susceptible to incubation in dH$_2$O and PBS (Fig. 5). The G' of Muc/Alg 2 hydrogels decreased from 21.9 Pa, as prepared, to 3.91 and 2.66 Pa after incubation in dH$_2$O and PBS, respectively. Interestingly, Muc/Alg 5 hydrogels were also affected by the incubation. In spite of increased weight and thickness after 6 hours of incubation, the G' of these hydrogels decreased from 56.1 Pa, as prepared, to 29.0 and 26.8 Pa when incubated in dH$_2$O and PBS, respectively. These findings corroborate the rheological results, as for Muc/Alg 5 hydrogels decreased G^*, η^* and G' were observed with respect to Alg 5 hydrogels, which was hypothesized to be associated with the interaction between mucin and Alg (Fig. 4b–d). The decreased G' after incubation might be linked to mucin loss through the incubation period. Muc/Alg 3 hydrogels, in their turn, did not display changes in G' showing their superiority to withstand incubation up to 6 hours (Fig. 5c).

The superior stability combined with their ability to model the viscoelastic properties of pathological airway mucus makes

Table 1 Mesh size (ξ) and shear modulus (G_∞) after fitting the GMM with the obtained rheological data of the developed mucus models

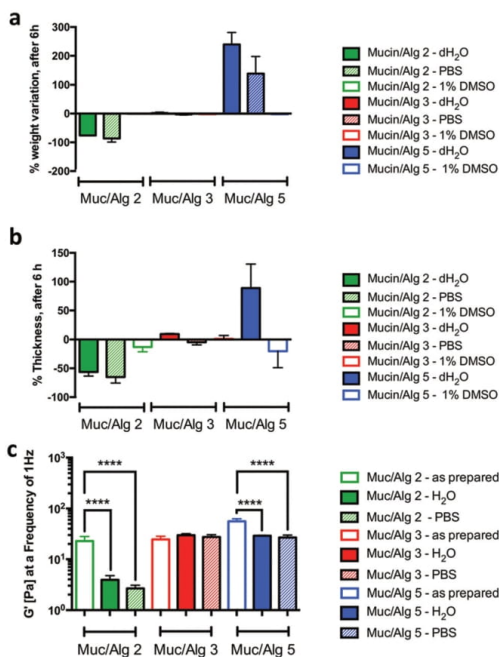|	Alg 2	Muc/Alg 2	Alg 3	Muc/Alg 3	Alg 5	Muc/Alg 5
Estimated ξ (nm) $\pm$ SD	53.7 $\pm$ 3.14	75.7 $\pm$ 1.67	50.7 $\pm$ 8.06	54.7 $\pm$ 5.35	42.9 $\pm$ 5.68	42.3 $\pm$ 1.21
G_∞ (Pa) $\pm$ SD	51.5 $\pm$ 8.66	18.1 $\pm$ 1.23	92.5 $\pm$ 27.2	49.3 $\pm$ 14.3	110 $\pm$ 18.0	104 $\pm$ 8.95

Fig. 5 Stability assessment of different Muc/Alg hydrogels. (a) Percentage of weight variation (w%); (b) percentage of thickness variation (h%); and (c) G' (Pa) on dH$_2$O, PBS and 1% DMSO, after 6 hours of incubation, at 25 °C. Significant differences were set for *$p < 0.05$; **$p < 0.01$; ***$p < 0.001$; ****$p < 0.0001$. Muc/Alg 2, Muc/Alg 3 and Muc/Alg 5 hydrogels are depicted in green, red and blue, respectively.

Muc/Alg 3 hydrogels the preferred candidate to serve as a platform for drug diffusion studies.

3.3 Drug diffusion through the airway mucus model

Passive diffusion is the predominant transport phenomenon experienced by drugs aiming at targeted tissues, and it involves going through both mucus and cell membranes. The diffusion of drugs depends on their permeability through both mucus and the lipid bilayer of epithelial cells. The PAMPA assay is a widely used high-throughput system that contains a lipid-infused artificial membrane and it was adopted, in this study, to simulate the passive transport characteristic of cell membranes. The PAMPA assay presents many advantages, such as it is cost-effective, easy- and ready-to-use, it has good reproducibility and good corroboration with the permeability studies conducted using Caco-2 cells, and ensures higher correlation of the obtained results across different laboratories.[60,61] Yet, the PAMPA assay cannot take into consideration the diffusion of drugs through mucus, which is dependent on the mucus viscoelastic properties, mesh size, drug–mucin interactions, and drug solubility. In this work, we propose a mucus model that can be easily coupled to the PAMPA membrane to get descriptive information on the steric and interactive effects relevant during drug diffusion through the mucus barrier.

Currently, there is no standardized protocol to test drug permeability across lung mucus, whose duration differs from study-to-study. Herein, we have studied the permeability up to 6 hours, as recent studies focused on the permeation of both drugs and drug delivery systems through CF sputum, porcine intestinal mucus, and intestinal mucus models have been conducted up to 2, 2.5, 4 and 6 hours.[12,23,62–65] As proof of concept, the diffusion of three different drugs, namely acetylsalicylic acid (ASA), cephalexin and epirubicin, was tested across the developed airway mucus model (Muc/Alg 3 hydrogels). The mucus model was prepared over the PAMPA membrane system, and after crosslinking the different drugs were deposited on top of the mucus model (donator). At specific time points the release medium was collected from the receptor chamber (Fig. 6a). Drug diffusion through the PAMPA membrane was studied as control.

Mucin–drug interactions influence drug pharmacokinetics by reducing drug absorption.[18] In this sense, three different drugs with different degrees of interaction with mucin, dimensions, solubilities in water, and charges at pH 7.4 were selected (Table 2). In a previous study, it was determined that the K_A of cephalexin shows a moderate interaction with mucin.[18] Following the published method, the K_A of both ASA and epirubicin was evaluated in solution, which revealed low and high interactions, respectively. The obtained original data are presented in Table 2. ASA did not show any interaction with mucin, in agreement with what was also observed for mucin solutions (Table 2), and rapidly diffused through the Muc/Alg 3 hydrogels. Its concentration in the receptor chamber after 6 hours was above 90% with no significant differences and a similar diffusion profile (Fig. 6b). In accordance to what was observed in solution, cephalexin was able to interact with the mucin present within the mucus model, and this resulted in a different diffusion profile than that of PAMPA membranes.[18] After 6 hours, the percentage of cephalexin on Muc/Alg 3 hydrogels was 19.5% in comparison to the PAMPA membranes (83.4%; Fig. 6b). The mucin–cephalexin interaction is mainly governed by van der Waals and hydrogen bonds.[18] Our results indicate that this interactive capability is retained by mucin when included in the mucus model. Finally, it was determined that epirubicin shows a strong interaction with mucin in solution (Table 2). Accordingly, in the presence of Muc/Alg 3 hydrogels, the diffusion of epirubicin was strongly hampered with a release of 1.6% with respect to 50.4%, the percentage of drug diffused across the PAMPA membrane (Fig. 6b).

To discriminate between the steric effect *versus* the interactive effect, we performed a parallel experiment in Transwell® supports (*i.e.* not employing PAMPA) in which we compared Alg3 hydrogels *versus* Muc/Alg 3 hydrogels (Fig. S4, ESI†). For ASA, no effects were observed for both hydrogels, indicating no interaction with either mucin or alginate. Cephalexin exhibits a mild interaction with mucin (Table 2) that, together with the higher molecular weight compared to ASA, may have played a role in reducing its mobility through both Alg 3 and Muc/Alg 3 hydrogels (Fig. S4, ESI†). The two hydrogels did not affect the diffusion in the same way (Fig. S4, ESI†), supporting the hypothesis that van der Waals interactions with mucin, described in solution[18] and observed in the diffusion studies conducted
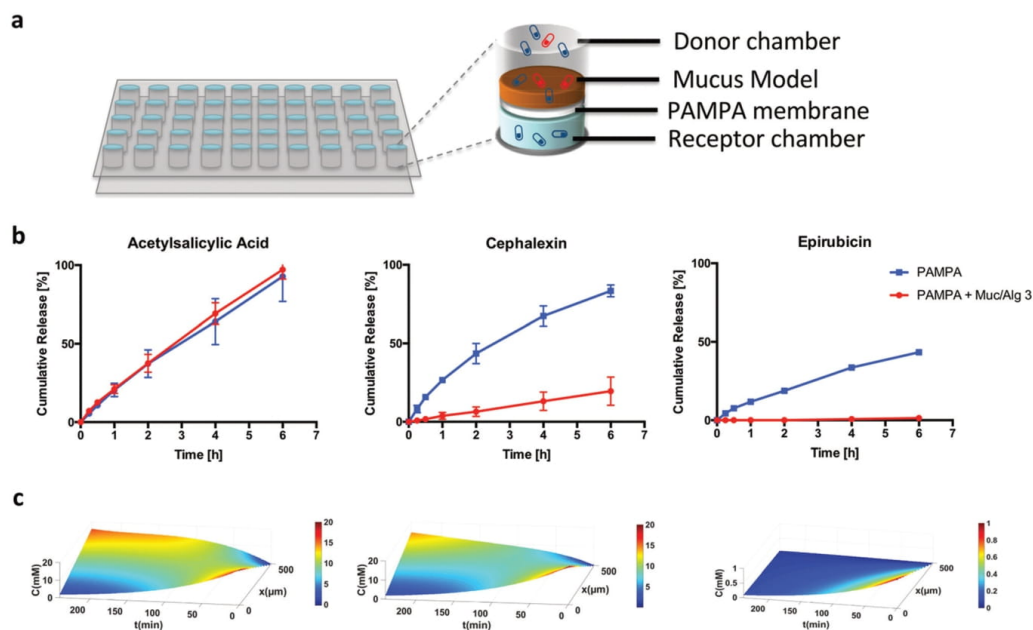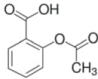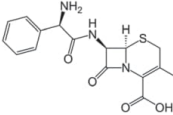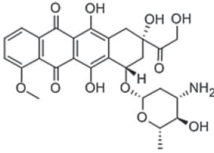
Fig. 6 Drug diffusion tests through the developed airway mucus model. (a) Drug diffusion experimental setup; (b) cumulative release of acetylsalicylic acid, cephalexin and epirubicin through the empty PAMPA plate (blue line) and in the presence of Muc/Alg 3 hydrogels (red line); and (c) mathematical model of the diffusion profile of the different drugs within the mucus model.

Table 2 Physicochemical features of acetylsalicylic acid (ASA), cephalexin and epirubicin. References are added for the data derived from previous work, while all the other data are original data obtained in this work

	Acetylsalicylic acid	Cephalexin	Epirubicin
Chemical structure			
Molecular weight (g mol^{-1})	180.159[69]	347.389[70]	543.529[71]
Charge at pH 7.4^a	100% negative	60% negative	80% positive
		40% zwitterion	20% zwitterion
Water solubility (mg ml^{-1})	4.60[69]	1.79[70]	0.0930[71]
van der Waals surface area^a	246	433	713
Constant of association with mucin (K_a) (M^{-1}) × 10^4	No interaction	0.610[18]	7.76
Constant of dissociation with mucin (K_d) (M) ×10^{-4}	No interaction	1.64[18]	0.130
P_{app} through PAMPA membrane (10^{-6} cm s^{-1})	26.6 ± 1.21	14.9 ± 2.50	9.07 ± 2.59
P_{app} through PAMPA membrane + Muc/Alg 3 (10^{-6} cm s^{-1})	25.8 ± 0.762	5.96 ± 2.95	0.640 ± 0.305

^{a} Both molecular weight and van der Waals surface area of acetylsalicylic acid, cephalexin and epirubicin were calculated using MarvinSketch 16.8.15.0 by ChemAxon (https://www.chemaxon.com).

through PAMPA + Muc/Alg 3 hydrogels (Fig. 6), could be involved in slowing down cephalexin diffusion. The high interaction of epirubicin with mucin resulted in a very low amount of epirubicin passing through the Muc/Alg 3 hydrogels. The comparison with the diffusion profile of hydrogels composed solely of Alg brings interesting points to discriminate the mucin

interaction from steric interaction. Although Alg 3 hydrogels reduced epirubicin diffusion, the major effects were seen when mucin is present in the model.

To better understand the diffusion profile of the different drugs through the mucus model, a mathematical model was developed based on the convection–diffusion equation (eqn (10)),

in which the diffusion force is mainly governed by a concentration gradient (Fig. 6c).

$$\frac{\partial C}{\partial t} = D\nabla^2 - \nabla(C \times v) \tag{10}$$

where C is the drug concentration at time t, D is the diffusion coefficient, ∇ is the Laplace operator (which has three coordinates, including x, y and z) and v is the velocity of the mucus model. Different mathematical models have been developed to study drug release from hydrogels when these are applied as drug delivery systems.[66,67] Yet, herein the aim of the developed mathematical model is to study the drug diffusion across the hydrogel, which acts as a barrier.[68] As in this study, the mucus does not move and the drugs only diffuse in the x direction of the orthonormal Cartesian reference system, the convection–diffusion equation was simplified into:

$$\frac{\partial c}{\partial t} = D\frac{\partial^2 c}{\partial x^2} \tag{11}$$

As boundary conditions it was considered that drug concentration in $x = 0$ (apical layer of the mucus model) changes with time in an exponential manner and the concentration in x equal to thickness is assumed to change as measured in drug diffusion tests and reported in Fig. 6b for each drug. The interpolation function takes into consideration the different behaviour of each drug in the mucus model. As initial conditions it was admitted that at $x = 0$ and $t = 0$ the concentration is equal to C_0 (initial concentration), while in all the other points (so $x \neq 0$) the concentration is 0 at $t = 0$. By applying the mathematical model, it is possible to assess the topographical drug diffusion profile inside of the mucus model (Fig. 6c). The drug diffusion profile of both ASA and cephalexin is similar, though a slower diffusion was observed for cephalexin, most probably related to its interaction with mucin.[18] The diffusion of epirubicin through the mucus model is extremely slow, with epirubicin retained in the upper layers of the mucus model (Fig. 6c). The nature of this interaction is unknown, although it can be hypothesised that the molecular weight, the high van der Waals area, and the positive charge at the considered pH (Table 2) could each play a role or synergistically contribute to the interaction. According to the present results, it is not possible to identify which is the determinant characteristic of the strong interaction of this drug with mucin.

4 Conclusions

Aiming at disassembling the complexity of mucus to provide an easy-to-use and easy-to-produce tool, we have developed a viscoelastic hydrogel, with mucin and alginate as major components, to model the compositional and structural features of mucus for early drug discovery. The mucus model can be easily coupled to state-of-the-art diffusion models (e.g. PAMPA membranes), expanding their potential to render a more realistic picture of drug diffusion through the mucus barrier. In fact, the proposed model was effective in discriminating between both steric and interactive barriers of mucus towards drugs selected for their different chemical–physical and dimensional characteristics.

The mesh size of the hydrogel, estimated by applying the generalized Maxwell model, corroborates the drug diffusion results, giving an insight into the diffusion mechanism. A mathematical model to represent the diffusion was developed to describe the drug diffusion profile through the proposed mucus model. In a broader sense, this set of combined experimental methods and mathematical modelling can be proposed for in depth characterization in the development of hydrogel-based *in vitro* models, whenever the viscoelastic properties, the mesh size, and the diffusion mechanisms are key features to be studied.

It is relevant to highlight that the production method allows easy incorporation, in a modular approach, of other components (e.g. albumin, phospholipids, among others) to further recreate the chemical composition of mucus, while allowing the determination of the contribution of each component to drug diffusion. The proposed mucus model can be exploited as a high throughput screening platform either for cystic fibrosis mucus or other pathological mucus, such as mucus of chronic obstructive pulmonary disease, which unveils its potential for a wider range of applications as a fast screening tool for early drug discovery.

Conflicts of interest

There are no conflicts to declare.

Acknowledgements

Notes and references

1 F. Taherali, F. Varum and A. W. Basit, *Adv. Drug Delivery Rev.*, 2018, **124**, 16–33.
2 A.-C. Groo and F. Lagarce, *Drug Discovery Today*, 2014, **19**, 1097–1108.
3 A. Lechanteur, J. das Neves and B. Sarmento, *Adv. Drug Delivery Rev.*, 2018, **124**, 50–63.
4 J. Hughes, S. Rees, S. Kalindjian and K. Philpott, *Br. J. Pharmacol.*, 2011, **162**, 1239–1249.
5 E. Lionta, G. Spyrou, D. Vassilatis and Z. Cournia, *Curr. Top. Med. Chem.*, 2014, **14**, 1923–1938.
6 J. V. Fahy and B. F. Dickey, *N. Engl. J. Med.*, 2010, **363**, 2233–2247.
7 V. J. Broughton-Head, J. R. Smith, J. Shur and J. K. Shute, *Pulm. Pharmacol. Ther.*, 2007, **20**, 708–717.
8 N. N. Sanders, E. V. A. N. Rompaey, S. C. D. E. Smedt and J. Demeester, *Crit. Care Med.*, 2001, **164**, 486–493.
9 P. G. Bhat, D. R. Flanagan and M. D. Donovan, *J. Pharm. Sci.*, 1996, **85**, 624–630.
10 C. A. McCaslin, D. N. Petrusca, C. Poirier, K. A. Serban, G. G. Anderson and I. Petrache, *J. Cystic Fibrosis*, 2015, **14**, 70–77.

4950 | *J. Mater. Chem. B*, 2019, **7**, 4940–4952

This journal is © The Royal Society of Chemistry 2019

81

11 S. M. Kreda, C. W. Davis and M. C. Rose, *Cold Spring Harbor Perspect. Med.*, 2012, **2**, a009589.

12 J. S. Suk, S. K. Lai, Y.-Y. Wang, L. M. Ensign, P. L. Zeitlin, M. P. Boyle and J. Hanes, *Biomaterials*, 2009, **30**, 2591–2597.

13 T. Yu, J. Chisholm, W. J. Choi, A. Anonuevo, S. Pulicare, W. Zhong, M. Chen, C. Fridley, S. K. Lai, L. M. Ensign, J. S. Suk and J. Hanes, *Adv. Healthcare Mater.*, 2016, **5**, 2745–2750.

14 S. Yuan, M. Hollinger, M. E. Lachowicz-Scroggins, S. C. Kerr, E. M. Dunican, B. M. Daniel, S. Ghosh, S. C. Erzurum, B. Willard, S. L. Hazen, X. Huang, S. D. Carrington, S. Oscarson and J. V. Fahy, *Sci. Transl. Med.*, 2015, **7**, 276ra27.

15 Q. Xu, L. M. Ensign, N. J. Boylan, A. Schön, X. Gong, J.-C. Yang, N. W. Lamb, S. Cai, T. Yu, E. Freire and J. Hanes, *ACS Nano*, 2015, **9**, 9217–9227.

16 N. Barbero, M. Coletti, F. Catalano and S. Visentin, *Int. J. Pharm.*, 2018, **535**, 438–443.

17 J. X. Huang, M. A. T. Blaskovich, R. Pelingon, S. Ramu, A. Kavanagh, A. G. Elliott, M. S. Butler, A. B. Montgomery and M. A. Cooper, *Antimicrob. Agents Chemother.*, 2015, **59**, 5925–5931.

18 C. Pontremoli, N. Barbero, G. Viscardi and S. Visentin, *Bioorg. Med. Chem.*, 2015, **23**, 6581–6586.

19 A. Horsley, K. Rousseau, C. Ridley, W. Flight, A. Jones, T. A. Waigh and D. J. Thornton, *J. Cystic Fibrosis*, 2014, **13**, 260–266.

20 D. A. Norris and P. J. Sinko, *J. Appl. Polym. Sci.*, 1997, **63**, 1481–1492.

21 M. Dawson, E. Krauland, D. Wirtz and J. Hanes, *Biotechnol. Prog.*, 2004, **20**, 851–857.

22 A. W. Larhed, P. Artursson and E. Björk, *Pharm. Res.*, 1998, **15**, 66–71.

23 M. Boegh, S. G. Baldursdóttir, A. Müllertz and H. M. Nielsen, *Eur. J. Pharm. Biopharm.*, 2014, **87**, 227–235.

24 M. Boegh, M. García-Díaz, A. Müllertz and H. M. Nielsen, *Eur. J. Pharm. Biopharm.*, 2015, **95**, 136–143.

25 M. Anwarul Hasan, C. F. Lange and M. L. King, *J. Nonnewton. Fluid Mech.*, 2010, **165**, 1431–1441.

26 Y. Yang, M. D. Tsifansky, C.-J. Wu, H. I. Yang, G. Schmidt and Y. Yeo, *Pharm. Res.*, 2010, **27**, 151–160.

27 M. T. Cook, S. L. Smith and V. V. Khutoryanskiy, *Chem. Commun.*, 2015, **51**, 14447–14450.

28 S. Lum, P. Gustafsson, H. Ljungberg, G. Hulskamp, A. Bush, S. B. Carr, R. Castle, A.-F. Hoo, J. Price, S. Ranganathan, J. Stroobant, A. Wade, C. Wallis, H. Wyatt and J. Stocks, *Thorax*, 2007, **62**, 341–347.

29 H. Wilkens, B. Weingard, A. Lo Mauro, E. Schena, A. Pedotti, G. W. Sybrecht and A. Aliverti, *Thorax*, 2010, **65**, 808–814.

30 D. B. Hill, P. A. Vasquez, J. Mellnik, S. A. McKinley, A. Vose, F. Mu, A. G. Henderson, S. H. Donaldson, N. E. Alexis, R. C. Boucher and M. G. Forest, *PLoS One*, 2014, **9**, e87681.

31 S. L. McGill and H. D. C. Smyth, *Mol. Pharmaceutics*, 2010, **7**, 2280–2288.

32 S. S. Dhanisha, C. Guruvayoorappan, S. Drishya and P. Abeesh, *Crit. Rev. Oncol. Hematol.*, 2018, **122**, 98–122.

33 V. J. Schömig, B. T. Käsdorf, C. Scholz, K. Bidmon, O. Lieleg and S. Berensmeier, *RSC Adv.*, 2016, **6**, 44932–44943.

34 C. V. Robinson, M. R. Elkins, K. M. Bialkowski, D. J. Thornton and M. A. Kertesz, *J. Med. Microbiol.*, 2012, **61**, 1644–1653.

35 J. M. Flynn, D. Niccum, J. M. Dunitz and R. C. Hunter, *PLoS Pathog.*, 2016, **12**, e1005846.

36 M. O. Henke, G. John, M. Germann, H. Lindemann and B. K. Rubin, *Am. J. Respir. Crit. Care Med.*, 2007, **175**, 816–821.

37 J. A. Dodge, *Dev. Period Med.*, 2015, **19**, 9–13.

38 H. Matsui, B. R. Grubb, R. Tarran, S. H. Randell, J. T. Gatzy, C. W. Davis and R. C. Boucher, *Cell*, 1998, **95**, 1005–1015.

39 N. Nikravesh, O. G. Davies, I. Azoidis, R. J. A. Moakes, L. Marani, M. Turner, C. J. Kearney, N. M. Eisenstein, L. M. Grover and S. C. Cox, *Adv. Healthcare Mater.*, 2019, 1801604.

40 R. Zhang, L. Lei, Q. Song and X. Li, *Colloids Surf., B*, 2019, **175**, 569–575.

41 B. N. Sathy, A. Daly, T. Gonzalez-Fernandez, D. Olvera, G. Cunniffe, H. O. McCarthy, N. Dunne, E. Jeon, E. Alsberg, T. L. H. Donahue and D. J. Kelly, *Acta Biomater.*, 2019, **88**, 314–324.

42 E. Ruvinov, T. Tavor Re'em, F. Witte and S. Cohen, *J. Orthop. Translat.*, 2019, **16**, 40–52.

43 L. Raddatz, A. Lavrentieva, I. Pepelanova, J. Bahnemann, D. Geier, T. Becker, T. Scheper and S. Beutel, *J. Funct. Biomater.*, 2018, **9**, 63.

44 S. Hafeez, H. Ooi, F. Morgan, C. Mota, M. Dettin, C. van Blitterswijk, L. Moroni and M. Baker, *Gels*, 2018, **4**, 85.

45 C. Taylor, J. Pearson, K. Draget, P. Dettmar and O. Smidsrod, *Carbohydr. Polym.*, 2005, **59**, 189–195.

46 R. Popeski-Dimovski, *Carbohydr. Polym.*, 2015, **123**, 146–149.

47 K. Y. Lee and D. J. Mooney, *Prog. Polym. Sci.*, 2012, **37**, 106–126.

48 B. E. Larsen, J. Bjørnstad, E. O. Pettersen, H. H. Tønnesen and J. E. Melvik, *BMC Biotechnol.*, 2015, **15**, 29.

49 A. Fuongfuchat, A. M. Jamieson, J. Blackwell and T. A. Gerken, *Carbohydr. Res.*, 1996, **284**, 85–99.

50 J.-K. Yan, L.-X. Wu, W.-Y. Qiu, Y.-Y. Wang, Z.-C. Ding and W.-D. Cai, *RSC Adv.*, 2017, **7**, 50441–50448.

51 E. A. Nunamaker, K. J. Otto and D. R. Kipke, *J. Mech. Behav. Biomed. Mater.*, 2011, **4**, 16–33.

52 M. A. LeRoux, F. Guilak and L. A. Setton, *J. Biomed. Mater. Res.*, 1999, **47**, 46–53.

53 C. K. Kuo and P. X. Ma, *Biomaterials*, 2001, **22**, 511–521.

54 S. K. Lai, Y.-Y. Wang, D. Wirtz and J. Hanes, *Adv. Drug Delivery Rev.*, 2010, **61**, 86–100.

55 I. Fernández Farrés and I. T. Norton, *Food Hydrocolloids*, 2014, **40**, 76–84.

56 B. Menchicchi, J. P. Fuenzalida, A. Hensel, M. J. Swamy, L. David, C. Rochas and F. M. Goycoolea, *Biomacromolecules*, 2015, **16**, 924–935.

57 G. Turco, I. Donati, M. Grassi, G. Marchioli, R. Lapasin and S. Paoletti, *Biomacromolecules*, 2011, **12**, 1272–1282.

58 M. Grassi, C. Sandolo, D. Perin, T. Coviello, R. Lapasin and G. Grassi, *Molecules*, 2009, **14**, 3003–3017.

59 H. B. Eral, V. López-Mejías, M. O'Mahony, B. L. Trout, A. S. Myerson and P. S. Doyle, *Cryst. Growth Des.*, 2014, **14**, 2073–2082.

This journal is © The Royal Society of Chemistry 2019

J. Mater. Chem. B, 2019, **7**, 4940–4952 | **4951**

82

60 M. Á. Cabrera-Pérez, M. B. Sanz, V. M. Sanjuan, M. González-Álvarez and I. G. Álvarez, *Concepts and Models for Drug Permeability Studies*, Elsevier, 2016, pp. 3–29.

61 E. Naderkhani, J. Isaksson, A. Ryzhakov and G. E. Flaten, *J. Pharm. Sci.*, 2014, **103**, 1882–1890.

62 N. N. Sanders, S. C. De Smedt, E. van Rompaey, P. Simoens, F. de Baets and J. Demeester, *Am. J. Respir. Crit. Care Med.*, 2000, **162**, 1905–1911.

63 J. S. Suk, S. K. Lai, N. J. Boylan, M. R. Dawson, M. P. Boyle and J. Hanes, *Nanomedicine*, 2011, **6**, 365–375.

64 H. Friedl, S. Dünnhaupt, F. Hintzen, C. Waldner, S. Parikh, J. P. Pearson, M. D. Wilcox and A. Bernkop-Schnürch, *J. Pharm. Sci.*, 2013, **102**, 4406–4413.

65 F. Lagarce, A.-C. Groo, P. Saulnier, J.-C. Gimel, J. Gravier, C. Ailhas and J.-P. Benoit, *Int. J. Nanomed.*, 2013, 4291.

66 B. Amsden, *Macromolecules*, 1998, **31**, 8382–8395.

67 D. Caccavo, S. Cascone, G. Lamberti and A. A. Barba, *Mol. Pharmaceutics*, 2015, **12**, 474–483.

68 Y. Cu and W. M. Saltzman, *Adv. Drug Delivery Rev.*, 2009, **61**, 101–114.

69 PubChem, Aspirin, https://pubchem.ncbi.nlm.nih.gov/compound/2244, accessed 12 February 2019.

70 PubChem, Cephalexin, https://pubchem.ncbi.nlm.nih.gov/compound/27447, accessed 12 February 2019.

71 PubChem, Epirubicin, https://pubchem.ncbi.nlm.nih.gov/compound/41867, accessed 12 February 2019.

83

Cystic fibrosis mucus model to design more efficient drug therapies

The author's contributions to the appended manuscript consist of all the experimental work, data analysis, and manuscript preparation. Data interpretation, in particular the effect of calcium on permeability as well as assessment of chemical variability, and manuscript revision was performed with the contribution from coauthors.

The manuscript was featured on the Front Cover of Molecular Pharmaceutics (Volume 19, Issue 2)
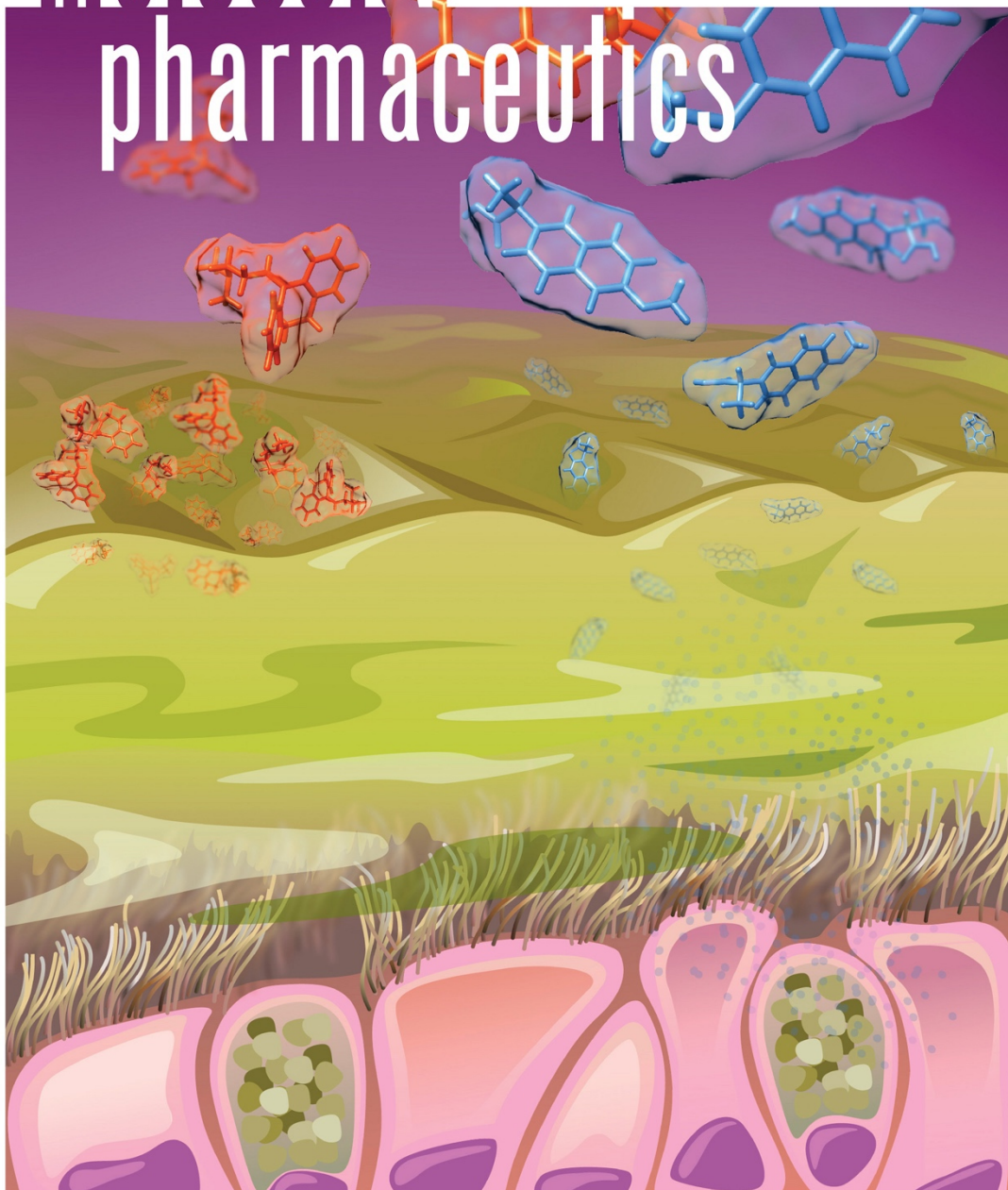
Cystic Fibrosis Mucus Model to Design More Efficient Drug Therapies

Cosmin Butnarasu,* Giulia Caron, Daniela Peneda Pacheco, Paola Petrini, and Sonja Visentin*

ACCESS | Metrics & More | Article Recommendations | Supporting Information

ABSTRACT: Mucus represents a strong barrier to tackle for oral or pulmonary administered drugs, especially in mucus-related disorders. This study uses a pathological cystic fibrosis (CF) mucus model to investigate how mucus impacts the passive diffusion of 45 *ad hoc* commercial drugs selected to maximize physicochemical variability. An *in vitro* mucosal surface was recreated by coupling the mucus model to a 96-well permeable support precoated with structured layers of phospholipids (parallel artificial membrane permeability assay, PAMPA). Results show that the mucus model was not a mere physical barrier but it behaves like an interactive filter. In nearly one-half of the investigated compounds, the diffusion was reduced by mucus, while other drugs were not sensitive to the mucus barriers. We also found that permeability can be enhanced when drug—calcium salts are formed. This was confirmed with cystic fibrosis sputum as a rough *ex vivo* model of CF mucus. Since the drug discovery process is characterized by a high rate of failure, the mucus platform is expected to provide an efficient support to early reduce the number of poor-performing drug candidates.

KEYWORDS: mucus, drugs, permeability, PAMPA, HTS
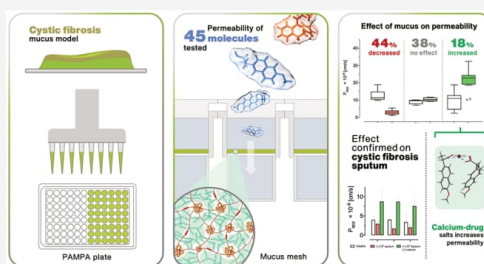
1. INTRODUCTION

The human body is constantly exposed to environmental threats. To counteract potential noxious agents, all of the wet epithelia are covered with a layer of mucus.[1] Mucus is a dynamic semipermeable network with a heterogeneous composition. It consists of ~95% water, with the remaining 5% comprising electrolytes, lipids, DNA fragments, and proteins.[2] Maintaining the gel-like properties and keeping together such a huge amount of water require a strong yet flexible skeleton. The tough job is carried out by mucins.[3] Mucins are long polymeric glycoproteins having a high molecular weight (640 kDa[4]), consisting of a peptide backbone to which a huge amount of carbohydrate chains are attached. Up to 80% of their total weight is due to a large number of O-glycosylated chains.[4,5] Such an architecture enables the exchange of nutrients, water, gases, and hormones while being impermeable to most bacteria and pathogens.[1,6]

Although mucus production is needed to avoid environmental threats, either overproduction or a dysfunctional clearance of mucus is a hallmark of all mucus-related pathologies[7] such as cystic fibrosis (CF). In these disorders, an overexpression of mucins, accumulation of extracellular DNA as well as cellular debris, and the persistent presence of bacteria confer mucus stasis, leading to a vicious cycle of infection and inflammation that can be chronically sustained.[8,9] Moreover, the lack of function of the cystic fibrosis

transmembrane conductance regulator (CFTR) protein leads to a dehydrated form of mucus, which is characterized by a reduced mesh size (60—300 nm)[10] in comparison to physiological mucus (497—503 nm).[11] As a result, in CF and bronchiectasis, daily sputum production is a crucial marker for physicians to evaluate disease severity and treatment response.[12]

Despite the great advancements in disease management of the last decades, pulmonary failure remains the main cause of morbidity and mortality in CF patients.[13] Physicians have, therefore, developed advanced clearance techniques (ACTs) based on coughing maneuvers to get rid of the viscous mucus. In addition, CF patients manage their disease by following a regular treatment with medications, mainly antibiotics (*i.e.*, aztreonam, tobramycin, levofloxacin) and anti-inflammatory drugs (*i.e.*, high-dose ibuprofen[14]). Yet, to enter into the systemic circulation, drugs administered by oral, pulmonary, nasal, or rectal routes should cross mucus barriers to reach their target. In the context of cystic fibrosis, the pathological
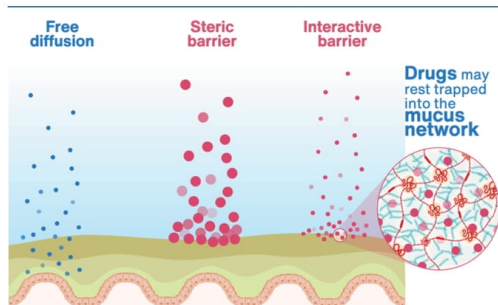
A

mucus can strongly limit the absorption of drugs that do not exhibit these difficulties under normal physiological conditions. Two main mechanisms are expected to affect drug diffusion through mucus: steric and interactive filtering (Figure 1).[1,6,15,16] Oligomers of secreted mucins connect with each

Figure 1. Steric and interactive barriers of mucus. Drugs larger than the mesh spacing between mucin fibers are stacked within mucus because they are too big to cross the mucus mesh. Similarly, drugs smaller than the mesh but able to interact with mucus components are equally retained by mucus. On the contrary, particles that are small enough and relatively inert to any of the mucus components can freely diffuse through the mucus layer and eventually be absorbed.

other creating a complex network that filters molecules bigger than the size of the mesh spacing between mucin fibers[15] (steric filter). Molecules small enough to penetrate the mucin mesh are subjected to interactive filtering, which is mainly governed by the structural complexity of mucins. On the highly glycosylated hydrophilic regions, negative charges are exposed due to the presence of sialic acid. On these substrates, hydrogen bonding and electrostatic interactions can be established with polar and hydrophilic molecules. Moreover, cysteine-rich domains are glycan-free and usually fold into hydrophobic regions on which lipophilic molecules can attach. Finally, other mucus components such as lipids, antimicrobial peptides (defensins, histatins, collectins, *etc.*), lytic enzymes (lysozyme), and antibodies (IgA and IgG) have the potential to interact with drugs.

Developing *in vitro* models of pulmonary pathological mucus is, therefore, a much-needed step in modern drug discovery to find new CF pharmacological treatments. Today, the most popular *in vitro* models for assessing permeability/absorption of drugs and drug candidates are based on artificial membranes, such as parallel artificial membrane permeability assay (PAMPA),[17] systems based on cells, such as Caco-2[18] and MDCK,[19] and systems based on site-specific tissues.[20] Notably, none of them takes mucus specifically into account. In recent years a variety of mucus models have been proposed.[21] The proposed models include gastrointestinal mucin-based solutions,[22,23] reconstituted oral mucus gels,[24] multilayered polyelectrolyte films,[25] and *in vitro* cell culture models incorporating airway mucus or mucus-producing cells.[26] Falavigna et al. developed a mucus phospholipid vesicle-based permeation assay that has been used for permeability screening of drugs and formulations.[27]

Recently, we developed an *in vitro* pathological mucus model, which simplifies mucus complexity but still mimics the chemical composition, structural features, and viscoelastic

properties of CF mucus.[28] The latter are achieved by taking advantage of the internal gelation of alginate in the presence of calcium ions. Alginate is an extracellular exopolysaccharide component of mucoid *P. aeruginosa*, a hallmark of CF infection, and has been shown to protect bacteria against certain antibiotics as well as escape the immune system.[29,30] To reproduce the interactive and steric filters of CF mucus, we used commercially available unpurified mucin-type III from the porcine stomach. One may argue that commercial mucins are different in terms of the structure and viscoelastic properties from native mucins. Indeed, commercial mucins may fail to form hydrogels at acidic pH, are only partially purified, and are inferior in inhibiting virus infection compared to natively purified mucins obtained in the lab.[5] It is also known that high concentrations of calcium can react with native mucin inducing the shrinking of the protein.[31] However, this phenomenon does not happen with commercial mucins, as the extraction process reduces the presence of groups able to interact with calcium ions. However, the aim of our pathological mucus model is to have an easy to use and easy to reproduce *in vitro* model suitable for average throughput screening to be used in early drug discovery. Thus, even if in the lab extracted mucins are qualitatively superior to commercial mucins, the time-consuming and expensive procedures of purification, extraction, and concentration at the laboratory level are not adapted for our purposes.

In this study, we intended to expand the applicability and the understanding of our *in vitro* cystic fibrosis mucus model in relation to CF patient sputum as well. To reach this aim we (i) selected 45 commercially available drugs to cover a large drug chemical space domain, (ii) performed PAMPA measurements in the absence of mucus and assessed the physicochemical determinants of apparent permeability (P_{app}), (iii) coupled the developed pathological mucus model with PAMPA to mimic *in vitro* cystic fibrosis airway mucosal surface; the permeability in the presence of mucus was compared with the P_{app} obtained in the absence of mucus, and (iv) measured drug permeability in the presence of cystic fibrosis patient sputum to support the conclusion drawn from the *in vitro* model, herein, presented.

Overall, this study highlights the challenges of reproducing *in vitro* the complexity of cystic fibrosis dysfunctional mucus. As a first screening tool of poorly permeable molecules, a fully tunable *in vitro* mucus model, easy to reproduce, and mimicking both the composition and the rheological properties of CF mucus could be of high usefulness in the early drug discovery.

2. EXPERIMENTAL SECTION

2.1. Computational Part. The drug SMILES codes were retrieved from DrugBank.[32] The csv file of the approved drugs was downloaded from DrugBank (last updated on 3 January 2021). The csv file was transformed into an xlsx file using Microsoft Excel (v. 16.43). The SMILES of CFTR$_{inh}$-172, which is a noncommercial drug acting as an inhibitor of the CFTR protein, was retrieved from PubChem.[33] Molecular properties were calculated with DataWarrior (ver. 5.5.0, openmolecules.org) and include physicochemical properties, druglikeness-related properties, various atom and ring counts, molecular shape, flexibility, as well as functional groups (Table S2). The molecular charge at pH 7.4 was retrieved from MarvinSketch (Marvin 20.20, 2020, ChemAxon).

The data set was analyzed with the principal component analysis (PCA) tool implemented in DataWarrior. The

correlation matrix of the descriptors was calculated using DataWarrior and represented as a heatmap.

2.2. Materials. Mucin from the porcine stomach (PGM type III, bound sialic acid 0.5−1.5%, partially purified powder), sodium salt of alginic acid, calcium carbonate, D-(+)-gluconic acid δ-lactone (GDL) ≥99.0%, and sodium chloride used to develop the airway mucus model were all purchased from Merck (Germany). Permeability experiments were carried out on Corning Gentest Pre-coated PAMPA, 353015, USA plates. Millipore grade water (resistivity: 18.2 MΩ·cm at 25 °C) was obtained from an in-house Millipore system. Acetonitrile, ammonium acetate, and dimethyl sulfoxide (DMSO) were of the highest available grade and purchased from Sigma-Aldrich. The drugs used in this study were all commercially available (Figure S1). Stock solutions were prepared in DMSO and stored at 4 °C.

2.3. Mucus Model. The mucus model used herein can be exploited as a platform for drug diffusion either for cystic fibrosis mucus or other mucus-related disorders such as mucus of chronic obstructive pulmonary disease (COPD), which unveils its potential for a wide range of applications in drug discovery. The mucus model was prepared as previously described.[28] Briefly, a 21 mg/mL alginate sodium salt solution was dissolved in a 16.3 mg/mL NaCl solution, under slow magnetic agitation. In parallel, a 43.7 mg/mL mucin suspension was prepared in mQ water and left under slow agitation overnight. The alginate and mucin solutions were mixed at a 1:4 proportion using two jointed luer-lock syringes. Then, the alginate and mucin suspension was mixed with a suspension of 7 mg/mL CaCO$_3$ prepared in a 16.3 mg/mL NaCl solution. Next, a 70 mg/mL GDL solution was freshly prepared in 16.3 mg/mL NaCl and mixed with the previously prepared suspension (alginate, mucin, and CaCO$_3$) at a proportion of 1:6. Finally, 40 μL of the mucus model was pipetted directly over the PAMPA membrane in the donor compartment, producing a hydrogel of approximately 500 μm in thickness. The donor plate of the PAMPA was then carefully shacked to uniformly distribute the volume of mucus over the entire well surface and to get rid of any air bubbles. Afterward, the mucus within the plate was left to cross-link for 24 h before the addition of drug solutions. Throughout the time course of the permeability experiment, the CF mucus model remained stable with respect to weight and thickness variations. In fact, we previously determined that after 6 h of incubation in an aqueous medium, mucus undergoes a thickness variation below 10%, which was considered acceptable for our experimental purpose.[28]

2.4. PAMPA Assay. The apparent permeability (P_{app}) and the effect of mucus on permeability were experimentally determined through PAMPA and mucus−PAMPA assays, respectively. Stock solutions of all drugs were prepared in DMSO at a concentration of 10 mg/mL. Donor solutions of drugs were prepared in phosphate-buffered saline (PBS) (10 mM, pH 7.4, 5% DMSO) at a concentration between 100 and 500 μM, depending on the drugs' specific solubility. Each donor well was filled with 200 μL of drug solution, while the acceptor wells were filled with 300 μL of PBS. The donor plate was then placed on top of the acceptor plate, so the artificial membrane was in contact with the buffer solution below. A lid was placed on top of the donor plate and the whole PAMPA plate was incubated at room temperature for 5 h. At the end of the incubation period, the plates were separated, and the volume of the acceptor wells was collected. Concentrations of

drugs in each acceptor well were quantified either by high-performance liquid chromatography-ultraviolet (HPLC-UV) or high-performance liquid chromatography-mass spectrometry (HPLC-MS). The apparent permeability coefficient (P_{app}) was expressed using eq 1 derived from Fick's law[34] for steady-state conditions

$$P_{app} = \frac{dQ/dt}{C_0 \times A} \tag{1}$$

where dQ is the quantity of drug expressed as moles permeated into acceptor compartment at time t (18 000 s), C_0 is the initial concentration in the donor well, and A is the area of the well membrane (0.3 cm^2). P_{app} was used as an average of all of the measures.

The same PAMPA experimental setup was adopted when assessing the effect of individual components of mucus. In particular, we evaluated how PGM, NaCl, alginate hydrogel, and calcium impact permeability. For this purpose, the passive diffusion was measured in the presence of each one of these chemicals, each of which was individually added in the donor compartment of the PAMPA. In brief, 40 μL of the alginate gel was deposited over the phospholipid membrane of the donor compartment prior to the addition of the drug solution. The influence of PGM was assessed by filling the donors with a suspension of drug containing 4.16 mg/mL PGM (the PGM concentration donor compartment). Similarly, drug donor solutions containing 1.67 mM CaCl$_2$ or 20 mM NaCl were used when investigating the impact of calcium and NaCl over permeability.

2.5. Cystic Fibrosis Sputum. Sputum collected from cystic fibrosis patients was used as a model of a complex biological matrix representative of CF mucus. We measured the permeability of some of the drugs of our data set using the CF sputum—PAMPA system, and compared the results with the permeability obtained in the presence of our mucus model. Sputum samples were a kind concession of Prof. A. Ghigo from the Department of Molecular Biotechnology of the University of Turin. Spontaneously expectorated sputum was collected into sterile containers and was processed as described by Oriano et al.[35] Briefly, samples were processed getting first rid of saliva. Then, they were diluted 8× in PBS, vortexed until sputum dissolution, and centrifuged for 15 min at 3000*g*. Overall, 40 μL of sputum was deposited over the PAMPA membrane in the bottom of the top plate, and eventually, 200 μL of a drug solution was inserted over the layer of CF sputum, while 300 μL of PBS was inserted into the bottom plate of the PAMPA. Then, two plates were coupled and incubated for 5 h. At the end of 5 h, the plates were split and the amount of drug diffused into the bottom plate was quantified. Similarly, to test the effect of calcium over the permeability of the drug, we formed drug−calcium complexes by dissolving the same into PBS containing calcium at the same concentration present in the cystic fibrosis mucus model. The permeability of calcium−drug complexes was measured through the CF sputum PAMPA system, as previously described.

2.6. Quantification. All compounds, except ebselen, benzoic acid, and 3-aminophenol, were analyzed and quantified by HPLC-MS/MS using a Varian HPLC equipped with a 410 autosampler and an Ascentis C18 column (10 cm × 2.1 mm, 3 μm). Gradient mobile phases composed of acetonitrile and water 0.1% formic acid or ammonium acetate 5 mM pH 6.6 as organic and aqueous phases, respectively,
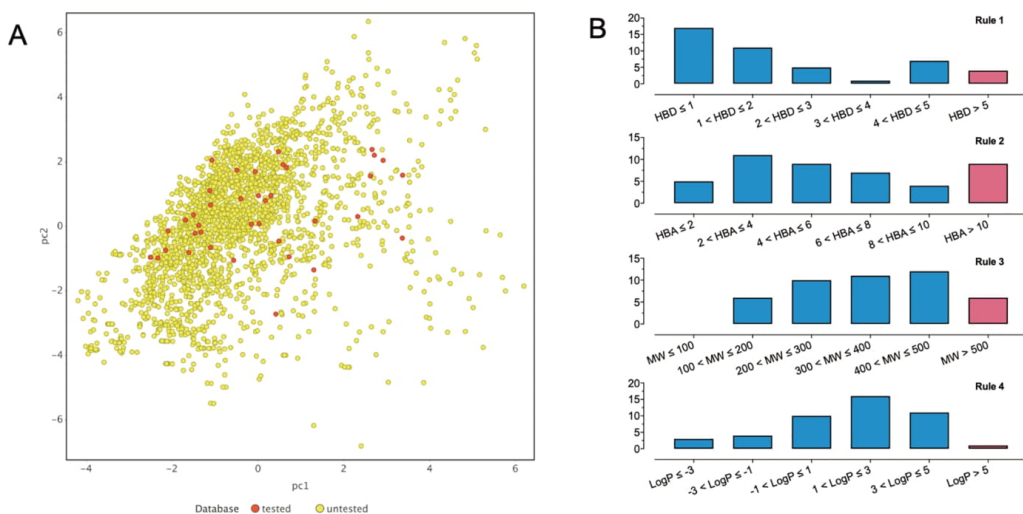
Figure 2. (A) Distribution of the tested drugs (red dots) within the DrugBank database of approved drugs (yellow dots) having total molecular weight ≤1000 Da. (B) Classification and distribution based on Lipinski's rule of five (Ro5) (B). Compounds that violate the Ro5 for each molecular descriptor are represented by the red bars.

were pumped at a flow rate of 200 μL/min. A flow of 200 μL/min and an injection volume of 10 μL were used. Compounds were detected on a Varian 320 MS TQ Mass Spectrometer equipped with an electrospray ionization (ESI) source operating in a positive or negative mode, depending on the drugs' method. The detector was used in a multiple reaction monitoring (MRM) mode, and the transitions of each drug are reported in Table S1.

Ebselen, benzoic acid, and 3-aminophenol were quantified on an HPLC Varian ProStar equipped with a 410 autosampler and a PDA 335 LC Detector. The analysis was conducted on an IAM column (Regis, 10 cm × 4.6 cm 10 μm packing 300 Å pore size) using ammonium acetate and acetonitrile as aqueous and organic mobile phases, respectively. The flow rate was 1 mL/min.

2.7. Statistical Analysis. A minimum of four replicates were conducted for each compound on each experimental method (with or without the mucus model), some of which were repeated on different PAMPA plates as well. Results are expressed as mean ± standard deviation (SD). Student's t-test was applied to detect the statistical significance between the permeability recorded with and without mucus. A $p < 0.05$ was considered to be a statistically significant difference.

3. RESULTS AND DISCUSSION

3.1. Data Set Selection: Assessment of Chemical Heterogeneity. We included in our data set a number of anti-inflammatory (ibuprofen, dexamethasone) and antibacterial drugs (tobramycin, ceftazidime, aztreonam, ciprofloxacin, tetracycline) commonly employed in the cystic fibrosis therapy regimes. To properly evaluate the performances of our CF mucus model, we expanded the data set up to 45 compounds considering it a reasonable number of drugs to be investigated, with good variability in terms of chemical properties (see below).

To assess the distribution of our data set within the entire drug chemical space, we first downloaded the DrugBank database of approved drugs. From DrugBank's database, we retrieved the SMILES code for each compound and used them to calculate molecular descriptors (see Methods, Table S2). Using drugs as observations and the selected molecular descriptors as variables, we then computed principal component analysis (PCA). The drugs within our data set are small molecules; therefore, we focused on compounds of total molecular weight <1000 Da (yellow dots in Figure 2A). The variance explained by PC1 and PC2 using 30 molecular descriptors is about 60%. In the score plot defined by PC1 and PC2, it is possible to appreciate a good distribution of the tested drugs within the chemical space (red dots in Figure 2A).

To assess chemical variability within our data set, we also evaluated Lipinski's rule of five (Ro5) molecular descriptor distribution (the number of the hydrogen bond donors (HBD), the number of the hydrogen bond acceptors (HBA), the molecular mass (MW), and the octanol−water partition coefficient (log P)). Figure 2B shows that all of the descriptor categories are well represented by the data set.

3.2. Validation of the Permeability Setup to Measure P_{app}. Before evaluating the effect of mucus on drug permeability, we determined and validated permeability in the absence of mucus through an artificial cellular membrane since our method differs from the standard PAMPA protocol (Figure 3A). In fact, in our setup (modified setup), mucus was placed over the PAMPA membrane (a filter plate precoated with structured layers of phospholipids) in the top well, as this is the only way to have a physical support that can sustain mucus. Thus, diffusion took place from the top to the bottom well, and the respective drugs were quantified only in the acceptor compartment (bottom well).

Data obtained with our original setup (Table 1) were first validated using a subset of compounds taken from the paper of

D
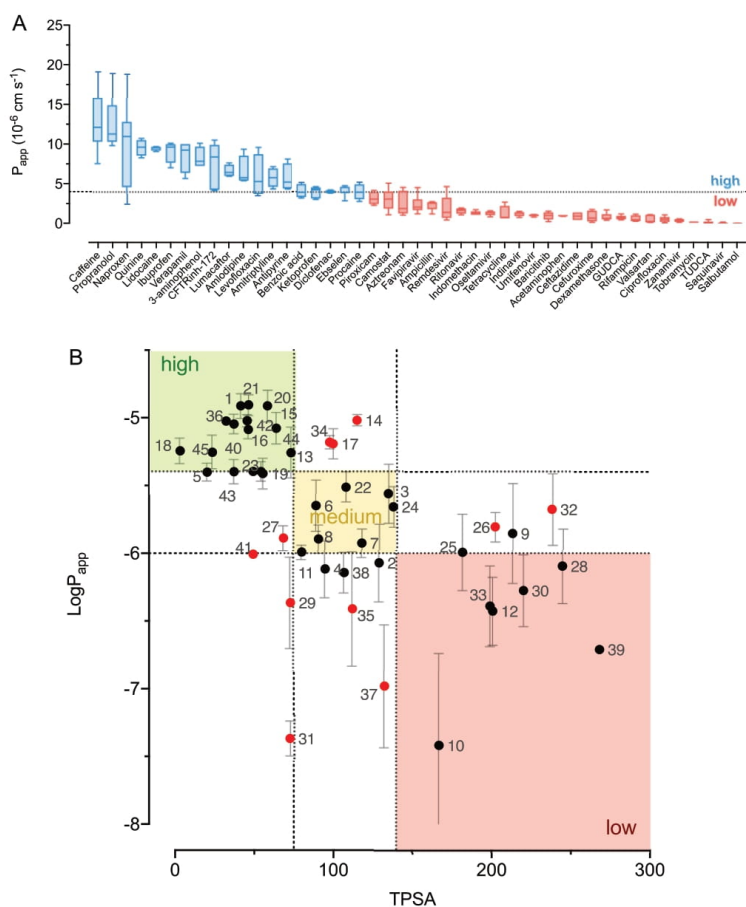
Figure 3. Classification in high and low permeable compounds (A) of the tested drugs based on the determined apparent permeability (P_{app}) Data set grouping within permeability categories (B): permeability classification: green = high, yellow = medium, and red = low. The P_{app} threshold between high-medium and medium-low permeable compounds was set at 4 and 1×10^{-6}, respectively. TPSA threshold between high-medium and medium-low permeable compounds was set at 75 and 140 Å^2, respectively. The number beneath each dot refers to the drug name (see Figure S1 and Table 2).

Chen et al.,[36] (Table S3 and Figure S2) using the same artificial membrane (r^2 = 0.610, Figure S2). Notably, compounds as propranolol and caffeine known for being high permeable[37,38] could clearly be discriminated from low permeable compounds.

Then, we determined which molecular descriptors mostly govern permeability in our system. To do so, a correlation matrix between apparent permeability (P_{app}) and a pool of molecular descriptors (Figure S3, and see Methods) was calculated. The highest correlation (r^2 = 0.303) was found to exist with topological polar surface area (TPSA, the surface sum over all polar atoms or molecules, mainly oxygen and nitrogen, also including their attached hydrogen atoms) and to a minor extent with hydrogen bond donor and acceptor groups (HBD and HBA). In particular, the higher the TPSA, the lower the P_{app}. This is in line with the literature[39] and again confirms the reliability of our system.

Finally, we verified whether TPSA can distinguish high from low permeable compounds. Although a definitive threshold is missing, in the standard PAMPA setup the P_{app} value for distinguishing low from highly permeable compounds is frequently set at 1.5×10^{-6} cm/s.[36] However, in a modified setup (diffusion from the top to the bottom well), the permeability threshold is higher.[40,41] Here, we used 4×10^{-6} and 1×10^{-6} cm/s to distinguish high, medium, and low permeable molecules. Figure 3B shows that TPSA values of 140[42] and of 75 Å^2[43,44] are able to predict the permeability class of the investigated data set.

In addition to the discrimination based on the total polar surface area, we plotted the high and low permeable compounds in the chemical space based on their chemical properties. For this purpose, we computed principal component analysis using as variables the molecular descriptors calculated from DataWarrior. Indeed, we can

E

Table 1. Summary of P_{app} Recorded on PAMPA and the Effect the Mucus Model Played over Permeability with the Respective P_{app} Variations[a]

Nr	Compound	MW (g/mol)	Lipophilicity	P_{app} PAMPA ($\pm$ SD) $\times 10^{-6}$ [cm/s]	P_{app} Mucus-PAMPA ($\pm$ SD) $\times 10^{-6}$ [cm/s]	Effect of mucus on P_{app}
1	Propranolol	259.3	medium	12.56 ($\pm$ 2.9)	2.84 ($\pm$ 1.4)	Decreased (−1)
5	Ebselen	274.2	low	4.01 ($\pm$ 0.6)	1.82 ($\pm$ 0.8)	Decreased (−1)
8	Oseltamivir	312.4	medium	1.30 ($\pm$ 0.3)	0.32 ($\pm$ 0.1)	Decreased (−1)
11	Umifenovir	477.4	medium	1.03 ($\pm$ 0.1)	0.18 ($\pm$ 0.0)	Decreased (−1)
12	Zanamivir	332.3	medium	0.42 ($\pm$ 0.2)	0.02 ($\pm$ 0.0)	Decreased (−1)
13	Levofloxacin	361.4	low	5.94 ($\pm$ 2.7)	0.00 ($\pm$ 0.0)	Decreased (−1)
14	CFTRinh-172	409.4	medium	7.35 ($\pm$ 2.9)	3.84 ($\pm$ 1.2)	Decreased (−1)
15	Verapamil	454.6	medium	8.57 ($\pm$ 2.0)	0.53 ($\pm$ 0.2)	Decreased (−1)
16	3-aminophenol	109.1	low	8.28 ($\pm$ 1.4)	0.74 ($\pm$ 0.6)	Decreased (−1)
17	Amlodipine	408.9	medium	6.60 ($\pm$ 1.9)	0.00 ($\pm$ 0.0)	Decreased (−1)
18	Amitriptyline	277.4	high	5.80 ($\pm$ 1.2)	0.00 ($\pm$ 0.0)	Decreased (−1)
19	Procaine	236.3	low	4.00 ($\pm$ 1.0)	0.00 ($\pm$ 0.0)	Decreased (−1)
20	Caffeine	194.2	low	12.70 ($\pm$ 3.5)	6.43 ($\pm$ 4.2)	Decreased (−1)
25	Tetracycline	444.4	high	1.22 ($\pm$ 1.0)	0.00 ($\pm$ 0.0)	Decreased (−1)
26	Ritonavir	721.0	high	1.60 ($\pm$ 0.4)	0.61 ($\pm$ 0.2)	Decreased (−1)
31	Salbutamol	239.3	low	0.04 ($\pm$ 0.0)	0.01 ($\pm$ 0.0)	Decreased (−1)
34	Lumacaftor	452.4	medium	6.64 ($\pm$ 0.8)	5.40 ($\pm$ 0.3)	Decreased (−1)
36	Lidocaine	234.3	high	9.47 ($\pm$ 0.3)	0.05 ($\pm$ 0.1)	Decreased (−1)
38	GUDCA	449.6	medium	0.76 ($\pm$ 0.3)	0.22 ($\pm$ 0.3)	Decreased (−1)
42	Quinine	324.4	low	9.54 ($\pm$ 1.0)	6.66 ($\pm$ 0.6)	Decreased (−1)
3	Camostat	398.4	medium	3.04 ($\pm$ 1.3)	3.28 ($\pm$ 2.9)	None (0)
4	Dexamethasone	392.5	medium	0.85 ($\pm$ 0.4)	0.46 ($\pm$ 0.4)	None (0)
6	Favipiravir	157.1	high	2.44 ($\pm$ 1.1)	3.17 ($\pm$ 1.3)	None (0)
7	Indinavir	613.8	low	1.22 ($\pm$ 0.3)	0.94 ($\pm$ 0.7)	None (0)
9	Remdesivir	602.6	low	1.86 ($\pm$ 1.6)	1.63 ($\pm$ 1.5)	None (0)
10	Saquinavir	670.9	high	0.08 ($\pm$ 0.1)	0.10 ($\pm$ 0.1)	None (0)
24	Ampicillin	349.4	low	2.29 ($\pm$ 0.6)	1.34 ($\pm$ 0.7)	None (0)
28	Ceftazidime	546.6	low	0.93 ($\pm$ 0.5)	1.14 ($\pm$ 1.0)	None (0)
29	Ciprofloxacin	331.3	low	0.54 ($\pm$ 0.3)	0.31 ($\pm$ 0.3)	None (0)
30	Rifampicin	823.0	high	0.61 ($\pm$ 0.4)	0.19 ($\pm$ 0.1)	None (0)
32	Aztreonam	435.4	low	2.45 ($\pm$ 1.5)	1.64 ($\pm$ 0.6)	None (0)
33	Cefuroxime	424.4	low	0.87 ($\pm$ 0.7)	0.16 ($\pm$ 0.2)	None (0)
35	Valsartan	435.5	low	0.56 ($\pm$ 0.5)	0.44 ($\pm$ 0.5)	None (0)
37	TUDCA	499.7	high	0.17 ($\pm$ 0.2)	0.04 ($\pm$ 0.1)	None (0)
39	Tobramycin	467.5	high	0.19 ($\pm$ 0.0)	0.25 ($\pm$ 0.1)	None (0)
40	Ibuprofen	206.3	medium	9.09 ($\pm$ 1.4)	10.33 ($\pm$ 1.2)	None (0)
45	Antipyrine	188.2	medium	5.75 ($\pm$ 1.7)	6.19 ($\pm$ 2.6)	None (0)
2	Baricitinib	371.4	high	0.99 ($\pm$ 0.8)	2.68 ($\pm$ 2.1)	Increased (+1)
21	Naproxen	230.3	low	9.57 ($\pm$ 3.9)	22.02 ($\pm$ 6.1)	Increased (+1)
22	Piroxicam	331.4	high	3.15 ($\pm$ 0.8)	6.63 ($\pm$ 0.1)	Increased (+1)
23	Diclofenac	296.2	medium	4.03 ($\pm$ 0.2)	5.06 ($\pm$ 0.1)	Increased (+1)
27	Indomethacin	357.8	medium	1.32 ($\pm$ 0.3)	2.54 ($\pm$ 0.9)	Increased (+1)
41	Acetaminophen	151.2	medium	0.99 ($\pm$ 0.1)	6.22 ($\pm$ 0.9)	Increased (+1)
43	Benzoic acid	122.1	medium	4.06 ($\pm$ 0.9)	9.91 ($\pm$ 0.9)	Increased (+1)
44	Ketoprofen	254.3	low	4.04 ($\pm$ 0.7)	9.24 ($\pm$ 1.2)	Increased (+1)

[a]Drugs were classified as low lipophilic if $\log P$ was ≤ 1; medium lipophilic when $1 < \log P \leq 3$, and high lipophilic when $\log P > 3$. The terms increased/decreased are used only if the difference in permeability is statistically significant. Student's t-test was applied to detect statistical significance between the permeability recorded with and without mucus. $p < 0.05$ was considered to be a statistically significant difference. For better and immediate visualization of lipophilicity, a three-colour scale is used based on the drug's partition coefficient (logP) value: yellow, green and blue for high (logP> 3), medium (1< logP < = 3), low (logP < = 1) lipophilicity, respectively. Analogously, the effect of mucus is displayed on a three-colour scale using red, yellow, and green for decreased (−1), none (0) and increased (+1) permeability, respectively.

observe a good separation of the two groups on the first principal component (see Figure S4A−C).

Overall, we validated the consistency of the experimentally determined P_{app} in the absence of mucus and confirmed that the P_{app} values can be used as benchmarks when assessing the effect of mucus in a mucus−PAMPA system.

3.3. Permeation Studies in the Presence of a Mucus Model. The mucus model was adapted to the PAMPA plate by directly pipetting it on top of the phospholipid membrane in the donor compartment. As all of the wet epithelia of the human body are covered by mucus, drugs administered by oral or pulmonary routes have to cross both the mucus layer and

F

the cellular membrane to be absorbed to be effective. With our adapted mucus–PAMPA system, we are expecting to be able to mimic *in vitro* the interface at mucosal surfaces. (Figure 4).
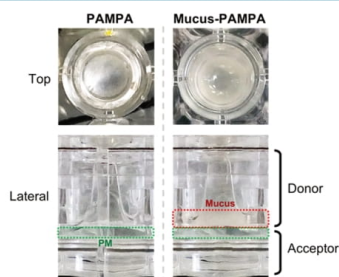
Figure 4. Comparison between PAMPA and the mucus–PAMPA system. At the top, the upper view of the PAMPA wells, and at the bottom, the lateral view of the donor and acceptor compartments. Dashed lines highlight the mucus layer and the phospholipid membrane (PM).

The effect of mucus was measured in terms of variations of permeability and was considered statistically significant only if the *p*-value between the means of the two groups (PAMPA and mucus–PAMPA) was <0.05. A summary of P_{app} with and without mucus is reported in Table 1, while the detail of each drug tested is reported in SI (Figure S6).

Three kinds of mucus-induced effects were observed (Table 1 and Figure 5A): (a) in the presence of mucus, 44% drugs showed a decreased permeability, (b) 38% had no statistically significant variation, and (c) 18% had an increased permeability. Among the compounds for which diffusion was reduced by mucus, we cannot outline any dependency on drugs' lipophilicity. In fact, mucus reduced the permeability of both hydrophilic and lipophilic drugs, which is in agreement with the findings of Boegh et al.,[24] using a biosimilar mucus on Caco-2 cells, and Falavigna et al.,[27] with a mucin–PVPA system. Data suggest that the CF pathological mucus model did not act as a mere physical barrier. Instead, it behaves like an interactive filter, as different structures interacted differently with mucus. This can be attributed to low-affinity interactions taking place during the diffusion process across the mucus layer and is mostly dependent on the structure of mucins. In fact, due to the complex architecture of mucins, hydrophobic
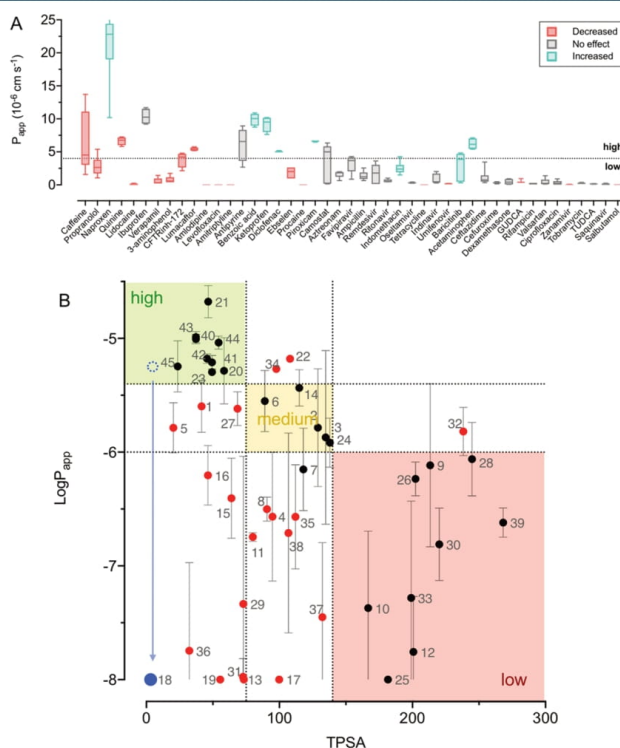
Figure 5. Impact of mucus over permeability. (A) Permeability recorded in the presence of mucus. (B) Grouping within permeability categories of the 45 compounds tested (permeability classification: green = high, yellow = medium, red = low). The P_{app} threshold of high-medium and medium-low is set at 4 and 1 × 10^{-6}, respectively. The TPSA threshold of high-medium and medium-low is set at 75 and 140 Å^2, respectively. The number beneath each dot refers to the drug name (see Figure S1 and Table 2). As an example, the focus is pointed on the variation of permeability of amitriptyline (nr 18, blue dot) in the absence and the presence of mucus.

drugs can be retained by the naked domains of the peptide core of mucin, while hydrophilic drugs can entangle with the branched oligosaccharides. In addition to the interactive filter orchestrated by mucins through hydrophobic, electrostatic, and hydrogen bonding interactions, mucins can also hinder the diffusion of xenobiotics also through a size filtering mechanism dependent on the mucin mesh. To estimate the mesh size of our mucus model, we applied the generalized Maxwell model (GMM), as described in our previous work.[28] The estimated mesh size was 54.7 ± 5.35 nm, which is in good agreement with what is currently reported in the literature related to pathological mucus. Considering that our data set is composed of only small molecules, thus much smaller than the mesh of our mucus model, we believe that the steric filter had a minor impact on drug diffusion.

Once we had assessed the effect that mucus played on P_{app} (*i.e.*, decreased, no effect, increased) of each compound, we then wanted to quantitatively compute its activity of mucus. Thus, we assigned numerical values to each effect, namely, -1, 0, $+1$ for when the permeability was decreased, unvaried, and increased, respectively. The effect of mucus over permeability varies without any apparent relation to any of the molecular descriptors selected, as shown by the correlation matrix (Figure S3). In fact, the relation between the P_{app} and TPSA registered in the absence of mucus does not hold true anymore. If previously we could correctly predict the permeability of almost 80% of the tested compounds, after the addition of mucus, we see that only 53% of the molecules have their permeability correctly predicted (Figure 5B). For instance, in the absence of mucus, amitriptyline (compound nr. 18) belongs to the high permeable group as it has low TPSA and high P_{app}; in contrast, the presence of mucus strongly decreases its permeability. Amitriptyline is a highly lipophilic drug, though being positively charged at pH 7.4. Such a reduction in permeability that we observe may be the result of combined retention due to interactions with the lipophilic domains and the negatively charged glycans of mucin. As amitriptyline, many other drugs have their permeability decreased (see Table 1 and Figure 5).

With the drug diffusion studies on the mucus–PAMPA system, we demonstrate that the pathologic cystic fibrosis mucus model can strongly influence the permeability of drugs. Theoretically, if the observed effects would have been similar for all compounds, one could reasonably state that the rate-limiting factor could be the longer diffusive pathway when mucus is present. That said, this hypothesis should be discarded as we have found that for some drugs, the presence of the pathological mucus model may increase permeability. These results are discussed in the next session.

3.4. Increased Permeability in the Presence of Pathological Mucus. We expected the mucus model to reduce or have no effect on the permeability of drugs. Figure 5A clearly reports that some of the compounds we tested (such as naproxen) presented a higher permeability in the presence of mucus than in its absence. Among the tested drugs, 18% (baricitinib, naproxen, piroxicam, diclofenac, indomethacin, acetaminophen, benzoic acid, ketoprofen) had a significant increase in permeability in the presence of mucus. In respect of the entire data set, the increased-permeability group share some chemical–physical properties; they are relatively small molecules (MW < 380 Da, total surface area < 270 Å^2), lipophilic ($c \log P > 1$), have medium-low polarity (PSA < 130 Å^2), and six out of eight are negatively charged at pH 7.4.

3.4.1. Role of the Mucus Components in the Enhancement of Permeability. To isolate the driving force of the increased diffusion rate observed in the presence of our mucus model, we disassembled the mucus and measured the permeability of naproxen in the presence of each one of the components of mucus. For this purpose, we selected naproxen as a model drug as it is the most remarkable compound for which the permeability increases with mucus (Figure S6). The main components of our mucus model are (a) PGM, which is used to mimic the composition of CF mucus; (b) alginate, because it is produced by mucoid *P. aeruginosa* infecting the CF mucus; (c) CaCO$_3$, used to cross-link alginate; and (d) NaCl, which is necessary to reproduce the salinity of CF mucus. Thus, we performed a PAMPA assay where naproxen solutions were prepared in PBS buffer containing either PGM, NaCl, or calcium in the same concentrations used in the mucus model. As for the alginate gel, this was deposited on the bottom of the top compartment of the PAMPA the day before the experiment, so as to allow alginate to cross-link (top of Figure 6).
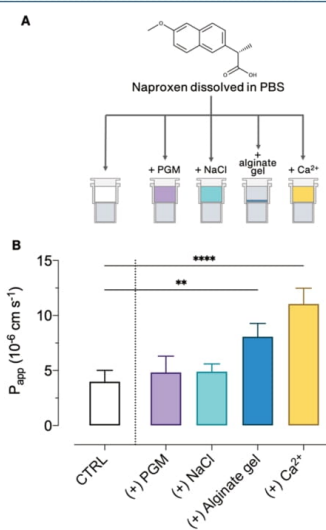

Figure 6. (A) Experimental setup used to isolate the effect of each one of the components of mucus. (B) Permeability of naproxen recorded in the presence of individual components of mucus.

We observed that while the diffusion rate in the presence of PGM or NaCl did not undergo major variations, in the other two systems (*i.e.*, the alginate gel and CaCl$_2$), a net increase in permeability was obtained. It is worth noting that the alginate gel contains calcium, as this is necessary to cross-link the alginate solution and, hence, to form the hydrogel matrix. The most probable scenario explaining such activity could rely on ion pairing, as it is commonly known that Ca^{2+} ions have a strong affinity for O, N, or F atoms because the metal acts as a Lewis acid and thus forms complexes with many ligands.[45] The binding of calcium ions is highly selective and can form asymmetric complexes that consist of a large radius. The formation of the naproxen–calcium complex was confirmed

H
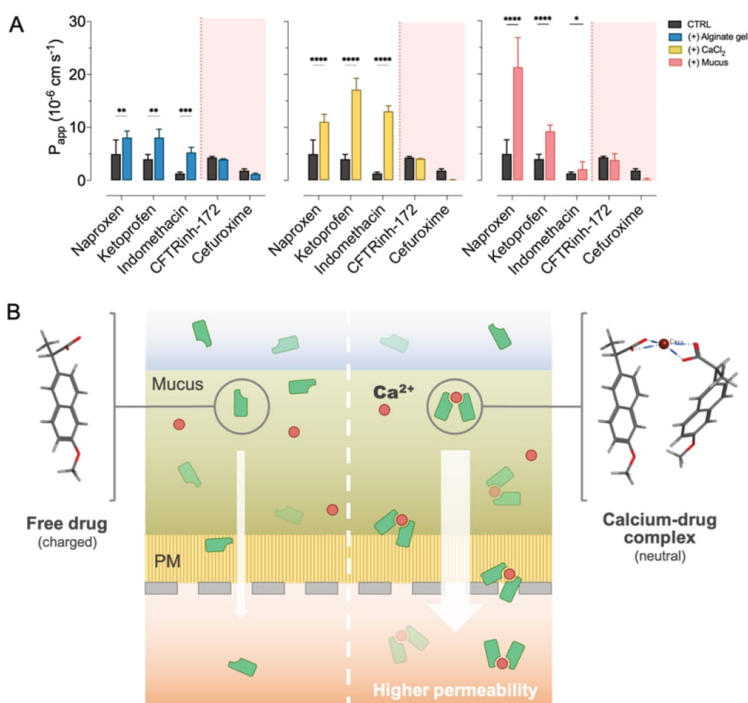
Figure 7. Effect of calcium over the permeability of some anions at pH 7.4. (A) Naproxen, ketoprofen, and indomethacin have higher diffusion rates when calcium is present. CFTR$_{inh}$-172 and cefuroxime do not undergo permeability variations in the presence of calcium. Two-way analysis of variance (ANOVA) comparing each group's mean with the mean of other group was used to compute statistical analysis. (B) Schematic representation of the calcium–naproxen complex and the passive diffusive mechanism through the mucus–PAMPA system.

experimentally by recording the ESI-MS spectrum (Figure S7, SI).

3.4.2. Role of Calcium. Once we isolated Ca^{2+} as the reason for the increased permeability, we then wanted to understand if this phenomenon is dependent on the negative charge borne by some of the drugs. Tests were repeated with ketoprofen and indomethacin as anions on which mucus increased their respective permeabilities, as well as CFTR$_{inh}$-172 and cefuroxime as anions with reduced and unvaried permeability (negative controls) in the presence of mucus, respectively. For naproxen, ketoprofen, and indomethacin, permeability increased in the presence of the alginate hydrogel and got even higher in the presence of only CaCl$_2$ (Figure 7A). It has been reported that these three drugs and other nonsteroidal anti-inflammatory drug agents (NSAIDs) can form complexes with calcium.[45−47] Interestingly, Ogiso and colleagues report that the absorption of indomethacin calcium salt on rat abdominal skin is significantly higher than that from indomethacin alone.[47] When forming complexes with calcium, naproxen, ketoprofen, and indomethacin are neutralized; they shift from a negatively charged form to exhibiting no relative charge. The neutralization implies a decrease of polarity in favor of lipophilicity, which we think actually favors the diffusion through the artificial phospholipid membrane of PAMPA (Figure 7B). It should be noted that, when drug–calcium complexes are formed, the molecular descriptors are completely different from those of the free drugs and cannot

be easily calculated. In addition, the higher permeability observed with CaCl$_2$ could be due to the larger availability of free Ca^{2+} in solution. In fact, in the system containing alginate, despite having the same Ca^{2+} concentration, part of it is not available because of the ion's cross-linking with alginate. On the contrary, we observe that the permeability of CFTR$_{inh}$-172 and cefuroxime is not influenced by the presence of calcium, even though they are also considered anionic drugs.

Overall, we hypothesized that drug–calcium salts have higher passive diffusion rates through the PAMPA phospholipid artificial membrane in comparison to the not-complexed drug. However, the formation of calcium salts is not merely dependent on the negative charge, as not all of the anionic drugs included in the data set enhanced permeability.

3.4.3. CF Patient Sputum Validation. Next, we wanted to understand if the results recorded in the presence of our mucus model can be reproduced using a more complex biological matrix to mimic CF sputum. For this purpose, we employed CF sputum as it is often considered a rough *ex vivo* model of CF mucus, and we measured the permeability of naproxen, ketoprofen, and indomethacin. In fact, a hallmark of diseases such as CF, COPD, and bronchiectasis is the excessive production of sputum. As a consequence of the altered physicochemical properties, the diseased sputum contains higher concentrations of inflammatory mediators, lytic enzymes (*i.e.*, neutrophil elastase), and bacterial colonization. However, due to the high variability among patients, which

I
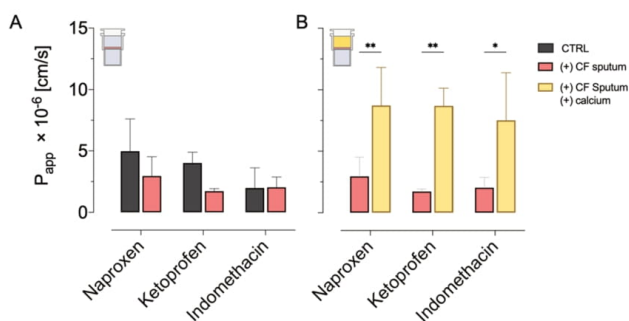
Figure 8. Effect of calcium over the permeability of naproxen, ketoprofen, and indomethacin in the presence of cystic fibrosis (CF) sputum. (A) Permeability of the three drugs measured on the CF sputum—PAMPA system, and compared with PAMPA (CTRL). (B) Increase of permeability through the CF sputum—PAMPA system, after the formation of calcium—drug complexes. Two-way ANOVA was used to compute statistical analysis.

depends on the diseases' stage, the measurements performed with CF sputum may have low reproducibility.

Given the high concentration of calcium in our mucus model, we wanted to find out if the permeability of some negatively charged drugs is overestimated when using the mucus model developed by us. As expected, in the presence of the CF sputum, the permeability of naproxen, ketoprofen, and indomethacin was decreased, even though the variation was not statistically significant (Figure 8A). Such a reduction could be the result of interactions with neutrophil elastase and proteases also present at high concentrations in the CF sputum. Mandel et al.[48] reported higher concentrations of calcium (136 ± 33 $\mu g/mL$) in submaxillary saliva of CF patients as opposed to healthy people (71 ± 19 $\mu g/mL$). Based on these values, we can estimate almost a $10\times$ higher concentration of calcium in our model than that of the *in vivo* scenario. Therefore, we can speculate that the permeability of some negatively charged drugs might be overestimated with our CF mucus model.

Despite this, we establish evidence indicating that some negatively charged drugs can form calcium—drug salts, which have higher diffusion rates on PAMPA in comparison to the free drugs. In terms of permeability, these salts might be less affected by the barrier effect of mucus. Thus, we wondered if this mechanism can be exploited to increase the permeability of naproxen, ketoprofen, and indomethacin through CF sputum. For this purpose, we repeated the permeability test through CF sputum, this time suspending the drugs into PBS containing calcium. As shown in Figure 8B, the permeability of all three drugs was significantly higher for the samples containing calcium. This is likely a consequence of the formation of calcium complexes, which increased more than twice the permeability of the drugs through CF sputum.

Even though the concentration of calcium in the CF mucus is reported to be lower than that of our mucus model, the impact that calcium can play on permeability is clear. Drug calcium salts might have better biological activities and should be considered when formulating drugs. For instance, high-dose ibuprofen taken constantly for years has been shown to significantly reduce the progression of the lung disease in cystic fibrosis.[14] It would be interesting to investigate if better health outcomes could be reached using a calcium formulation.

4. CONCLUSIONS

For the purpose of the present research, we used an *in vitro* pathological cystic fibrosis mucus model to explore how it can impact over permeability of a data set of 45 compounds. Overall, our data suggest that the activity of mucus is complex to be predicted. Determining the specific effects limiting the permeability of drugs through mucus was out of the scope of this work. Yet, it was found that the mucus was not only a physical barrier for the permeability of drugs but also behaved as a dynamic filter as well. The permeability of most of the compounds was reduced, while others were not affected by the barriers of mucus. A poor correlation of the effect of mucus on permeability was found for all of the selected molecular descriptors. These findings represent additional evidence of the further need for reliable *in vitro* mucus models to be used for drug screening, especially in mucus-related disorders.

We also ascertained that calcium, which is one of the components of our mucus model, enhanced the permeability of a small group of drugs. This was most likely the result of the complexation with the drug. The observed increased-permeability effect induced by calcium was also achieved through cystic fibrosis sputum, further highlighting the potential of using drugs as calcium salts to pursue higher absorption rates *in vivo*. Additionally, calcium-based formulations could offer new potentialities for the repositioning of the current therapies as well.

■ ASSOCIATED CONTENT

ⓢ Supporting Information

The Supporting Information is available free of charge at https://pubs.acs.org/doi/10.1021/acs.molpharmaceut.1c00644.

> Additional tables with the LC-MS and LC-UV conditions, the molecular descriptors selected, and the comparison of the herein measured P_{app} with reference values are reported; additional figures reporting the molecular structure of the tested compounds, the correlation plot between the herein measure P_{app} and reference P_{app} values, the correlation matrix, PCA plots, parallel analysis, detailed comparison of permeability recorded without and with the cystic fibrosis mucus model, and the ESI-MS spectrum of naproxen—calcium complex are reported (PDF)

■ AUTHOR INFORMATION

Corresponding Authors

Cosmin Butnarasu − *Department of Molecular Biotechnology and Health Science, University of Torino, Torino 10135, Italy;* ● orcid.org/0000-0001-8620-3391;
Email: cosminstefan.butnarasu@unito.it

Sonja Visentin − *Department of Molecular Biotechnology and Health Science, University of Torino, Torino 10135, Italy;*
Email: sonja.visentin@unito.it

Authors

Giulia Caron − *Department of Molecular Biotechnology and Health Science, University of Torino, Torino 10135, Italy;* ● orcid.org/0000-0002-2417-5900

Daniela Peneda Pacheco − *Department of Chemistry, Materials and Chemical Engineering, Giulio Natta-Politecnico di Milano, Milano 20133, Italy; Bac3Gel Lda, TagusPark—Edificio Inovacao II, Porto Salvo 2740-122, Portugal*

Paola Petrini − *Department of Chemistry, Materials and Chemical Engineering, Giulio Natta-Politecnico di Milano, Milano 20133, Italy;* ● orcid.org/0000-0003-3735-2432

Complete contact information is available at:
https://pubs.acs.org/10.1021/acs.molpharmaceut.1c00644

Notes

The authors declare the following competing financial interest(s): Daniela Peneda Pacheco is Co-founder and CTO of Bac3Gel Lda; Sonja Visentin and Paola Petrini are Co-founders.

■ ABBREVIATIONS USED

CF, cystic fibrosis; COPD, chronic obstructive pulmonary disease; PAMPA, parallel artificial membrane permeability assay.; PBS, phosphate-buffered saline; HPLC-MS, high-pressure liquid chromatography-mass spectrometry; DMSO, dimethyl sulfoxide; P_{app}, apparent permeability; GDL, D-(+)-gluconic acid δ-lactone; MRM, multiple reaction monitoring; PCA, principal component analysis; Ro5, Lipinski rule of five; NSAID, nonsteroidal anti-inflammatory drug

■ REFERENCES

(1) Cone, R. A. Barrier Properties of Mucus. *Adv. Drug Delivery Rev.* **2009**, *61*, 75−85.
(2) Hansson, G. C. Mucus and Mucins in Diseases of the Intestinal and Respiratory Tracts. *J. Intern. Med.* **2019**, *285*, 479−490.
(3) Bansil, R.; Turner, B. S. Mucin Structure, Aggregation, Physiological Functions and Biomedical Applications. *Curr. Opin. Colloid Interface Sci.* **2006**, *11*, 164−170.
(4) Mejías-Luque, R.; Cobler, L.; de Bolós, C. Atlas of Genetics and Cytogenetics in Oncology and Haematology. *Atlas Genet. Cytogenet. Oncol. Haematol.* **2011**, *14*, 566−569.
(5) Schömig, V. J.; Lieleg, B. T.; Berensmeier, S.; et al. An Optimized Purification Process for Porcine Gastric Mucin with Preservation of Its Native Functional Properties. *RSC Adv.* **2016**, *6*, 44932−44943.
(6) Murgia, X.; Loretz, B.; Hartwig, O.; Hittinger, M.; Lehr, C. The Role of Mucus on Drug Transport and Its Potential to Affect Therapeutic Outcomes. *Adv. Drug Delivery Rev.* **2018**, *124*, 82−97.
(7) Fahy, J. V.; Dickey, B. F. Airway Mucus Function and Dysfunction. *N. Engl. J. Med.* **2010**, *363*, 2233−2247.
(8) Mitri, C.; Xu, Z.; Bardin, P.; Corvol, H.; Touqui, L.; Tabary, O. Novel Anti-Inflammatory Approaches for Cystic Fibrosis Lung Disease: Identification of Molecular Targets and Design of Innovative Therapies. *Front. Pharmacol.* **2020**, *11*, No. 01096.
(9) Meldrum, O. W.; Chotirmall, S. H. Mucus, Microbiomes and Pulmonary Disease. *Biomedicines* **2021**, *9*, No. 675.
(10) Suk, J. S.; Lai, S. K.; Wang, Y. Y.; Ensign, L. M.; Zeitlin, P. L.; Boyle, M. P.; Hanes, J. The Penetration of Fresh Undiluted Sputum Expectorated by Cystic Fibrosis Patients by Non-Adhesive Polymer Nanoparticles. *Biomaterials* **2009**, *30*, 2591−2597.
(11) Yu, T.; Chisholm, J.; Choi, W. J.; Anonuevo, A.; Pulicare, S.; Zhong, W.; Chen, M.; Fridley, C.; Lai, S. K.; Ensign, L. M.; Suk, J. S.; Hanes, J. Mucus-Penetrating Nanosuspensions for Enhanced Delivery of Poorly Soluble Drugs to Mucosal Surfaces. *Adv. Healthcare Mater.* **2016**, *5*, 2745−2750.
(12) Murray, M. P.; Pentland, J. L.; Turnbull, K.; MacQuarrie, S.; Hill, A. T. Sputum Colour: A Useful Clinical Tool in Non-Cystic Fibrosis Bronchiectasis. *Eur. Respir. J.* **2009**, *34*, 361−364.
(13) Turcios, N. L. Cystic Fibrosis Lung Disease: An Overview. *Respir. Care* **2020**, *65*, 233−251.
(14) Konstan, M. W.; Byard, P. J.; Hoppel, C. L.; Davis, P. B. Effect of High-Dose Ibuprofen in Patients with Cystic Fibrosis. *N. Engl. J. Med.* **1995**, *332*, 848−854.
(15) Boegh, M.; Nielsen, H. M. Mucus as a Barrier to Drug Delivery - Understanding and Mimicking the Barrier Properties. *Basic Clin. Pharmacol. Toxicol.* **2015**, *116*, 179−186.
(16) Sigurdsson, H. H.; Kirch, J.; Lehr, C. M. Mucus as a Barrier to Lipophilic Drugs. *Int. J. Pharm.* **2013**, *453*, 56−64.
(17) Kansy, M.; Senner, F.; Gubernator, K. Physicochemical High Throughput Screening: Parallel Artificial Membrane Permeation Assay in the Description Of of Passive Absorption Processes. *J. Med. Chem.* **1998**, *41*, 1007−1010.
(18) Artursson, P.; Palm, K.; Luthman, K. Caco-2 Monolayers in Experimental and Theoretical Predictions of Drug Transport. *Adv. Drug Delivery Rev.* **2012**, *64*, 280−289.
(19) Di, L.; Whitney-Pickett, C.; Umland, J. P.; Zhang, H.; Zhang, X.; Gebhard, D. F.; Lai, Y.; Federico, J. J., III; Davidson, R. E.; Smith, R.; Reyner, E. L.; Lee, C.; Feng, B.; Rotter, C.; Varma, M. V.; Kempshall, S.; Fenner, K.; El-kattan, A. F.; Liston, T. E.; Troutman, M. D. Development of a New Permeability Assay Using Low-Efflux MDCKII Cells. *J. Pharm. Sci.* **2011**, *100*, 4974−4985.
(20) Sarmento, B. *Concepts and Models for Drug Permeability Studies - Cell and Tissue Based In Vitro Culture Models*; 1st ed., Woodhead Publishing, 2015.
(21) Lock, J. Y.; Carlson, T. L.; Carrier, R. L. Mucus Models to Evaluate the Diffusion of Drugs and Particles. *Adv. Drug Delivery Rev.* **2018**, *124*, 34−49.
(22) Butnarasu, C.; Barbero, N.; Pacheco, D.; Petrini, P.; Visentin, S. Mucin Binding to Therapeutic Molecules: The Case of Antimicrobial Agents Used in Cystic Fibrosis. *Int. J. Pharm.* **2019**, *564*, 136−144.
(23) Norris, D. A.; Sinko, P. J. Effect of Size, Surface Charge, and Hydrophobicity on the Translocation of Polystyrene Microspheres through Gastrointestinal Mucin. *J. Appl. Polym. Sci.* **1997**, *63*, 1481−1492.
(24) Boegh, M.; Baldursdóttir, S. G.; Müllertz, A.; Nielsen, H. M. Property Profiling of Biosimilar Mucus in a Novel Mucus-Containing in Vitro Model for Assessment of Intestinal Drug Absorption. *Eur. J. Pharm. Biopharm.* **2014**, *87*, 227−235.
(25) Onnainty, R.; Usseglio, N.; Bonafé Allende, J. C.; Granero, G. Exploring a New Free-Standing Polyelectrolyte (PEM) Thin Film as a Predictive Tool for Drug-Mucin Interactions: Insights on Drug Transport through Mucosal Surfaces. *Int. J. Pharm.* **2021**, *604*, No. 120764.
(26) Grainger, C. I.; Greenwell, L. L.; Lockley, D. J.; Martin, G. P.; Forbes, B. Culture of Calu-3 Cells at the Air Interface Provides a Representative Model of the Airway Epithelial Barrier. *Pharm. Res.* **2006**, *23*, 1482−1490.

(27) Falavigna, M.; Klitgaard, M.; Brase, C.; Ternullo, S.; Škalko-Basnet, N.; Flaten, G. E. Mucus-PVPA (Mucus Phospholipid Vesicle-Based Permeation Assay): An Artificial Permeability Tool for Drug Screening and Formulation Development. *Int. J. Pharm.* **2018**, *537*, 213−222.

(28) Pacheco, D. P.; Butnarasu, C. S.; Briatico Vangosa, F.; Pastorino, L.; Visai, L.; Visentin, S.; Petrini, P. Disassembling the Complexity of Mucus Barriers to Develop a Fast Screening Tool for Early Drug Discovery. *J. Mater. Chem. B* **2019**, *7*, 4940−4952.

(29) Hentzer, M.; Teitzel, G. M.; Balzer, G. J.; Heydorn, A.; Molin, S.; Givskov, M.; Parsek, M. R. Alginate Overproduction Affects Pseudomonas Aeruginosa Biofilm Structure and Function. *J. Bacteriol.* **2001**, *183*, 5395−5401.

(30) Leid, J. G.; Willson, C. J.; Shirtliff, M. E.; Hassett, D. J.; Parsek, M. R.; Jeffers, A. K. The Exopolysaccharide Alginate Protects *Pseudomonas aeruginosa* Biofilm Bacteria from IFN-γ-Mediated Macrophage Killing. *J. Immunol.* **2005**, *175*, 7512−7518.

(31) Forstner, J. F.; Forstner, G. G. Effects of Calcium on Intestinal Mucin: Implications for Cystic Fibrosis. *Pediatr. Res.* **1976**, *10*, 609−613.

(32) Wishart, D. S.; Knox, C.; Guo, A. C.; Shrivastava, S.; Hassanali, M.; Stothard, P.; Chang, Z.; Woolsey, J. DrugBank: A Comprehensive Resource for in Silico Drug Discovery and Exploration. *Nucleic Acids Res.* **2006**, *34*, 668−672.

(33) Kim, S.; Chen, J.; Cheng, T.; Gindulyte, A.; He, J.; He, S.; Li, Q.; Shoemaker, B. A.; Thiessen, P. A.; Yu, B.; Zaslavsky, L.; Zhang, J.; Bolton, E. E. PubChem in 2021: New Data Content and Improved Web Interfaces. *Nucleic Acids Res.* **2021**, *49*, D1388−D1395.

(34) Sharifian Gh, M. Recent Experimental Developments in Studying Passive Membrane Transport of Drug Molecules. *Mol. Pharm.* **2021**, *18*, 2122−2141.

(35) Oriano, M.; Terranova, L.; Sotgiu, G.; Saderi, L.; Bellofiore, A.; Retucci, M.; Marotta, C.; Gramegna, A.; Miglietta, D.; Carnini, C.; Marchisio, P.; Chalmers, J. D.; Aliberti, S.; Blasi, F. Evaluation of Active Neutrophil Elastase in Sputum of Bronchiectasis and Cystic Fibrosis Patients: A Comparison among Different Techniques. *Pulm. Pharmacol. Ther.* **2019**, *59*, No. 101856.

(36) Chen, X.; Murawski, A.; Patel, K.; Crespi, C. L.; Balimane, P. V. A Novel Design of Artificial Membrane for Improving the PAMPA Model. *Pharm. Res.* **2008**, *25*, 1511−1520.

(37) Teixeira, L.; de, S.; Chagas, T. V.; Alonso, A.; Gonzalez-alvarez, I.; Bermejo, M.; Polli, J.; Rezende, K. R. Biomimetic Artificial Membrane Permeability Assay over Franz Cell Apparatus Using Bcs Model Drugs. *Pharmaceutics* **2020**, *12*, 1−16.

(38) Sugano, K.; Takata, N.; Machida, M.; Saitoh, K.; Terada, K. Prediction of Passive Intestinal Absorption Using Bio-Mimetic Artificial Membrane Permeation Assay and the Paracellular Pathway Model. *Int. J. Pharm.* **2002**, *241*, 241−251.

(39) Artursson, P.; Bergström, C. A. S. Intestinal Absorption: The Role of Polar Surface Area. *Methods Princ. Med. Chem.* **2003**, 339−357.

(40) Di, L.; Kerns, E. H.; Fan, K.; McConnell, O. J.; Carter, G. T. High Throughput Artificial Membrane Permeability Assay for Blood-Brain Barrier. *Eur. J. Med. Chem.* **2003**, *38*, 223−232.

(41) Köllmer, M.; Mossahebi, P.; Sacharow, E.; Gorissen, S.; Gräfe, N.; Evers, D. H.; Herbig, M. E. Investigation of the Compatibility of the Skin PAMPA Model with Topical Formulation and Acceptor Media Additives Using Different Assay Setups. *AAPS PharmSciTech* **2019**, *20*, No. 89.

(42) Matsson, P.; Kihlberg, J. How Big Is Too Big for Cell Permeability? *J. Med. Chem.* **2017**, *60*, 1662−1664.

(43) Hitchcock, S. A.; Pennington, L. D. Structure-Brain Exposure Relationships. *J. Med. Chem.* **2006**, *49*, 7559−7583.

(44) Shityakov, S.; Neuhaus, W.; Dandekar, T.; Förster, C. Analysing Molecular Polar Surface Descriptors to Predict Blood-Brain Barrier Permeation. *Int. J. Comput. Biol. Drug Des.* **2013**, *6*, 146−156.

(45) Tang, B.; Wang, J.; Wang, Q.; Xiao, Y.; Huang, Y.; Liao, X.; Li, H. Calcium(II)−Naproxen Complex: Synthesis, Characterization, and Interaction with Human Serum Albumin. *Spectrosc. Lett.* **2016**, *49*, 404−411.

(46) Atassi, F.; Mao, C.; Masadeh, A. S.; Byrn, S. R. Solid-State Characterization of Amorphous and Mesomorphous Calcium Ketoprofen. *J. Pharm. Sci.* **2010**, *99*, 3684−3697.

(47) Ogiso, T.; Ito, Y.; Iwaki, M.; Atago, H. Absorption of Indomethacin and Its Calcium Salt through Rat Skin: Effect of Penetration Enhancers and Relationship between in Vivo and in Vitro Penetration. *J. Pharmacobio-Dyn.* **1986**, *9*, 517−525.

(48) Mandel, I. D.; Eriv, A.; Kutscher, A.; Denning, C.; Thompson, R. H.; Kessler, W.; Zegarelli, E. Calcium and Phosphorus Levels in Submaxillary Saliva. *Clin. Pediatr.* **1969**, *8*, 161−164.

L

Cystic Fibrosis Mucus Model to Design More Efficient Drug Therapies

Cosmin Butnarasu [*a], Giulia Caron [a], Daniela Peneda Pacheco [b,c], Paola Petrini [b], Sonja Visentin [*a]

[a] *University of Torino, Department of Molecular Biotechnology and Health Science, Via Quarello 15, 10135 Torino, Italy*
[b] *Department of Chemistry, Materials and Chemical Engineering, Giulio Natta-Politecnico di Milano, Piazza Leonardo da Vinci 32, 20133 Milano, Italy*
[c] *Bac3Gel Lda, TagusPark – Edificio Inovacao II, 2740-122 Porto Salvo, Portugal.*

Corresponding author: sonja.visentin@unito.it, cosminstefan.butnarasu@unito.it,

Supporting Material

Tables

Table S1. Analytical conditions of the investigated compounds on LC-MS and LC-UV.

Table S2. Molecular descriptors. Principal Component Analysis was computed using all descriptors except for P_{app} and *Effect of mucus on P_{app}*.

Table S3. Comparison of the permeability data for some of the tested compounds with what previously reported by Chen *et al*.[1]

Figures

Figure S1: Structures of the tested drugs.

Figure S2: Correlation of the P_{app} obtained in the PAMPA system with the permeability reported by Chen *et al*.[1]

Figure S3. Correlation matrix.

Figure S4. Principal component analysis of the dataset.

Figure S5. Selection of components based on parallel analysis. By retaining only those PCs with eigenvalues greater than the 95th percentile of the simulated eigenvalues, it is ensured that the variance explained by these PCs likely represents "real" variance and not variance due to noise.

Figure S6. Comparison of the permeability recorded on PAMPA without (blue) and with mucus (red) for the tested compounds.

Figure. S7. The ESI-MS spectrum of the naproxen-calcium complex.

Table S1. Analytical conditions of the investigated compounds on LC-MS and LC-UV.

#	Compounds	Mobile phases	Polarity	Parent ion	Fragment ion	CE (V)	UV detection (nm)
1	Propranolol		+	259.9	116.1	-11.5	
2	Baricitinib		+	371.7	186.2	-34.5	
3	Camostat		+	399	296.1	-18	
4	Dexamethasone		+	372.8	237.1	-20	
6	Favipiravir		-	155.5	112.7	13	
7	Indinavir		+	614.2	421.1	-26.5	
8	Oseltamivir		+	313	166.2	-15	
9	Remdesivir		+	603.1	200	-41.5	
10	Saquinavir		+	671.3	570.2	-25	
11	Umifenovir		+	479.2	433.9	-15	
12	Zanamivir		+	333.2	273.9	-15.5	
13	Levofloxacin		+	362	317.9	-16.5	
14	CFTR$_{inh}$-172		-	408.2	363.9	7	
15	Verapamil		+	455.4	164.9	-21	
17	Amlodipine		+	409.2	237.7	-14.5	
18	Amitriptyline		+	278.2	90.8	-19	
19	Procaine		+	237.2	99.8	-13	
20	Caffeine		+	195.1	137.8	-15.5	
22	Piroxicam	H2O FA 0.1% - ACN	+	332	94.8	-17.5	
23	Diclofenac		+	296	213.9	-35	
24	Ampicillin		+	350	105.8	-21	
25	Tetracycline		+	445.2	409.8	-14.5	
26	Ritonavir		+	721	296	-20	
28	Ceftazidime		+	547.4	79.8	-9.5	
29	Ciprofloxacin		+	331.9	230.8	-38.5	
30	Rifampicin		+	823.6	791	-13	
31	Salbutamol		+	240	147.9	-18.5	
32	Aztreonam		-	433.9	95.7	16	
34	Lumacaftor		+	453.3	413.1	-18.5	
35	Valsartan		-	434.2	349.7	15	
36	Lidocaine		+	235.1	85.6	-14	
37	TUDCA		-	498.7	123.5	16.5	
38	GUDCA		-	448.7	74	12	
39	Tobramycin		+	468	324	-13	
41	Acetaminophen		+	152	109.8	-20	
42	Quinine		+	325	307	-18	
44	Ketoprofen		+	255.1	104.7	-22	
45	Antipyrine		+	189	76.8	-32.5	
21	Naproxen		-	229	169.4	13	
27	Indomethacin	Ammonium acetate 5 mM pH 6.6 - ACN	-	356.2	312	6	
33	Cefuroxime		-	423.3	206.9	9.5	
40	Ibuprofen		-	205	160.5	5.5	
41	Ebselen	Ammonium acetate 5 mM pH 6.6 - ACN					263
42	3-aminophenol						236
43	Benzoic acid						230

2

Table S2. Molecular descriptors. Principal Component Analysis was computed using all descriptors except for P_{app} and *Effect of mucus on P_{app}*.

#	Molecular descriptor	Origin
1	Charge at pH 7.4	MarvinSketch
2	P_{app} (PAMPA)	Experimental
3	Effect of mucus on P_{app}	
4	Total Molweight	DataWarrior
5	cLogP	
6	cLogS	
7	H-Acceptors	
8	H-Donors	
9	Total Surface Area	
10	Relative PSA	
11	Total Polar Surface Area	
12	Druglikeness	
13	Shape Index	
14	Molecular Flexibility	
15	Molecular Complexity	
16	Non-H Atoms	
17	Non-C/H Atoms	
18	Electronegative Atoms	
19	Stereo Centers	
20	Rotatable Bonds	
21	Rings Closures	
22	Aromatic Atoms	
23	sp3-Atoms	
24	Symmetric Atoms	
25	Small Rings	
26	Aromatic Rings	
27	Amides	
28	Amines	
29	Alkyl-Amines	
30	Aromatic Amines	
31	Aromatic Nitrogens	
32	Basic Nitrogens	
33	Acidic Oxygens	

Table S3. Comparison of the permeability data for some of the tested compounds with what reported in the literature.

Compound	P_{app} PAMPA (± SD) ×10^{-6} [cm/s]		P_{app} PAMPA literature reference (± SD) ×10^{-6} [cm/s] [1]	
Propranolol	12.56	(± 2.9)	10.32	(± 2.4) [1,2]
Naproxen	9.57	(± 3.9)	6.03	(± 0.6)
Caffeine	12.70	(± 3.5)	9.89	(± 1.5)
Ibuprofen	9.09	(± 1.4)	10.73	(± 1.6)
Verapamil	8.57	(± 2.0)	8.75	(± 0.5)
Diclofenac	4.03	(± 0.2)	6.95	(± 0.3)
Antipyrine	5.75	(± 1.7)	7.51	(± 1.4)
Ketoprofen	4.04	(± 0.7)	4.13	(± 0.4)
Piroxicam	3.15	(± 0.8)	4.96	(± 0.7)

4
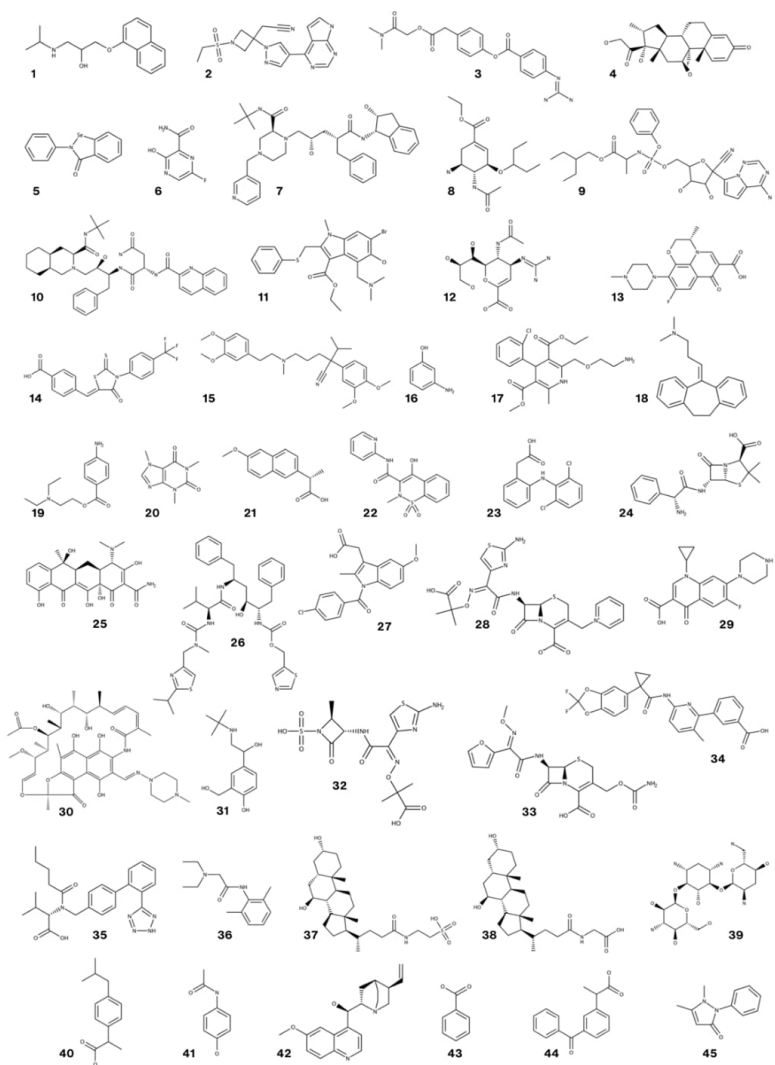
Figure S1. Structures of the tested drugs. (1) propranolol, (2) baricitinib, (3) camostat, (4) dexamethasone, (5) ebselen, (6) favipiravir, (7) indinavir, (8) oseltamivir, (9) remdesivir, (10) saquinavir, (11) umifenovir, (12) zanamivir, (13) levofloxacin, (14) CFTR$_{inh}$-172, (15) verapamil, (16) 3-aminophenol, (17) amlodipine, (18) amitriptyline, (19) procaine, (20) caffein, (21) naproxen, (22) piroxicam, (23) diclofenac, (24) ampicillin, (25) tetracycline, (26) ritonavir, (27) indomethacin, (28) ceftazidime, (29) ciprofloxacin, (30) rifampicin, (31) salbutamol, (32) aztreonam, (33) cefuroxime, (34) lumacaftor, (35) valsartan, (36) lidocaine, (37) tauroursodeoxycholic acid, (38) glycoursodeoxycholic acid, (39) tobramycin, (40) ibuprofen, (41) acetaminophen, (42) quinine, (43) benzoic acid, (44) ketoprofen, (45) antipyrine.
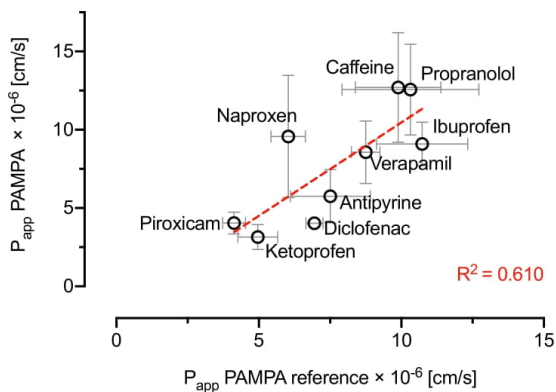
Figure S2. Comparison between PAMPA permeability obtained with the modified setup and PAMPA permeability reported by Chen *et al.*, using the same artificial membrane. Data used in this plot are listed in Table S3.
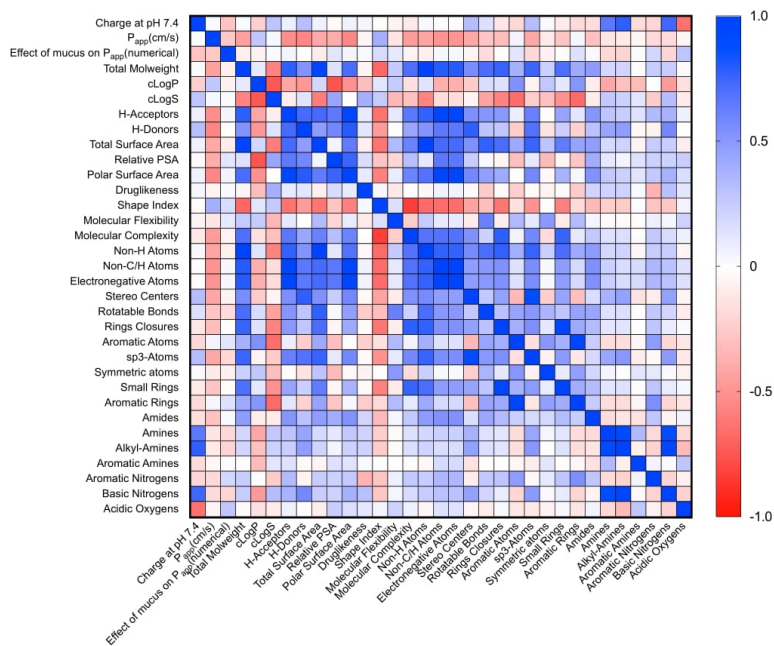
Figure S3. Correlation matrix

In addition to the discrimination of the high and low permeable compounds based on the topological polar surface area (TPSA), we tried to understand if the two groups could be discriminated within the chemical space based on their chemical properties. To better appreciate any existing difference between the two groups, we computed a principal component analysis (PCA). In brief, PCA is a multivariate technique that is used to reduce the dimension of the dataset while retaining as much information from the data as possible, alongside maximizing the variance of the data by defining principal components. The results are represented by score and loadings plots in Fig S2 A and S2 C. The PC score graph (Fig. S2 A) provides a visual representation of the dimension reduction achieved by PCA, while the PC loadings plot (Fig. S2 C) represent the correlation between variables and the principal components.

Based on parallel analysis which is a method for selecting principal components that accounts for variance in the data due to random error or noise (Fig. S3), four components have been selected accounting for 74% of the variance. With PC 1 and PC2 about 55% of the variance was explained and high and low permeable compounds can be discriminated on PC 1 which accounts for the highest variance. As expected, the loadings plot shows that permeability is negatively correlated with molecular descriptors associated with polarity (i.e., PSA, HBD, HBA), as they are arranged in a specular fashion with respect to the scores of the highly permeable group. Yet, a negative correlation is observed also with descriptors linked to molecular complexity (i.e., total molecular weight, non-H atoms, total surface area), and apparently no relation with lipophilicity (cLogP). This, for some extent, is somehow contradictory as numerous significant correlations between lipophilicity and drug passive permeation have been established.

The distribution of the tested drugs in the chemical space based on their behavior in the presence of mucus is challenging to interpret (Fig. S2 B). In the score plot, a general overlap of the three groups is observed, making it difficult to discriminate between each category.
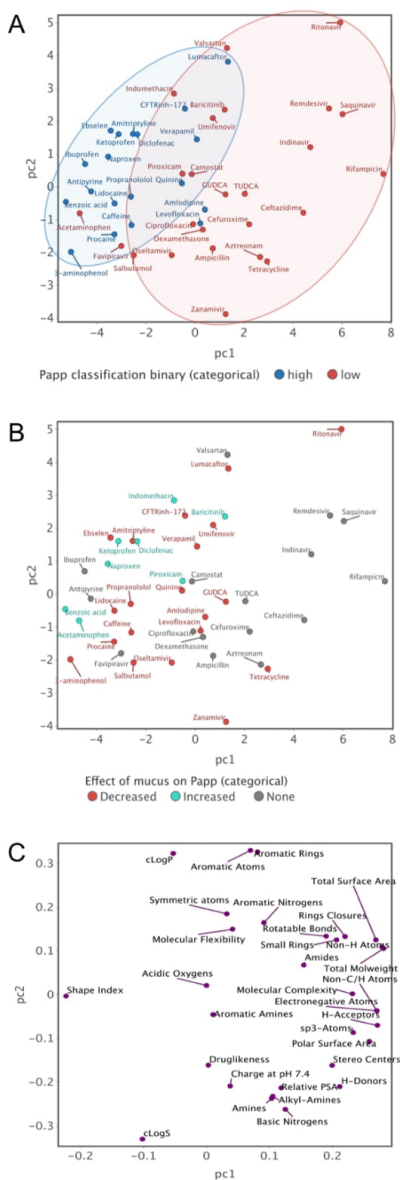
Figure S4. Principal component analysis of the dataset. (Fig S2 A) score plot colored based on the classification in high and low permeability. The blue and red circles define the discrimination of the two categories on the first principal component. (Fig S2 B) score plot colored by the effect of mucus over the permeability in the mucus-PAMPA system. Here we cannot see a clear discrimination on any of the principal

components between the three categories. (Fig. S2 C) loading plot representing the correlation between the variables and the principal components.
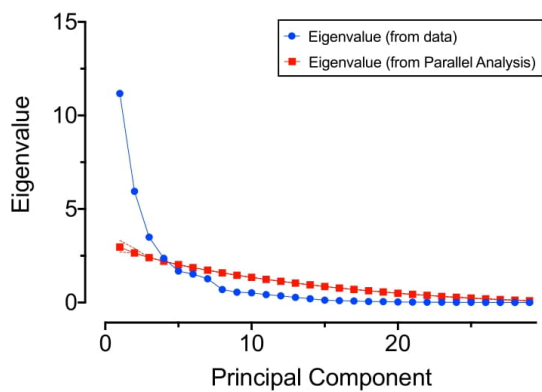
Figure S5. Selection of components based on parallel analysis. By retaining only those PCs with eigenvalues greater than the 95th percentile of the simulated eigenvalues, it is ensured that the variance explained by these PCs likely represents "real" variance and not variance due to noise.
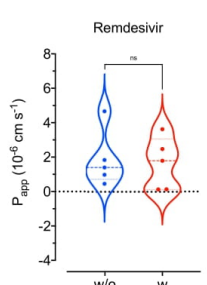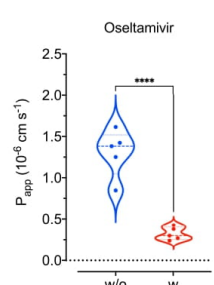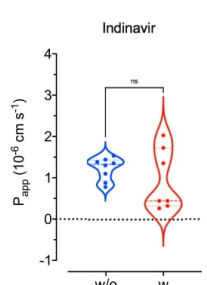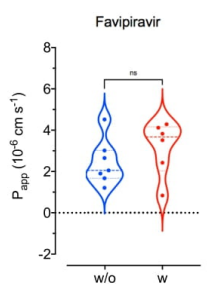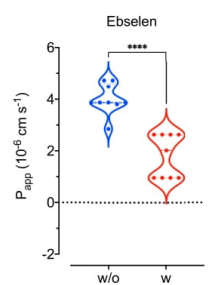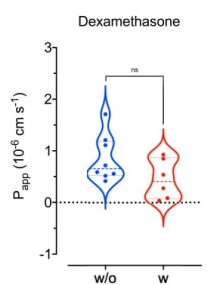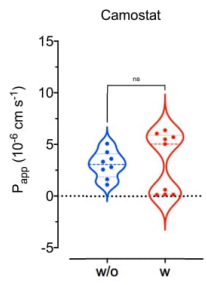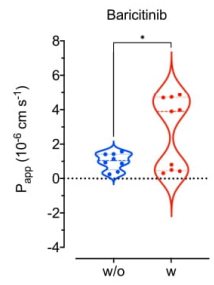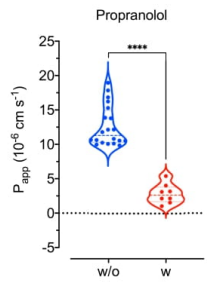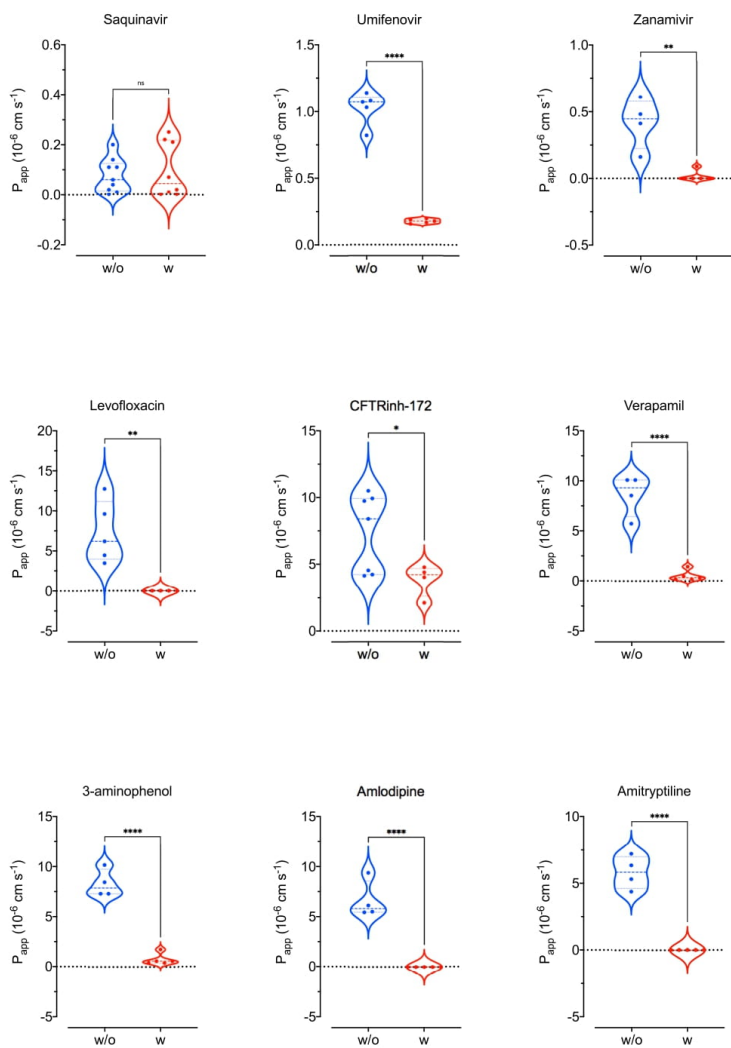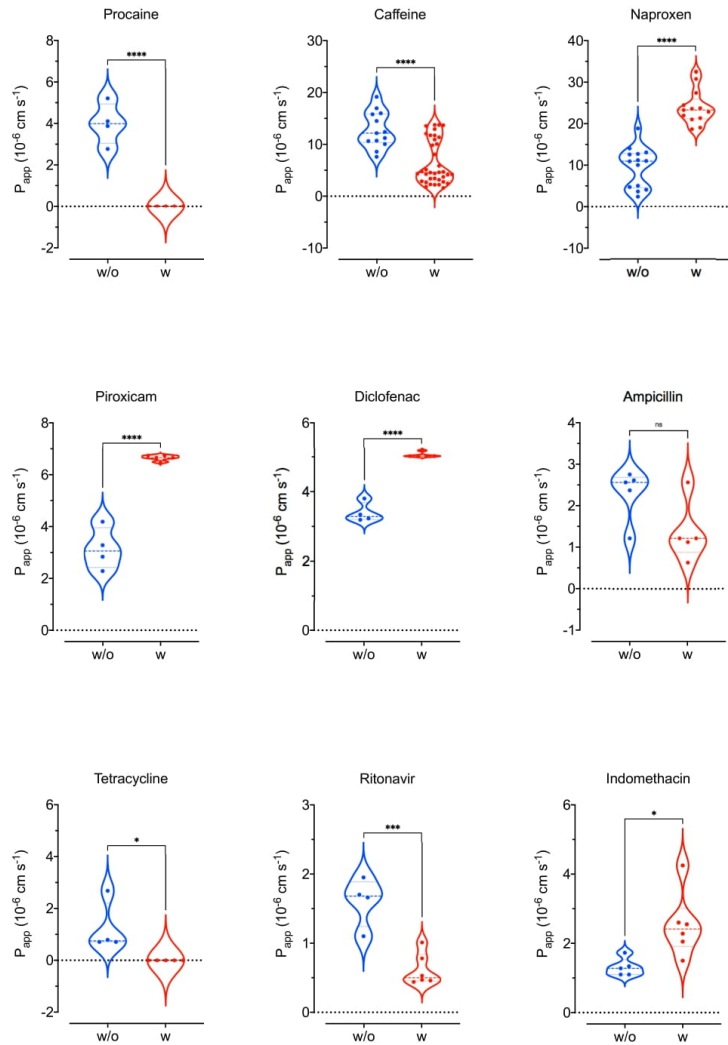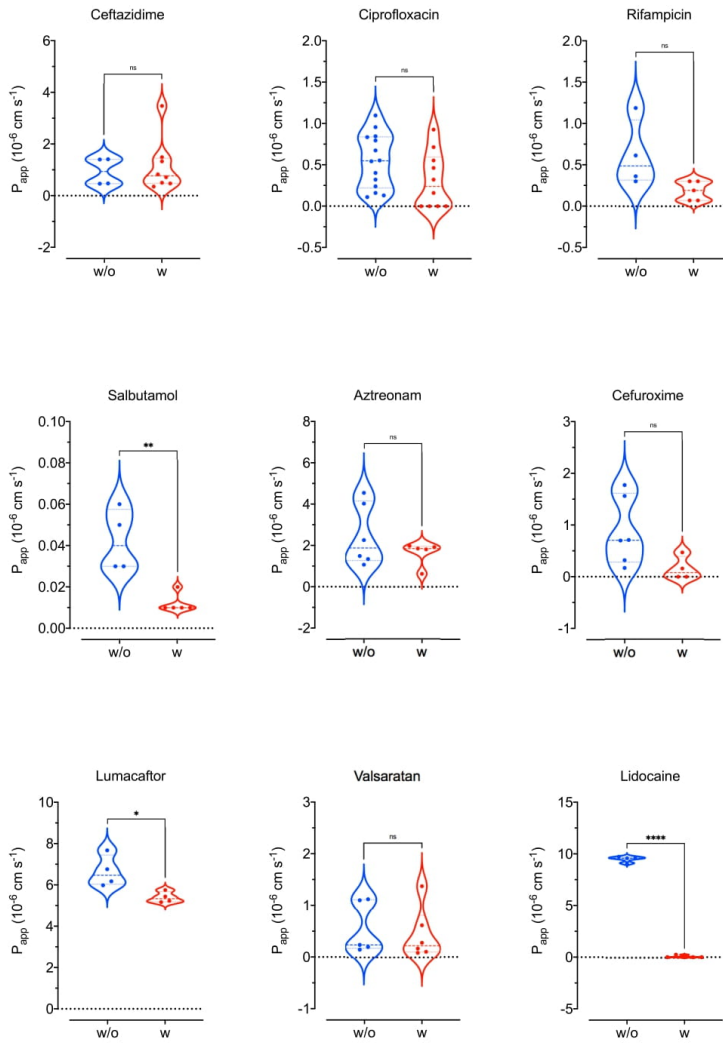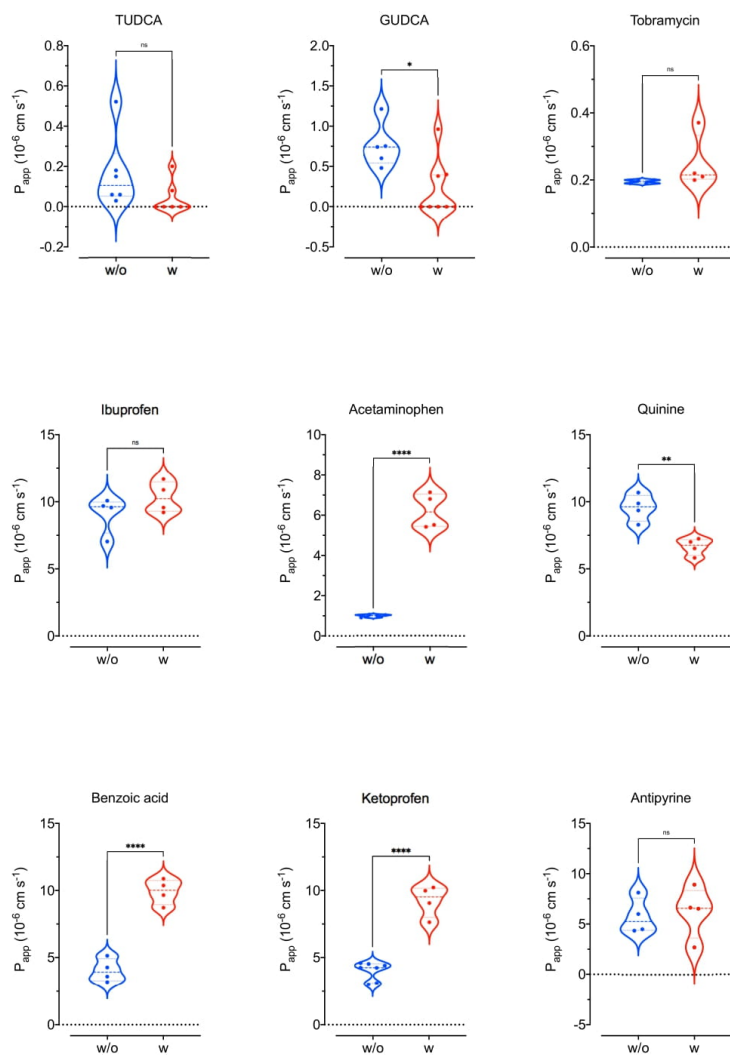
Figure S6. Comparison of the permeability recorded on PAMPA without (blue) and with mucus (red) for the tested compounds.
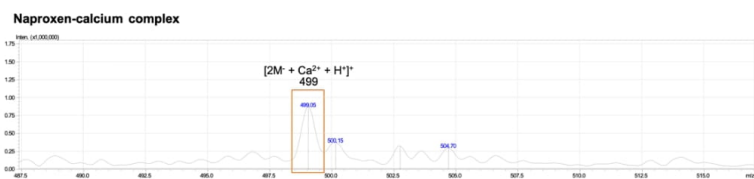
Figure. S7. The ESI-MS spectrum of the naproxen-calcium complex.

References

(1) Chen, X.; Murawski, A.; Patel, K.; Crespi, C. L.; Balimane, P. V. A Novel Design of Artificial Membrane for Improving the PAMPA Model. *Pharm. Res.* **2008**, *25* (7), 1511–1520. https://doi.org/10.1007/s11095-007-9517-8.

(2) Kerns, E. H.; Di, L.; Petusky, S.; Farris, M.; Ley, R.; Jupp, P. Combined Application of Parallel Artificial Membrane Permeability Assay and Caco-2 Permeability Assays in Drug Discovery. *J. Pharm. Sci.* **2004**, *93* (6), 1440–1453. https://doi.org/10.1002/jps.20075.

Mucosomes: intrinsically mucoadhesive glycosylated mucin nanoparticles as multi drug delivery platform

The attached manuscript is in form of submitted manuscript (original article).

The author's contributions to the appended manuscript consist of part of the experimental work (synthesis, drug encapsulation, size, glycosylation, spectroscopic, stability, and mucosal diffusion characterization), data analysis, and major part of manuscript preparation. Planning and execution of experiments, data interpretation, and writing the manuscript were performed with the contribution from coauthors.

Mucosomes: intrinsically mucoadhesive glycosylated mucin nanoparticles as multi drug delivery platform

Cosmin Butnarasu[1*], Paola Petrini[2], Francesco Bracotti[1], Visai Livia[3,4], Giuseppe Guagliano[2], Alessandra Fiorio Pla[5], Ettore Sansone[5], Sara Petrillo[1] and Sonja Visentin[1*]

[1] *University of Turin, Department of Molecular Biotechnology and Health Science, via Quarello 15, 10135 Torino, Italy*

[2] *Department of Chemistry, Materials and Chemical Engineering "Giulio Natta", Politecnico di Milano, Italy*

[3] *Molecular Medicine Department (DMM), Center for Health Technologies (CHT), UdR INSTM, University of Pavia, Pavia, Italy*

[4] *Department of Occupational Medicine, Toxicology and Environmental Risks, Istituti Clinici Scientifici (ICS) Maugeri, IRCCS, Pavia, Italy*

[5] *Department of Life Sciences and Systems Biology, University of Torino, via Accademia Albertina 13, 10123 Torino, Italy*

*Corresponding author: <u>cosminstefan.butnarasu@unito.it</u>, <u>sonja.visentin@unito.it</u>

Abstract

Mucus is a complex barrier to overcome during pharmacological treatment and it is one of the major challenges faced by transmucosal drug delivery. The overproduction of mucus during respiratory diseases like cystic fibrosis, COPD and also COVID-19, impedes pulmonary delivery of therapeutics. Here we introduce a novel class of intrinsically mucoadhesive and glycosylated mucin-based nanoparticles that have been named "mucosomes". They were designed for improving drug absorption and residence time in the nasal epithelial. The mucoadhesive properties and surface glycosylation are naturally inherited from mucin, which is the most important protein constituting mucus. The synthesis, the functionalization with glycans, and the encapsulation of the desired compound are obtained through a lean one-pot synthesis. Mucosomes can be efficiently loaded with small- and macro- molecules with different physicochemical properties. Furthermore, we have proved the intrinsic mucoadhesive properties of

mucosomes, the presence of functional glycans, and their biocompatibility *in vitro* and *in vivo*. Given their unique properties, mucosomes represent a groundbreaking nanosystem that could be broadly applied in different pathological contexts, especially in mucus-related disorders.

1. Main

In spite of advances in technology and knowledge of human diseases, the translation of these benefits into therapeutic advances has been far slower than expected.[1] Pharmaceutical companies are spending more and more to come up with fewer drugs. Furthermore, since finding new therapeutic solutions has become so difficult, the cost and time to bring new drugs to market nearly doubled in the last decades, requiring on average an investment of $2.6 billion in 12 years.[2,3] This is coupled with a high probability of failure at the jump from preclinical studies to clinical trials, making drug development a highly risky investment. The World Health Organization (WHO) calls for new and more effective strategies to treat the various diseases that take the heaviest toll on the developing world.[4,5] For example, given the current pace, the development of new antimicrobial drugs is unlikely to solve the global emergence of microbial pathogen resistance.[6]

There is the need to reinvent the way in which current drugs are delivered, focusing on different mechanisms of action and improving the efficiency of delivery systems to make them more selective for the specific body district and the type of targeted environment. Within the anti-infective scenario, for example, there is a shift towards not killing the pathogen yet interfering with their pathogenic mechanism.[6] In the anti-adhesion therapy of infectious agents, protein-glycans interactions modulate adhesion, invasion and immune evasion of bacteria and viruses.[7–10] Protein-glycans interactions are crucial not only for infectious pathogens. Changes in the glycosylation profile of cell surface adhesion molecules, such as selectin ligands, integrins, and mucins, have been implicated also in tumor microenvironment.[11–14] For example, overexpression of sialic acid on the cell surface increases repulsion between adjacent cells and facilitates entrance into the bloodstream, promoting metastasis.[11,15] These features could be sharply targeted, switching from generic, all-purpose, delivery systems to pathology-specific or tissue-specific ones.

Nanocarriers, lipid and protein nanoparticles (NPs), are nowadays employed to deliver drugs, genetic material, or a contrast agent, facing the problems of safety, efficacy, bioavailability, dose–response, targeting ability, and personalization. So far, a plethora of nanoparticles have been documented with a wide range of applications in medicine and biology. Among them, lipid nanoparticles are one of the most preferred platforms for numerous formulations.[16] During the last 30 years their application was explored and validated in numerous fields, spacing from the administration of pulmonary antibiotic drugs (e.g. Arikayce®), to the embedding and delivery of genetic material, including the latest mRNA vaccines against COVID-19.[17,18] Alternatively, protein-based nanoparticles have demonstrated advantageous features in oncology. Albumin-bound paclitaxel nanoparticles (nab-paclitaxel, Abraxane®) are used as a second-line treatment against breast metastatic cancer, and up to now, are the only protein-based nanosystem marketed. This pioneering success story provides a glimpse into the opportunities behind this class of nanoparticles as drug vehicles. Several other protein drug carriers, like silk fibroin, gelatin, and gliadin, are currently under development.[19–21]

Except for the intravenous administration, all the other routes imply overcoming or interacting with physiological barriers, to exert the desired pharmacological effect. The first barrier interspaced between the external environment and all the wet surfaces of our body is mucus. Mucus acts as a primary innate defensive barrier, playing a crucial role in preventing pathogens from reaching the inner districts of the organism and expelling them through tightly regulated clearance mechanisms.[22,23] The mucus retention is governed by interactions with its components. Among them, mucins orchestrate most of the interplays. Mucins are long polymeric glycoproteins characterized by a peptide backbone rich in carbohydrates chains terminated by sialic acid.[24] But mucus can equally represent a barrier to overcome also for the absorption of drugs and NPs.[25] Particularly, in mucus-related disorders, such as cystic fibrosis (CF), chronic obstructive pulmonary disease (COPD) and bronchial asthma, characterized by an overproduction of mucus. Often, in these cases, the low efficacy treatment is the result of the inability of therapeutics to overcome the mucus barrier.[26,27]

Nevertheless, mucus is not only an obstacle to surpass. One of the strategies pursued to improve the performance of pharmaceutical drug formulations consists in adoption of mucoadhesive drug delivery systems. In fact, adhesion of chemicals to mucous membranes or a mucus-covered surface prolongs the contact with adsorption sites,

overcoming the challenge of short retention time.[28] Over the years, several mucoadhesive polymers for drug delivery applications have been investigated, including natural polymers as alginates[29] and chitosan[30], but also synthetic as poly acrylic acid[31] and poly vinyl pyrrolidone.[32] However, obtaining mucoadhesive drug delivery systems is not straightforward. Usually, it requires *ad hoc* derivatization procedures which are time consuming and expensive. The pharmaceutical industry, despite the great interest, adopts in most of the cases less expensive solutions, such as simply increasing the amount of active ingredient rather than designing mucoadhesive drug delivery systems.[33]

We identified the need to design drug delivery systems specifically targeting mucus and able to carry active pharmaceutical ingredients, avoiding though successive functionalization steps. By taking inspiration from our primary defensive mechanism, the mucus, we used mucin glycoproteins to develop a completely new system with multiple potential applications, including drug delivery, gene-therapy, and diagnostic. The ability of mucins to directly engage with an extremely wide spectrum of both pathogens and molecules was selected as a strategy to produce nanosystems for drug delivery, with in mind the specific challenge of mucoadhesion.

We, therefore, introduce a novel category of nanosystems, named *mucosomes*, glycosylated and mucoadhesive nanoparticles, composed of mucins, and inspired from the very same characteristics of mucus (Fig. 1a).

2. Results

2.1. Synthesis of stable mucosomes

Proteins and other macromolecules can condensate in nanostructures by desolvation process. Usually, organic solvent (*e.g.*, alcohol, acetone) is added dropwise to an aqueous solution of protein under stirring to dehydrate the protein leading to protein self-assembly and nanoparticles (NPs) formation.[34,35] Similarly to other proteins, native mucin is also described to form reversible nanoparticles.[36] Building up from the state-of-art knowledge, we set-up a synthetic method to produce, in one single step, mucin-based nanoparticles, having in mind the need of preserving the protein glycosylation, and avoiding the successive synthetic steps commonly employed to produce glycosylated nanoparticles.[37,38] We also believed that the possibility to produce and load nanoparticles with drugs within the same synthetic procedure would favor a lean

preparation. The "produce-and-load" single step overcomes the limits of successive loading and expands the diversity of molecules that can be loaded. In fact, drug loading into pre-formed nanoparticles is a challenge. Because passive loading is an equilibrium process depending on the ratio between intraparticle and extra particle volume, the encapsulation efficiency is low and the formulation has to be purified from the non-encapsulated drug.[39] Moreover, the encapsulation efficiency for high-molecular-weight molecules has been reported to be generally low, namely far below 50%.[40] We, therefore, developed a production method based on desolvation, which allows simultaneous loading of drugs with encapsulation efficiencies spanning from 21% to 94% (see section 3.7).

But the agile process for production and drug loading is not enough. For the applicability of the systems, the stability in physiological condition, until the NPs and their payloads reach the target sites, is another important issue. This should be associated with the possibility to produce nanoparticles that can be stored until use, and/or resuspended in a medium without aggregation. To face these challenges, the desolvation method alone was not effective. The desolvation mechanism was paired with a secondary process, the chemical crosslinking, and PEG was used to minimize aggregation. We called the novel class of protein nanoparticles, formed by the synergy of the double mechanism of desolvating the protein with organic solvent and crosslinking with glutaraldehyde, "mucosomes". After conversion of mucin into mucosomes, the nanoparticles were purified by several centrifugation cycles. Uncondensed mucin monomers and small mucin fragments were quantified in the supernatant volumes and the calculated yield of condensation is approximately 25%. The formation of mucin nanoparticles can be appreciated when comparing the absorbance spectra of free mucin and mucosomes (Fig. 1g), as the characteristic band of PGM at 258 nm, resulting mainly from the phenylalanine residues, strongly flattens after the formation of nanoparticles. Also, the scattering of the mucosomes is significantly higher as a result of the formation of nanoparticulate in suspension.[41] The secondary structure of mucin (Fig. 1h) strongly changes after the folding of the protein into nanoparticles as observed by circular dichroism. The predicted secondary structure of mucin varies from 29.2% α-helix and 6.4% β-strand, to 11.7% and 27.8% respectively, representative of mucosomes.

Moreover, it is worth mentioning that mucosomes are synthesized starting from commercially available porcine gastric mucin. The advantages of using the commercial

protein are multiple in terms of scalability, availability and production costs. On the other hand, it might be true that laboratory-purified mucins are qualitatively superior and contain fewer impurities.[42,43] However, extracting and purifying mucin at a laboratory scale is, up to now, time-consuming and highly expensive. For pharmaceutical purposes, the lack of efficient and scalable extraction and purification processes are one of the main obstacles to use lab-purified mucins.

2.2. Morphological characterization of mucosomes

Important factors of nanosystems influencing their bioavailability are the size and the morphology. The size and the morphology of mucosomes were evaluated by transmission electron microscopy (TEM), field-emission scanning electron microscopy (FESEM), energy-dispersive X-ray analysis (EDX), dynamic light scattering analysis (DLS) and nano-tracking analysis (NTA).

Mucosomes have a spherical shape with the size in the range of 150-300 nm (TEM analysis, Fig. 1b). FESEM measurements (Fig. 1c) corroborated the result (spherical nanoparticles of about 200 nm diameter). The observed nanoparticles are largely composed of C and to a lesser extent of O, N and S (Fig. 1d, EDX analysis). Such composition reflects the protein nature of the mucosomes.

By microscopy techniques, such as TEM and FESEM, samples are analyzed in a dried form. But as the physiological environment is relevant for their use, the size distribution profile in a liquid environment was evaluated by the DLS and NTA techniques (Fig. 1e-f). The mucosomes exhibited a population of nanoparticles around 230 (± 86) nm (DLS measurements), while the mean size values obtained by NTA are slightly smaller (170 ± 124 nm) than the measured size given by DLS. Even though by both techniques only one population is observed, the size distribution of mucosomes is moderately high. According to the polydispersity index (PDI 0.63 ± 0.13) and the span values (span 2.03 ± 0.21), it can be inferred that, within the same population, there is a wide range of size variation. A combination of high dilution factors for NTA and the different sizing principles of the two techniques are likely linked to the slight differences detected. Yet, both the results obtained in suspension are in agreement with the size observed by TEM and FESEM analysis. Similar sizes (300 nm) are reported for a reversible nanosystem based on mucin, produced by glycerol-induced condensation.[36]

Mucin is a negatively charged protein and, when assembled into mucosomes, they acquire a negative charge. The repulsion of negatively charged NPs might prevent their agglomeration and maintain their stability. The measured zeta potential (ZP) of mucosomes, an indicator of the stability of colloidal dispersions, was measured by NTA (-20.8 ± 0.8 mV in phosphate buffer pH 7.4). Although they result with negative ZP, it is, however, below the recognized minimal values necessary for colloids to be stable in solution (ZP > ±30 mV).[44] For this reason, a resuspension step is needed immediately before use.

Mucosomes can be stored in suspension at different temperatures, in particular at room temperature, 4° and 40 °C. After an initial increase of the absorbance at 258 nm in the first day of storage, the values remained overall constant up to the longest test time, 60 days (Fig. 1i). The sample stored at 40 °C presented the highest increase of absorbance. The increase of absorbance is linked to nanoparticle degradation as the disaggregation of mucosomes can release mucin in the solution. Following one of the approaches usually adopted to increase the long-term stability of polymeric nanoparticles, mucosomes were lyophilized and the stability tests repeated. Lyophilized mucosomes are more stable over time with respect to liquid formulations of the same as the absorbances of the lyophilized samples are less subjected to variations over time when compared to the samples stored in suspension (Fig. 1j). Mucosomes therefore can undergo lyophilization, an approach in line with the ones commonly adopted for other polymeric nanoparticles.
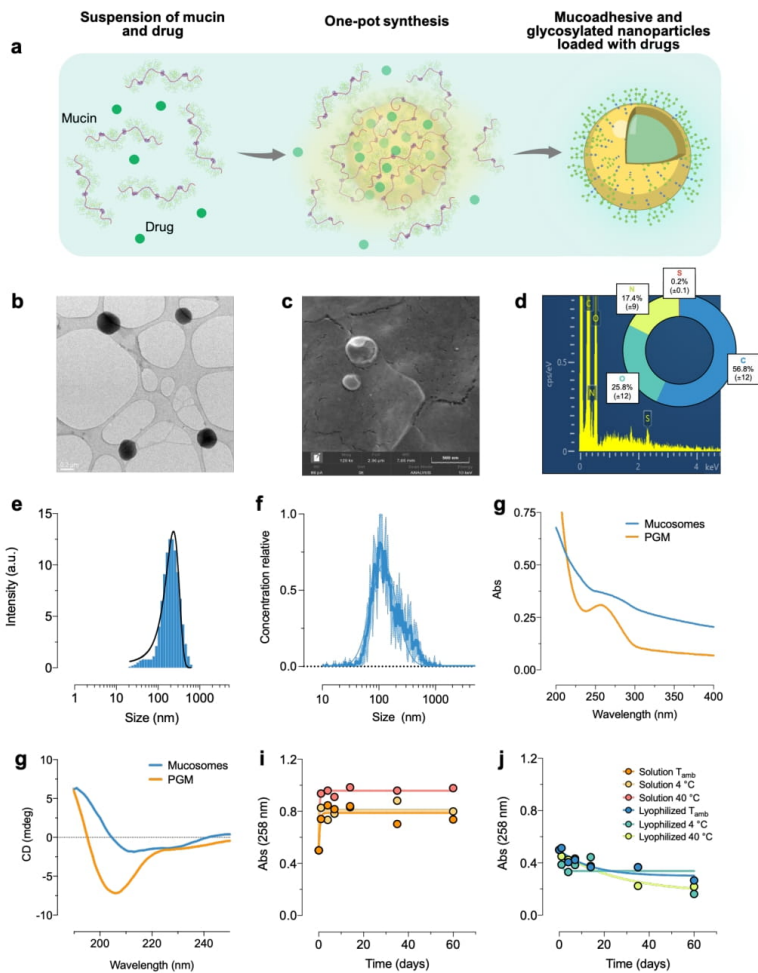
Figure 1. Mucosomes are nanoparticles of ~200 nm, of spherical shape, atomic composition mainly based on C, O and N, and are bioinspired from mucus. (a) Mucin glycoprotein, which is the backbone of mucus, is used to synthesize the mucosomes. The nanoparticles can be efficiently loaded with different compounds. The peptide core of mucin is highly glycosylated and glycans are preserved even after the formation of nanoparticles. (b) Representative transmission electron microscopy images (scale bar = 0.2 μm) and (c) field emission scanning electron microscopy analysis (scale bar = 0.5 μm) representing the size and the morphology of the mucosomes. (d) EDX spectrum depicting

2.3.   Characterization of glycosylation

The mucin used to synthesize the mucosomes is a highly glycosylated protein, meaning that the peptide core of mucin is densely coated with sugars called glycans. The "sugar-coating" of mucin gives them a huge water-binding capacity and also makes the protein resistant to proteolysis. The amount of glycans retained on mucosomes after the synthetic procedure was evaluated by a colorimetric periodic acid-Schiff (PAS) staining of oxidized vicinal hydroxyls present on glycans. The amount of glycans detected on mucosomes is similar to the amount present on the free protein, without statistical difference between the two (Fig. 2a). In addition to PAS staining, we also specifically tested sialic acid groups, as a complementary proof of the surface glycosylation of mucosomes. Sialic acid is the general name for nine carbon acidic sugars with *N* or *O*-substituted derivatives.[45] It is widely distributed within the mucin structure and has been shown to serve as a receptor for bacteria and viruses in particular for *Pseudomonas aeruginosa* in the lower respiratory tract.[46,47] The sialic acid assay used was an improved Warren method,[48] in which sialic acid is oxidized to formyl pyruvic acid. This reacts with thiobarbituric acid forming a pink-colored product that can be detected by fluorometric detection (ex = 550 nm, em = 585 nm). The concentration of sialic acid found for mucosomes is comparable with that of mucin (Fig. 2b). Taken together, the results obtained from the PAS staining and the sialic acid assay, it is possible to conclude that the mucin glycosylation is maintained even after the synthetic process, and the mucosomes can be considered as glycosylated nanoparticles.

The glycans present on mucosomes retain their reactivity, and this was assessed by studying the binding of mucosomes to a lectin glycoprotein known to bind mucin.[49] Lectins are ubiquitous carbohydrate-binding proteins of nonimmune origin. Among

them, concanavalin A (Con A) is known to bind α-glucosides, mannosides and biopolymers having these sugar configurations. Previous studies proved that Con A is able to bind mucin.[50] Con A has an intensive fluorescence at 350 nm which is quenched upon the addition of increasing concentrations of mucosomes (Fig. 2c). Based on the percentage of bound mucosomes to Con A, the estimated equilibrium concentration of mucosomes inducing half of the maximum binding is 30.2 μg/mL (Fig. 2d). The interaction with Con A was confirmed also by a chromatographic method. In particular, it was quantified the eluted amount of mucosomes through a chromatographic column, prepacked with a Con A-containing resin (Fig. 2e). The retention volumes and the amount of recovered samples of mucin and mucosomes were fully comparable (PGM recovery 83 ± 17%, mucosomes recovery 77 ± 20%).
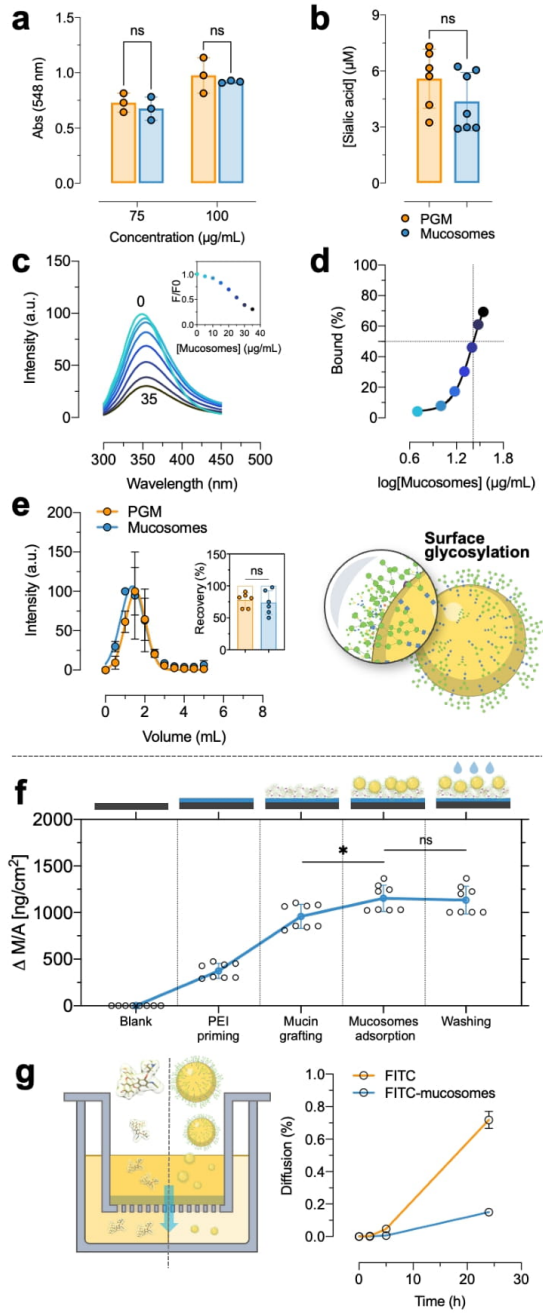
2.4. Mucoadhesive properties

The mucoadhesion of nanocarriers was tested to evaluate if they possess the great added value, from the pharmaceutical formulation view, to prolong the residence time and bioavailability of the encapsulated drug at the mucosal surface.[33,51] The mucoadhesive formulations are key features for the emerging intranasal applications, which is increasingly considered a valid option for local or systemic delivery of many therapeutic agents.[52] Moreover, biodegradable and mucoadhesive polymeric carriers seem to be the most promising candidate for mucosal vaccine delivery.[52]

As a matter of fact, liposomes are consolidated and the most used nanocarriers in the field of drug discovery. Liposomes are directed to intracellular drug delivery, although they are not necessarily suitable to reach mucosal surfaces because of their lack of mucoadhesive properties. Only positively charged liposomes exhibit mucoadhesion, but, as a side effect, their biocompatibility is reduced.[53–55] Different approaches to obtain mucoadhesive liposomes include surface derivatization with other polymers such as alginate, chitosan, pectin, Eudragit and Carbopol, with processes that can increase the complexity of the synthetic process with impact on yields, costs, and additional purification and characterization steps.[29,56–59]

The hypothesis is that, since mucosomes are bioinspired from mucus, and because of their mucin-based composition, they might be endowed with mucoadhesive properties. This hypothesis was assessed by QCM-D analysis. The test was studied at pH 7.4, pH at which mucin (BSM) is negatively charged due to its isoelectric point around 3.[60] The

1   adsorption of mucosomes to a mucin layer, previously produced onto the quartz crystal,

2   resulted in a resonance frequency shift of -25 ± 1 Hz which was calculated to correspond

3   to a deposited mass of 196 ±10 ng/cm^2. After the washing step, the frequency increased

4   by 10% (2,5 ± 0,5 Hz), which corresponds to a mass loss of 20,5 ± 7 ng/cm^2. The loss

5   can be attributed to the removal of weakly bound NPs (Fig. 2f).

6   It could be argued that measuring the mucoadhesive properties using mucin to mimic

7   mucus could be a too simplistic model. Therefore, we tested the ability of mucosomes

8   to interact/cross a tridimensional layer of mucus and deliver the encapsulated

9   compound. Fluorescein isothiocyanate was encapsulated (encapsulation efficiency, 49

10   ± 12 %) and the ability of mucosomes to cross a layer of a pathological mucus model.[61]

11   The kinetics of diffusion of the FITC-loaded mucosomes through the mucus layer was

12   slower than that of the free dye for the whole duration of the test (up to 24h) (Fig. 2g).

13   This implies a longer residence time within mucus and, therapeutically speaking, a

14   higher drug bioavailability and persistence within the mucosal surface. Such a feature

15   could be an advantage in mucus-related disorders (*e.g.,* cystic fibrosis, COPD, other

16   mucoid infections and some inflammatory states), where mucus clearance is hindered.

17   In fact, the permanent presence of bacteria participates in the inflammatory process

18   contributing to a vicious cycle where mucus alteration, infection, and inflammation are

19   elements tightly intertwined and difficult to separate. Because of this complex

20   pathological milieu, formulations able to increase the residence time of the drug within

21   mucus are desirable in order to prolong its therapeutic activity.

1

*Figure 2. Mucosomes are glycosylated nanoparticles with mucoadhesive properties which are stable over time as lyophilized powder. The presence of carbohydrates on the surface of mucosomes is demonstrated by a Periodic acid-Schiff (PAS) staining **(a)** and by derivatization and fluorometric detection of sialic acid **(b)**. The amount of carbohydrates is compared with the native protein. The interaction of mucosomes with Concanavalin A (Con A) was studied by steady-state fluorescence spectroscopy **(c)** and the equilibrium binding constant is calculated using a non-linear fit **(d)**. Interaction of mucosomes with Con A was investigated also by a chromatographic method. **(e)** Depicts the elution volumes of PGM and mucosomes from a Sepharose column prepacked with Con A, while the inset shows the recovery of the injected amount of sample. Mucoadhesive properties of mucosomes were studied by QCM analysis **(f)**. The mucosomes at first adsorbs over the BSM-PEI layer and remains adsorbed even after two washing cycles with PBS. The mucoadhesive properties were investigated also by measuring their diffusion through a pathological mucus model **(g)**. The diffusion of FITC loaded into mucosomes was lower with respect to free FITC. This result proved that mucosomes are able to increase the residence time of FITC within the mucus model*

2.5.   Biological activity

Mucosomes are well-tolerated by HeLa cells cultured up to 72h in presence of different concentrations of mucosomes (up to 2 μg/mL) (Fig. 3a). The upper limit before cytotoxicity was found to be 10 μg/mL, but only after 72h of incubation (Fig. 3b). These results are comparable or even less toxic than other organic nanosystems tested on the same cell line, like poly-caprolactone conjugated albumin nanoparticles,[62] chitosan-gold nanoparticles.[63] Conversely, albumin nanoparticles and liposomes induce less cytotoxic effects when tested on HeLa cell line.[62,64]

Nanocarriers able to cross the cellular membrane could be of interest if the aim would be to deliver active ingredients intracellularly. In order to isolate the signal of the nanoparticles around the cellular environment, mucosomes were loaded with FITC. However, before conducting the *in vitro* studies on cells, it was of fundamental importance to know the release kinetics of the encapsulated dye. Such information is crucial to state with certainty that the signal recorded by confocal microscopy truly corresponds to the FITC loaded into mucosomes rather than to the released dye. For this purpose, the passive release of FITC was investigated by dialysis. A slow kinetics is observed in the first 24h, followed by a step increase of release in the following days.

The total amount released after the first 24h is below 1%; the same being 11% after 7 days of monitoring (Fig. 3c). Given that the cellular localization tests are conducted within 24h, it is possible to say that the recorded emission of FITC corresponds to mucosomes with the dye. Results indicate that mucosomes are partially internalized and they colocalize with lysosomes (Fig. 3d, e). However, the specific internalization mechanism was not further investigated. Previous studies have shown a relationship between the size of nanoparticles and the endocytic pathway. Particles with a size below 200 nm were internalized into non-phagocytic, murine melanoma cells B16-F10 via clathrin-mediated endocytosis [65,66], while particles larger than 500 nm have been known to enter phagocytic cells via phagocytosis pathways.[67] Thus, since mucosomes are nanoparticles of about 200 nm, they might be internalized by endocytosis.
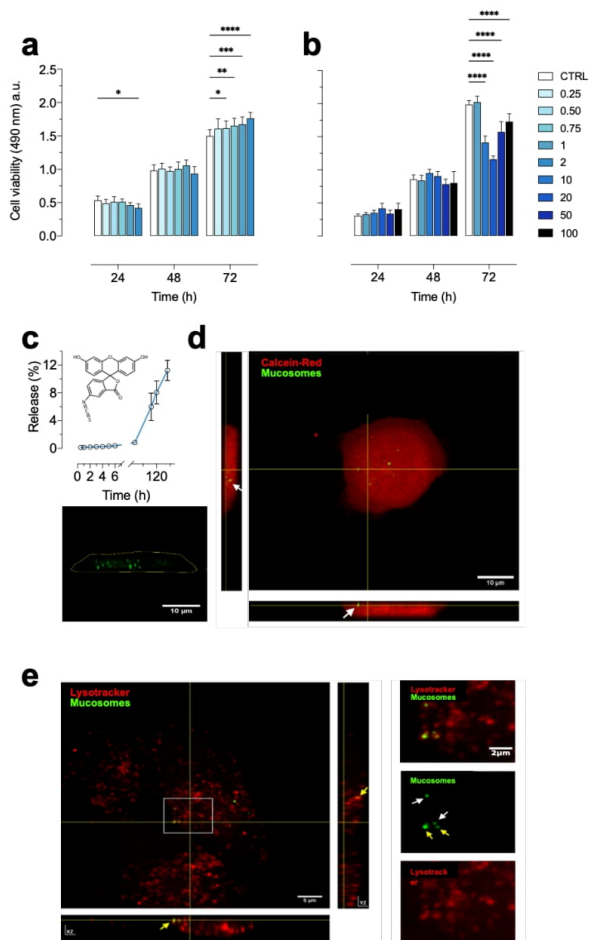
1

2 *Figure 3. Mucosomes are cytocompatible on HeLa cells, internalized and partially*

3 *colocalized with lysosomes. (a-b) MTS cytotoxicity assay on HeLa cells after incubation*

4 *with different concentrations (µg/ml) of mucosomes and monitored at different time*

5 *points of a representative experiment. Data in the bar graph represent mean ± SD (n = 8*

6 *technical replicates). (c) The release profile of FITC loaded into mucosomes investigated*

7 *by dialysis. (d) Confocal microscopy images of HeLa cells incubated with FITC-loaded*

8 *mucosomes. The red signal is referred to Calcein-Red (ex: 561 nm), while the green signal*

9 *is referred to FITC-loaded mucosomes (ex: 490 nm). The arrows on the sidebars point out*

Nanoparticles can exert important immunological effects, such as interactions with immune cells, triggering of the inflammatory response, activation of the complement cascade, or activation of antigenic-specific hypersensitivity reactions. Immunotoxicological heterogeneity is a hallmark of nanomedicine, and therefore a critical hurdle for immune safety evaluation. The effect of mucosomes on RAW 264.7 cells, a cell line of mouse macrophages commonly used to assess inflammatory activity *in vitro,* was studied. The administration of exogenous materials could induce macrophages to secrete pro-inflammatory cytokines, chemical messengers regulating the innate and adaptive immune system. The pro-inflammatory response of the cells treated with mucosomes was analyzed by evaluating IL-1B, IL-6 and TNF-α cytokines mRNA expression. The stimulation with mucosomes showed a minimal immune response as compared with controls untreated conditions. In particular, the transcription of proinflammatory cytokines was not significantly increased for the lower mucosome concentration, while a significant increase in IL-1B and IL-6 was observed starting from 0.5 µg/mL. Mucosomes, at any tested concentration, did not induced TNFα production. However, LPS (1 µg/mL), which is known to activate antigen-presenting cells, induced a strong increase in all the 3 tested cytokines transcription (Fig. 4a).

The intravenous route offers several advantages even when coming to nanoparticles administration; it provides almost instantaneous response and allows fine control of the drug concentration within the body. Blood is in fact the first tissue nanoparticles come in contact with when administered intravenously, therefore it is of crucial importance to understand the biological response at this level. Several nanomaterials have been shown to alter blood coagulation pathways producing unwanted side effects. For example polystyrene nanoparticles activate intrinsic coagulation in a size-dependent fashion,[67] while cationic polyamidoamine dendrimers induce platelet

1   aggregation. [68,69] Another study reported that anionic liposomes shortened coagulation

2   time *in vitro* and induced reversible aggregation of platelets both *in vitro* and *in vivo*

3   through a factor XII- and XI-mediated mechanism.[70,71] Mucosomes did not induced

4   alterations of the coagulation cascade when lyophilized mucosomes were added to

5   human blood samples, and, in particular, the prothrombin time (PT), the activated

6   partial prothrombin time (APPT) and the concentration of fibrinogen, antithrombin, D-

7   dimer, factor VIII and factor XI remained in the physiologically acceptable ranges

8   without significant variations (Fig. 4b).
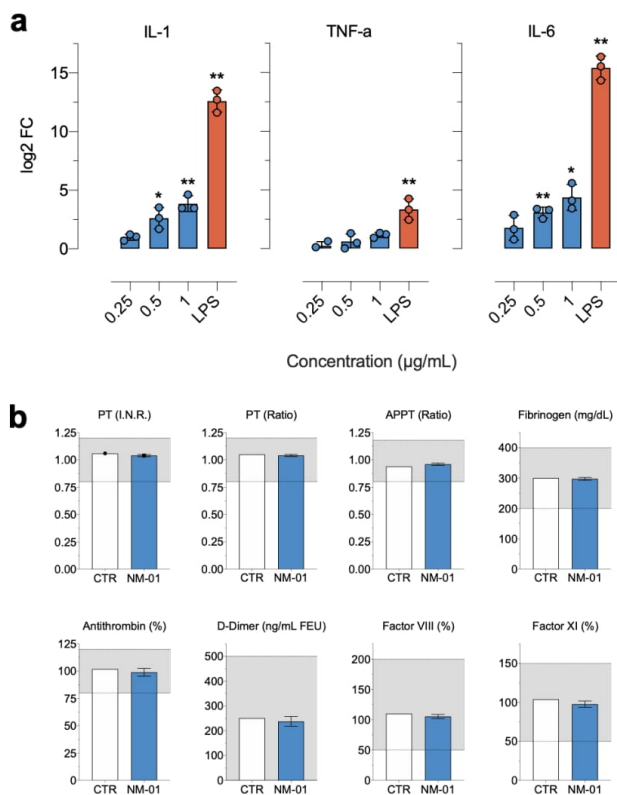
9

10

11   *Figure 4. Mucosomes are not immunogenic and do not alter the coagulation*

12   *cascade. (a) IL-1B, IL-6 and TNF-α mRNA expression on RAW 264.7 cells stimulated with*

2.6. The potential of mucosomes to be used for intranasal drug delivery

Considering the mucoadhesive properties of mucosomes, it is reasonable to consider that they could be a promising candidate for intranasal administration of drugs. The application of nebulizers for the pulmonary delivery of drug-loaded mucoadhesive vehicles represents a noninvasive and portable mode of administration with high efficacy owing to optimal retention of the active ingredients at the target site.[72]

HeLa cells are a standardized cell line, yet far from modeling the airway epithelium. Therefore, diffusion studies of FITC-loaded mucosomes were conducted on an *in vitro* reconstituted 3D human nasal epithelium (MucilAir™), cultured at the air-liquid interface (Fig. 5a). After 5h of incubation, the diffusion rate of the FITC delivered by mucosomes was slower as compared with FITC. Given that the MucilAir™ cell model is mucus producing, and mucosomes have proved to spend more time within mucus (Fig. 2g), we can assume that the lower diffusion of FITC-loaded mucosomes can be the result of a longer residence time within mucus. When compared with the non-cell-based diffusion test (Fig. 2g), the amount of diffused FITC through the cell model is higher. This can be explained since it has been previously proved that in addition to transcellular and paracellular passive diffusion, fluorescein can also be actively transported.[73] To ascertain the effect of dispensing mucosome-based suspensions using nasal spray pumps, the shape stability of the inoculum was evaluated (Fig. 5b). We were interested in evaluating the possibility of shear induced nanoparticle degradation.[74] The TEM analysis showed that after dispensing with a generic intranasal spray pump device, the integrity of mucosomes was not altered (Fig. 5c).
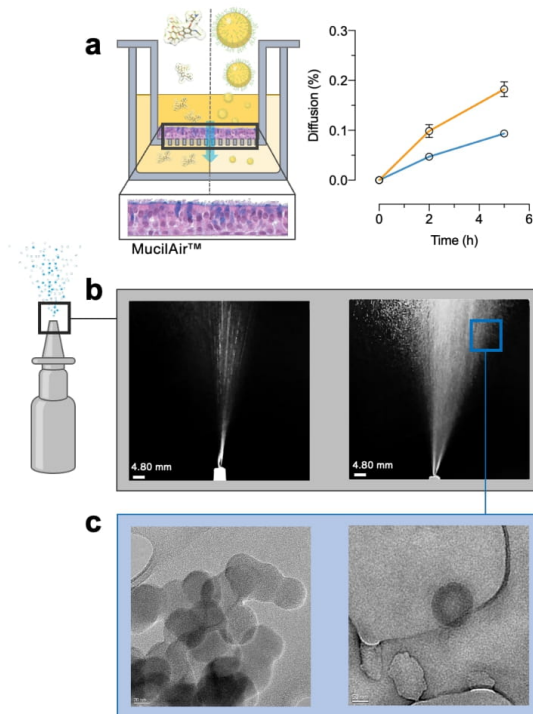
Figure 5. Mucosomes maintain shape integrity after spray nebulization and attach to the nasal epithelium (a) Mucosomes proved to increase the residence time of FITC within an in vitro cell model of the human airway epithelium. (b) Schematic representation of the intranasal spray pump device and the spray geometry. (c) Representative TEM images of the mucosome nanoparticles after nebulization through the generic intranasal spray pump device.

2.7. *In vivo* biodistribution and toxicity

The biodistribution of novel nanoparticles is a parameter of extreme importance during the development of novel drug delivery systems. Once nanoparticles are introduced into the physiological environment, their biodistribution can be affected by many factors, including nanoparticles chemical-physical properties, physiological environment characteristics, and the route of administration, among which intravenous injection is one of the most widely used and studied methods. Before investigating the

biodistribution of mucosomes, at first, the stability in a more biologically complex environment was tested. In fact, after intravenous administration the nanocarrier might undergo enzymatic degradation which could lead to particle degradation. To test this hypothesis, a stability assay of FITC-loaded mucosomes incubated with a generic protease was conducted. The rationale behind such an experiment is to determine if mucosome are sensitive to the activity of proteolytic enzymes that could be encountered after IV administration. If mucosomes are susceptible to protease activity, a higher release of the encapsulated compound should be expected. Indeed, it was found that the fluorescence intensity of the dye increases over time in the presence of protease (Fig. 6a). This result suggests that mucosomes are sensitive to the proteolytic activity of the enzyme. After 30h of incubation with the protease, the release of FITC is just 1.6x higher with respect to the absence of the enzyme (Fig. 6a). However, even though this appoints mucosomes as being enzyme susceptible, it is worth mentioning that such an experiment was conducted in an extremely controlled environment containing only the substrate (mucosomes) and the enzyme. The *in vivo* interaction may be less "aggressive" as the catalytic enzyme site might be subjected to endogenous competition.

To be able to perform biodistribution studies, it was mandatory to load mucosomes with a fluorescent dye suitable for *in vivo* imaging tests. It is essential that the absorption and emission wavelength of the dye fall in a spectral region in which the interference with the biological matrix is minimal. For this purpose, a polymethine dye (Cy5.5) was selected because it emits at 720 nm. In this spectral region, the biological tissues are "transparent", therefore it is possible to isolate and monitor only the signal coming from the fluorescent dye. Cy5.5 was encapsulated with an efficiency of 30 ± 8%. Similarly to what was done with FITC, a release study of Cy5.5 was conducted to make sure that the signal recorded can truly be ascribed to the dye encapsulated within mucosomes. The release of Cy5.5 is below 1% even after 96 h, and the same remains below 5% after 200h (Fig. 6b). Next, the *in vivo* biodistribution of Cy5.5-loaded mucosomes after administering a dose of 400 µg/mL of mucosomes containing 13 nmol of Cy5.5 in the caudal vein of mice was investigated (Fig. 6c). The biodistribution in lungs, liver, spleen, heart and kidney was monitored up to 48 h. According to the slow release of Cy5.5 (Fig. 6b), we can state that the monitored Cy5.5 signal corresponded to Cy5.5-loaded mucosomes. An intense signal was observed at all the examined time points. Notably, in the first 4 hours, the strongest signals were reported in the liver and
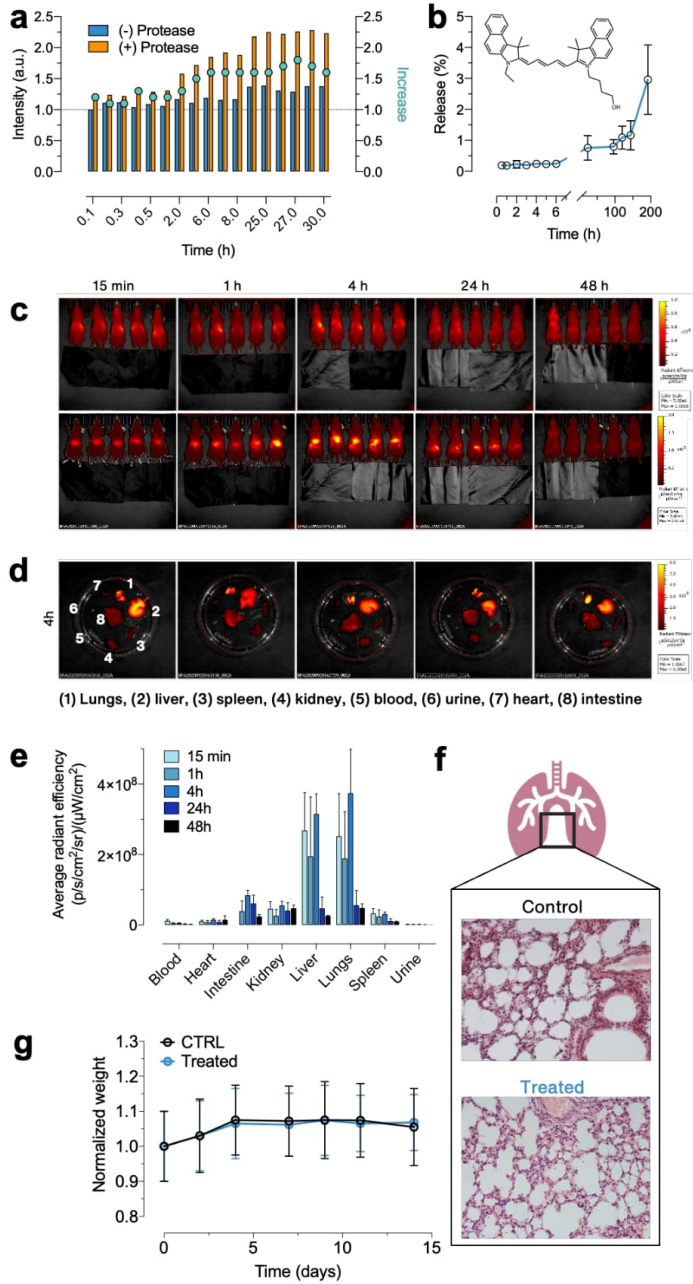
lungs (Fig. 6d), although significant fluorescent intensity also appears in the kidneys and intestine (Fig. 6e). After 24 hours and, even more, at 48 hours after injection, a weak signal was observed in all the monitored organs. Overall, the highest distribution of mucosomes was achieved in the lungs. This might suggest that mucosomes could have an intrinsic tropism for mucosal tissues, even when administered by the parenteral route. In addition to the qualitative analysis, the amount of Cy5.5-mucosome localized in some of the investigated organs was quantitatively measured. The lungs and the kidney of one of the mice sacrificed one hour after the injection were randomly selected. The amount of Cy5.5-mucosome present in the lungs represented 4.15% of the total administered dose, while at the same time point only 0.51% of the total dose was detected at kidney level. These results are in good agreement with what was previously observed by optical microscopy.

Because the lungs have been demonstrated to be the organ with the highest distribution of mucosomes, it was interesting to evaluate if the presence of the nanoparticles could somehow affect tissue physiology. Thus, histology studies have been carried out on the explanted lungs. No signs of tissue inflammation were detected in the treated animals (Fig. 6f).

Besides the assessment of biodistribution sites, the main goal of *in vivo* studies was to determine if mucosomes truly represent a biocompatible nanocarrier. Toxicity studies have been conducted by injecting 100 μg of empty mucosomes (400 μg/mL) intravenously into the caudal vein of five healthy mice. Injection of saline solution was administered into the other five mice as control. Animals were weighed three times a week and monitored for clinical signs. Within the monitoring time period (14 days), the animals remained healthy as no weight variations were observed and no abnormal clinical signs were manifested (Fig. 6g).

According to *in vivo* biodistribution and toxicity studies conducted on mice, we can state that mucosomes distribute mainly in the lungs and liver, and they are gradually eliminated from the body after 48 hours without clinically evident signs of toxicity.

a

Intensity (a.u.) / Increase

(-) Protease
(+) Protease

Time (h): 0.1 0.3 0.5 2.0 6.0 8.0 25.0 27.0 30.0

b

Release (%)

Time (h)

c

15 min   1 h   4 h   24 h   48 h

d

4h

(1) Lungs, (2) liver, (3) spleen, (4) kidney, (5) blood, (6) urine, (7) heart, (8) intestine

e

Average radiant efficiency
(p/s/cm²/sr)/(µW/cm²)

15 min
1h
4h
24h
48h

Blood Heart Intestine Kidney Liver Lungs Spleen Urine

f

Control

Treated

g

Normalized weight

CTRL
Treated

Time (days)

1

22

Figure 6. Mucosomes distribute mainly in the lungs and liver without inducing toxic effects. (a) stability of FITC-loaded mucosomes in the presence of a generic protease. (b) Release profile of Cy5.5-loaded mucosomes studied by dialysis (MWCO 3.5 kDa). (c) in vivo optical imaging of real-time mice after administration of Cy5.5-loaded mucosomes. (d) Representative ex vivo optical imaging of mice organs sacrificed at the end of biodistribution tests. (e) Quantitative fluorescence intensities of organs from ex vivo images. (f) Histological analysis of Cy5.5-loaded mucosomes in lungs of treated and untreated mice. The mucosomes were stained with alcian blue. (g) Weight monitoring of treated and untreated mice after administration of mucosomes.

2.8. Drug encapsulation

One of the most important characteristics of drug nanocarriers is the ability to be efficiently loaded with active ingredients. So far, mucosomes have been loaded with two fluorescent dyes, FITC and Cy5.5, with good encapsulation efficiencies. Given the physicochemical properties of mucosomes, they could be advantageous in pathological contexts characterized by infection and inflammation strictly intertwined. Drug delivery systems based on polymers are reported to improve the performance of existing antimicrobial compounds.[75-78] Thus, oseltamivir, ceftazidime and dexamethasone have been selected as three models of antiviral, antibacterial and anti-inflammatory drugs, respectively. Overall, a good encapsulation efficiency (EE) was observed (Fig. 7a). The antiviral oseltamivir is the drug with the highest EE (85 ± 0.7%), followed by the antimicrobial ceftazidime (44 ± 8%). On the contrary, the steroidal anti-inflammatory dexamethasone is the least encapsulated (21 ± 13%). Deciphering the mechanisms governing the loading efficiency of drugs within mucosomes can be tricky. To find out if EE depends on any molecular property, we performed a correlation matrix with several molecular descriptors. To maximize the chemical variability, also FITC and Cy5.5 were included for the computation as they all belong to the class of small molecules (MW < 1 kDa). A negative correlation (R^2=0.97) between EE and drugs' molecular complexity was found (Fig. 7b). Molecular complexity is calculated by the number of distinct structural fragments, which one can construct from a molecule by just cutting parts off. The more distinct fragments, the more complex the molecule.[79] According to this relationship, it was found that the lower the molecular complexity, the higher the entrapment efficiency.

In addition to nanosystems carrying small molecules, today a soaring interest is addressed to the development of nanocarriers suitable for the delivery of macromolecules. Protein and nucleic-acid based therapeutics have made important progress in the treatment of a variety of human diseases.[80,81] Given the high binding capability of mucins, we investigated if this property could be exploited to encapsulate macromolecules within mucosomes.[27,82–84] A small peptide nucleic acid (TCACTAGATG, MW < 10 kDa,)[85] and human serum albumin (MW < 100 kDa) were selected as representative models of nucleic acids and proteins, respectively. The two macromolecules showed excellent encapsulation efficiencies, despite their high molecular weight. Interestingly, the PNA decamer has been encapsulated with an efficiency of 94%. PNA is a synthetic analogue of DNA in which the ribose phosphate backbone has been replaced by a polyamide chain. Previous experimental and theoretical studies on the ionization and lipophilic properties of PNA derivatives have proved how PNA is overall a hydrophilic macromolecule, even though the backbone is not charged as for DNA and RNA.[86,87] And because mucin is densely coated with carbohydrate chains, which represent strong hydrophilic domains, it is reasonable to speculate that PNA binds mostly on the glycosylated portions of mucin by H-bonding mechanism. Similarly, even though albumin is a high molecular weight protein (66.4 kDa) it was encapsulated into mucosomes with an efficiency of 48%. Albumin can form complexes with mucin,[88] most probably by hydrophobic interactions;[89] this could explain the overall high encapsulation into mucosomes.
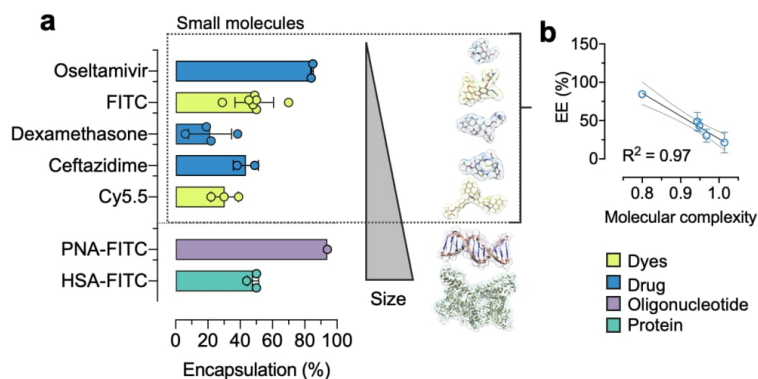
Figure 7. Mucosomes can be loaded with compounds spanning a wide range of molecular weights and physicochemical properties, and to increase residence time

1 *at mucosal surfaces. The entrapment efficiency of oseltamivir, fluorescein*
2 *isothiocyanate (FITC), dexamethasone, ceftazidime, cyanine 5.5 (Cy5.5), peptide nucleic*
3 *acid bioconjugated with FITC (PNA-FITC) and human serum albumin bioconjugated with*
4 *FITC (HSA-FITC) was calculated based on the amount of free compound recovered from*
5 *the washing volumes **(a)**. Among the small molecules encapsulated, a good correlation*
6 *was observed between entrapment efficiency (EE) and drug molecular complexity **(b)**.*

7

8 ### 3.   Conclusions

9 In this study we presented mucosomes, a novel nanosystem obtained through a
10 desolvation method of mucin glycoproteins. We got inspiration from the unique
11 properties of mucus, our first-line of defense, to develop a cutting-edge technology that
12 exploits the mucus' natural mucoadhesive and binding capacity. The synthesis, the
13 functionalization with glycans, and the loading with the desired active compound can
14 be obtained in only one reaction pot. In summary, it was proved that mucosomes are
15 spherical nanoparticles of about 200 nm, naturally endowed with mucoadhesive
16 properties, and stable over time when formulated as a lyophilized powder. Since mucin
17 is highly glycosylated, it was proved that after the desolvation process the glycans are
18 preserved and still reactive on the surface of mucosomes. Because of the unique
19 physicochemical properties inherited from mucin, mucosomes are able to encapsulate
20 active ingredients spanning over a wide range of molecular weights. The *in vitro*
21 biological tests showed that mucosomes can reach the intracellular compartment
22 without significant cytotoxic effects on HeLa cells. They showed low immunogenicity as
23 cytokine production on macrophages was minimal compared to a well-known
24 immunogenic agent (LPS), and also, mucosomes proved to be inert over the coagulation
25 cascade. *In vivo* tests showed that mucosomes are not toxic on mice, and distribute
26 mainly in the lungs and the liver. Within the monitored organs the concentration of
27 mucosomes gradually decreased over time suggesting that the nanoparticles do not
28 lead to accumulation in tissues, a problem that usually can induce organ-specific toxic
29 effects.

30 The possibility to deliver active ingredients using mucosomes would offer several
31 advantages over conventional systems in terms of mucoadhesive properties and
32 targeted delivery. Especially in pathological conditions where the mucus barrier
33 represents an obstacle to overcome in order to eradicate the disease. The mucoadhesive
34 property would ensure permanence of the encapsulated drug within the mucus layer,

while the presence of surface glycans would mediate the engagement of glycoproteins expressed by pathogens such as bacteria and viruses. Drugs would be released more closely to pathogens, limiting the adverse effects and maximizing the effectiveness. Given these unique features, we believe mucosomes could be a promising drug platform for mucosal delivery.

4. Experimental section

4.1. Materials

Mucin from porcine stomach (Type III, bound sialic acid 0.5-1.5%, partially purified powder), mucin from bovine submaxillary gland (BSM), polyethylenimine hydrochloride (PEI), Schiff's reagent, sialic acid assay kit (MAK314), lectin from Concanavalin A Type IV, ready-to use column prepacked with Con A Sepharose (HiTrap® Con A 4B), glutaraldehyde 70% solution, polyethylene glycol (PEG) 6000, ethanol, sialic acid assay kit, alginate, D-(+)-Glucono-delta-lactone, $CaCO_3$, oseltamivir, fluorescein isothiocyanate, cyanine 5.5, ceftazidime, dexamethasone, peptide nucleic acid and human serum albumin were all obtained from Merck (Italy). Transwell® permeable supports were purchased from Corning. All other reagents were of analytical grade and used as received. Millipore grade water (resistivity: 18.2 MΩ cm at 25 °C) was obtained from an in-house Millipore system.

4.2. Synthesis and purification of mucosomes

Mucosomes were prepared by a proprietary process (application PCT: PCT/IB2021/055450) employing a desolvation technique. Briefly, protein nanoparticle formation was achieved by slowly adding ethanol as a desolvation agent to a suspension of mucin. After protein desolvation, particle cross-linking was achieved by adding aqueous glutaraldehyde. PEG 6000 was added to minimize aggregation of the particles. Mucosomes purification was carried out by centrifugation of nanoparticle suspension at 10.000 RPM for 10 minutes at 4 °C. The supernatants were discarded and the sedimented nanoparticles were dispersed in mQ water using an ultrasound bath (1 minute, room temperature, 45 kHz, 130W). These purification steps were repeated five times.

4.3.   Characterization of mucosomes

The formation of mucosomes was characterized by UV-Vis spectroscopy and the absorption spectrum was compared with that of the native protein. The size and shape of mucosomes were monitored by transmission electron microscopy (TEM) and field emission scanning electron microscopy (FESEM). TEM samples were prepared by drop-coating the mucosomes at a concentration of 0.1 mg/mL in water, into the carbon-coated copper grid, and their size and morphology were characterized using a TEM (JEOL 3010-UHR TEM operating at an accelerating voltage of 300.00 kV). The chemical elements present in the nanoparticles were evaluated through energy-dispersive X-ray spectroscopy (EDX). The FESEM sample was prepared at the same concentration and was analyzed using a FIB-FESEM/EBSD//TOF-SIMS Tescan S9000G.

The size distribution profile of mucosomes was determined by dynamic light scattering (DLS, Malvern Zetasizer) and nanoparticle tracking analysis (NTA, ZetaView® - Particle Metrix). DLS measurements were performed after an equilibration time of 60 s which allowed samples to reach the temperature of 25 °C. A 5 mg/mL mucosome sample was diluted 1:50,000 in ultra-pure water. The sample was measured in size and zeta potential in scatter mode (488 nm laser). Triplicate measurements were performed for each sample.

The UV-Vis absorption spectra were measured by a UH5300 Hitachi spectrophotometer at room temperature using a quartz cuvette (1 cm pathway length). Stability over time of mucosomes stored in suspension and as a lyophilized powder at different temperatures (T_{amb}, 4 and 40 °C) was also evaluated by measuring the variation of the absorbance at 258 nm of samples (100 µg/mL) at specific time points up to 60 days in comparison with the absorbance of freshly prepared samples. The shape integrity of mucosomes was investigated also after nebulization through an intranasal spray pump device. Mucosome were suspended in water at a concentration of 1 mg/mL and nebulized using the spray device. The nebulized volume was collected and after 1:10 dilution with mQ water was analyzed by TEM microscopy as previously described. Suspensions of 0.05 mg/mL of PGM and mucosomes were scanned in the far-UV spectral range over the wavelength region 190-250 nm with a scanning speed of 50 nm min^{-1} using a Jasco J-815 spectropolarimeter equipped with a Xe arc lamp, using a quartz circular cuvette (path length 1 mm). CD spectra deconvolution and prediction of protein secondary structure were performed with K2D3 online software.[90]

4.4. Drug loading into mucosomes

Oseltamivir, fluorescein isothiocyanate (FITC), dexamethasone, ceftazidime, cyanine 5.5 (Cy5.5), peptide nucleic acid (PNA) and human serum albumin (HSA) have been encapsulated within mucosomes. The drugs were solubilized into the mucin aqueous suspension prior to the desolvation step. The PNA was synthesized as previously described.[85] Before encapsulation, HSA and PNA were bioconjugated with FITC following the reported protocol.[91] The excess of FITC was 50-fold the moles of HSA or PNA. After bioconjugation, the derivative was immediately purified using a Sephadex® G-25 desalting column and PBS (20 mM, 150 mM NaCl, pH 7.2) as eluent to evaluate the FITC labeling efficiency, the dye/protein ratio (D/P) of the conjugates was determined by the absorption spectra of the labelled HSA and PNA, registered in PBS, according to the relationship reported in Equation 1:[92]

$$\frac{D}{P} = \frac{A_{max}\varepsilon_{prot}}{(A_{280} - cA_{max})\varepsilon_{dye}} \qquad Eq.\,1$$

where A_{280} is the absorbance of the conjugate at 280 nm; A_{max} is the absorbance of the conjugate at the maximum absorbance of the corresponding FITC; c is a correction factor that must be used to adjust the amount of A_{280} contributed by the dye because FITC also absorbs at 280 nm; c equals the A_{280} of the dye divided by A_{max} of the dye (c=0.29); ε_{prot} and ε_{dye} are the molar extinction coefficients for the HSA or PNA and FITC, respectively.

Encapsulation efficiency was indirectly calculated by quantifying the drug released in the supernatants obtained throughout the purification steps. The released amount of FITC, Cy5.5, PNA-FITC and HSA-FITC were detected by fluorescence spectroscopy using a Horiba Jobin Yvon Fluorolog 3 TCSPC fluorimeter equipped with a 450-W xenon lamp and a Humamatsu R928 photomultiplier. FITC and Cy5.5 were excited at 490 and 645 nm respectively, while detection was measured at the maximum of fluorescence for each dye (λ_{FITC} = 520 nm, $\lambda_{Cy5.5}$ = 715 nm). Oseltamivir, dexamethasone and ceftazidime were quantified by HPLC-MS/MS using a Varian HPLC equipped with a 410 autosampler and an Ascentis C18 column (10 cm x 2.1 mm, 3 μm) and detected on a Varian 320 MS TQ Mass Spectrometer equipped with an electrospray ionization (ESI) source operating

in positive mode. The detector was used in multiple reaction monitoring (MRM) mode. The amount released was quantified based on linear calibration standard curves. The encapsulation efficiency was determined according to Equation 2:

$$EE\ (\%) = \frac{amount\ of\ drug\ in\ supernatant\ volume\ (mg)}{initial\ amount\ of\ drug\ (mg)} \times 100 \qquad Eq.\ 2$$

Release studies were performed for the two dyes, FITC- and Cy5.5-loaded mucosomes. The dye-loaded mucosomes were suspended in a volume of mQ H_2O to obtain a drug concentration of 1 mg/mL. Drug-loaded mucosomes (800 µL) were placed in dialysis tubes (MWCO 3,500 Da), with an additional external volume of 29 mL of water, yielding a total volume of release medium of 30 mL. The release was performed at room temperature under magnetic stirring. At regular intervals, 1 mL samples were withdrawn and replaced with an equal volume of fresh water. The concentration of FITC and Cy5.5 was measured by fluorescence spectroscopy and quantified on 7-point calibration curves as previously described. Experiments were repeated in triplicate.

The computational part was performed starting from the SMILES of the drugs and the dyes. The SMILES were retrieved from MarvinSketch (Marvin 20.20, 2020 ChemAxon) after drawing the molecular structure. Molecular properties were calculated with DataWarrior (ver. 5.5.0, openmolecules.org) and include physicochemical properties, druglikeness related properties, various atom and ring counts, molecular shape, complexity, flexibility as well as functional groups. The correlation matrix was calculated using DataWarrior.

4.5.   Diffusion of loaded mucosomes through mucous membranes

Diffusion of FITC-loaded mucosomes was tested through a cystic fibrosis mucus model using Transwell® permeable supports. The mucus model was prepared as described by Pacheco et al.[61] Briefly, the cystic fibrosis mucus model was prepared using a modular approach mixing mucin from porcine stomach, alginate, $CaCO_3$ suspension and D-(+)-Glucono-delta-lactone solution. The mucus model (40 µL) was pipetted over the Transwell® membrane. The donor compartments of the Transwell® containing mucus model were then carefully shaken to uniformly distribute the mucus over the Transwell® surface and to remove any air bubbles. Then, the mucus model was left to

crosslink overnight. Successively, FITC-loaded mucosomes (200 μL of a 1 mg/mL suspension in mQ water) were inserted into the donor compartment of the Transwell® plate, while 600 μL of mQ water were placed into the acceptor compartment. The donor and acceptor compartments were then joined together and incubated. After 2 and 5 hours, the entire acceptor volume was collected and replaced with fresh water.

Similarly, diffusion experiments were performed through an *in vitro* cell model of the human airway epithelium (MucilAir™, Epithelix). MucilAir™ cell cultures are reconstituted from human primary basal, ciliated and goblet cells characterized by mucus production, active cilia beating, active ion transport and tight junctions. Cells were cultivated, according to manufacturer instructions, using the recommended medium. Cells were cultivated at the air-liquid interface on Transwell® inserts for one month before the experiments. Cells were treated with FITC or FITC-loaded mucosomes (containing 0.6 μg/mL FITC) and donor and acceptor compartments were collected after 2- and 5-hours analyses

The amount of FITC diffused in the acceptor compartment was quantified by fluorescence spectroscopy as previously described in section 2.4. The diffusion of the free FITC was used as a control.

4.6. Assessment of surface glycosylation

To evaluate the glycosylation of mucosomes, a periodic acid assay was performed with periodic acid and Shiff's reactive. Briefly, the periodic acid oxidizes vicinal hydroxyls on sugars to aldehydes or ketones, which reacts with Schiffs' reagent to give a magenta colour. The intensity of the staining is proportional to the amount of glycans. Initially, PGM standards were prepared at 75 and 100 μg/mL. In parallel, mucosomes were prepared at the same concentrations of PGM. Then, 10 μL of 50% w/v periodic acid has been added to 7 mL of 7% v/v acetic acid. Subsequently, the PGM standards and mucosomes samples were incubated under agitation for 2 hours and eventually centrifuged at 10,000 RPM for 45 min at 4°C. At the end of centrifugation, the previously prepared solution of periodic acid (180 μL) has been added to 600 μL of the supernatants. After 2 hours of incubation at 37°C, 60 μL of Schiff reagent was added to each sample. The resulting solutions were kept in the dark for 30 minutes before measuring the UV-Vis spectrum in a wavelength range of 400-700 nm.

1 In addition to the periodic acid assay, we used a complementary method to assess the

2 surface glycosylation of mucosomes. We quantified the content of free sialic acid which

3 is one of the most common glycans present on mucins. The sialic acid assay used was

4 an improved Warren method,[48] in which sialic acid is oxidized to formyl pyruvic acid.

5 This reacts with thiobarbituric acid forming a pink colored product that can be detected

6 by fluorometric detection. In brief, sialic acid standards for calibration curve were

7 prepared by adding 5 μL of 10% trichloroacetic acid (TCA) to 20 μL of each standard.

8 Similarly, 10 μL of 10% TCA were added to 40 μL of mucosomes at the concentration of

9 1 mg/mL. Samples were vortexed and centrifuged at 14,000 RPM for 10 minutes, then

10 25 μL of the supernatants were transferred to clean tubes. Each sample was then

11 oxidized and let stand at room temperature for 60 minutes. After, the color reaction was

12 started by adding 50 μL of a reactive dye and heating for 10 minutes at 100 °C. Samples

13 were diluted 1:1 with DMSO, centrifuged at 14,000 RPM for 10 minutes and eventually

14 sialic acid was quantified by fluorometric procedure (λ_{ex} = 550 nm, λ_{em} = 585 nm). The

15 sialic acid concentration of each sample was calculated according to Equation 3:

16 $$[Sialic\ acid](\mu M) = \frac{Fluorescence\ sample\ -\ Fluorescence\ blank}{Slope\ (\mu M^{-1})} \times dilution\ factor \quad Eq.3$$

17

18 ### 4.7.   Interaction with Concanavalin A

19 The interaction between mucosomes and concanavalin A (Con A) was investigated by

20 steady-state fluorescence spectroscopy using a Horiba Jobin Yvon Fluorolog 3 TCSPC

21 fluorimeter equipped with a 450-W xenon lamp and a Humamatsu R928

22 photomultiplier. A constant concentration of Con A (10 μg/mL) prepared in PBS was

23 titrated with increasing concentrations of mucosomes (5, 10, 15, 20, 25, 30, 35 μg/mL)

24 prepared as previously described. Samples were excited at 280 nm and emission was

25 recorded in the spectral range over the wavelength region 300-450 nm. Equilibrium

26 association constant was obtained after a non-linear fitting of the percentage of the

27 bound mucosomes versus the concentration of mucosomes.

28 Interaction with Con A was also investigated using a 1 mL HiTrap Con A 4B Column. A

29 1 mg/mL suspension of mucosomes was injected into the ready-to-use column

30 prepacked with Con A Sepharose 4B and 0.5 mL fractions were collected and analyzed

31 by UV-Vis spectroscopy. 20 mM Tris-HCl, 0.5 M NaCl, 1 mM $MnCl_2$, 1 mM $CaCl_2$, pH 7.4

32 was used as elution buffer. The same experiment was repeated with mucin which was

33 used as a reference. The amount of eluted mucosomes and mucin was monitored by

measuring the absorbance at 258 nm, and the concentration was calculated using a calibration curve.

4.8. Mucoadhesion

Mucoadhesion was studied by monitoring the interaction of mucosomes with mucin (BSM, mucin from bovine submaxillary glands, type I-S) in real-time using a dissipative quartz crystal microbalance QCM (QCM-Z500, KSV Instruments, Finland). Briefly, QCM measures the change in frequency of an oscillating quartz crystal in response to the adsorption of material to the crystal surface. A mass deposited onto the surface of the crystal results in a decrease in its resonant frequency.[93] The QCM response to viscoelastic layers is modelled using a Voigt model to calculate the deposited mass density.[94] In this work, crystals having a diameter of 1.5 cm, a fundamental frequency of 5 MHz, and gold electrodes (100 nm and roughness of 0.9 ± 0.2 nm) were used. The crystal was mounted into a Teflon chamber having a volume of 2 mL.

As a first step, polyethyleneimine hydrochloride (PEI, average MW 25,000 Da, c=0,1 mg/mL in 0.01 M) was deposited onto the surface of the quartz crystal to impart a positive charge for the following deposition of mucin (c=0.1 mg/mL in PBS 0.01 M). Namely, PEI and mucin were alternatively introduced into the chamber and left in contact with the crystal for 10 min. This time of deposition was enough to reach saturation adsorption for both molecules. After each deposition step, PBS 0.01 M was poured into the chamber and left in contact with the crystal for 1 min to remove the unabsorbed molecules. Finally, mucosomes were introduced into the chamber and left to interact with the mucin layer for 30 min, followed by two washing steps of 15 min each. The frequency change of the crystal was continuously recorded during the experiments and data analysis was performed using the QCM Impedance Analysis software (KSV Instruments, version 3.11).

4.9. Cytotoxicity

The MTS assay was employed to evaluate the cell viability of HeLa cells treated with mucosomes. Briefly, HeLa cells were seeded in each well of a 96 well plate at a density of $2.5 \cdot 10^3$ cells/well and cultured in a humidified 5% CO_2 incubator at 37 °C for 24h. The cells were then treated with mucosomes at various concentrations (0, 0.25, 0.5, 0.75, 1, 2, 10, 20, 50, 100 µg/mL) in culture medium, and cells cultured without

mucosomes acted as controls. Then, MTS reagent was added to each well. The cells were further incubated for another 4 hours. After incubation the plate was shaken briefly and the optical density (OD) at 490 nm was measured. The cell viability was estimated according to equation 4:

$$Cell\ viability\ (\%) = \left[\frac{OD_t}{OD_e}\right] \times 100 \qquad\qquad Eq.\ 4$$

where OD_e was the absorbance value estimated from cells without mucosomes and OD_t was the absorbance estimated in the presence of mucosomes.

4.10. Cellular uptake

Cellular uptake on HeLa cells of mucosomes was studied by confocal microscopy. For this purpose, mucosomes were loaded with fluorescein isothiocyanate (FITC). The cells were seeded onto sterile culture dishes at a concentration of $2.5 \cdot 10^5$ cells/well and cultured overnight (DMEM 10% FBS) prior to the experiments. After 24 h, the DMEM 10% FBS growth medium was aspirated and substituted with a growth medium containing 10 µg/mL of FITC loaded mucosomes. After having incubated culture dishes at 37°C for 5 h and 20 h, the modified growth medium was removed. The cells were treated with Calcein AM (CellTraceTM, calcein red-orange, Molecular Probe®, Life Technology) to obtain a red-fluorescent cytoplasm. The calcein was diluted with HBSS (Hanks' Balanced Salt Solution) to a 250 nM concentration and then incubated for 30 minutes at 37°C. Before the observations by confocal microscopy, the cells were washed twice with HBSS and fixed at 37°C with a 4% PFA (paraformaldehyde) solution for 2 min. Images were acquired over the three-axis of space (x, y, z) to reconstruct the entire cell volume. To visualize the samples by CLSM (Confocal Laser Scanning Microscopy) a DABCO MIX mounter was used. CLSM was performed with a TCS Leica SP8 X (Leica Microsystem) equipped with a scanner with DPSS laser (561 nm, to monitor calcein) and laser Ar (488 nm, to monitor fluorescein). The resulting images were obtained by an oil immersion lens (HC PLAPO CS2 63X / 1.4 A.N). The reconstruction of the 3D images helped to understand the uptake of the mucosomes. Images were analysed with ImageJ software (Rasband, W. S., ImageJ, U. S. National Institutes of Health, Bethesda, Maryland, USA, https://imagej.nih.gov/ij/, 1997- 2017). To assess the intracellular localization of mucosomes, HeLa cells were treated with 10 µg/mL of FITC-loaded mucosomes. After treatment, the cells were incubated overnight and marked with Lysotracker-Red (ex: 561 nm), a red fluorescent dye for labelling and tracking of acidic

organelles in live cells (*i.e.* lysosomes). Fluorescence was monitored as previously described.

4.11. RNA extraction and quantitative real-time PCR analysis

Murine macrophage cell line, Raw 264.7, was used to study cytokine levels after stimulation with mucosomes. The cDNA levels of the pro-inflammatory cytokines IL-1B, IL-6 and TNF-α, have been tested by Real-Time PCR technique. Cells were treated with mucosomes at three doses (0.25, 0.5, 1 µg/mL). Untreated cells were used as negative control while lipopolysaccharide (LPS 1 µg/mL) was used as a positive control. Before the RNA extraction, the cells were observed by light microscopy to evaluate their viability and morphology.

RNA extraction and quantitative real-time PCR (qRT-PCR) analyses were performed as previously described.[95] Briefly, total RNA was extracted using PureLink RNA Mini Kit (Thermo Fisher Scientific, Waltham, MA USA) and 0.5-1 μg of total RNA were transcribed into complementary DNA (cDNA) by High-Capacity cDNA Reverse Transcription Kit (Thermo Fisher Scientific, Waltham, MA USA). qRT-PCR was performed using the following TaqMan™ Gene Expression Assays: Il1β, Mm00434228_m1; Il-6, Mm00446190_m1; TNFα, Mm00443258_m1 (Thermo Fisher Scientific Waltham, MA USA). qRT-PCR was performed on a QuantStudio™ 6 Flex Real-Time PCR System (Thermo Fisher Scientific, Waltham, MA USA) and the analyses were done using QuantStudio Real-Time PCR software. Transcript abundance, normalized to 18s messenger ribonucleic acid (mRNA) expression, is expressed as Log2 of the fold change over a calibrator sample.

4.12. Assessment of the effect of mucosomes on the coagulation system

The effect of mucosomes on blood coagulation was investigated *in vitro*. Blood samples were collected from healthy consenting volunteers who had not taken any medication in the 7 days previous to the tests. The test was carried out with nanoparticles in blood samples at a final concentration of 0.5 mg/mL and compared with samples not treated with mucosomes. After 30 min the addition of mucosomes, blood tubes were centrifuged at 2,000 g for 15 min at room temperature to separate the corpuscular part from the plasma fraction. The prothrombin time (PT), the activated partial prothrombin

1　time (APPT) and the concentration of fibrinogen, antithrombin, D-dimer, factor VIII and

2　factor XI were estimated by the automatic coagulometer ACL TOP 750 Las. Each sample

3　was repeated in triplicate.

4

5　### 4.13.　Stability of mucosomes to protease

6　The stability toward a degradation enzyme of FITC-loaded mucosomes was

7　investigated using a protease from bovine pancreas (Merck, Italy, code P4630). The

8　protease degrades proteins by hydrolyzing the peptide bond. FITC-loaded mucosomes

9　were synthesized as previously described. A 1 mg/mL sample of FITC-loaded

10　mucosomes suspended in 10 mM PBS, and a 0.01 mg/mL of protease prepared in the

11　same buffer, were mixed in a 100:1 ratio. Afterwards, the mixture was incubated at 37

12　°C. FITC-loaded mucosomes without the protease were used as control. At specific time

13　points, 100 µL of the mucosome mixture was withdrawn and mixed with 83 µL of 110

14　mM trichloroacetic acid (TCA), which was used to block the activity of the protease. The

15　effect of the enzyme was measured by quantifying the amount of FITC released in the

16　environment. FITC was detected by fluorescence spectroscopy using a Horiba Jobin

17　Yvon Fluorolog3 TCSPC spectrofluorometer (ex: 490 nm).

18

19　### 4.14.　*In vivo* biodistribution and toxicity

20　The biodistribution of cyanine 5.5 (Cy5.5)-loaded mucosomes was investigated on

21　healthy naked female Envigo mice via tail vein injection. The distribution profiles of

22　Cy5.5-loaded mucosomes in the heart, liver, spleen, lung and kidney over different time

23　periods (15 min, 1h, 4h, 24h, 48h) were comparatively investigated by fluorescence

24　spectroscopy. The emission of Cy5.5 was monitored at 720 nm. A suspension of 400

25　µg/mL of Cy5.5-loaded mucosomes was prepared in PBS and 250 µL (containing 13

26　nmol Cy5.5) were injected into mice (n=10). Animals were randomly divided into two

27　groups and 15 min, 1h, 4h, 24h and 48h post-injection mice were anaesthetized with

28　sevoflurane and monitored by optical imaging. After imaging, the mice were sacrificed

29　and liver, spleen, kidney, lung and heart were excised for *ex vivo* optical imaging

30　acquisition. A drop of urine (where present) and blood were aspired and imaged as well.

31　The analysis was performed with the Living Image IVIS software.

32　In addition to the qualitative analysis, Cy5.5 was also quantified in the lungs and

33　kidneys of one of the mice. Organs were extracted, weighted and suspended in 10 mL

of ethyl acetate. Then, organs were homogenized using an Ultra-Turrax® T-25 for 2 minutes and sonicated for another 2 minutes. In order to separate the corpuscular part from the solubilized material, the homogenate was centrifuged at 10,000 rpm for 10 minutes. The supernatant was collected and filtered through a 0.45 µm PTFE filter. Eventually, the Cy5.5 within the obtained solutions was quantified by fluorescence spectroscopy using a 7-points calibration curve, as previously described.

Similarly, the *in vivo* toxicity of empty mucosomes was evaluated on the same animal model. A 400 µg/mL of mucosomes was prepared in PBS and 250 µL were injected into the caudal vein of healthy mice (n=5). Saline was used as a control (n=5). Animals were weighed three times a week and monitored for 14 days after administration. Mice were euthanized humanely 2 weeks after injection of empty mucosomes.

References

1. Pushpakom, S. *et al.* Drug repurposing: Progress, challenges and recommendations. *Nat. Rev. Drug Discov.* **18**, 41–58 (2018).

2. Freedman, D. H. Hunting for New Drugs with AI. *Nature* **576**, S49–S53 (2019).

3. DiMasi, J. A., Grabowski, H. G. & Hansen, R. W. Innovation in the pharmaceutical

industry: New estimates of R&D costs. *J. Health Econ.* **47**, 20–33 (2016).

4.   Antimicrobial Resistance Division; Global Antimicrobial Resistance
     Surveillance System; Global Antimicrobial Resistance Surveillance System
     (GLASS); SurveillancePrevention&Control *et al. Global antimicrobial resistance*
     and use surveillance system (GLASS) report. World Health Organisation. (2021).

5.   Katsuno, K. *et al.* Hit and lead criteria in drug discovery for infectious diseases
     of the developing world. *Nat. Rev. Drug Discov.* **14**, 751–758 (2015).

6.   Eissa, A. M., Abdulkarim, A., Sharples, G. J. & Cameron, N. R. Glycosylated
     Nanoparticles as Efficient Antimicrobial Delivery Agents. *Biomacromolecules*
     17, 2672–2679 (2016).

7.   Ofek, I., Hasty, D. L. & Sharon, N. Anti-adhesion therapy of bacterial diseases:
     Prospects and problems. *FEMS Immunol. Med. Microbiol.* **38**, 181–191 (2003).

8.   Li, Y. *et al.* The Importance of Glycans of Viral and Host Proteins in Enveloped
     Virus Infection. *Front. Immunol.* **12**, 1–12 (2021).

9.   Te Riet, J., Joosten, B., Reinieren-Beeren, I., Figdor, C. G. & Cambi, A. N-glycan
     mediated adhesion strengthening during pathogen-receptor binding revealed
     by cell-cell force spectroscopy. *Sci. Rep.* **7**, 1–12 (2017).

10. Poole, J., Day, C. J., Von Itzstein, M., Paton, J. C. & Jennings, M. P.
     Glycointeractions in bacterial pathogenesis. *Nat. Rev. Microbiol.* **16**, 440–452
     (2018).

11. Mereiter, S., Balmaña, M., Campos, D., Gomes, J. & Reis, C. A. Glycosylation in the
     Era of Cancer-Targeted Therapy: Where Are We Heading? *Cancer Cell* **36**, 6–16
     (2019).

12. Chen, J. *et al.* Variation in carbohydrates between cancer and normal cell
     membranes revealed by super-resolution fluorescence imaging. *Adv. Sci.* **3**,
     (2016).

13. Munkley, J. The role of sialyl-Tn in cancer. *Int. J. Mol. Sci.* **17**, (2016).

14. Wi, D. H., Cha, J. H. & Jung, Y. S. Mucin in cancer: a stealth cloak for cancer cells.
     BMB Rep. **54**, 344–355 (2021).

15. Torres-Pérez, S. A., Torres-Pérez, C. E., Pedraza-Escalona, M., Pérez-Tapia, S. M.
     & Ramón-Gallegos, E. Glycosylated Nanoparticles for Cancer-Targeted Drug

Delivery. *Front. Oncol.* **10**, 1–10 (2020).

16. Tenchov, R., Bird, R., Curtze, A. E. & Zhou, Q. Lipid Nanoparticles from Liposomes to mRNA Vaccine Delivery, a Landscape of Research Diversity and Advancement. *ACS Nano* **15**, 16982–17015 (2021).

17. Hou, X., Zaks, T., Langer, R. & Dong, Y. Lipid nanoparticles for mRNA delivery. *Nat. Rev. Mater.* **6**, 1078–1094 (2021).

18. Shirley, M. Amikacin Liposome Inhalation Suspension: A Review in Mycobacterium avium Complex Lung Disease. *Drugs* **79**, 555–562 (2019).

19. Freitag, T. L. *et al.* Gliadin Nanoparticles Induce Immune Tolerance to Gliadin in Mouse Models of Celiac Disease. *Gastroenterology* **158**, 1667-1681.e12 (2020).

20. Pham, D. T. & Tiyaboonchai, W. Fibroin nanoparticles: a promising drug delivery system. *Drug Deliv.* **27**, 431–448 (2020).

21. Carvalho, J. A. *et al.* Preparation of gelatin nanoparticles by two step desolvation method for application in photodynamic therapy. *https://doi.org/10.1080/09205063.2018.1456027* **29**, 1287–1301 (2018).

22. Adnane, M., Meade, K. G. & O'Farrelly, C. Cervico-vaginal mucus (CVM) – an accessible source of immunologically informative biomolecules. *Vet. Res. Commun.* **42**, 255–263 (2018).

23. Bustamante-Marin, X. M. & Ostrowski, L. E. Cilia and mucociliary clearance. *Cold Spring Harb. Perspect. Biol.* **9**, (2017).

24. Devine, P. L. & McKenzie, I. F. C. Mucins: Structure, function, and associations with malignancy. *BioEssays* **14**, 619–625 (1992).

25. Butnarasu, C., Caron, G., Pacheco, D. P., Petrini, P. & Visentin, S. Cystic Fibrosis Mucus Model to Design More Efficient Drug Therapies. *Mol. Pharm.* (2022). doi:10.1021/acs.molpharmaceut.1c00644

26. Prandota, J. Clinical Pharmacology of Antibiotics and Other Drugs in Cystic Fibrosis. *Drugs* **35**, 542–578 (1988).

27. Huang, J. X. *et al.* Mucin Binding Reduces Colistin Antimicrobial Activity. *Antimicrob. Agents Chemother.* **59**, 5925–5931 (2015).

28. Dat Pham, Q. *et al.* Mucoadhesion: mucin-polymer molecular interactions. *Int. J.*

Pharm. **610**, 121245 (2021).

29. Shtenberg, Y. *et al.* Mucoadhesive alginate pastes with embedded liposomes for local oral drug delivery. *Int. J. Biol. Macromol.* **111**, 62–69 (2018).

30. Sogias, I. A., Williams, A. C. & Khutoryanskiy, V. V. Why is Chitosan Mucoadhesive? *Biomacromolecules* **9**, 1837–1842 (2008).

31. Park, H. & Robinson, J. R. Mechanisms of Mucoadhesion of Poly(acrylic Acid) Hydrogels. *Pharm. Res.* **4**, 457–464 (1987).

32. Jaipakdee, N., Pongjanyakul, T. & Limpongsa, E. Preparation and characterization of poly (vinyl alcohol)-poly (vinyl pyrrolidone) mucoadhesive buccal patches for delivery of lidocaine HCL. *Int. J. Appl. Pharm.* **10**, 115–123 (2018).

33. Salama, M. M. & Elzoghby, A. O. Chapter 6 - Mucoadhesive nanoparticles as promising drug delivery systems. in (eds. Kesharwani, P., Taurin, S. & Greish, K. B. T.-T. and A. of N. N.) 113–136 (Academic Press, 2021). doi:https://doi.org/10.1016/B978-0-12-820466-5.00006-5

34. Elzoghby, A. O., Elgohary, M. M. & Kamel, N. M. Implications of Protein- and Peptide-Based Nanoparticles as Potential Vehicles for Anticancer Drugs. *Adv. Protein Chem. Struct. Biol.* **98**, 169–221 (2015).

35. Davidov-Pardo, G., Joye, I. J. & Mcclements, D. J. Food-Grade Protein-Based Nanoparticles and Microparticles for Bioactive Delivery: Fabrication, Characterization, and Utilization. *Adv. Protein Chem. Struct. Biol.* **98**, 293–325 (2015).

36. Yan, H. *et al.* Reversible Condensation of Mucins into Nanoparticles. *Langmuir* **34**, 13615–13625 (2018).

37. Moratz, J., Klepel, F. & Ravoo, B. J. Dynamic glycosylation of liposomes by thioester exchange. *Org. Biomol. Chem.* **15**, 5089–5094 (2017).

38. Budhadev, D. *et al.* Glycan-Gold Nanoparticles as Multifunctional Probes for Multivalent Lectin–Carbohydrate Binding: Implications for Blocking Virus Infection and Nanoparticle Assembly. *J. Am. Chem. Soc.* **142**, 18022–18034 (2020).

39. Kneidl, B., Peller, M., Winter, G., Lindner, L. H. & Hossann, M. Thermosensitive liposomal drug delivery systems: state of the art review. *Int. J. Nanomedicine* **9**,

4387–4398 (2014).

40. Ullmann, K., Leneweit, G. & Nirschl, H. How to Achieve High Encapsulation Efficiencies for Macromolecular and Sensitive APIs in Liposomes. *Pharmaceutics* **13**, (2021).

41. Wang, X. & Cao, Y. Characterizations of absorption, scattering, and transmission of typical nanoparticles and their suspensions. *J. Ind. Eng. Chem.* **82**, 324–332 (2020).

42. Schoemig, V., Isik, E., Martin, L. & Berensmeier, S. Solid liquid liquid extraction of porcine gastric mucins from homogenized animal material. *RSC Adv.* **7**, 39708–39717 (2017).

43. Marczynski, M. *et al.* Structural Alterations of Mucins Are Associated with Losses in Functionality. *Biomacromolecules* **22**, 1600–1613 (2021).

44. Kumar, A. & Dixit, C. K. 3 - Methods for characterization of nanoparticles. in (eds. Nimesh, S., Chandra, R. & Gupta, N. B. T.-A. in N. for the D. of T. N. A.) 43–58 (Woodhead Publishing, 2017). doi:https://doi.org/10.1016/B978-0-08-100557-6.00003-1

45. Baos, S. C., Phillips, D. B., Wildling, L., McMaster, T. J. & Berry, M. Distribution of Sialic Acids on Mucins and Gels: A Defense Mechanism. *Biophys. J.* **102**, 176–184 (2012).

46. Bjarnsholt, T. *et al.* Pseudomonas aeruginosa biofilms in the respiratory tract of cystic fibrosis patients. *Pediatr. Pulmonol.* **44**, 547–558 (2009).

47. Kahl, B. C. Staphylococcus aureus and Pseudomonas aeruginosa Respiratory Tract Coinfection - What Can We Learn from Animal Models? *J. Infect. Dis.* **217**, 854–856 (2018).

48. WARREN, L. The thiobarbituric acid assay of sialic acids. *J. Biol. Chem.* **234**, 1971–1975 (1959).

49. Jeffers, F. *et al.* Mucin–lectin interactions assessed by flow cytometry. *Carbohydr. Res.* **345**, 1486–1491 (2010).

50. Surolia, A. *et al.* Studies on the interaction of concanavalin A with glycoproteins. *Adv. Exp. Med. Biol.* **55**, 95–115 (1975).

51. Cui, F., Qian, F. & Yin, C. Preparation and characterization of mucoadhesive

polymer-coated nanoparticles. *Int. J. Pharm.* **316**, 154–161 (2006).

52. Shakya, A. K., Chowdhury, M. Y. E., Tao, W. & Gill, H. S. Mucosal vaccine delivery: Current state and a pediatric perspective. *J. Control. Release* **240**, 394–413 (2016).

53. Smistad, G., Jacobsen, J. & Sande, S. A. Multivariate toxicity screening of liposomal formulations on a human buccal cell line. *Int. J. Pharm.* **330**, 14–22 (2007).

54. Li, Y. *et al.* Cationic liposomes induce cytotoxicity in HepG2 via regulation of lipid metabolism based on whole-transcriptome sequencing analysis. *BMC Pharmacol. Toxicol.* **19**, 1–13 (2018).

55. Filion, M. C. & Phillips, N. C. Toxicity and immunomodulatory activity of liposomal vectors formulated with cationic lipids toward immune effector cells. *Biochim. Biophys. Acta - Biomembr.* **1329**, 345–356 (1997).

56. De Leo, V., Milano, F., Agostiano, A. & Catucci, L. Recent Advancements in Polymer/Liposome Assembly for Drug Delivery: From Surface Modifications to Hybrid Vesicles. *Polymers* **13**, (2021).

57. Jung, I. W. & Han, H. K. Effective mucoadhesive liposomal delivery system for risedronate: Preparation and in vitro/in vivo characterization. *Int. J. Nanomedicine* **9**, 2299–2306 (2014).

58. Abdellatif, M. M. *et al.* Formulation and characterization of sertaconazole nitrate mucoadhesive liposomes for vaginal candidiasis. *Int. J. Nanomedicine* **15**, 4079–4090 (2020).

59. Karn, P. R., Vanić, Z., Pepić, I. & Škalko-Basnet, N. Mucoadhesive liposomal delivery systems: The choice of coating material. *Drug Dev. Ind. Pharm.* **37**, 482–488 (2011).

60. Shogren, R., Gerken, T. A. & Jentoft, N. Role of glycosylation on the conformation and chain dimensions of O-linked glycoproteins: light-scattering studies of ovine submaxillary mucin. *Biochemistry* **28**, 5525–5536 (1989).

61. Pacheco, D. P. *et al.* Disassembling the complexity of mucus barriers to develop a fast screening tool for early drug discovery. *J. Mater. Chem. B* **7**, 4940–4952 (2019).

62. Dong, C. *et al.* A Protein–Polymer Bioconjugate-Coated Upconversion

Nanosystem for Simultaneous Tumor Cell Imaging, Photodynamic Therapy, and Chemotherapy. *ACS Appl. Mater. Interfaces* **8**, 32688–32698 (2016).

63. Martínez-Torres, A. C. *et al.* Chitosan gold nanoparticles induce cell death in hela and MCF-7 cells through reactive oxygen species production. *Int. J. Nanomedicine* **13**, 3235–3250 (2018).

64. Casadó, A. *et al.* Improved selectivity and cytotoxic effects of irinotecan via liposomal delivery: A comparative study on Hs68 and HeLa cells. *Eur. J. Pharm. Sci.* **109**, 65–77 (2017).

65. Peñaloza, J. P. *et al.* Intracellular trafficking and cellular uptake mechanism of PHBV nanoparticles for targeted delivery in epithelial cell lines. *J. Nanobiotechnology* **15**, 1 (2017).

66. Ehrlich, M. *et al.* Endocytosis by Random Initiation and Stabilization of Clathrin-Coated Pits. *Cell* **118**, 591–605 (2004).

67. Oh, N. & Park, J.-H. Endocytosis and exocytosis of nanoparticles in mammalian cells. *Int. J. Nanomedicine* **9**, 51–63 (2014).

68. Dobrovolskaia, M. A. *et al.* Nanoparticle Size and Surface Charge Determine Effects of PAMAM Dendrimers on Human Platelets in Vitro. *Mol. Pharm.* **9**, 382–393 (2012).

69. Jones, C. F. *et al.* Cationic PAMAM Dendrimers Disrupt Key Platelet Functions. *Mol. Pharm.* **9**, 1599–1611 (2012).

70. Zbinden, G., Wunderli-Allenspach, H. & Grimm, L. Assessment of thrombogenic potential of liposomes. *Toxicology* **54**, 273–280 (1989).

71. Ilinskaya, A. N. & Dobrovolskaia, M. A. Nanoparticles and the blood coagulation system. Part II: safety concerns. *Nanomedicine* **8**, 969–981 (2013).

72. Prasher, P. & Sharma, M. Mucoadhesive nanoformulations and their potential for combating COVID-19. *Nanomedicine* **16**, 2497–2501 (2021).

73. Berginc, K., Žakelj, S., Levstik, L., Uršič, D. & Kristl, A. Fluorescein transport properties across artificial lipid membranes, Caco-2 cell monolayers and rat jejunum. *Eur. J. Pharm. Biopharm.* **66**, 281–285 (2007).

74. Makidon, P. E. *et al.* Characterization of Stability and Nasal Delivery Systems for Immunization with Nanoemulsion-Based Vaccines. *J. Aerosol Med. Pulm.*

1   *Drug Deliv.* **23**, 77–89 (2009).

2   75. Thorn, C. R., Thomas, N., Boyd, B. J. & Prestidge, C. A. Nano-fats for bugs: the
3   benefits of lipid nanoparticles for antimicrobial therapy. *Drug Deliv. Transl.*
4   *Res.* **11**, 1598–1624 (2021).

5   76. Forier, K. *et al.* Lipid and polymer nanoparticles for drug delivery to bacterial
6   biofilms. *J. Control. Release* **190**, 607–623 (2014).

7   77. Canaparo, R. *et al.* Recent Developments in Antibacterial Therapy: Focus on
8   Stimuli-Responsive Drug-Delivery Systems and Therapeutic Nanoparticles.
9   *Molecules* **24**, (2019).

10 78. Dua, K., Shukla, S. D., Tekade, R. K. & Hansbro, P. M. Whether a novel drug
11   delivery system can overcome the problem of biofilms in respiratory diseases?
12   *Drug Deliv. Transl. Res.* **7**, 179–187 (2017).

13 79. von Korff, M. & Sander, T. About Complexity and Self-Similarity of Chemical
14   Structures in Drug Discovery BT - Chaos and Complex Systems. in (eds.
15   Stavrinides, S. G., Banerjee, S., Caglar, S. H. & Ozer, M.) 301–306 (Springer
16   Berlin Heidelberg, 2013).

17 80. Yu, M., Wu, J., Shi, J. & Farokhzad, O. C. Nanotechnology for protein delivery:
18   Overview and perspectives. *J. Control. Release* **240**, 24–37 (2016).

19 81. Bost, J. P. *et al.* Delivery of Oligonucleotide Therapeutics: Chemical
20   Modifications, Lipid Nanoparticles, and Extracellular Vesicles. *ACS Nano* **15**,
21   13993–14021 (2021).

22 82. Butnarasu, C., Barbero, N., Pacheco, D., Petrini, P. & Visentin, S. Mucin binding
23   to therapeutic molecules: The case of antimicrobial agents used in cystic
24   fibrosis. *Int. J. Pharm.* (2019). doi:10.1016/j.ijpharm.2019.04.032

25 83. Witten, J., Samad, T. & Ribbeck, K. Molecular Characterization of Mucus
26   Binding. *Biomacromolecules* **20**, 1505–1513 (2019).

27 84. Falavigna, M., Stein, P. C., Flaten, G. E. & di Cagno, M. P. Impact of Mucin on
28   Drug Diffusion: Development of a Straightforward In Vitro Method for the
29   Determination of Drug Diffusivity in the Presence of Mucin. *Pharmaceutics* **12**,
30   (2020).

31 85. Barbero, N. *et al.* Is it possible to study the kinetic parameters of interaction
32   between PNA and parallel and antiparallel DNA by stopped-flow fluorescence?

J. Photochem. Photobiol. B Biol. **163**, 296–302 (2016).

86.   Thakare, P. *et al.* Acid-base and lipophilic properties of peptide nucleic acid derivatives. *J. Pharm. Anal.* **11**, 638–645 (2021).

87.   Egholm, M. *et al.* PNA hybridizes to complementary oligonucleotides obeying the Watson-Crick hydrogen- bonding rules. *Lett. to Nat.* **87**, 507–513 (1992).

88.   Feiler, A. A., Sahlholm, A., Sandberg, T. & Caldwell, K. D. Adsorption and viscoelastic properties of fractionated mucin (BSM) and bovine serum albumin (BSA) studied with quartz crystal microbalance (QCM-D). *J. Colloid Interface Sci.* **315**, 475–481 (2007).

89.   List, S. J., Findlay, B. P., Forstner, G. G. & Forstner, J. F. Enhancement of the viscosity of mucin by serum albumin. *Biochem. J.* **175**, 565–571 (1978).

90.   Louis-Jeune, C., Andrade-Navarro, M. A. & Perez-Iratxeta, C. Prediction of protein secondary structure from circular dichroism using theoretically derived spectra. *Proteins Struct. Funct. Bioinforma.* **80**, 374–381 (2012).

91.   Hermanson, G. *Bioconjugate Techniques*. (2008).

92.   Barbero, N. *et al.* A transient kinetic study between signaling proteins: The case of the MEK-ERK interaction. *Chem. Sci.* **2**, 1804–1809 (2011).

93.   Marx, K. A. Quartz Crystal Microbalance: A Useful Tool for Studying Thin Polymer Films and Complex Biomolecular Systems at the Solution–Surface Interface. *Biomacromolecules* **4**, 1099–1120 (2003).

94.   Viitala, T., Hautala, J. T., Vuorinen, J. & Wiedmer, S. K. Structure of Anionic Phospholipid Coatings on Silica by Dissipative Quartz Crystal Microbalance. *Langmuir* **23**, 609–618 (2007).

95.   Petrillo, S. *et al.* Heme accumulation in endothelial cells impairs angiogenesis by triggering paraptosis. *Cell Death Differ.* **25**, 573–588 (2018).

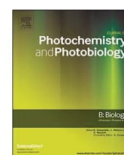The author's contributions to the appended manuscript consist of all the experimental work and manuscript preparation; data interpretation was done together with the contribution from coauthors.

Squaraine dyes as fluorescent turn-on sensors for the detection of porcine gastric mucin: A spectroscopic and kinetic study

Cosmin Butnarasu[a], Nadia Barbero[b], Claudia Barolo[b], Sonja Visentin[a],*

[a] *Department of Molecular Biotechnology and Health Sciences, University of Torino, Via Gioacchino Quarello 15A, 10135 Torino, Italy*
[b] *Department of Chemistry, NIS Interdepartmental and INSTM Reference Centre, University of Torino, Via Pietro Giuria 7, 10125 Torino, Italy*

A B S T R A C T

Mucin-type glycoproteins are the principal components of mucus which cover all the mucosal surfaces of the human body. The mucus and mucins are essential mediators of the innate immune system, however in the last decades mucins have been identified even as an important class of cancer biomarkers. Luminogenic materials with fluorescence turn-on behavior are becoming promising materials because of their advantages of label free, relatively inexpensive and simple to use properties for biological detection and imaging. Squaraines are luminogens characterized by high fluorescence in organic media but poor emission in aqueous environments due to their tendency to self-aggregate. Herein we investigate the interaction between porcine gastric mucin (PGM) and several squaraines in aqueous media. While squaraine dyes showed low fluorescence intensity and quantum yield in water, as a result of the formation of aggregates, an enhancement of fluorescence up to 45-fold was achieved when PGM was added. PGM was detected in a linear range of 10–300 μg/mL with a limit of detection of 800 ng/mL. The assay was used to quantify mucin in diluted human serum samples and recoveries of 94.9–116.2% were achieved. To the best of our knowledge, this is the easiest and convenient method for mucin detection in the reported literature.

1. Introduction

Mucins are a family of long polymeric glycoconjugates having high molecular weight, produced by goblet cells in the gastrointestinal, respiratory, reproductive, pancreatic, hepatic and renal epithelium. Structurally, mucins are formed by a long peptide core at which glycans are linked (Fig. 1 A). So far, two major classes of mucins have been identified: secreted mucins, further divided as gel-forming and non-gel forming, and transmembrane mucins [1–3]. Gel-forming mucins assemble into polymers creating a complex network representing the skeleton around which mucus is formed [4]. The primary function of mucus is to protect the underlying surfaces from environmental stressors. Beside its protective function, in pathological conditions, mucus can become a concentrate of pathogens and cellular debris as well as a barrier for drug absorption as a result of its altered physico-chemical properties. Alterations or overexpression of mucus are associated with diseases like chronic obstructive pulmonary disease (COPD), asthma, cystic fibrosis and several types of cancer [5]. Particularly, in the last years, great attention was addressed to expression of mucins in various cancers such as pancreatic adenocarcinomas [6,7], colon and rectal cancer [8], breast cancer [9], ovarian cancer [10] and gastric

carcinoma [11]. Maker et al. [12] found that high-risk patients for intraductal papillary mucinous neoplasms of the pancreas have elevated cyst fluid concentrations of MUC2 and MUC4, and increased serum levels of MUC5AC. Significantly high serum levels of mucin were found also in patients with breast cancer and in patients with oral lichen planus. Bademler et al. reported that the average serum levels of MUC2 in breast cancer patients was 198 vs 54 ng/mL (with spikes even at 668 ng/mL), while Agha-Hosseini et al. found a concentration of 614.8 ng/mL (± 63) of mucin in serum of patients with oral lichen planus [13,14]. It is well known that the early diagnosis is a key factor for outcome, treatments, and healthcare. Thus, the identification and detection of specific and sensitive biomarkers have become extremely important in the last decades [12,13,15–17].

Up until now, various methods for membrane-bound mucin MUC1 detection have been developed such as antibody-based enzyme-linked immunosorbent assays and aptamer-based electrochemical and fluorescence techniques [18–21]. However, these methods often have limitations including relative instability, complex production, difficult purification processes, and time-consuming. Therefore, the search for better alternatives is still running. Among the above mentioned methods, fluorometric assays have received remarkable attention due

---

* Corresponding author.
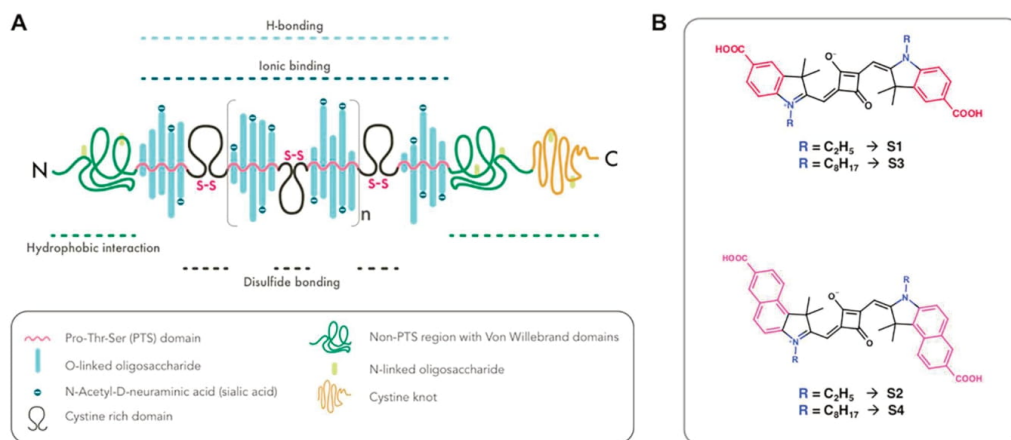 *E-mail address:* sonja.visentin@unito.it (S. Visentin).

Fig. 1. Molecular structures of PGM (A, adapted from Butnarasu et al. [34]) and the squaraine dyes (B).

to their convenience, unparalleled sensitivity, simplicity, rapid implementation, noninvasive monitoring capability and usability in biological samples [22]. Thus, the interest in developing new dyes that can non-covalently bind specific proteins for their detection is rising up. Fluorescent probes with absorption and emission in the near infrared (NIR) region (650–900 nm) are useful for practical biological applications as NIR signal detection does not suffer of self-absorption and autofluorescence typical of biological matrices.

Among promising biological fluorescent probes, polymethine dyes (cyanine and squaraines) are characterized by sharp and intense absorption and emission in the visible up to the NIR region. Squaraine dyes are produced by condensation reactions between squaric acid and electron-rich substrates. Squaraines were studied extensively and such research covered numerous areas ranging from photophysical to biological applications [23–25]. Moreover, we can easily design and modify their structure to get NIR molecules, perfectly matching the phototherapeutic window (650–850 nm), simply by tuning the lateral functional groups [26,27]. However, as most of fluorescent probes, in physiological conditions, squaraine dyes tend to form aggregates that lead to fluorescence quenching therefore limiting their wide applications. As reported in previous studies, squaraine dyes exhibit a fluorescence turn-on when bound to proteins which translate in an increase in fluorescence intensity, quantum yield and lifetime due to the changes in the surrounding environment [28–32]. Saito et al. reported an artificial fluorescent receptor for saccharides (mainly fructose) by modifying a squaraine dye with boronic acid. The sensor was used to detect PGM solutions, however they recorded a mild turn-on of fluorescence intensity [33].

In the present paper we report our results about a spectroscopic, thermodynamic and kinetic study of the interaction between commercial porcine gastric mucin (PGM) and four squaraine dyes with different substitutions (Fig. 1 B). The squaraines differ on the nature of the lateral moieties (i.e. indolenine vs benzoindolenine) and on the length of the alkyl chains (i.e. C2 vs C8). Interactions were carried out by means of UV–Vis, circular dichroism and fluorescence spectroscopies. Moreover, we evaluate the possibility of using these squaraine dyes as probes for mucin detection in serum samples. We report a new fluorometric "turn-on" detection of mucin based on the aggregation/deaggregation of squaraine dyes in different environments. As far as we know, no reports have been published to date on the application of squaraine dyes as fluorescent probes in testing mucin detection in human serum samples.

2. Experimental Section

2.1. Materials

All reagents were of analytical reagent grade. Millipore grade water was obtained from an in-house Millipore system (resistivity: 18.2 MΩ cm at 25 °C). Mucin from porcine stomach (PGM type III, bound sialic acid 0.5–1.5%, partially purified powder) was purchased from Sigma Aldrich. PGM solutions were prepared in phosphate buffer (PBS) 2 mM. Since PGM itself is a water insoluble material, in order to facilitate solubility and obtain homogeneous suspensions, dispersions of mucin were sonicated for two minutes at room temperature. Squaraine dyes were prepared as previously described [35]. Mother solutions of the dyes (500 μg/mL) were prepared in DMSO and dilutions for the experiments (in the μM range) were performed in PBS.

2.2. Spectroscopic Measurements

UV–Vis absorption spectra were measured by a UH5300 Hitachi spectrophotometer at room temperature, using 1 cm pathway length quartz cuvettes. The UV measurements were made in the range of 500–750 nm. Squaraine dyes concentration was kept constant (2 μM) and PGM changed over the range 0–300 μg/mL.

Circular dichroism measurements were performed using a Jasco J-815 CD spectrophotometer. The spectra were collected in a range of 185–250 nm in a 0.5 mm light path using a scan speed of 50 nm/min. Each spectrum is the average of three scans.

Fluorescence emission spectra in steady state mode were acquired at room temperature using a Horiba Jobin Yvon Fluorolog 3 TCSPC fluorimeter equipped with a 450-W Xenon lamp and a Hamamatsu R928 photomultiplier.

Fluorescence spectra were recorded in the range of 615–750 nm for S1, 625–800 nm for S3 and 645–800 nm for S2 and S4. The excitation wavelength was fixed on the squaraine hypsochromic shoulder of absorbance: 595 nm for S1, 605 nm for S3 and 625 nm for S2 and S4. A constant concentration of squaraine dye (1 μM for S1 and S2, and 0.1 μM for S3 and S4) was analyzed by successive increasing the concentration of PGM.

Fluorescence experiments were also performed in a time drive mode in order to check whether and when the solution reached the stability; fluorescence intensity of a constant concentration of squaraine and PGM was registered over time at specific time points.

The absolute quantum yield was determined by means of an integrating sphere combining Quanta-φ with Fluorolog 3. The reported quantum yields are the average of the values obtained after three measurements using three different dye solutions.

Fluorescence lifetimes were measured by the time correlated single photon counting method (Horiba Jobin Yvon) using a 636 nm Horiba Jobin Yvon NanoLED as excitation source and an impulse repetition frequency of 1 MHz positioned at 90° with respect to a TBX-04 detector. Lifetimes were calculated using DAS6 decay analysis software.

2.3. Serum Test

To assess applicability for detecting PGM in complex matrices, we performed measurements in diluted human serum (HS). Serum samples were prepared as following. To a volume of HS, an equal volume of cold 50% *w/v* trichloroacetic acid (TCA) was added. The sample was vortexed for one minute and then stored at -20 °C for 15 min. Next, the sample was centrifuged at 13.000 rpm for 15 min at 4 °C. The supernatant was collected and centrifuged again using the same settings. Eventually, the supernatant was collected, neutralized with NaOH 1 M and 1% diluted HS samples were prepared. Spiked samples were prepared by addition of different concentrations of PGM to the diluted HS.

3. Results and Discussion

3.1. Spectroscopic Measurements

The absorption and emission of squaraine dyes are strongly influenced by the environment [30]. First the UV/Vis absorption spectra of the four squaraines were recorded in different solvents (Fig. 2). All the four squaraines are freely soluble in DMSO giving one principal band at 656, 684, 659 and 686 nm attributing it to the monomeric form of S1, S2, S3 and S4 respectively, and a slight shoulder at lower wavelengths. The absorption spectra of the four squaraines in water are blue-shifted with a decreased absorbance that is a consequence of the reduced solubility. This is particularly evident for S3 and S4 where the monomeric band is almost absent, and the absorption spectrum is characterized by the large H-aggregate band. Except for S1, the addition of surfactants (SDS or Pluronic F-127, 0.05 wt%) to the aqueous solution leads to an increase in absorption of the band corresponding to the monomeric form. The major changes in absorption are achieved with the non-ionic surfactant (Pluronic F-127). Since the concentration of surfactants are below their critical micelle concentration (CMC), the surfactant molecules are expected to be not aggregated. As proposed by Y. Xu et al. [29] it is possible that the negative charge of SDS interacts with the positively charged (even if delocalized) nitrogen of the squaraines,
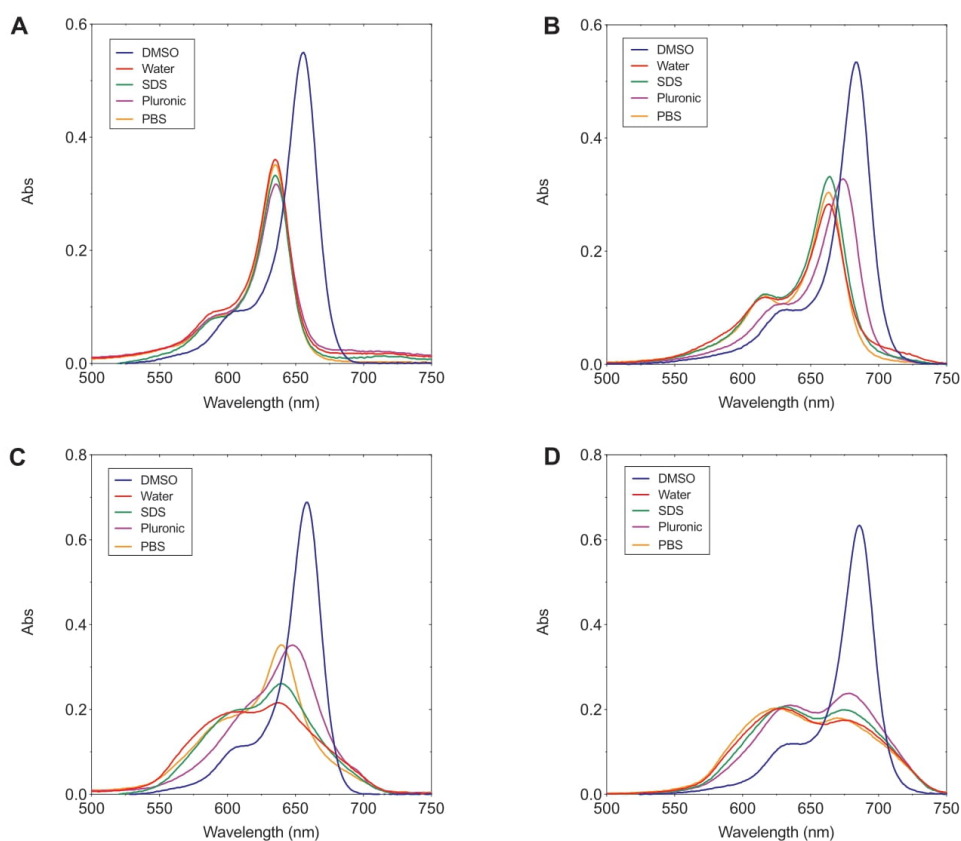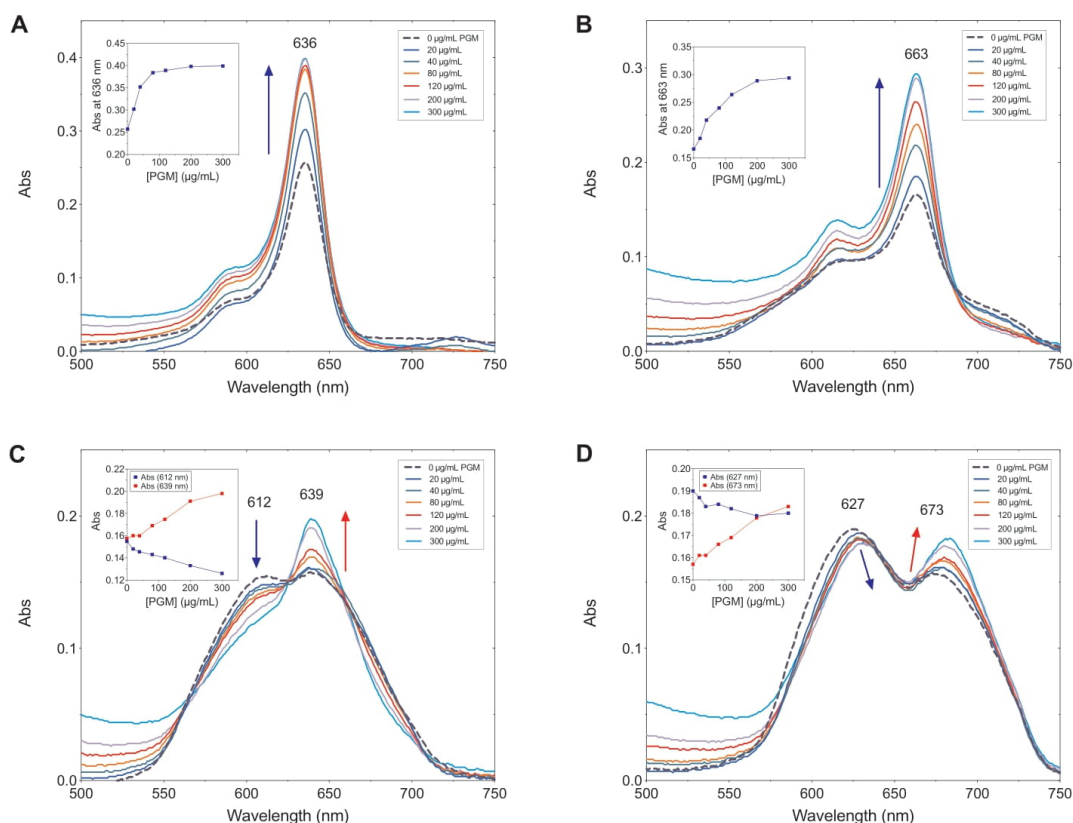

Fig. 2. UV/Vis absorption spectra of a 2 μM solution of S1 (A), S2 (B), S3 (C), S4 (D) recorded in different solvents.

3

161

Fig. 3. UV/Vis absorption spectra of S1 (A), S2 (B), S3 (C) and S4 (D) alone (bold dashed line) and upon addition of porcine gastric mucin (PGM). The inset shows the absorbance response to PGM concentration.

making them more soluble in water thus less aggregated. Likewise, the hydrophobic poly(propylene)-oxide (PPO) segments of the amphiphilic surfactant (Pluronic F-127) may entangle with the indolenine or benzoindolenine moieties of the squaraine resulting in an increased water solubility. An increase in solubility, even if particularly evident only for S3, is achieved with phosphate buffer (2 mM, pH 7.4). At pH 7.4 the carboxylic groups on the lateral moieties of squaraines are completely deprotonated consequently resulting in an increased solubility in water.

The interaction between each squaraine and PGM was firstly monitored by UV/Vis absorption spectroscopy keeping the squaraine concentration constant (1 μM) with a subsequent increase amount of PGM (Fig. 3). Since mucin "solutions" are actually suspensions, with the increasing of the concentration of the protein we observe an increase of the absorption baseline which is the result of the suspended mucin strands. Addition of increasing amounts of PGM to the solutions of the short-chain squaraines, S1 and S2, results in an increased absorption (hyperchromism) of their bands at 636 and 663 nm respectively. The absorption spectra of the two squaraines with the longer chains, S3 and S4, are characterized by two large bands; the first band at shorter wavelength assignable to H-aggregates, while the second one at longer wavelength accountable to the monomeric form of the squaraine. In the

case of S3, addition of PGM resulted in a gradually increase of the band at 639 nm and a decrease of the H-aggregate band at 612 nm. A similar trend was observed also for S4. Here, not only the bands at 627 and 673 nm decreased and increased but were also 4 and 10 nm red-shifted respectively. Overall, these results suggest that in presence of PGM a lower amount of H-aggregates is present and probably the protein interacts with the monomeric form of the squaraine dye. However, the exact mechanism of interaction is not fully understood with only this technique.

As reported also in our previous studies, all the herein studied squaraines have excellent emission properties in organic solvents which is gradually decreased, due to an aggregation quenching effect (AQE), upon addition of increasingly amount of water [23,28,36]. The loss of fluorescent features of squaraines as a result of the aggregation phenomenon is widely reported in literature [30,37–41]. When the concentration of PGM was increased in the test system, a gradual enhancement in the fluorescence intensity was observed (Fig. 4). In fact, the emission intensity of S1 at about 642 nm increased about 3 times, while for S2 the fluorescence intensity increased about 4 times and the original emission peak at 670 nm was 7 nm red-shifted. Interestingly, the major turn-on of fluorescence was recorded for the complexes with
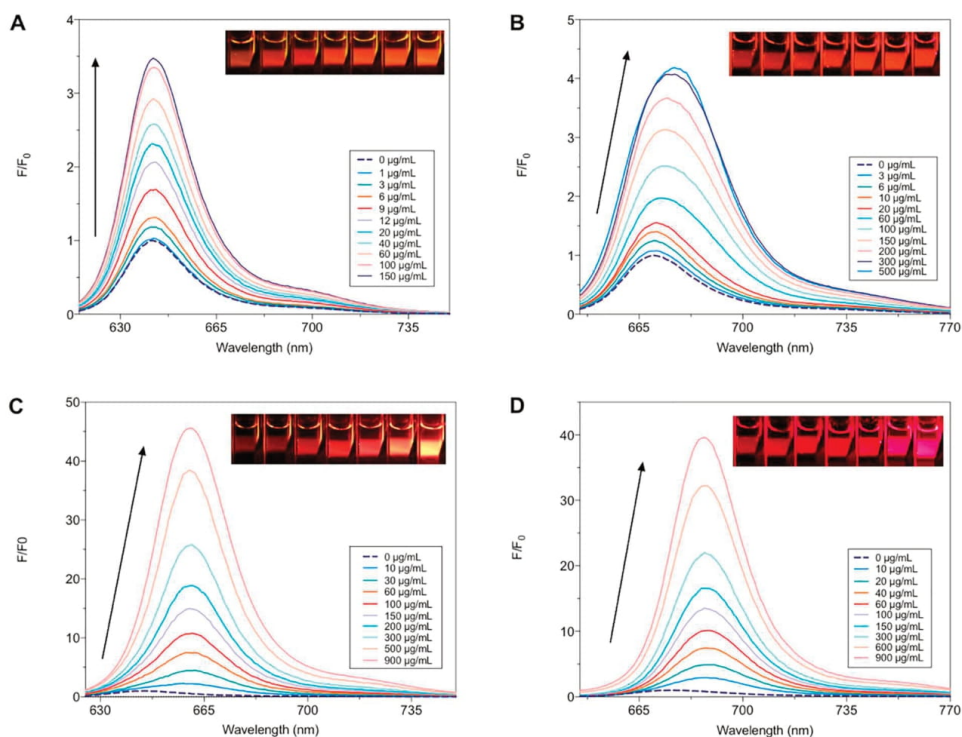
Fig. 4. Steady-state fluorescence intensity changes of S1 (A), S2 (B), S3 (C) and S4 (D) upon addition of PGM. The inset show the increase of emission visible on the surface of cuvette.

the analogue squaraine dyes with longer alkyl chains (S3 and S4). Indeed, upon addition of PGM, the maximum emission wavelength of S3 shifted from 645 to 660 nm and the fluorescence intensity increased by almost 45-fold. Similarly, a red-shift from 676 to 687 nm with a 40-fold emission enhancement was observed for the S4/PGM complex. The PGM-induced increase of fluorescence is visible even by naked eye when the beam of the spectrofluorometer is passing the quartz cuvette (insets on Fig. 4).

The observed increase of fluorescence and the red-shift after the introduction of PGM indicated environmental changes surrounding the squaraine chromophore. Squaraine aggregates may entangle with the hydrophobic domains of mucin. Once the contact is established, single dye molecules could be released from the aggregate to freely interact with the protein (inset in Fig. 10). As mentioned above, the emission spectra of the monomeric form of the squaraines can be registered in organic solvents like DMSO. In Fig. 5 it can be seen that, except for S1, the emission profile of squaraines recorded in aqueous solutions of mucin are shifted toward the profile of squaraines registered in DMSO. Moreover, it is noteworthy to mention that the emission intensity of S3-PGM complex is almost intense (> 80%) as the emission of S3 alone recorded in DMSO. These observations suggest that the emission turn-on may be attributed to an increase in the hydrophobicity of the environment surrounding the squaraine due to the hydrophobic domains of mucin. To test if the dye-protein interaction is somehow dependent by the hydrophobic domains of mucin we recorded the emission of

squaraines in presence of PGM at pH 2. It is known that at acidic pH, the hydrophobic domains of mucin are involved in non-covalent crosslinks via hydrophobic associations [3,42]. As can be seen in Fig. 5, at acidic pH the emission intensity of the squaraines in presence of mucin is reduced. These results indicate that the acidic-induced modification of the structure of mucin makes less effective the contact with squaraine aggregates, so giving a reduced turn-on of fluorescence.

To further confirm the hypothesis that the nature of the binding forces involved in the interaction of squaraines with PGM are of hydrophobic nature, we performed a thermodynamic study. Squaraines with the major ratio of F/F_0 (i.e. S3 and S4) were analyzed. A constant concentration of squaraine was titrated with mucin at different temperatures (288, 296, 310 K) and the fluorescence spectra were recorded. According to the values of enthalpy and entropy changes, the model of interaction between two chemical species can be summarized as: (i) $\Delta H° > 0$ and $\Delta S° > 0$ are indicative of binding guided by hydrophobic forces; (ii) $\Delta H° < 0$ and $\Delta S° < 0$ interactions through van der Waals interactions and hydrogen bonds; (iii) $\Delta H° < 0$ and $\Delta S° > 0$ are indicative of electrostatic interactions [34]. The various thermodynamic parameters, enthalpy change ($\Delta H°$), entropy change ($\Delta S°$) and Gibbs free energy change ($\Delta G°$) were calculated using the van't Hoff equation (Eqs. (1) and (2)) as mentioned below:

$$lnK = -\frac{\Delta H°}{RT} + \frac{\Delta S°}{R}$$
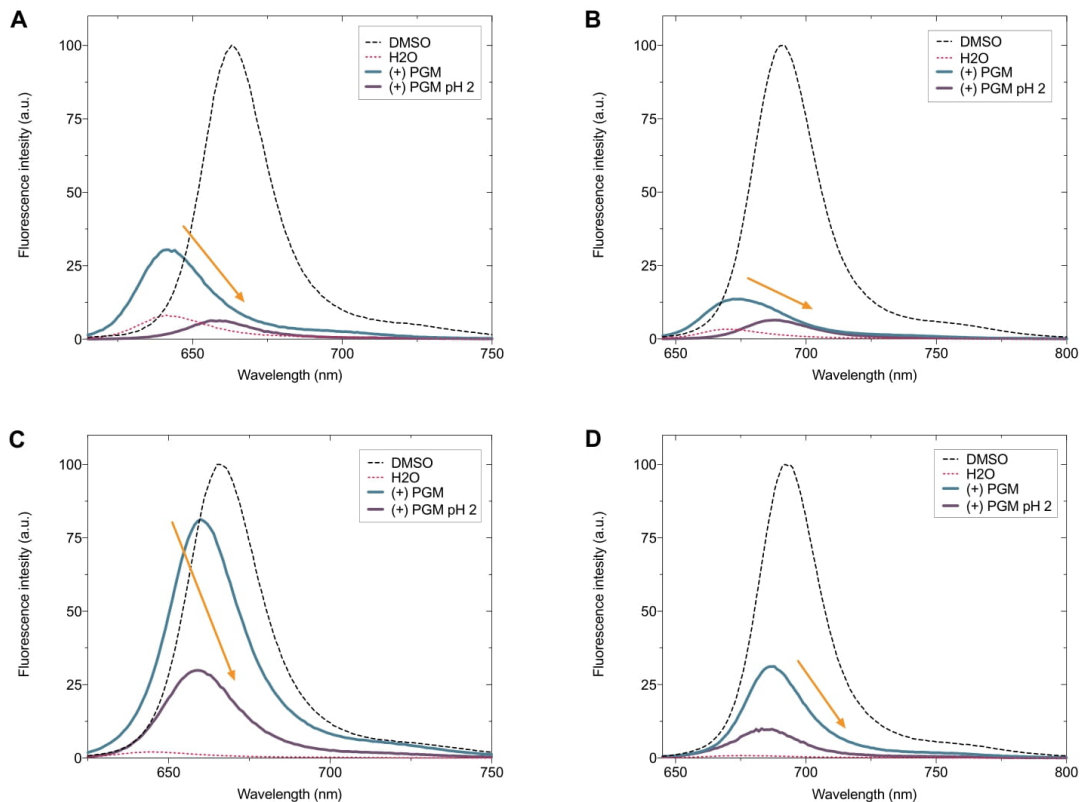
(1)

5

163

Fig. 5. Steady-state fluorescence intensity of S1 (A), S2 (B), S3 (C) and S4 (D) registered in DMSO, in water, in aqueous solutions of PGM and in aqueous solutions of PGM adjusted at pH 2.
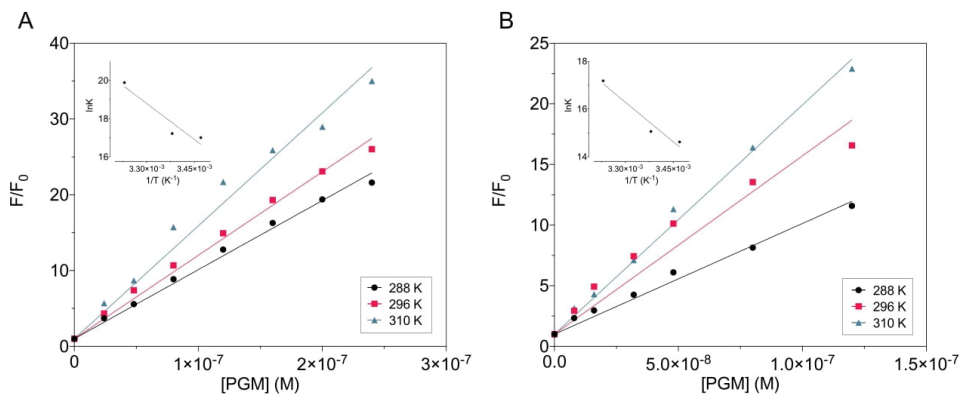

Fig. 6. Stern-Volmer plots of S3- and S4- PGM complexes recorded at different temperatures. Van't Hoff plots are reported as insets.

164

Table 1
Thermodynamic parameters for S3- and S4-PGM complexes at various temperatures.

Compound	T (K)	$\Delta G°$(KJ mol^{-1})	$\Delta H°$ (KJ mol^{-1})	$\Delta S°$ (J K^{-1} mol^{-1})
S3	288	−40.7		
	296	−42.4	101.8	491.8
	310	−51.2		
S4	288	−35.0		
	296	−37.1	89.1	429.2
	310	−44.3		

Table 2
Quantum yields (Φ, expressed as percent) of the studied squaraines in absence and presence of PGM. Data are the mean of three measurements.

Dye	Φ	Φ (+) PGM	Increase of Φ
S1	3.1	3.6	1.2
S2	3.4	4.1	1.2
S3	1.5	9.8	6.7
S4	0.2	2.8	12.2

$$\Delta G° = \Delta H° - T\Delta S° = -RTlnK \qquad (2)$$

where R is the universal gas constant (8.314 J K^{-1} mol^{-1}), K corresponds to K_A at specific temperatures and T is the absolute temperature. The results are presented in Fig. 6 and Table 1. The negative $\Delta G°$ value indicates that the binding processes of squaraine to mucin are spontaneous at the corresponding temperatures. The $\Delta H°$ and $\Delta S°$ values are both positive demonstrating that hydrophobic forces play the major role in the interaction of squaraines with PGM.

As a result of the formation of aggregates, each squaraine exhibited very low fluorescence quantum yield in aqueous medium (QY 1–3%) however, after addition of PGM an increase of the QY was recorded (Table 2). As shown in Fig. 7, the major increase in fluorescence QY was achieved by the squaraines with the longer alkyl chains. Among the four squaraines studied, S3 and S4 are the most lipophilic having logP 7.6 and 9.8 respectively (calculated with MarvinSketch, Chemaxon [43]). A high lipophilicity implies a scarce capacity to solubilize in water consequently we can assume that S3 and S4 are most prone to form aggregates in aqueous media.

In order to characterize possible changes in the secondary structure of mucin caused by the interaction with the squaraines, we compared the circular dichroism spectra of mucin alone and after addition of the dyes. The CD spectrum of PGM presents a maximum at 190 nm and a minimum at 208 nm (Fig. 8). This is characteristic of proteins with α-helix, β strand and aperiodic secondary structure [44]. After addition of squaraines, it can be observed that there was a slight increase of both the band without any significant shifts. These observations imply that the interaction of squaraines with mucin causes a very small change in secondary structure of the protein.

3.2. Binding and Kinetic Results of Squaraines with PGM

Conscious of the fact that the squaraine dyes exhibit different binding and interaction kinetics based on the complexity of their molecular structure [28,45], in order to investigate the interaction between PGM and the four squaraines we performed time-resolved and kinetics fluorescent studies.
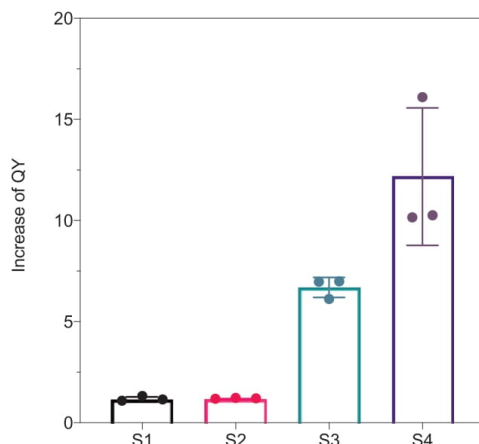
Fig. 7. The increase of fluorescence quantum yield of squaraines in water (2% DMSO) after addition of mucin.

At first, binding constants were obtained by plotting the ratio of the maximum values of fluorescence intensity of the squaraine/PGM complex on the maximum of fluorescence of squaraine alone (F/F_0), against the increasing PGM concentration (Fig. 9). Data were fitted with a nonlinear least-squares procedure, based on Eq. (3) [46].

$$\frac{F}{F_0} = \frac{F_{max}[Q]}{K_D + [Q]} \qquad (3)$$

where $[Q]$ is the concentration of PGM, F_{max} is the maximum increase of fluorescence achieved by the Sq-PGM complex formed at saturation and K_D is the equilibrium dissociation constant.

In order to reduce the inner filter effect, we used concentrations of mucin lower than 1 mg/mL; however, such a concentration is not enough for S3-PGM and S4-PGM to reach a complete plateau but enough to overtake the linear range. Emission spectra were recorded after waiting for the equilibrium of the squaraine-protein complexes (almost 20 min for S2- and S3-PGM complexes and 6 h for S4-PGM complex). The monomeric form of mucin weights about 640 kDa however, the extraction and purification processes alter the final protein structure [47], thus the precise value of the molecular weight is mutable. For the molecular weight of porcine gastric mucin we referred at the work of K. Jumel et al. [48]. Values of association (K_A) and dissociation (K_D) constant are reported in Table 3. We observe a dependence between the binding and the molecular structure of the squaraine. It seems like the bulkier the molecular structure of the squaraine the lowest the affinity toward mucin.

The kinetics of the squaraine-protein complexes was then investigated by checking the variation of the emission intensity over time, during incubation with a constant concentration of mucin. We considered as achievement of fluorescence stability the time after which no more increase in emission intensity was observed (Fig. 10). After one minute, fluorescence of S1-PGM complex was stable over time with no significant changes, while S2 and S3 required a longer time, 15 and 20 min respectively. Interestingly, a very long time was required for S4 which
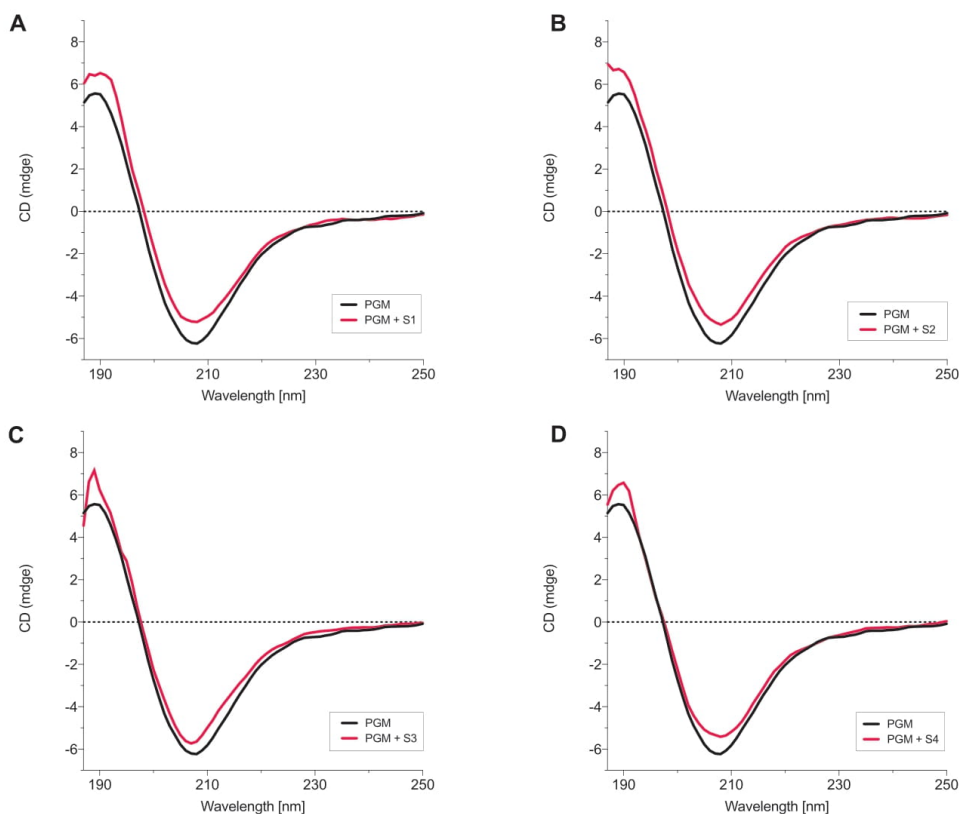
Fig. 8. Circular dichroism spectra of mucin alone and in the presence of S1 (A), S2 (B), S3 (C) and S4 (D).

reached the plateau after 360 min. Based on these results, we can assume that there is a relationship between the structure of the squaraine and the interaction with mucin, as previously found for the squaraine-bovine serum albumin interaction [28]. Evidently, the presence of short alkyl chains and indolenine groups (S1) allows a rapid kinetics. On the other hand, a slower kinetics is observed if the longer alkyl chains or the benzoindolenine groups are present (S2, S3), while the presence of both the structures on the same molecule (S4) involves a sum effect upon kinetics. It is also evident that the kinetic of the interaction has a great influence on the turn-on phenomenon: we observe a major increase of fluorescence with the long-lasting interactions (i.e. S4) while it is less evident for squaraines with fast kinetic (i.e. S1).

The complex formation between the squaraines with the major increase of quantum yield (i.e. S3 and S4) and mucin was further confirmed by analysis of lifetimes. Time-resolved fluorescence analysis indicated that S3 and S4 alone exhibits a biexponential decay (probably due to the presence of the dye alone and dye-aggregates), whereas triexponential decay (due to the formation of dye-protein aggregates) with significantly increased lifetime was observed in presence of PGM (Fig. 11).

3.3. Detection of S3 in Diluted Human Serum Samples

As the S3-PGM complex has the major increase in fluorescence, we chose to use S3 as probe to detect mucin in serum samples. The increase of F/F_0 upon increasing the PGM concentration has a linear relationship in the range 10–300 μg/mL, where F represents the maximum of fluorescence intensity of the complex and F_0 is the maximum of fluorescence intensity of S3 alone. We added different concentrations of PGM into the diluted serum samples and detected it again after an equilibration period time of 30 min. The concentration of PGM in diluted serum sample was calculated using the calibration curve (Fig. 9, inset in C). The calculated limit of detection (LOD) was 800 ng/mL. LOD was calculated according to the IUPAC definition of three times the deviation of the blank signal on the slope of the calibration curve (LOD = $3\sigma \, s^{-1}$). TCA was used to remove protein from the pure serum. The procedure of detection is illustrated in Fig. 12 and results are presented in Table 4: the recovery rates of different concentrations of PGM in diluted serum were from 94.9 to 116.2%. These results indicate that the squaraine S3 could act as a fluorescent probe for an accurate mucin detection in biological samples and has a great potential as an effective detection method for mucin detection in diagnostic applications.
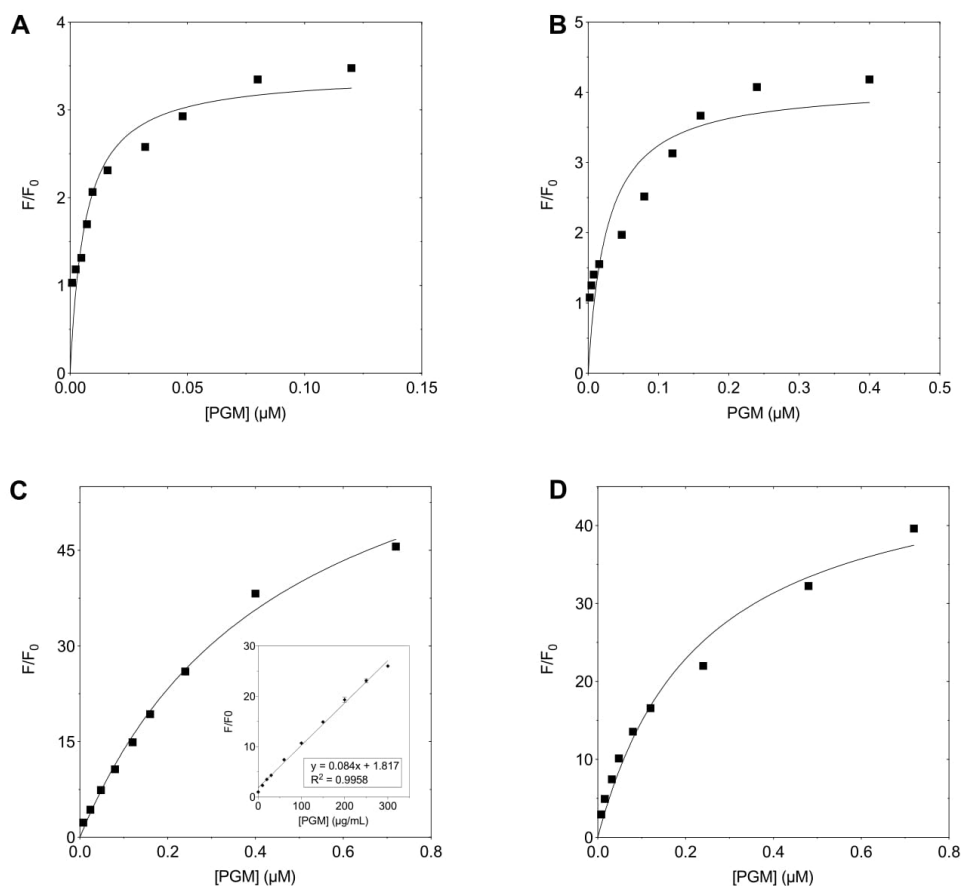
8

Fig. 9. Intensity maxima obtained at various PGM concentration for the monitoring of the S1-PGM (A), S2-PGM (B), S3-PGM (C) and S4-PGM (D) complexes formation. The curve is the fitting to a hyperbole equation for the evaluation of the binding constant. Inset (in C) is the linear relationship between F/F_0 and [PGM] ranging from 10 to 300 μg/mL.

Table 3
Association (K_A) and dissociation (K_D) constants of the squaraine-PGM complexes.

Compound	K_A (10^6 M^{-1})	K_D (10^{-7} M)
S1	156 (± 64)	0.064 (± 0.026)
S2	37.2 (± 15)	0.27 (± 0.11)
S3	2.78 (± 0.26)	4.57 (± 0.54)
S4	4.29 (± 0.81)	2.33 (± 0.44)

4. Conclusions

In summary, the interaction between porcine gastric mucin (PGM) and a series of squaraines with different substitutions was investigated. Thermodynamic and kinetic data were obtained. Squaraine dyes showed a structure-relationship influence upon the kinetic interaction with mucin, particularly the bulkier the molecular structure of squaraine, the slower the interaction. In addition, squaraine-mucin complexes displayed interesting emission characteristics since a fluorescence "turn-on" behavior was observed upon increasing additions of mucin in aqueous medium with a good increase of fluorescence quantum yield. Hydrophobic interactions play an important role in the binding of squaraines with mucin. These results make the herein squaraines as potential biosensors for different biological applications. In particular, squaraine S3 showed interesting fluorescence turn-on properties for mucin detection. This novel mucin detection has several significant advantages as it is simple, robust, cost efficiency, and has an acceptable sensitivity for mucin type III. Moreover, the proposed method could be a straightforward method for in vitro monitoring of mucin in microscopy applications. Further studies could be conducted on this path in order to design and develop new and more efficient squaraines for the detection of biomolecules as mucins.
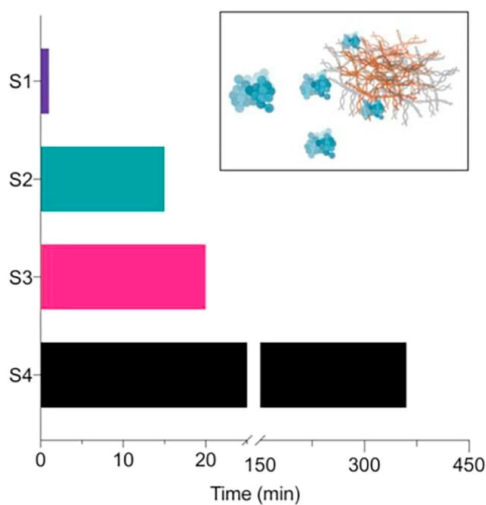
Fig. 10. Time-dependent fluorescence intensity of squaraines in the presence of a constant concentration of mucin. The times reported are the time after which no more increase of emission was observed. Inset reports a cartoon of the interaction between squaraine aggregates and mucin.

Table 4
Recovery of PGM from serum samples (*n* = 3). Data are mean ± standard deviation (SD).

Added PGM (μg/mL)	Detected (μg/mL)	Recovery (%)	SD (%, n = 3)
20	20.4	101.8	13.6
40	46.5	116.2	3.1
80	76.0	94.9	4.8

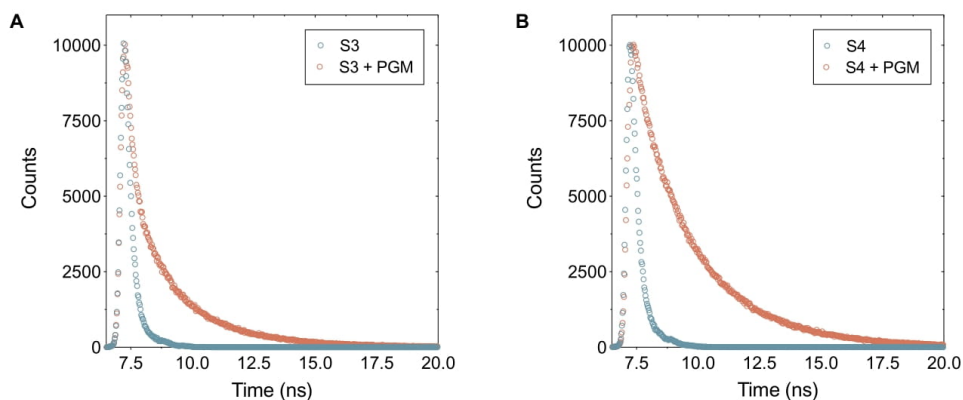**Declaration of Competing Interests**

Fig. 11. Time-resolved fluorescence analysis of S3 (A) and S4 (B) alone and in presence of PGM.
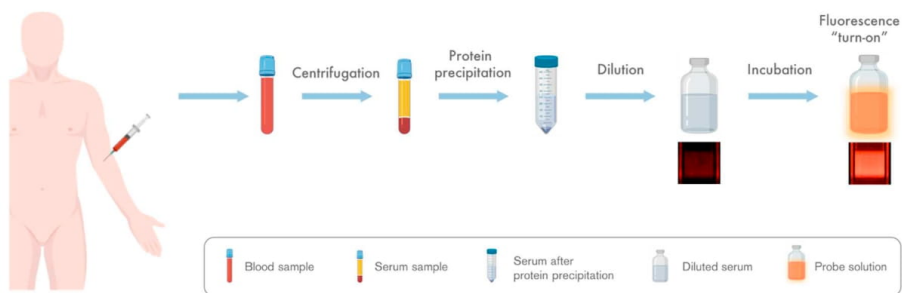

Fig. 12. Schematic illustration of serum samples preparation and detection. The square insets want to illustrate the emission enhancement visible on the surface of the cuvette when the beam of the spectrofluorometer passes through the cuvette without and with mucin.

References

[1] J. Ma, B.K. Rubin, J.A. Voynow, Mucins, mucus, and goblet cells, Chest. 154 (2017) 169–176, https://doi.org/10.1016/j.chest.2017.11.008.

[2] R. Bansil, B.S. Turner, The biology of mucus: composition, synthesis and organization, Adv. Drug Deliv. Rev. 124 (2018) 3–15, https://doi.org/10.1016/j.addr.2017.09.023.

[3] R. Bansil, B.S. Turner, Mucin structure, aggregation, physiological functions and biomedical applications, Curr. Opin. Colloid Interface Sci. 11 (2006) 164–170, https://doi.org/10.1016/j.cocis.2005.11.001.

[4] G.C. Hansson, Mucus and mucins in diseases of the intestinal and respiratory tracts, J. Intern. Med. 285 (2019) 479–490.

[5] S.K. Behera, A.B. Praharaj, B. Dehury, Exploring the role and diversity of mucins in health and disease with special insight into non-communicable diseases, Glycoconj. J. 32 (2015) 575–613, https://doi.org/10.1007/s10719-015-9606-6.

[6] H. Suh, K. Pillai, D.L. Morris, Mucins in pancreatic cancer: biological role, implications in carcinogenesis and applications in diagnosis and therapy, Am. J. Cancer Res. 7 (2017) 1372–1383.

[7] N. Jonckheere, N. Skrypek, I. Van Seuningen, Mucins and pancreatic Cancer, Cancers (Basel). 2 (2010) 1794–1812.

[8] S. Nakamori, D.M. Ota, K.R. Cleary, K. Shirotani, T. Irimura, MUC1 mucin expression as a marker of progression and metastasis of human colorectal carcinoma, Gastroenterology. 106 (1994) 353–361, https://doi.org/10.1016/0016-5085(94)90592-4.

[9] E.A. Rakha, R.W.G. Boyce, D.A. El-rehim, T. Kurien, A.R. Green, E.C. Paish, J.F.R. Robertson, I.O. Ellis, Expression of mucins (MUC1, MUC2, MUC3, MUC4, MUC5AC and MUC6) and their prognostic significance in human breast cancer, Mod. Pathol. 18 (2005) 1295–1304, https://doi.org/10.1038/modpathol.3800445.

[10] S.C. Chauhan, K. Vannatta, M.C. Ebeling, N. Vinayek, A. Watanabe, K.K. Pandey, M.C. Bell, M.D. Koch, H. Aburatani, Y. Lio, M. Jaggi, Expression and functions of transmembrane mucin MUC13 in ovarian Cancer, Cancer Res. 69 (2009) 765–775, https://doi.org/10.1158/0008-5472.CAN-08-0587.

[11] H.O. Duarte, D. Freitas, C. Gomes, J. Gomes, A. Magalhães, C.A. Reis, Mucin-type O -glycosylation in gastric carcinogenesis, Biomolecules. 6 (2016) 1–19, https://doi.org/10.3390/biom6030033.

[12] A.V. Maker, N. Katabi, M. Gonen, R.P. Dematteo, M.I.D. Angelica, Y. Fong, W.R. Jarnagin, M.F. Brennan, P.J. Allen, Pancreatic cyst fluid and serum mucin levels predict dysplasia in intraductal papillary mucinous neoplasms of the pancreas, Ann. Surg. Oncol. 18 (2011) 199–206, https://doi.org/10.1245/s10434-010-1225-7.

[13] S. Bademler, A. Zirtiloglu, M. Sari, M.Z. Ucuncu, E.B. Dogru, S. Karabulut, Clinical significance of serum membrane-bound Mucin-2 levels in breast cancer, Biomolecules. 9 (2019) 40.

[14] F. Agha-Hosseini, M. Imanpour, I. Mirzaii-Dizgah, M.S. Moosavi, Mucin 5B in saliva and serum of patients with oral lichen planus, Sci. Rep. 7 (2017) 5–10, https://doi.org/10.1038/s41598-017-12157-1.

[15] K. Chen, O. Blixt, H.H. Wandall, Mucins as biomarkers in cancer, Mucins and Cancer, Future Medicine Ltd, 2013, pp. 34–49, , https://doi.org/10.2217/fmeb2013.13.124.

[16] J.-Y. Shih, S.-C. Yang, C.-J. Yu, H.-D. Wu, Y.-S. Liaw, R. Wu, P.-C. Yang, Elevated serum levels of mucin-associated antigen in patients with acute respiratory distress syndrome, Am. J. Respir. Crit. Care Med. 156 (1997) 1453–1457.

[17] E. Danese, O. Ruzzenente, A. Ruzzenente, C. Iacono, Assessment of bile and serum mucin5AC in cholangiocarcinoma: diagnostic performance and biologic significance, Surgery. 156 (2014) 1218–1224, https://doi.org/10.1016/j.surg.2014.05.006.

[18] M.V. Croce, M.T. Isla-Larriain, S.O. Demichelis, J.R. Gori, M.R. Price, A. Segal-Eiras, Tissue and serum MUC1 mucin detection in breast cancer patients, Cancer Res. Treat. 81 (2003) 195–207.

[19] Y. Ding, J. Ling, H. Wang, J. Zou, K. Wang, X. Xiao, M. Yang, Fluorescent detection of mucin 1 protein based on aptamer functionalized biocompatible carbon dots and graphene oxide, Anal. Methods 7 (2015) 7792–7798, https://doi.org/10.1039/c5ay01608k.

[20] W. Wang, Y. Wang, H. Pan, S. Cheddah, C. Yan, Aptamer-based fluorometric determination for mucin 1 using gold nanoparticles and carbon dots, Microchim. Acta 186 (2019), https://doi.org/10.1007/s00604-019-3516-4.

[21] Y. He, Y. Lin, H. Tang, D. Pang, A graphene oxide-based fluorescent aptasensor for the turn-on detection of epithelial tumor marker mucin 1, Nanoscale. 4 (2012) 2054–2059, https://doi.org/10.1039/c2nr12061e.

[22] J. Shi, Q. Deng, C. Wan, M. Zheng, F. Huang, B. Tang, Fluorometric probing of the lipase level as acute pancreatitis biomarkers based on interfacially controlled aggregation-induced emission (AIE), Chem. Sci. 8 (2017) 6188–6195, https://doi.org/10.1039/C7SC02189E.

[23] J. Park, C. Barolo, F. Sauvage, N. Barbero, C. Benzi, P. Quagliotto, S. Coluccia, D. Di Censo, M. Grätzel, M.K. Nazeeruddin, G. Viscardi, Symmetric vs. asymmetric squaraines as photosensitisers in mesoscopic injection solar cells: A structure-property relationship study, Chem. Commun. 48 (2012) 2782–2784, https://doi.org/10.1039/c2cc17187b.

[24] L. Serpe, S. Ellena, N. Barbero, F. Foglietta, F. Prandini, M.P. Gallo, R. Levi, C. Barolo, R. Canaparo, S. Visentin, Squaraines bearing halogenated moieties as anticancer photosensitizers: synthesis, characterization and biological evaluation,

[25] M. Shimi, V. Sankar, M.K.A. Rahim, P.R. Nitha, S. Das, K.V. Radhakrishnan, K.G. Raghu, Novel glycoconjugated squaraine dyes for selective optical imaging of cancer cells, Chem. Commun. 53 (2017) 5433–5436, https://doi.org/10.1039/c6cc10282d.

[26] C.A. Bertolino, G. Caputo, C. Barolo, G. Viscardi, S. Coluccia, Novel heptamethine cyanine dyes with large stoke's shift for biological applications in the near infrared, J. Fluoresc. 16 (2006) 221–225, https://doi.org/10.1007/s10895-006-0094-8.

[27] B. Ciubini, S. Visentin, L. Serpe, R. Canaparo, A. Fin, N. Barbero, Design and synthesis of symmetrical pentamethine cyanine dyes as NIR photosensitizers for PDT, Dyes Pigments 160 (2019) 806–813, https://doi.org/10.1016/j.dyepig.2018.09.009.

[28] N. Barbero, C. Butnarasu, S. Visentin, C. Barolo, Squaraine dyes: interaction with bovine serum albumin to investigate supramolecular adducts with aggregation-induced emission (AIE) properties, Chem. - An Asian J. 14 (2019), https://doi.org/10.1002/asia.201900055.

[29] Y. Xu, Z. Li, A. Malkovskiy, S. Sun, Y. Pang, Aggregation control of Squaraines and their use as near-infrared fluorescent sensors for protein, J. Phys. Chem. B 114 (2010) 8574–8580.

[30] Y. Zhang, X. Yue, B. Kim, S. Yao, M.V. Bondar, K.D. Belfield, Bovine serum albumin nanoparticles with fluorogenic near-ir-emitting squaraine dyes, ACS Appl. Mater. Interfaces 5 (2013) 8710–8717, https://doi.org/10.1021/am402361w.

[31] V.S. Jisha, K.T. Arun, M. Hariharan, D. Ramaiah, Site-selective binding and dual mode recognition of serum albumin by a squaraine dye, J. Am. Chem. Soc. 128 (2006) 6024–6025, https://doi.org/10.1021/ja061301x.

[32] V.S. Jisha, K.T. Arun, M. Hariharan, D. Ramaiah, Site-selective interactions-Squaraine dye-serum albumin complexes with enhanced fluorescence and triplet yields, J. Phys. Chem. B 114 (2010) 5912–5919.

[33] S. Saito, T.L. Massie, T. Maeda, H. Nakazumi, C.L. Colyer, A long-wavelength fluorescent squarylium cyanine dye possessing boronic acid for sensing monosaccharides and glycoproteins with high enhancement in aqueous solution, Sensors (Switzerland). 12 (2012) 5420–5431, https://doi.org/10.3390/s120505420.

[34] C. Butnarasu, N. Barbero, D. Pacheco, P. Petrini, S. Visentin, Mucin binding to therapeutic molecules : the case of antimicrobial agents used in cystic fi brosis, Int. J. Pharm. 564 (2019) 136–144, https://doi.org/10.1016/j.ijpharm.2019.04.032.

[35] N. Barbero, C. Magistris, J. Park, D. Saccone, P. Quagliotto, R. Buscaino, C. Medana, C. Barolo, G. Viscardi, Microwave-assisted synthesis of near-infrared fluorescent indole-based squaraines, Org. Lett. 17 (2015) 3306–3309, https://doi.org/10.1021/acs.orglett.5b01453.

[36] J. Park, N. Barbero, J. Yoon, E. Dell'Orto, S. Galliano, R. Borrelli, J.H. Yum, D. Di Censo, M. Grätzel, M.K. Nazeeruddin, C. Barolo, G. Viscardi, Panchromatic symmetrical squaraines: a step forward in the molecular engineering of low cost blue-greenish sensitizers for dye-sensitized solar cells, Phys. Chem. Chem. Phys. 16 (2014) 24173–24177, https://doi.org/10.1039/c4cp04345f.

[37] F. Gao, Y. Lin, L. Li, Y. Liu, U. Mayerhöffer, P. Spenst, J. Su, J. Li, F. Würthner, H. Wang, Supramolecular adducts of squaraine and protein for noninvasive tumor imaging and photothermal therapy in vivo, Biomaterials. 35 (2014) 1004–1014, https://doi.org/10.1016/j.biomaterials.2013.10.039.

[38] Y. Xu, Q. Liu, X. Li, Y. Pang, A zwitterionic squaraine dye with a large stokes shift for in vivo and site-selective protein sensing w, Chem. Commun. (2012) 11313–11315, https://doi.org/10.1039/c2cc36285f.

[39] F. An, Z. Deng, J. Ye, J. Zhang, Y. Yang, C. Li, C. Zheng, X. Zhang, Aggregation-induced near-infrared absorption of squaraine dye in an albumin nanocomplex for photoacoustic tomography in vivo, Appl. Mater. Interfaces 6 (2014) 17985–17992.

[40] G.M. Paternò, L. Moretti, A.J. Barker, C. D'Andrea, A. Luzio, N. Barbero, S. Galliano, C. Barolo, G. Lanzani, F. Scotognella, Near-infrared emitting single squaraine dye aggregates with large stokes shifts, J. Mater. Chem. C 5 (2017) 7732–7738, https://doi.org/10.1039/c7tc01375b.

[41] G. Wang, W. Xu, Y. Guo, N. Fu, Near-infrared squaraine dye as a selective protein sensor based on self-assembly, Sensors Actuators B Chem. 245 (2017) 932–937, https://doi.org/10.1016/j.snb.2017.01.172.

[42] J. Caicedo, E.J. Perilla, Effect of pH on the rheological response of reconstituted gastric mucin, Ing. e Investig. 35 (2015) 43–48.

[43] MarvinSketch 18.28, ChemAxon, 2018.

[44] A. Jabrani, S. Makamte, E. Moreau, Y. Gharbi, A. Plessis, M. Sanial, V. Biou, Biophysical characterisation of the novel zinc binding property in suppressor of fused, Sci. Rep. 7 (2017) 2–11, https://doi.org/10.1038/s41598-017-11203-2.

[45] N. Barbero, S. Visentin, G. Viscardi, The different kinetic behavior of two potential photosensitizers for PDT, J. Photochem. Photobiol. A Chem. 299 (2015) 38–43, https://doi.org/10.1016/j.jphotochem.2014.11.002.

[46] C. Pontremoli, N. Barbero, G. Viscardi, S. Visentin, Mucin-drugs interaction: the case of theophylline, prednisolone and cephalexin, Bioorg. Med. Chem. 23 (2015) 6581–6586, https://doi.org/10.1016/j.bmc.2015.09.021.

[47] K. Bidmon, O. Lieleg, S. Berensmeier, An optimized purification process for porcine gastric mucin with preservation of its native functional properties, RSC Adv. 6 (2016) 44932–44943, https://doi.org/10.1039/C6RA07424C.

[48] K. Jumel, I. Fiebrig, S.E. Harding, Rapid size distribution and purity analysis of gastric mucus glycoproteins by size exclusion chromatography: multi angle laser light scattering, Biol. Macromol. 18 (1996) 133–139.